हैदराबाद विश्वविद्यालय
University of Hyderabad

Polymorphism in Single and Multiple Component Crystal Forms of Active Pharmaceutical Ingredients

A Thesis
Submitted for the Degree of
DOCTOR OF PHILOSOPHY
By

Battini Swapna

July 2021

School of Chemistry, University of Hyderabad (IoE), Hyderabad-500 046, India

प्रतिष्ठित संस्थान
INSTITUTION OF EMINENCE
राष्ट्रीय अपेक्षाएँ, वैश्विक मानक
National Needs, Global Standards

Polymorphism in Single and Multiple Component Crystal Forms of Active Pharmaceutical Ingredients

A Thesis
Submitted for the Degree of
DOCTOR OF PHILOSOPHY

By

Battini Swapna

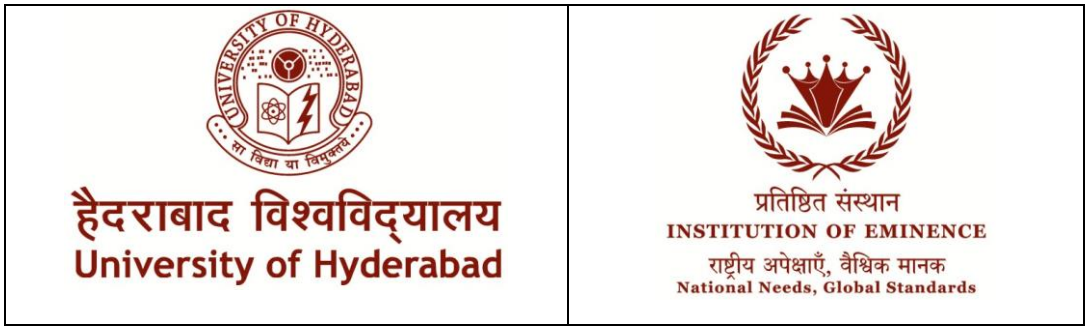

School of Chemistry
University of Hyderabad
Hyderabad 500046
Telangana
India

July 2021

Dedication

To

Amma & Nanna

DECLARATION

I hereby declare that the matter embodied in the thesis entitled **"Polymorphism in Single and Multiple Component Crystal Forms of Active Pharmaceutical Ingredients"** is the result of investigation carried out by me in the School of Chemistry, University of Hyderabad, Hyderabad, India, under the supervision of **Prof. Ashwini Kumar Nangia**.

In keeping with the general practice of reporting scientific observations, due acknowledgements have been made on the basis of the findings of other investigators. Any omission, which might have occurred by oversight or error, is regretted. This research work is free from Plagiarism. I hereby agree that my thesis can be deposited in shodganga/INFLIBNET. A report on plagiarism statistics from the University Librarian is enclosed.

B. Swapna

Battini Swapna
(11CHPH22)

Ashwini Nangia

Prof. Ashwini Kumar Nangia
(Supervisor)
University of Hyderabad

July 2021

Prof. Ashwini K. Nangia
School of Chemistry
University of Hyderabad
Central University P.O.
Hyderabad 500 046

CERTIFICATE

This is to certify that the thesis entitled **"Polymorphism in Single and Multiple Component Crystal Forms of Active Pharmaceutical Ingredients"** submitted by **Battini Swapna** holding registration number **11CHPH22** in partial fulfilment of the requirements for award of Doctor of Philosophy in the School of Chemistry is a bonafide work carried out by her under my supervision and guidance.

This thesis is free from plagiarism and has not been submitted previously in part or in full to this or any other University or Institution for award of any degree or diploma.

Parts of the thesis have been:

A. Published in following publication

Swapna, B.; Maddileti, D.; Nangia. A. *Cryst. Growth Des.* **2014,** *14,* 5991-6005.

Swapna, B.; Suresh, K.; Nangia. A. *Chem. Commun.* **2016,** *52,* 4037-4040.

Swapna, B.; Nangia. A. *Cryst. Growth Des.* **2017,** *17,* 3350-3360.

Swapna, B.; Mannava, M. K. C.; Nangia, A. *J. Pharm. Sci.* **2018**, *107,* 1667-1679.

B. Presented in the following conferences

1. ChemFest-2016
2. 17th Annual Dr. K. V. Rao Scientific Research Awards-2016-2017.

Further the student has passed the following courses towards fulfilment of course work requirement for Ph.D.

	Course No	Title	Credits	Pass/Fail
1.	CY-801	Research Proposal	3	Pass
2.	CY-805	Instrumental Methods A	3	Pass
3.	CY-840	Spectroscopic and other Physical Methods	3	Pass
4.	CY-841	Reactive Intermediates and Synthesis on Organic Chemistry	3	Pass

Prof. Ashwini Kumar Nangia

Thesis Supervisor

Prof. Ashwini K. Nangia
School of Chemistry
University of Hyderabad
Central University P.O.
Hyderabad 500 046

Dean

School of Chemistry

Dean
School of Chemistry
University of Hyderabad
P.O. Central University
Gachibowli, Hyderabad-500 046.

Acknowledgements

I express my deep sense of gratitude and profound thanks to my supervisor **Prof. Ashwini Kumar Nangia** for introducing me to the fascinating research field with highest degrees of freedom. His views on science and technology, optimistic way of approach and scientific administration are always admirable and inspiring. Throughout my Ph.D. tenure, he was always been approachable, helpful, and friendly. I will forever be grateful for being a part of his research family.

I take this opportunity to thank **Prof. K. C. Kumara Swamy**, Dean, School of Chemistry, and former Deans, Prof. M. Durga Prasad, Prof. M.V. Rajasekharan and all faculty members for providing the facilities needed for our research. I take this opportunity to thank my doctoral committee members **Prof. Samar Kumar Das** and **Prof. K. Lalitha Guruprasad** for their constant encouragement, discussions and support during my Ph.D. period.

I sincerely thank all the non-teaching staff of School of Chemistry for their help and assistance on various occasions. I specially thank to Mr. Gupta, Mr. Dilip, Mr. Abraham, Mr. Shetty, Mr. Mallaya Shetty, Mr. Vijay Bhaskar, Mr. Naik, Late Mr. Aleem, Smt. Geeta, Mr. David and Mr. Venkey anna, Mr. Durgesh, Mr. Mahinder, Mr. Satyanarayana, Mr. Turabuddin, Mr. Subramanyam, and Smt. Vijayalakshmi.

I am sincerely thankful to all my colleagues in School of Chemistry for fruitful scientific and social discussions and making my research life productive. I wish to thank UGC for fellowship, DST-SERB, UOH-UPE and UGC for providing required instruments, chemicals and facilities.

I am heartily thankful to Dr. K. Suresh, Dr. B. Geetha, Dr. Sudalai, Dr. Maddileti, Dr. Sudheer, M. Chaitanya, Dr. Anilkumar, Dr. Suryanarayana, Mr. Manish, Dr. Abhijit Mr. Sharath for being my generous co-workers, guides and friends. A special thanks to my lab seniors Dr. Anthony, Dr. Jagadeesh Babu, Dr. Bipul Sarma, Dr. Ranjit Thakuria, Dr. Naba Kamal Nath, Dr. Palash Sanphui, Dr. Suryanarayan and Dr. Rajesh Goud. I am glad to have a friendly working environment with Swarupa, P. Chaitanya, Vishwanath, Srikanth, Kranthi, Uday, Kiran, Divya, Dr. Ruchi, Dr. Daman, Dr. Abin.

I owe sincere and earnest thankfulness to my parents Shri. Battini Vishnumurthy and Smt. Bhagyamma and my brother Gopinath for everything. I am thankful to my sister-in-law Uma Rani and nephew Vivaan and niece Tiger and all other family members for their emotional association with me. I am heartily thankful to all my teachers and friends who constantly supported me throughout the period of my studies and boosted me morally and inspired me to be what I'm today.

Last but not the least, I would like to express respect and appreciation to my husband Venkatesh and my lovely son Rushank who have given me their unequivocal support throughout, as always, for which my mere expression of thanks likewise does not suffice.

swapna

SYNOPSIS

This thesis entitled **"Polymorphism in Single and Multiple Component Crystal Forms of Active Pharmaceutical Ingredients"** consists of seven chapters.

CHAPTER ONE

Introduction to Crystal Engineering and Pharmaceutical Solids

The term 'Supramolecular Chemistry' is used to describe 'chemistry beyond the molecule' and refers to the self-assembly of small molecules into complex solid state assemblies using non-covalent interactions. Crystal engineering is defined as "the understanding of intermolecular interactions such as hydrogen bonding, π-stacking, halogen bonding, electrostatic interactions, and van der Waals forces in the context of crystal packing and the utilization of such interactions in the design of new solids with desired physical and chemical properties". Crystal engineering is practiced by academic and industrial chemists for its ability to design novel pharmaceutical solids for drug development.

The design and synthesis of novel pharmaceutical solids has gained significant interest in recent years to alter the physicochemical properties of drugs. About 80% of marketed drugs are administered to patients as solid formulations (tablets, capsules, lyophilized powder forms) for reasons of economy, stability, mode of administration, ease of manufacture and storage. It is estimated that 40% of drugs in the market and over 80% of new chemical entities approved by the Food and Drug Administration (FDA) for use in the pharmaceutical industry are found to have limited aqueous solubility. Some drugs are known to exhibit physical stability (dissociation/decomposition) issues in the solid-state during manufacturing process and in different storage conditions, mainly under high humidity and/or ambient temperatures. Certain drugs, when exposed to UV light shows photostability problems such as photoisomerization, photodimerization and photodegradation. The management of these challenges along with enhanced therapeutic efficacy for active pharmaceutical ingredients (APIs) is the main goal for pharmaceutical scientists. Possible solutions to these issues in the solid formulation space are polymorphs, cocrystals, salts, amorphous, solvates/ hydrates etc. Owing to their hydrophilic/ hydrophobic nature, drugs exhibit physicochemical behavior which can be

controlled with coformers and additives, such as solubility, stability, bioavailability and dissolution rate for improved shelf-life and drug-patient compatibility. As a result, they play a crucial role in developing optimal formulations of drugs for better therapeutic efficacy.

Pharmaceutical solids can exist in different forms: thermodynamically stable crystalline and metastable polymorphs as well as amorphous forms. Crystalline solids have three-dimensional long-range order and periodicity but the structural interactions are short-range in amorphous solids. Amorphous solids can exist as amorphous solid dispersions and co-amorphous forms. Crystalline pharmaceutical solids can be further subdivided into single and multi-component compounds. The supramolecular family of multi-component solids includes cocrystals, salts, hydrates, solvates, eutectics, solid solutions etc. all of which can be used to enhancing specific physicochemical properties of active pharmaceutical ingredients. Cocrystals are solids that are neutral crystalline single-phase materials composed of two or more different molecular and/or ionic compounds generally in a stoichiometric ratio which are neither solvates nor simple salts. If at least one of the coformers is an API and the other component is pharmaceutically acceptable, then it is recognized as a pharmaceutical cocrystal. Salt cocrystals (SCCs) and ionic cocrystals (ICCs) are the two interesting subsets of cocrystals. SCCs are made up of a neutral molecule, which builds hydrogen bonds to a salt formed by its anion or cation. ICCs consist of an organic molecule and an inorganic salt that is in the same crystal lattice. A salt is formed by the transfer of a proton from an acid to a base. Hydrates and solvates are crystalline solids with water or solvent molecules incorporated in the crystal lattice structure. Solid solutions and eutectics are relatively less explored. Single-component solids may exist in multiple crystal structures which have different packing arrangements and/or conformations of molecules in the solid state, a phenomenon known as polymorphism. Polymorphs provide a unique opportunity to study the structure-property relationships of the same compound formed in different supramolecular environments. Solid form screening for the identification of novel API polymorphs is a rigorous exercise in the development of pharmaceutical drugs. This is because polymorphism can have a significant effect on pharmaceutical properties such as stability, solubility, bioavailability, hygroscopicity etc. Unlike single-component crystals and APIs, studies concerning polymorphism in cocrystals are not so widely reported. Since cocrystals are being considered as promising and patentable new solid forms for the development of drugs and materials, investigation of the polymorphic behavior of

cocrystals is just as important as that of single component crystals and APIs. Therefore, thorough screening of a drug molecule may result in any of the above mentioned solid forms for pharmaceutical applications. Diversity in the design of pharmaceutical solid forms is important because the pathological profile of a disease/infection might demand different formulations of a drug at various stages for effective treatment. In these situations, the wide range of physicochemical properties provided by the solid forms of an API would prove greatly beneficial.

The important point is that each of these solid forms can be advantageous for a specific application. Hence it is important to understand the nature and properties of diverse solid forms of drugs from a pharmaceutical perspective. This chapter specifically deals with the brief description of crystal engineering principles and pharmaceutical solids forms. It acts as a prelude to the working chapters of this thesis which deals with the design and discovery of various pharmaceutical solid forms of drugs and their physical behavior and physicochemical properties.

CHAPTER TWO

Cocrystals of the Tuberculosis Drug Isoniazid: Polymorphism, Isostructurality, and Stability

Isoniazid (INH) is an important active pharmaceutical ingredient (API) used in combination with rifampicin, pyrazinamide (PZA), and ethambutol for the treatment of tuberculosis, referred to as fixed dose combinations (3FDC, 4FDC). Tuberculosis (TB) is a major global health problem ranking as the second leading cause of death from a single infectious disease after HIV. WHO recommended FDCs against TB treatment for better patient compliance and lesser chances of developing drug resistance. However, serious concerns have been raised on the utility of these products due to quality problems such as stability and bioavailability of the formulation. Pure isoniazid is stable over long time periods at ambient as well as in accelerated stability conditions (40 °C, 75% RH), whereas in the FDC tablet formulations isoniazid undergoes degradation due to drug-drug interactions. Generally combinations of anti TB drugs are prescribed due to drug resistance and hence there is an immediate urgency to develop stable FDC formulations.

Pharmaceutical cocrystals may be defined as molecular complexes comprising of an API and one or more pharmaceutically acceptable cocrystal formers, usually selected from the list of US-FDA approved generally regarded as safe (GRAS) chemicals, which are in the solid-state at ambient conditions. Akin to single component systems such as active pharmaceutical ingredients (APIs), Cocrystals and salts also exhibit polymorphism. Polymorphism is the existence of more than one crystalline modification of the same compound in the solid-state. Even though single molecule polymorphism is classic whereas polymorphism in cocrystals is relatively recent. A complementary phenomenon to polymorphism is isostructurality, wherein two or more structurally related molecules have the same or similar crystal packing and/ or space group (i.e. isostructurality and isomorphism). Investigating the polymorphic behavior of an API is a critical part of the drug development process, because of its influence on pharmaceutical properties, such as solubility, stability, bioavailability, etc.

In this chapter, the cocrystal approach to improve the stability of anti-TB drug INH was examined by expanding the diversity of multi-component crystal structures. In INH, the principal functional groups are hydrazide and pyridine ring. The pyridine N atom is an excellent acceptor of hydrogen bond from acidic OH donor in the acid−pyridine heterosynthon. The hydrazide group has good hydrogen bond acceptor atoms (O and N) as well as donors (3 Hs). Both homo- (hydrazide N−H···O) and hetero-synthons (acid−pyridine O−H···N) are expected in the crystal structure. In this background, we performed liquid-assisted grinding (LAG) of INH with pharmaceutically acceptable GRAS coformers to prepare cocrystals. Novel crystalline multi-component forms were obtained with vanillic acid (VLA), ferulic acid (FRA), caffeic acid (CFA), and resorcinol (RES). Except INH-RES, the other cocrystals of INH-VLA, INH-FRA and INH-CFA are polymorphic. In order to obtain single crystals of these solid forms we used solution crystallization. Crystallization from different solvent mixtures afforded diffraction quality single crystals of all the solid forms except that of INH-CFA-Form-2 and INH-FRA-Form-2, which did not give diffraction quality single crystals even after several attempts. All cocrystals were found to be 1:1 (API: coformer) stoichiometry by X-ray diffraction. The composition of all the cocrystals was confirmed from the crystal structure, except that for INH-FRA-Form-2 and INH-CFA-Form-2, which were determined by ^{1}H NMR and ^{13}C ss-NMR. Structural analysis revealed that all the cocrystal structures containing acidic coformers are sustained by the robust acid–pyridine synthon (COOH···N_{arom}). The occurrence of this heterosynthon is in accordance

with the hydrogen bond hierarchy rule, except in INH-VLA-Form-1 and INH-FRA-Form-1 in which the hydroxyl–pyridine synthon (OH···N_{arom}) was observed. Interestingly, INH-VLA-Form-1 and INH-FRA-Form-1, which do not follow the hydrogen bond hierarchy rule, are 2D isostructural. Further, analysis of all the structures showed eight different kinds of supramolecular synthons (four homosynthons and four heterosynthons) in the cocrystals of INH with acid and hydroxyl functionality conformers. All the novel cocrystal forms were characterized by spectroscopic (FT-IR, FT-Raman, ^{13}C ss-NMR), thermal (DSC, HSM), X-ray diffraction (PXRD, single crystal XRD) techniques. The cocrystal forms were tested in accelerated ICH conditions of 40 ^{o}C and 75% RH for stability, and found that all the solid forms are stable for a test period of six months, except INH–RES cocrystal. Slurry conditions and grinding experiments suggest that Form-2 of INH-FRA and INH-VLA have good stability and Form-1 of INH-CFA is the most stable crystalline form of isoniazid.

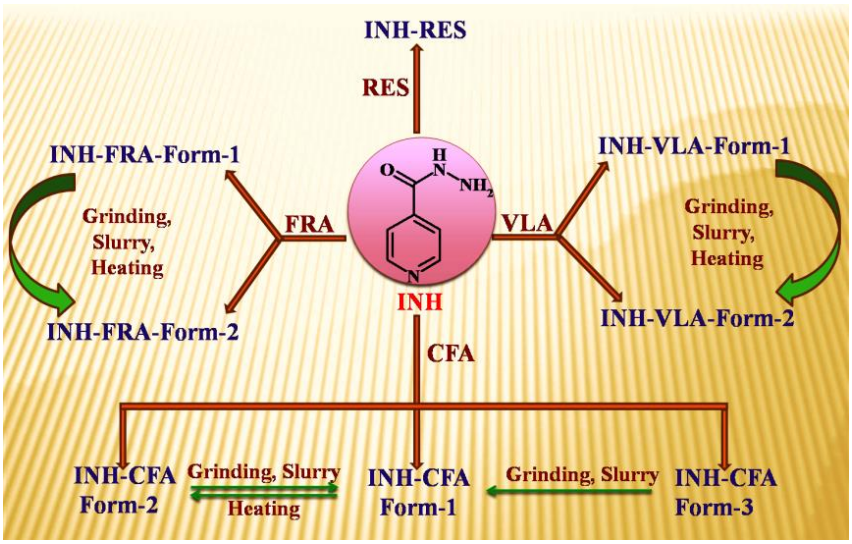

Figure 1: Figure representing cocrystal polymorphs of INH and their stability relationship.

CHAPTER THREE

Improved Stability of Tuberculosis Drug Fixed-Dose Combination Using Isoniazid-Caffeic acid and Vanillic acid Cocrystal

Tuberculosis (TB) is an airborne infectious disease caused by organisms of the Mycobacterium Tuberculosis complex. It is one of the top 10 leading causes of death worldwide. The first-line drugs recommended by WHO for the treatment of TB include Rifampicin (RIF), Isoniazid (INH), Pyrazinamide (PZA), and Ethambutol dihydrochloride (EDH). Since 1994, The WHO and International Union Against Tuberculosis and Lung Disease (IUATLD) recommended the use of fixed dose combination (2-drug, 3-drug and 4-drug FDCs) of these drugs for the treatment for tuberculosis over single-drug monotherapy tablets, for preventing the emergence of multidrug-resistant tuberculosis, and for better patient/ doctor compliance, simpler treatment and management of drug supply. In 1999 a 4-drug FDC tablet was included in the WHO Model List of Essential Drugs which comprises a combination of four anti-tuberculosis drugs namely, Rifampicin (RIF), Isoniazid (INH), Pyrazinamide (PZA), and Ethambutol dihydrochloride (EDH). Despite its numerous advantages, the 4-FDC tablet is known to exhibit quality and stability problems, including poor bioavailability of rifampicin and instability of anti-TB drugs during storage. When marketed FDC tablets in packed and unpacked state containing RIF, INH, PZA and EDH were stored under ICH (International Conference on Harmonisation of Technical Requirements for Registration of Pharmaceuticals for Human Use) accelerated stability conditions of 40 °C and 75% RH, extensive physical changes such as color fading, red bleeding and significant decomposition of RIF was observed. Isonicotinyl hydrazone (HYD) is the major degradation product in the mixture, which is formed by the interaction of the imino group of 3-formyl rifampicin of RIF with the hydrazine group of isoniazid under acidic conditions. Due to the hygroscopic nature of EDH, it attracts moisture and creates acidic environment in the formulation and thereby increases the rate of decomposition of RIF. Discoloration and conversion of the solid tablet to sticky, gummy mass is a common problem (Figure 3.1). Treatment of tuberculosis with poor-quality drugs, will result in treatment failures and development of drug resistance. With this background, WHO and IUATLD gave a joint statement that only FDC tablets of good quality and proven bioavailability of RIF should be used. In this regard, cocrystals of INH with several GRAS conformers were reported in chapter 1 where INH-CFA-form 1 and INH-VLA form 2 cocrystals showed good stability compared to the reference drug. In the present study, we replaced INH with stable cocrystals of INH in the 4-drug FDC formulation to improve the stability and prepared FDC INH-VLA (PZA + EDH + RIF + INH-VLA cocrystal) and FDC INH-CFA (PZA + EDH + RIF + INH-CFA cocrystal)

cocrystal batches and compared their stability with FDC reference batch (PZA + EDH + RIF + INH) after storage at accelerated conditions of 40 °C/ 75% RH for a period of one month. Stability studies showed that the physical stability of the cocrystal formulation was superior by PXRD and SEM analysis, and chemical purity was analyzed by HPLC. FDC-INH-CFA cocrystal batch exhibited greater stability compared to FDC-INH-VLA cocrystal and FDC reference drug batches. The superior stability of INH-CFA cocrystal is attributed to the presence of stronger hydrogen bonds and cyclic O–H···O synthon in the crystal structure.

Figure 3.1: Decomposition of 4-FDC tablets (a, e) on the shelf after storage at accelerated conditions of 40 °C/ 75% RH for a period of 2 days (c, g) and 5 days (d, h).

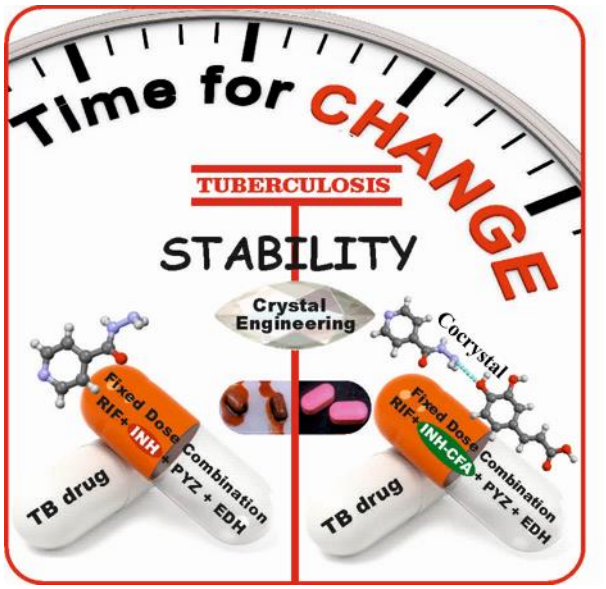

Figure 3.2: Improved stability of fixed dose tuberculosis drug through INH-Caffeic acid cocrystal.

CHAPTER FOUR

Color Polymorphs of Aldose Reductase Inhibitor Epalrestat: Configurational, Conformational and Synthon Differences

Epalrestat (5-[(1Z, 2E)-2-methyl-3-phenylpropenylidene]-4-oxo2-thioxo-3-thiazolidineacetic acid; EPR) is a non-competitive and reversible aldose reductase inhibitor (ARI), used to treat diabetic complications such as diabetic neuropathy, nephropathy, retinopathy, and cataract. By inhibiting aldose reductase enzyme, EPR reduces the accumulation of intracellular sorbitol, which is believed to be the cause of diabetic complications. Among all the recent carboxylic acid ARIs, EPR is the only ARI given marketing approval as a therapeutic drug for diabetic complications. EPR was developed in 1983 and since then has been marketed in Japan, China, India and Bangladesh. EPR is stable in the dark but isomerizes very easily upon photoirradiation even under a room light in solution to give four isomers and the structures of these four isomers were reported on the basis of NMR and UV spectroscopic techniques.

Polymorphism (supramolecular isomers) and configurational isomers (R/S, cis-trans, diastereomers) are related phenomena which can influence the structure and property of

molecules. Polymorphism is the ability of a chemical substance to exist in multiple crystal structures which have different packing arrangements and/or conformations of molecules in the solid state. Configurational isomerism may be stated as the same molecular formula exhibiting different orientation of groups in space (stereoisomers) or about double bond (geometric isomers). Configurational isomers are considered to be stable and not inter convertible at room temperature (possible to isolate), in contrast to conformers which are interconvertible readily at room temperature. Whereas isomerism is a molecular feature, polymorphism is about the supramolecular arrangements of molecules in the solid state. Polymorphism of crystalline materials, especially for drugs, is an area of immense interest and value to the pharmaceutical industry. Polymorphs can exhibit different physicochemical properties, such as solubility, dissolution rate, chemical and physical stability, melting point, color, filterability, density, flow properties and bioavailability. Hence an exhaustive solid form screen of all polymorphs (including hydrates, solvates, as well as salts and cocrystals) is a standard protocol for understanding the crystal landscape of a drug molecule.

In this chapter, we report five crystalline polymorphs and an amorphous phase of Epalrestat together with configurational isomerism and color behavior. Form I (deep red), form II (deep orange), form III (bright yellow), form IV (yellow), form V (orange) are in the E,Z configuration of the drug, and a Z,Z isomer (bright yellow). Two pathways are identified for polymorph conversion: direct transformation of E,Z isomer and another pathway via the Z,Z isomer to the E,Z polymorphs. Crystal form I, II, III (E,Z isomer) and Z,Z isomer structures were established by X-ray diffraction, and the remaining forms IV, V and amorphous state were characterized by spectroscopic (FT-IR, Raman, ^{13}C ss-NMR), thermal (DSC, HSM), and powder XRD techniques. Phase transformations were studied by VT-PXRD, DSC and HSM analysis. From a pharmaceutical perspective, the stability of polymorphs was established by grinding, solvent slurry and thermal conditions: Form I (thermodynamic) > Form II > Form V > Form III > Form IV (least stable).

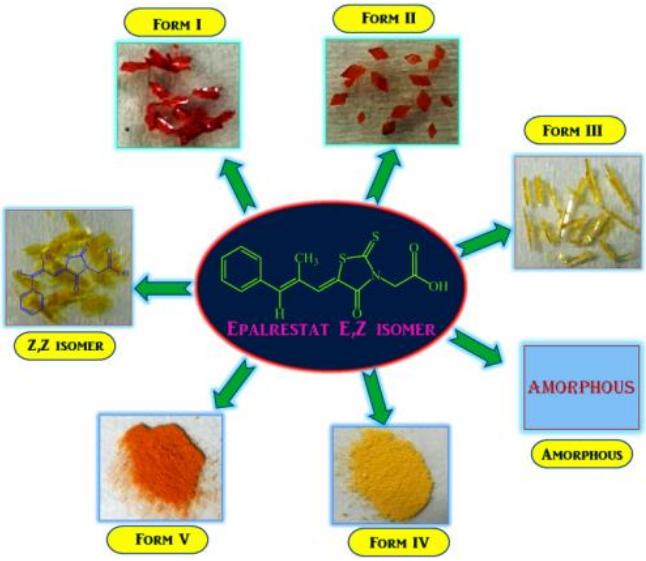

Figure 3: Photographs of different colored EPR polymorphs: deep red – form I, deep orange – form II, orange – form V; bright yellow – form III, yellow – form IV, and bright yellow – Z,Z isomer.

CHAPTER FIVE

Epalrestat–Cytosine Cocrystal and Salt Structures: Attempt to Control *E,Z* → *Z,Z* Isomerization

In chapter 4, we discussed color polymorphism in Epalrestat (EPR) (E,Z isomer) and its Z,Z isomer. But we couldn't control E,Z to Z,Z isomerization of EPR upon photoirradiation through polymorph screening. In this chapter we attempted to control E,Z to Z,Z isomerization of EPR through solid form screen of EPR with cytosine (CYT). The crystallization outcome of EPR and CYT could be a salt, cocrystal, or salt cocrystal hybrid based on an intermediate ΔpK_a value of 1.35. In the present study we have obtained novel salt polymorphs EPR^{-}–CYT-H^{+} form I and form II, salt-cocrystal hybrid and salt hydrate (EPR^{-}–CYT-H^{+}–H_2O, 1:2:1) forms of EPR with CYT using different techniques such as solution crystallization from different solvents, solvent assisted grinding, and controlled heating experiments. All the solid forms were fully characterized by spectroscopic (FT-IR, solution ^{1}H NMR), thermal (differential scanning calorimetry (DSC), hot-stage microscopy (HSM) and thermo gravimetric analysis (TGA), and X-ray diffraction techniques (single crystal and powder X-ray diffraction

(PXRD)). To our knowledge, this is the first report on salt and salt-cocrystal hybrid products for the same components under different crystallization conditions. The 2-amino-pyrimidinium−carboxylate two-point heterosynthon was observed in the crystal structure of EPR^{-}–CYT-H^{+} form I and form II solvated structures. The stoichiometry of EPR^{-}–CYT-H^{+} form II ethanol and n-propanol salt solvates was estimated as 1:1:0.036 and 1:1:0.043, respectively, by ^{1}H NMR spectroscopy. CYT-$H^{+}\cdots H^{+}$-CYT base-pairing was observed in the crystal structure of salt-cocrystal hybrid and salt hydrate.

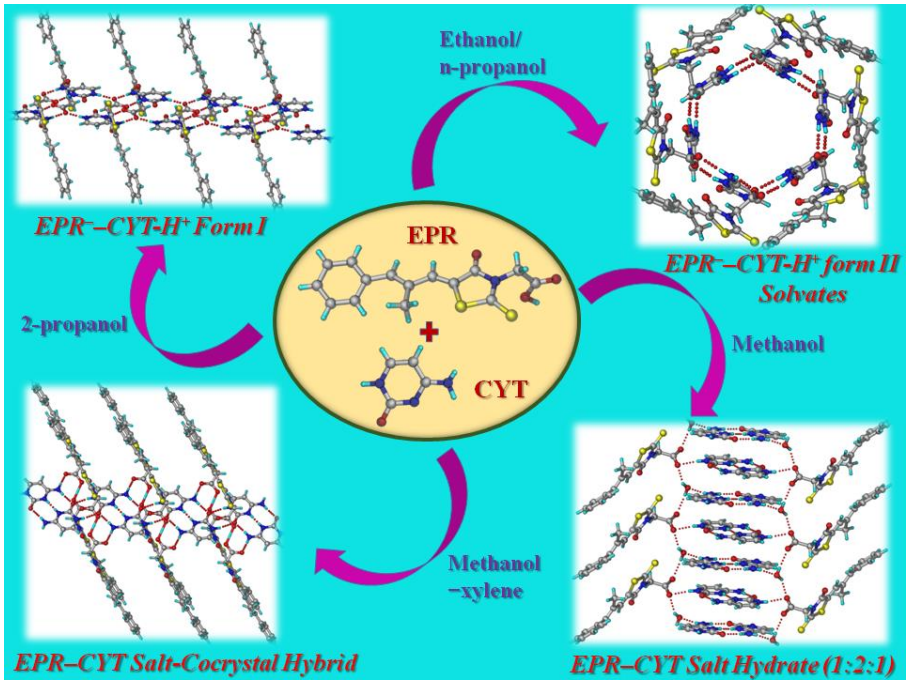

Figure 4: Figure representing the crystal structures of novel salt polymorphs EPR^{-}–CYT-H^{+} form I and solvated form II, salt-cocrystal hybrid and salt hydrate (EPR^{-}–CYT-H^{+}–H_2O, 1:2:1).

CHAPTER SIX

Improved Photostability of Aldose Reductase Inhibitor Epalrestat Through Cocrystallization

In the previous work (chapters 4 and 5), we are unsuccessful in controlling the E,Z to Z,Z photoisomerization of Epalrestat (EPR) through polymorph and salt screening. During the photostability studies, we found that EPR is undergoing photodimerization in

the solid state but it is not reported in the literature so far. Therefore, in this chapter we did cocrystal screening of EPR to control/stop the photoisomerization and photodimerization of EPR. Liquid assisted grinding (LAG) of EPR with several conformers resulted in cocrystals with conformers such as caffeine (CAF), acetamide (ACT), urea (URE), 4,4′-bipyridine (BPN) and 4-amino pyridine (AP). All the novel cocrystal forms were characterized by spectroscopic (FT-IR, ^{1}H NMR), thermal (DSC) and X-ray diffraction (powder XRD, single crystal XRD) techniques. Except EPR-BPN (1:0.5), all the cocrystals were found to be 1:1 (API:coformer) stoichiometry by X-ray diffraction. Solution crystallization of EPR and CAF grounded mixture from different solvent mixtures resulted in cocrystal polymorphs EPR-CAF Form I and EPR-CAF Form II. From X-ray crystal structures, it was found that C=C bonds lie parallel and separated less than 4.2 Å within the Schmidt's topochemical limit. Therefore, EPR and its cocrystal forms when exposed to UV light undergoing (2+2) cycloaddition in the solidstate. Peaks corresponding to EPR and EPR dimer in the ^{1}H NMR spectrum of EPR and all cocrystals except EPR-CAF Form II were similar after UV irradiation confirm the formation of type I head-tail dimer whereas EPR-CAF Form II gives type II head-tail dimer after UV irradiation. Percentage of EPR underwent for photodimerization reaction is different for different solid forms. All the solid forms were exposed to UV light for the period of 7 days and in the certain time intervals samples were withdrawn and their ^{1}H NMR spectroscopy studies were done. EPR-CAF form II undergoing 100% photodimerization within in time period of 10 min. Percentage of EPR remaining after photodimerization in EPR and its cocrystal forms is 30% (EPR), 86.7% (EPR-CFA Form I), 0% (EPR-CFA Form II), 50% (EPR-URE), 34% (EPR-4,4' BPN) and 55% (EPR-4AP). From the stability studies we conclude that EPR-CAF Form I is the most stable solid form in photodimerization reaction. All the cocrystal forms exposed to UV light in solution state and their photoisomerization studies were carried out through ^{1}H NMR spectroscopy. Unfortunately, all the cocrystal forms undergo photoisomerization and none of the cocrystals is able to stop/control the photoisomerization of EPR.

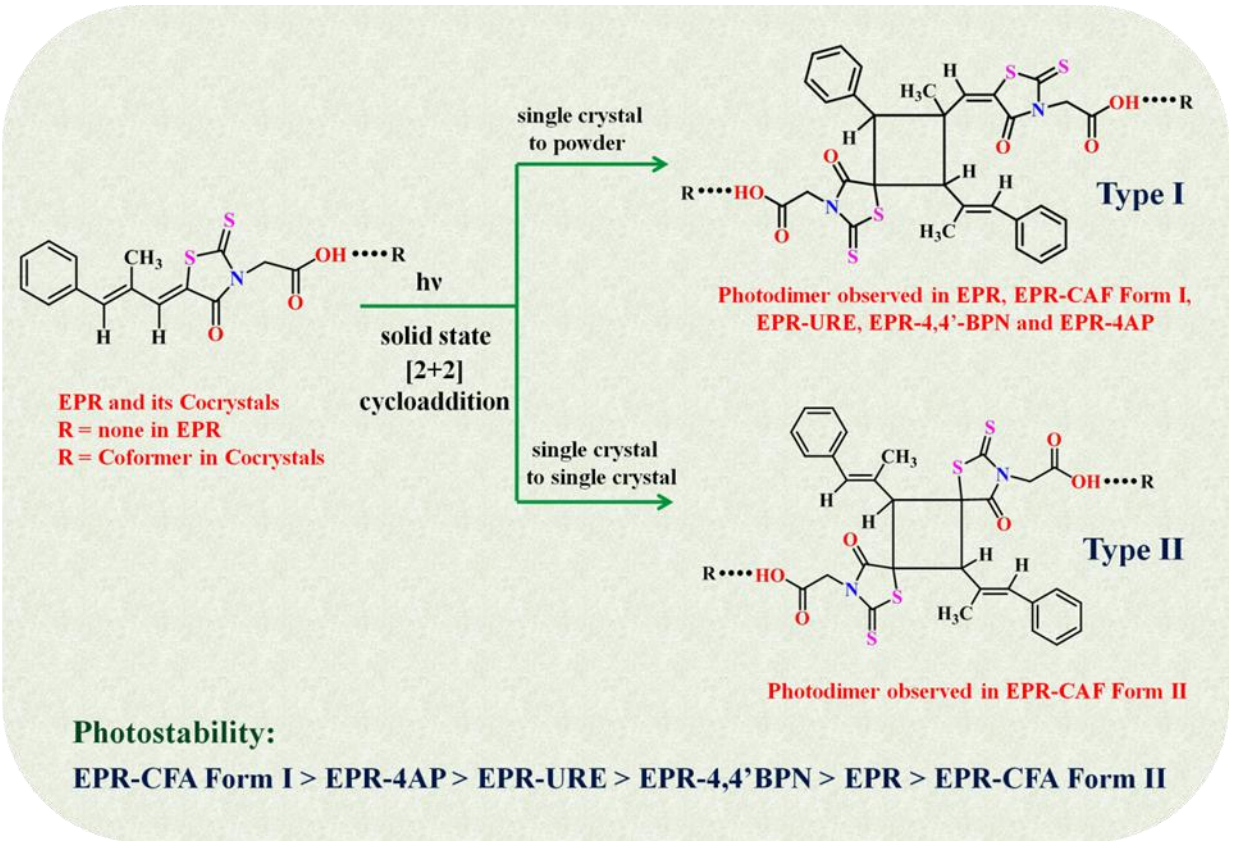

Figure 6: Figure representing photodimerization and improved photostability of Epalrestat by cocrystallization.

CHAPTER SEVEN

Conclusions and Future Prospects

From the above five working chapter the following implications and conclusions can be given. Crystal engineering principles and hydrogen bonding rules provides a wide-range of possibilities to design diverse pharmaceutical solid forms of Active Pharmaceutical Ingredients (APIs) with tailored physicochemical properties. Comprehensive studies on various pharmaceutical solid forms such as polymorphs, cocrystals and salts of several APIs were carried out with the intent of understanding and addressing the problems associated with those APIs. In chapter 2, novel cocrystals and cocrystal polymorphs of anti-TB drug Isoniazid were prepared and their stability studies were carried out.

Stability studies suggest that Form-2 of INH-FRA and INH-VLA have good stability and Form-1 of INH-CFA is the most stable crystalline form of isoniazid. In chapter 3, Study on the effect of these stable cocrystals (INH-CFA and INH-VLA) in stabilizing the 4-drug fixed dose combination (FDC) of Rifampicin, Isoniazid, Ethambutol dihydrochloride and Pyrazinamide in accelerated stability testing conditions showed that FDC-INH-CFA cocrystal batch exhibited greater stability compared to FDC-INH-VLA cocrystal and FDC reference drug batches. Five color polymorphs and an amorphous phase together with configuration isomerism of aldose reductase inhibitor Epalrestat (EPR) are studied and the stability relationship between polymorphs was established in chapter 4. Novel salt polymorphs EPR^{-}–CYT-H^{+} form I and form II, salt-cocrystal hybrid and salt hydrate (EPR^{-}–CYT-H^{+}–H_2O, 1:2:1) forms of Epalrestat with cytosine are discussed in chapter 5. In chapter 6, cocrystals of Epalrestat are obtained and their ability to decrease the photodimerization of parent compound was shown through photostability experiments.

CONTENTS

Declaration……. i

Certificate ……..... iii

Acknowledgements……..... v-vi

Synopsis ……..... vii-xx

Contents …… xxi-xxiii

Chapter 1

Introduction to Crystal Engineering and Pharmaceutical Solids **1-44**

1.1 Supramolecular Chemistry…….. 2
1.2 Crystal Engineering…..……... 3
1.3 Intermolecular Interactions…… 5
1.4 Supramolecular Synthons ……... 8
1.5 Hydrogen bond competition-Etter's rules …….……... 9
1.6 Introduction to Pharmaceutical Solids ……..... 10
1.7 Classification of Pharmaceutical Solids…….…… 10
1.7.1 Amorphous Forms …….……. 13
1.7.2 Polymorphism……..... 14
1.7.2.1 Classification of polymorphs……. 17
1.7.2.2 Generation of polymorphs ……..... 22
1.7.2.3 Kinetic vs. Thermodynamic polymorph……... 22
1.7.2.4 Polymorphism in Pharmaceutical industry……... 25
1.7.3 Solvates and Hydrates - Pseudopolymorphism …… 26
1.7.4 Pharmaceutical Salts ……... 28
1.7.5 Pharmaceutical Cocrystals……..……..... 30
1.8 Conclusions……..... 35
1.9 References……..…….….... 36

Chapter 2

Cocrystals of the Tuberculosis Drug Isoniazid: Polymorphism, Isostructurality, and Stability **45-98**

2.1 Introduction ……... 46
2.2 Literature reports on Isoniazid……... 48
2.3 Preparation of INH cocrystals…… 49
2.4 Results and Discussion…….. 50
2.4.1 Crystal Structure Description ……..... 54
2.4.2 Powder X-ray Diffraction……..... 61
2.4.3 Spectroscopic Characterization ……. 65
2.4.4 Thermal Analysis……..…….. 73
2.4.5 Slurry and Grinding…….. 76
2.4.6 Polymorph Stability ……...……... 85
2.5 Conclusions……..... 87
2.6 Experimental Section……. 88

2.7 References..... 92

Chapter 3

Improved Stability of Tuberculosis Drug Fixed-Dose Combination Using Isoniazid-Caffeic acid and Vanillic acid Cocrystal **99-128**

3.1 Introduction..... 100
3.2 Literature reports on Tuberculosis drugs..... 102
3.2.1 Decomposition of Rifampicin in the presence of Isoniazid..... 104
3.3 Results and Discussion..... 107
3.3.1 Crystal Structures..... 108
3.3.2 Physical Stability..... 111
3.3.3 Chemical stability by HPLC analysis..... 118
3.4 Conclusions..... 123
3.5 Experimental Section..... 123
3.6 References..... 126

Chapter 4

Color Polymorphs of Aldose Reductase Inhibitor Epalrestat: Configurational, Conformational and Synthon Differences **129-175**

4.1 Introduction..... 130
4.2 Literature Reports on Epalrestat..... 131
4.3 Results and Discussion..... 132
4.3.1 Crystal Structure Analysis..... 136
4.3.2 Conformational analysis and color polymorphism..... 139
4.3.3 Spectroscopic Analysis..... 141
4.3.4 Powder X-ray Diffraction Analysis..... 146
4.3.5 Phase Transformations in EPR Polymorphs..... 153
4.3.6 Polymorphic Stability under ICH Conditions..... 159
4.3.7 Grinding and Slurry experiments..... 162
4.3.8 Photostability Study of EPR polymorphs..... 164
4.4 Conclusions..... 166
4.5 Experimental Section..... 167
4.6 References..... 172

Chapter 5

Epalrestat–Cytosine Cocrystal and Salt Structures: Attempt To Control E,Z → Z,Z Isomerization **176-215**

5.1 Introduction..... 177
5.2 Epalrestat - Literature Reports 178
5.3 Results and Discussion..... 179
5.3.1 Crystal structure Analysis..... 184
5.3.2 Powder X-ray Diffraction..... 193
5.3.3 Spectroscopic Analysis..... 197
5.3.4 Thermal Analysis..... 201
5.3.5 Photostability Study of EPR–CYT Crystal Forms..... 206
5.4 Conclusions..... 209
5.5 Experimental Section..... 209

5.6 References…….. 213

Chapter 6

Improved Photostability of Aldose Reductase Inhibitor Epalrestat Through Cocrystallization **216-260**

6.1 Introduction…… 217
6.2 Literature Reports on Epalrestat…… 218
6.3 Preparation of Epalrestat Cocrystals…….. 219
6.4 Results and Discussion.....…….. 220
6.4.1 Crystal Structure Description……..... 224
6.4.2 Powder X-ray diffraction Analysis……..... 234
6.4.3 Infrared Spectroscopy…… 237
6.4.4 Thermal Analysis……..…….. 239
6.4.5 Photostability Studies……. 240
6.4.6 Correlating reactivity with molecular crystal packing……... 250
6.5 Conclusions……..... 252
6.6 Experimental Section……. 252
6.7 References…….. 257

Chapter 7

Conclusions and Future Prospects **261-264**

9.1 Conclusions…… 261
9.2 Future Prospects……. 263
About the Author…….. 265
List of Publications……... 267
Participation in Symposia, Workshops & Conferences…… 269

CHAPTER ONE

Introduction to Crystal Engineering and Pharmaceutical Solids

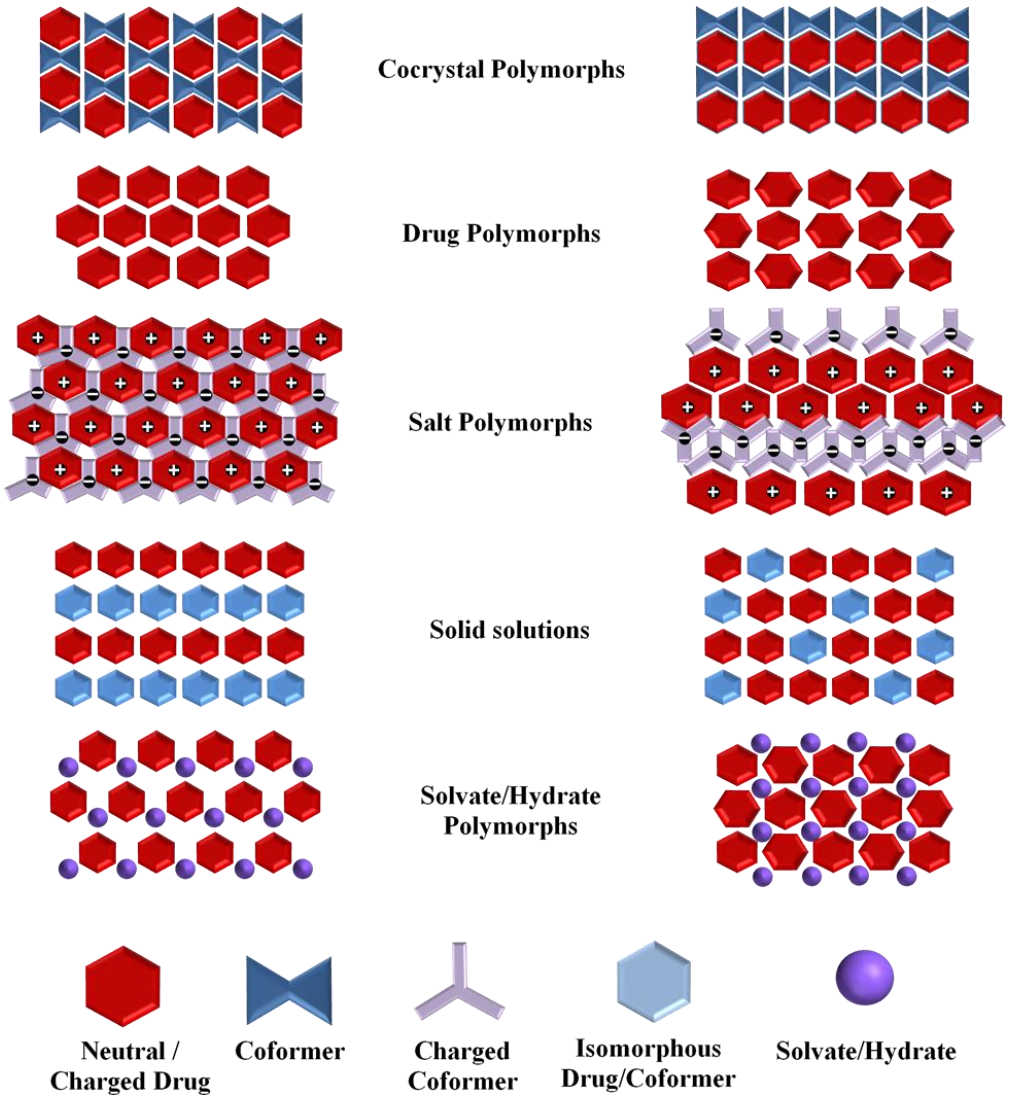

1.1 Supramolecular chemistry

The concept of a molecule is important in chemistry since Friedrich Wöhler synthesised urea[1] from ammonium cyanate in 1828. The molecule was then fortified as a decisive factor in understanding the physicochemical properties of a compound through the efforts of classical chemists. However, some of a compound's fundamental properties, such as its melting point, are bulk properties that are determined by the assembly of molecules rather than the molecule itself. Hence, a shift from this classic thought towards 'supramolecular chemistry'[2-3] was imminent. Philosophical foundations for supramolecular chemistry were established by Emil Fischer in 1894 when he related the enzyme-substrate interactions to a 'Lock and Key' mechanism[4]. This model subsequently formed the fundamental principles for the now-popular concepts of molecular recognition and host-guest chemistry. In 1948, H. M. Powell presented the organic crystal of hydroquinone clathrates as a network[5], which was the first modern stimulation of supramolecular thinking. Pedersen's serendipitous discovery of crown ethers in 1967, followed by Donald Cram and Jean-Marie Lehn's pioneering work in developing molecules with structure-specific non-covalent interactions and high selectivity, laid the foundation for modern supramolecular chemistry. The functional definition[6] of supramolecular chemistry was given by Jean-Marie Lehn in 2002 as: "*Supramolecular Chemistry aims at developing highly complex chemical systems from components interacting by non-covalent intermolecular forces*". In essence, the term can be applied to any scheme in which individual building blocks self-assemble to form an entirely new structure that is distinct from the individual building blocks. 'Supramolecular chemistry', also known as 'non-covalent chemistry' or 'Lego chemistry', is used to describe 'chemistry beyond the molecule'[3] is highlighted in Figure 1.1, which illustrates the relationship between molecular and supramolecular chemistry in terms of both structure and function.[7-8] Today, several areas, like dynamic covalent chemistry, complexation, biomimetics, molecular self-assembly, template-directed synthesis and molecular imprinting, are inspired by supramolecular chemistry principles[2,3,6]. Molecular self assembly is divided into two categories: 1) solution state dynamics of host-guest molecules, which are inspired by complex enzymatic reactions in biological systems referred to as molecular recognition

and 2) the understanding and design of solid-state intermolecular interactions, which is popularly known as 'Crystal Engineering[9-11]'.

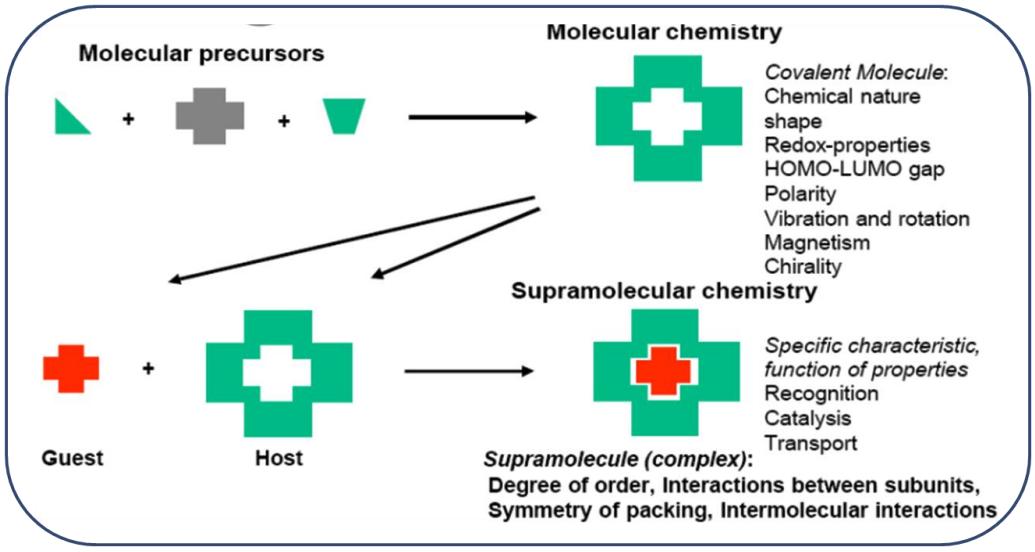

Figure 1.1 Comparison between the scope of molecular and supramolecular chemistry according to Lehn (adapted from ref. 3).

1.2 Crystal Engineering

The physical and chemical properties of molecular crystals are distinct from those of other types of crystalline solids. These properties are intimately related to the internal periodic arrangement of molecules. Crystal engineering arose from the need to understand the intermolecular interactions that exist in molecular solids in order to apply them in the construction of solid-state assemblies with tailored properties. In 1989, Desiraju defined crystal engineering[9] as "*the understanding of intermolecular interactions in the context of crystal packing and the utilization of such understanding in the design of new solids with desired physical and chemical properties*". Ever since R. Pepinsky[12] introduced the term crystal engineering to the literature in 1955 in the context of crystallization of organic ions with metal-containing complex ions, it has inspired the development of solid forms in pharmaceuticals[13], metal-organic frameworks[14] and nanostructures[13]. The quest of crystal engineering to answer the fundamental question: "*Given the molecular structure of a compound, what is its crystal structure?*" has significantly narrowed the gap in predicting

crystal structures of compounds from their molecular structures and vastly contributed to the understanding of intermolecular interactions in designing solid forms with predefined properties.

The evolution of crystal engineering began in the year 1921 by W. H. Bragg[15], who studied the unit cell parameters of naphthalene and anthracene and found that they were related: two of the axial lengths were nearly identical, while the third was 8.66 in naphthalene and 11.66 in anthracene. He concluded that the long direction of the molecules coincides with this third non-equal axis and that the width of a benzene ring is approximately 2.5 Å. This was possibly the earliest correlation between molecules and crystals, between crystal property and molecular property, of both naphthalene and anthracene compounds. Following that, J. M. Robertson,[16-17] a student of Bragg, made significant contributions on a large number of polynuclear aromatic hydrocarbons based on molecular thickness and molecular area. In addition, Bernal proposed molecular structures of phenanthrene related aromatic hydrocarbons from crystal unit cell parameters.[18] Although R. Pepinsky coined the term[12] "Crystal Engineering" in 1955, it was developed and expanded by G. M. J. Schmidt and coworkers between 1950 and 1970 in the context of organic solid state photochemical reactions in trans-cinnamic acids.[19-20] Based on the topochemical principle for photodimerization of alkenes via [2+2] cycloaddition reactions, they comprehensively established a correlation between crystal structure and their solid-state reactivity, and this approach has received a lot of attention in photochemical solid state reactions. They crystallized α-, β- and γ- forms of *trans*-cinnamic acids and photoirradiated them in the solid state, discovering that the α- and β- forms with an intermolecular distance of less than 4.2 Å underwent a cycloaddition reaction, resulting in α/β-truxillic acids, whereas the γ- form with a longer intermolecular distance of > 4.2 Å was photostable (Scheme 1.1).

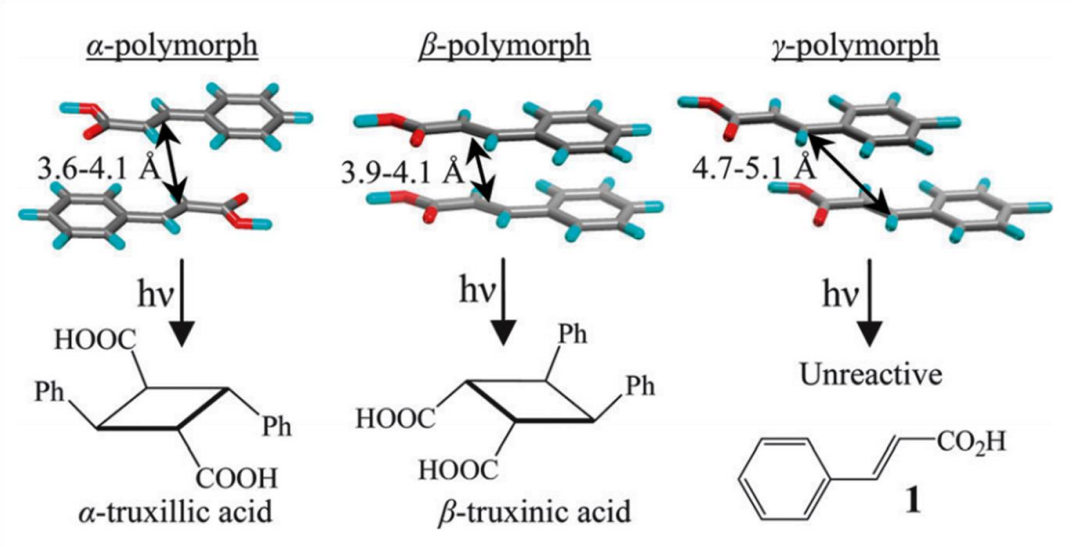

Scheme 1.1 Photo irradiation of α- and β- forms of trans-cinnamic acid with intermolecular distance of <4.2 Å has photodimerized to α- and β-truxillic acid respectively, whereas γ-form with intermolecular distance of >4.2Å was photo stable (Adapted from ref. 21)

1.3 Intermolecular interactions

A 'crystal' is a periodic arrangement of millions of molecules at an amazing level of precision. It is defined by Dunitz as '*a crystal is a perfect supermolecule—a super molecule par excellence*'.[22] while Lehn termed it as '*a very large supermolecule indeed*'[3]. The intermolecular interactions or non-covalent interactions that bind molecules in a crystal lattice are broadly classified into two types: isotropic medium range forces (C···C, C···H, H···H interactions) which define the shape, size and close packing; and anisotropic long-range forces which are electrostatic and include hydrogen bonds and hetero-atom interactions (O–H···O, N–H···O, C–H···O, C–H···N, O–H···π, halogen···halogen, nitrogen···halogen and so on). The importance of isotropic interactions is highlighted by A. I. Kitaigorodskii[23] who postulated the atom-atom potential method[24] for intermolecular interactions in crystal structures. This model describes crystals as being derived from efficient utilization of space during their formation, hence it is also popularly known as the 'principle of close packing'. Interaction energies of intermolecular interactions are now quite well established (Scheme 1.2).

Hydrogen bond[25-27] is the most widely used non-covalent interaction for the design and synthesis of supramolecular architectures. The early scientific literature on hydrogen bonds included reports from Werner[28] in 1902 and Hantzsch[29] in 1910 who referred the intermolecular interactions between ammonium salts by the term '*Nebenvalenz'* (minor valence). Latimer and Rodebush proposed that *'a free pair electrons on one water molecule can exert sufficient force on a hydrogen atom which is bonded to another water molecule, which consequently binds the two molecules together'*.[30] They defined the interaction as a *'weak bond'* involving hydrogen nuclei held between two Lewis octets. However, it was the chapter on hydrogen bonding in *'The nature of chemical bond*'[31] (Linus Pauling, 1939) that brought the subject of hydrogen bonding into the mainstream of science. The term *'hydrogen bond'* was coined by Linus Pauling and he defined the hydrogen bond as *"under certain conditions an atom of hydrogen is attracted by rather strong forces to two atoms instead of only one, so that it may be considered to be acting as a bond between them"*.[32] Later according to Pimentel and McClellan in the year 1960[33], a hydrogen bond is said to exist when (a) there is evidence of a bond, and (b) there is evidence that this bond specifically involves a hydrogen atom already bonded to another atom. Further Steiner and Saenger in 1993[34] and Desiraju and Steiner in 1999[35] also described the more general definition of hydrogen bond. In 2011, the International Union of Pure and Applied chemistry (IUPAC) established the following definition of hydrogen bonding: "*The hydrogen bond (designated as X-H···A, where acceptor A and donor X are electronegative atoms) is an attractive interaction between a hydrogen atom from a molecule or a molecular fragment X-H in which X is more electronegative than H, and an atom or a group of atoms in the same or a different molecule, in which there is evidence of bond formation*". [36] Hydrogen bonding interactions are formed between strong and weak donors and acceptors. The hydrogen bonding interactions can be investigated by a variety of experimental techniques such as X-ray diffraction, neutron diffraction, NMR, FT-IR and Raman spectroscopy as well as high energy diffraction and light sources. Depending on the interaction energy and the influence they have in determining and controlling the formation of supramolecular structures, hydrogen bonds are classified into three main categories: [35] very strong, strong, and weak (Table 1.1).

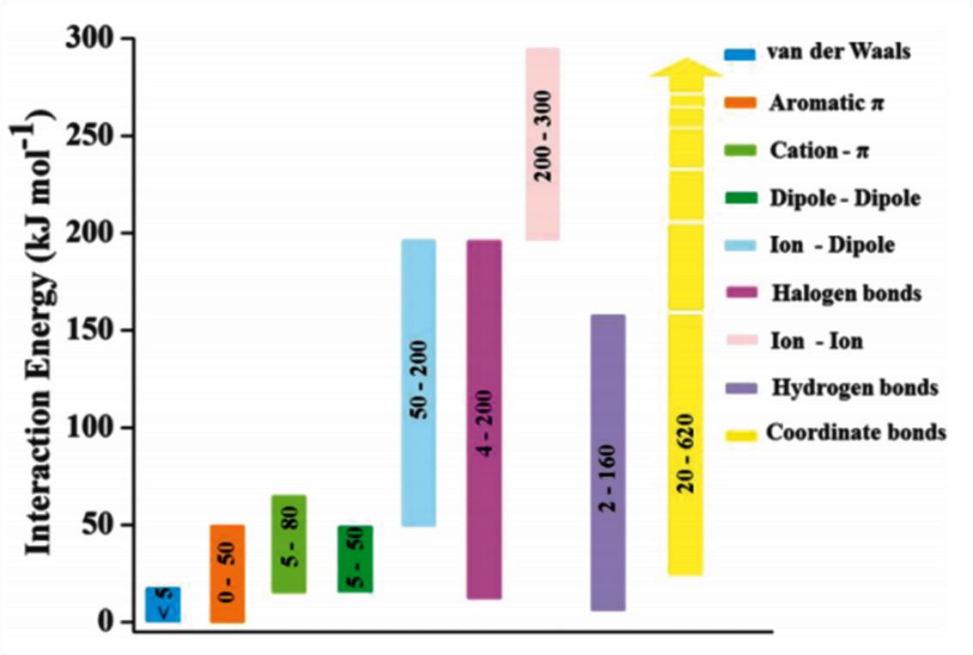

Scheme 1.2 Types of non-covalent interactions that have been exploited in supramolecular chemistry and their range of interaction energies. (Adapted from ref. 37)

Table 1.1 Some properties of very strong, strong and weak hydrogen bonds

	Very strong	Strong	Weak
Bond Energy (Kcal/mol)	15-40	4-15	< 4
Examples	[F–H···F⁻]	O–H···O=C	C–H···O
IR *vs* relative shift	>25%	5-25%	< 5%
Bond lengths	H–A ≈ X–H	H···A > X–H	H···A >> X–H
Lengthening of X-H (Å)	0.05–0.2	0.01–0.05	≤ 0.01
***D* (X···A) range (Å)**	2.2–2.5	2.5–3.2	3.0–4.0
***d* (H···A) range (Å)**	1.2–1.5	1.5–2.2	2.0–3.0
Bonds shorter than vDW	100%	Almost 100%	30-80%
θ (X–H···A) range (°)	175–180	130–180	90–180
kT (at room temp.)	>25	7-25	<7
Effect on crystal packing	Strong	Distinctive	Variable
Covalency	Pronounced	Weak	Vanishing
Electrostatics	Significant	dominant	moderate

Adapted from ref. 35.

1.4 Supramolecular Synthons

The term 'Synthon' was coined by E. J. Corey[38] in 1967 to simplify the synthesis of complex molecules and natural products in a review article titled "General Methods for Construction of Complex Molecules". He defined synthon as "*Structural units within molecules which can be formed and/or assembled by known or conceivable synthetic operations*". Since its inception, a synthon has been regarded as a part of the molecule that contains crucial information about bond connectivity and stereochemical information.[39] Using these synthon strategies in constructing a complex molecule with due consideration to its stereochemical preferences is popularly known as "Retrosynthesis".[40] The term was later used to designate a synthetic building block rather than retrosynthetic fragmentation structures.[41] Desiraju recognised crystal engineering as a supramolecular equivalent of organic chemistry in his excellent monograph[9] published in 1989. In order to simplify the complex supramolecular architectures, Desiraju proposed the term as 'Supramolecular Synthon'[42] and it is defined as "*structural units within supermolecules which can be formed and/or assembled by known or conceivable intermolecular interactions*". The supramolecular synthon approach is advantageous in that it greatly simplifies the understanding of crystal structures. To understand and design robust supramolecular synthons, it is necessary to recognise the suitable functional groups that would result in a high yielding supramolecular reaction.[43] Zaworotko[44] sub-classified synthons as homosynthons and heterosynthons based on the interacting functional groups. If supramolecular synthon is formed between the same functional group it is called a homosynthon, and between two different functional groups is called as heterosynthon. Heterosynthons acid–pyridine[45], phenol–pyridine[46], aminopyridine–acid[47], acid–amide[48], phenol–amine[49], amide–pyridine-*N*-oxide[50], and sulfonamide–pyridine-*N*-oxide[51] are well exploited in crystal engineering (Scheme 1.3).

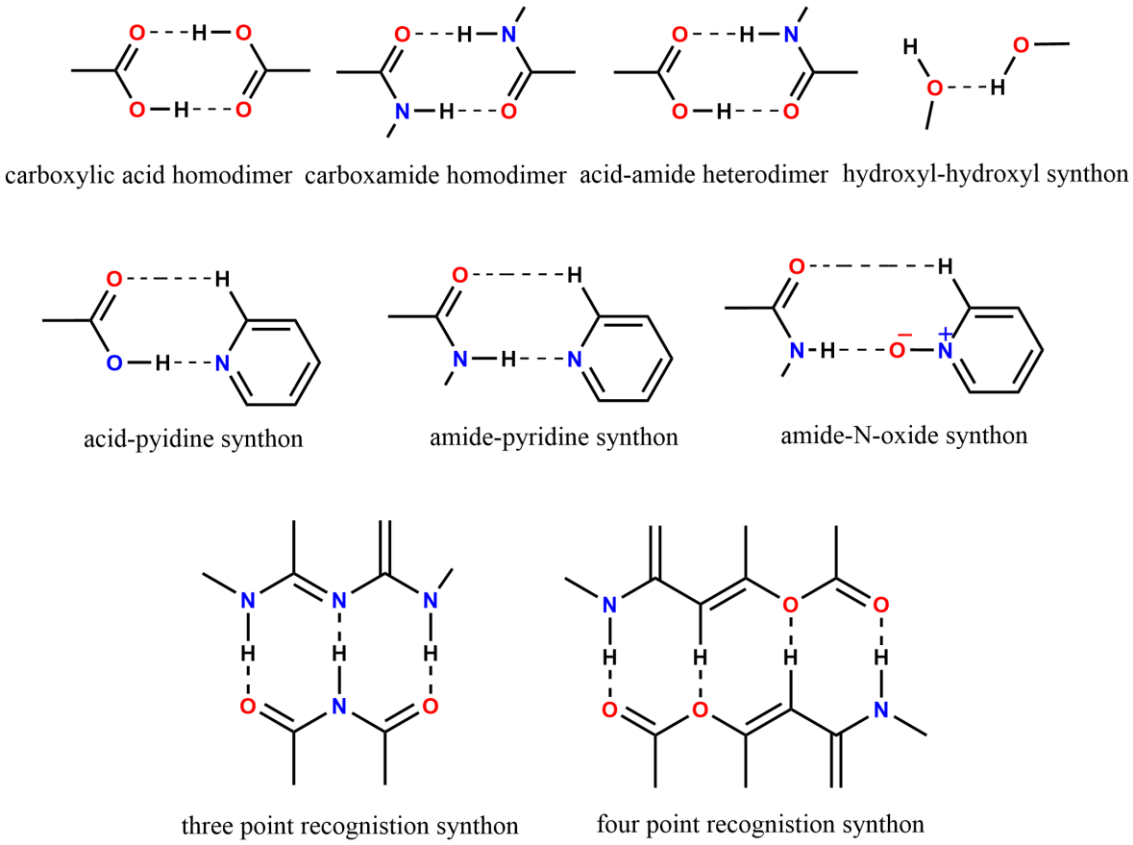

Scheme 1.3 Strong hydrogen bond homo/hetero synthons reported in literature.

1.5 Hydrogen bond competition - Etter's rules

To synthesize a desired crystal structure, one must first identify the functionalities that will generate predictable intermolecular interactions or synthons. It becomes more difficult in multifunctional molecules because of competition between similar strength of acceptor/donor groups. To comprehend the hydrogen bonding and competition in organic compounds, Etter proposed hydrogen bond rules, a fundamental rule is "*all acidic hydrogens available in a molecule will be used in hydrogen bonding in the crystal structure of that compound*."[52] A second rule, corresponding to the first one, is "*all good proton acceptors will be used in hydrogen bonding when there are available hydrogen-bond donors*." [53] And the third rule is "*the best hydrogen-bond donor and the best hydrogen acceptor will*

preferentially form hydrogen bonds to one another."[54] If the formation of a six-membered intramolecular hydrogen bond ring is possible, usually it will form in preference to other intermolecular hydrogen bonds. Functional group competitions in homomeric crystals or heteromeric cocrystals are used as a basis for categorising solid-state hydrogen bond preferences. The process entails determining which donors are chosen by a small number of acceptors or vice versa during crystallisation.

1.6 Introduction to Pharmaceutical Solids

The design and synthesis of novel pharmaceutical solids has gained significant interest in recent years to alter the physicochemical properties of drugs. About 80% of marketed drugs are administered to patients as solid formulations[55] (tablets, capsules, lyophilized powder forms) for reasons of economy, stability, mode of administration, ease of manufacture and storage. It is estimated that 40% of drugs in the market and over 80% of new chemical entities approved by the Food and Drug Administration (FDA) for use in the pharmaceutical industry are found to have limited aqueous solubility. Some drugs are known to exhibit physical stability (dissociation/decomposition) issues in the solid-state during manufacturing process and in different storage conditions, mainly under high humidity and/or ambient temperatures. Certain drugs, when exposed to UV light shows photostability problems such as photoisomerization, photodimerization and photodegradation. The management of these challenges along with enhanced therapeutic efficacy for active pharmaceutical ingredients (APIs) is the main goal for pharmaceutical scientists. Possible solutions to these issues in the solid formulation space are polymorphs, cocrystals, salts, amorphous, solvates/ hydrates etc. Owing to their hydrophilic/ hydrophobic nature, drugs exhibit physicochemical behavior which can be controlled with coformers and additives, such as solubility, stability, bioavailability and dissolution rate for improved shelf-life and drug-patient compatibility. As a result, they play a crucial role in developing optimal formulations of drugs for better therapeutic efficacy.

1.7 Classification of Pharmaceutical Solids

Generally pharmaceutical solids are broadly classified as thermodynamically stable crystalline and metastable amorphous forms. Crystalline solids have three-dimensional long-

range order and periodicity but the structural interactions are short-range in amorphous solids. Amorphous solids can exist as amorphous solid dispersions and co-amorphous forms. Crystalline pharmaceutical solids can be further subdivided into single and multi-component compounds. Single-component solids may exist in multiple crystal structures which have different packing arrangements and/or conformations of molecules in the solid state, a phenomenon known as polymorphism. The supramolecular family of multi-component solids includes cocrystals, salts, hydrates, solvates, eutectics, solid solutions etc. all of which can be used to enhancing specific physicochemical properties of active pharmaceutical ingredients. Polymorphism is possible in multicomponent crystalline solids such as salts, cocrystals, solvates etc. Cocrystals are solids that are neutral crystalline single-phase materials composed of two or more different molecular and/or ionic compounds generally in a stoichiometric ratio which are neither solvates nor simple salts. If at least one of the coformers is an API and the other component is pharmaceutically acceptable, then it is recognized as a pharmaceutical cocrystal. Salt cocrystals (SCCs) and ionic cocrystals (ICCs) are the two interesting subsets of cocrystals. SCCs are made up of a neutral molecule, which builds hydrogen bonds to a salt formed by its anion or cation. ICCs consist of an organic molecule and an inorganic salt that is in the same crystal lattice. A salt is formed by the transfer of a proton from an acid to a base. Hydrates and solvates are crystalline solids with water or solvent molecules incorporated in the crystal lattice structure. Solid solutions and eutectics are relatively less explored. Therefore, thorough screening of a drug molecule may result in any of the above mentioned solid forms for pharmaceutical applications. The classification of all pharmaceutical solids shown in Figure 1.2 and Scheme 1.4 depicts a summary of various approaches to drug solid form optimization. The following sections give a brief introduction to various solid forms that are studied in this thesis.

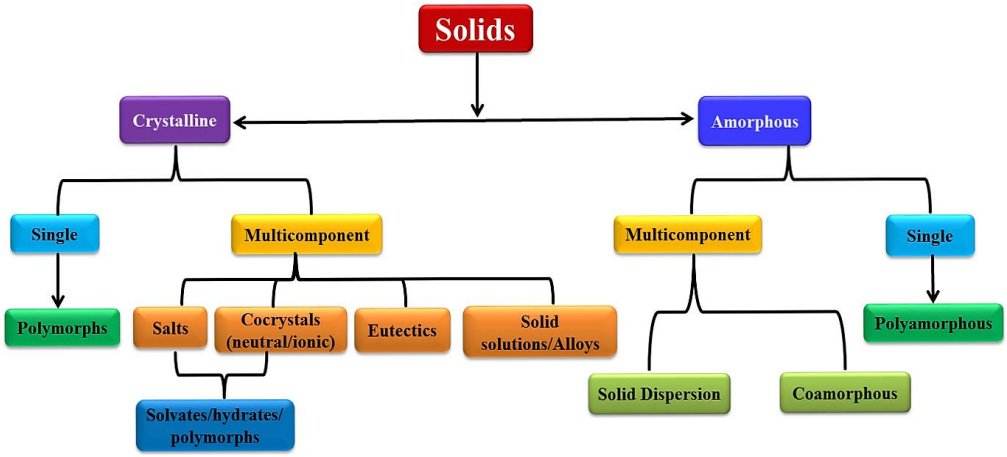

Figure 1.2 Classification of pharmaceutical solids based on the molecular packing in a crystal lattice into various solid state categories.

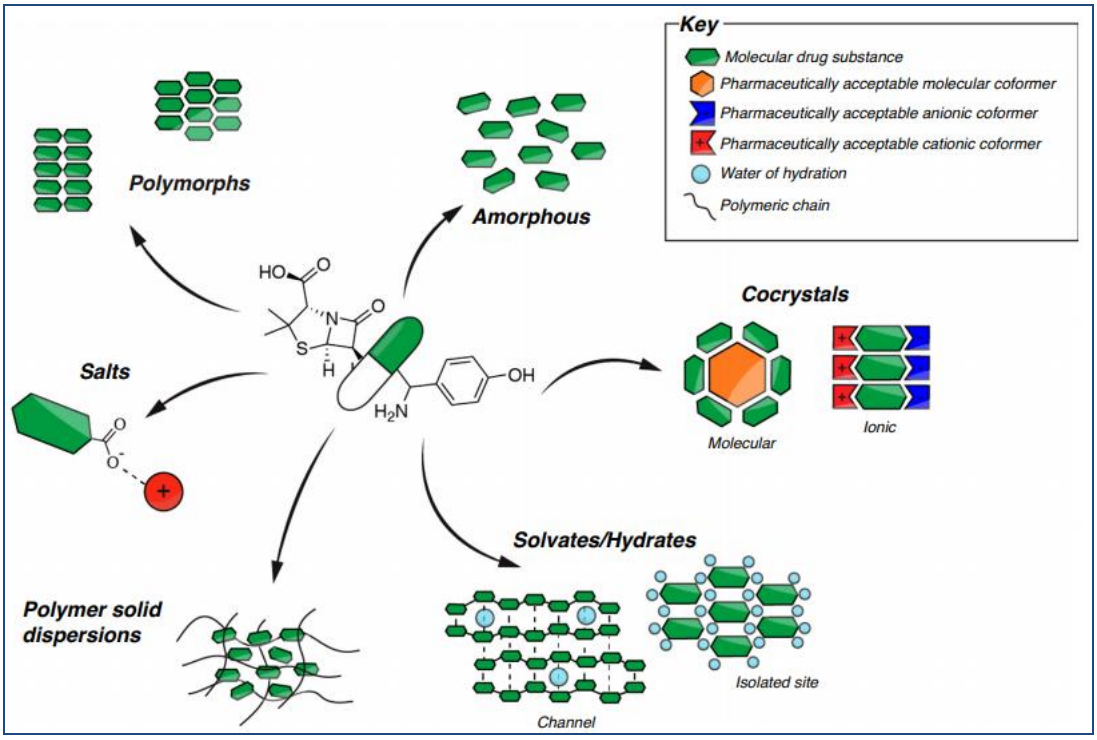

Scheme 1.4 Summary of various approaches to solid form optimisation. i.e; polymorphs, amorphous forms, salts, molecular and ionic cocrystals, hydrates/solvates, and solid dispersion (adapted from ref. 56).

1.7.1 Amorphous Forms

Amorphous solid forms have gained prominence in the pharmaceutical industry with their ability to increase the solubility and dissolution rate of Active Pharmaceutical Ingredients (APIs)[57]. However, unlike crystalline phases, amorphous compounds do not exhibit a regular diffraction pattern. These aperiodic solid forms can be made using a variety of techniques, including melt quenching, spray- and freeze-drying, milling, wet granulation[58], and most recently, manual grinding[59]. Of late, 'Co-amorphous'[60] compounds – amorphization of two or more neutral compounds in stoichiometric ratio have gained popularity because of their ability to improve parent drug solubility[61] (Figure 1.3).

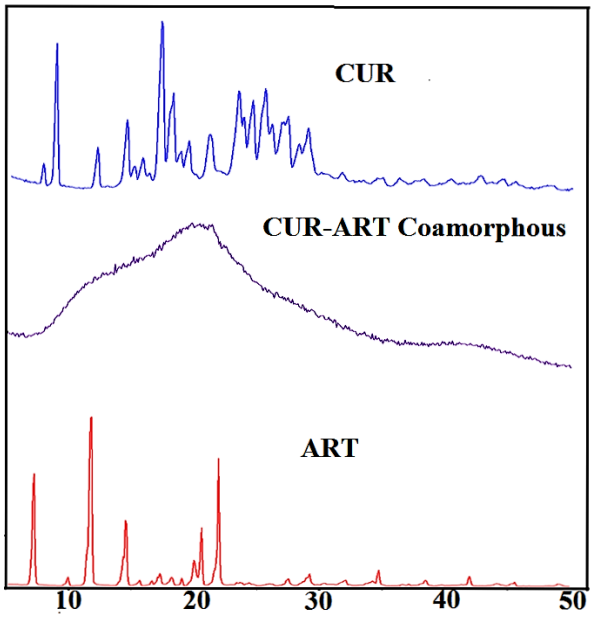

Figure 1.3 Comparison of Powder X-ray diffraction lines of coamorphous CUR-ART (1:1) with starting materials CUR and ART. (adapted from ref. 61)

An amorphous solid is characterized by its glass transition temperature (T_g). It is the temperature at which a glassy material (plastic) is converted to a rubbery phase while retaining some of the properties of the liquid[58]. Amorphous forms, like their crystalline counterparts, are known to exhibit polymorphism.[62-63] For example, polyamorphism in H_2O has been extensively studied[64-65], but the data interpretation is still debated because the diffraction pattern lacks any Bragg lines. On the one hand, the excess thermodynamic

functions of amorphous phases improve the solubility and dissolution rate of poorly soluble APIs. Several drug compounds, such as Itraconazole, Cefuroxime axetil, Lopinavir, Quinapril hydrochloride etc., are marketed either as purely amorphous forms or in combination with other solid forms[66]. But on the other hand, the higher enthalpy and entropy can be disadvantageous because they make the amorphous solid forms highly unstable. To stabilise the amorphous forms, several excipients such as alginic acid, polyvinyl pyrrolidone (PVP), methyl cellulose, polyethylene glycol (PEG) etc.[58] have been developed.

Chen et al.[35] recently discovered the structure of AlB4H11, an amorphous aluminoborane compound, by combining a density functional-based approach with experimental measurements using IR, NMR, and neutron vibrational spectroscopy (NVS). The use of such techniques to analyse the lattice structure of pharmaceutical amorphous solid forms could help with a better understanding of their molecular packing and intermolecular interactions, which could lead to more widespread use of these solid forms for improved drug efficacy.

1.7.2 Polymorphism

Polymorphism[68-70] (Greek: *poly* = many, *morph* = form) is a term used in a variety of disciplines to describe the diversity of nature. According to the Oxford Dictionary, this term was first used in 1656 in reference to the diversity of fashion[68]. In the area of crystallography, it is typically attributed to Mitscherlich[71] (1822, 1823), who recognised different crystal structures of the same compound in a number of arsenate and phosphate salts ($NaH_2AsO_4.H_2O$ and $NaH_2PO_4.H_2O$). In scientific terms, polymorphism is described as the ‘existence of a chemical substance in different crystalline arrangements’, and the different crystal forms are referred to as ‘polymorphs’. Berzelius[72] was the first to develop the term allotropism to describe the occurrence of an element existing in several crystal structures called allotropes. For example, carbon exists as four allotropes: diamond, graphite, fullerenes, and carbon nanotubes[73] (Figure 1.4). Polymorphism, on the other hand, is a term used in material science to describe the occurrence of a compound in different crystal structures. Therefore, in a broad sense, what polymorphs and polymorphism to a compound so are allotropes and allotropism is to an element[68].

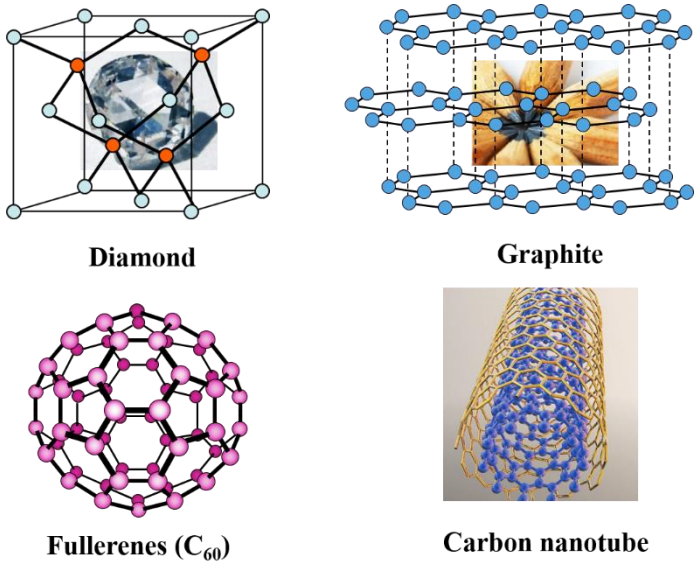

Figure 1.4: Allotropes of carbon showing different structures (adapted from ref. 73).

The importance of the polymorphism in the pharmaceuticals was brought to light by McCrone[69] who proposed the widely accepted definition that "*a solid crystalline phase of a given compound resulting from possibility of at least two different arrangements of the molecules of the compound in a solid state*". Later, Bernstein investigated the stability relationship between polymorphs and their phase transitions.[68,74-77] Friedrich Wöhler and Justus von Liebig discovered polymorphism in organic molecule for the first time in benzamide in 1832.[78] They discovered two polymorphs in a boiling benzamide solution that initially crystallised in silky needles when cooled, but were gradually replaced by rhombic crystals when left to stand. Similar to single components, polymorphism is possible in other classes of crystalline solids such as solvates, hydrates, salts, cocrystals and their solvates and hydrates, resulting in various solid forms as shown in Scheme 1.5. Therefore a single molecular entity can lead to the formation of multiple crystal forms.[79-80] Melting point, compressibility, flowability, stability, solubility, dissolution rate, and bioavailability are all important factors for selecting a suitable polymorph for effective drug administration.[68-70]

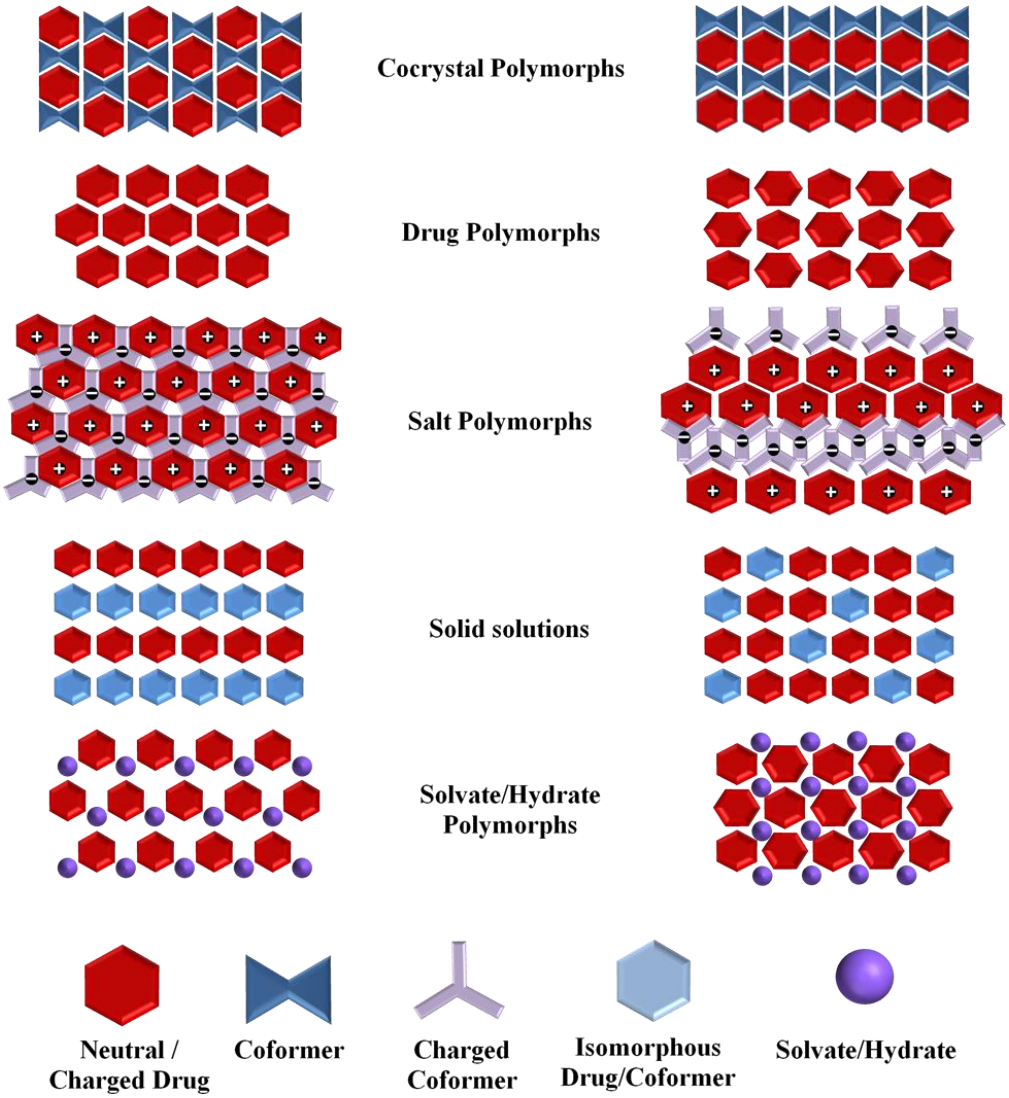

Scheme 1.5: Different kinds of possible polymorphism in single component or multiple component crystal forms of drugs.

1.7.2.1 Classification of polymorphs

Polymorphs (single or multicomponent) are referred to as "forms," "modifications," or "phases" in the literature, and are denoted by numerals (Arabic: 1,2, 3 etc. and Roman: I, II, III etc.) or alphabets (Greek: α, β, γ etc. and English: A, B, C etc.).[68] Polymorphs can be divided into three types based on structural differences.[81-82] i) Packing polymorphism ii)

Conformational polymorphism and iii) Synthon polymorphism (Figure 1.5). Conformational differences in molecular structure result in different crystal structures of the same molecule, which is known as 'conformational polymorphism'. Examples include dimorphs of oligothiophene derivative[83], N-acetyl cysteine (Figure 1.6)[84], and chiral and racemic tetramorphs of t-butyl fuchsone[85]. When the non-covalent interactions or supramolecular synthons of the same molecule differ in different crystal structures, this is referred to as 'synthon polymorphism'.[86-87] For example, carbamazepine molecules propagate through amide dimer in Form IV and amide catemer in form V[86-87] (Figure 1.7). When polymorphs differ in their overall three-dimensional crystal packing, they are referred to as 'packing polymorphs'.[82] In a broader sense, all polymorphs can be categorised under packing polymorphism, since all the polymorphs differ in their packing by default. This classification is subjective, because two or more types of polymorphism can coexist in each polymorphic system. For example, conformational and synthon polymorphism distinguishes the trimorphs of anti-diuretic drug Furosemide[88] (Figure 1.8) and synthon and packing polymorphism coexist in the tetramorphs of anti-tubercular drug Pyrazinamide[89] (Figure 1.9). In addition, Figures 1.10 and 1.11 discussed polymorphism in each cocrystal[90] and salt[91].

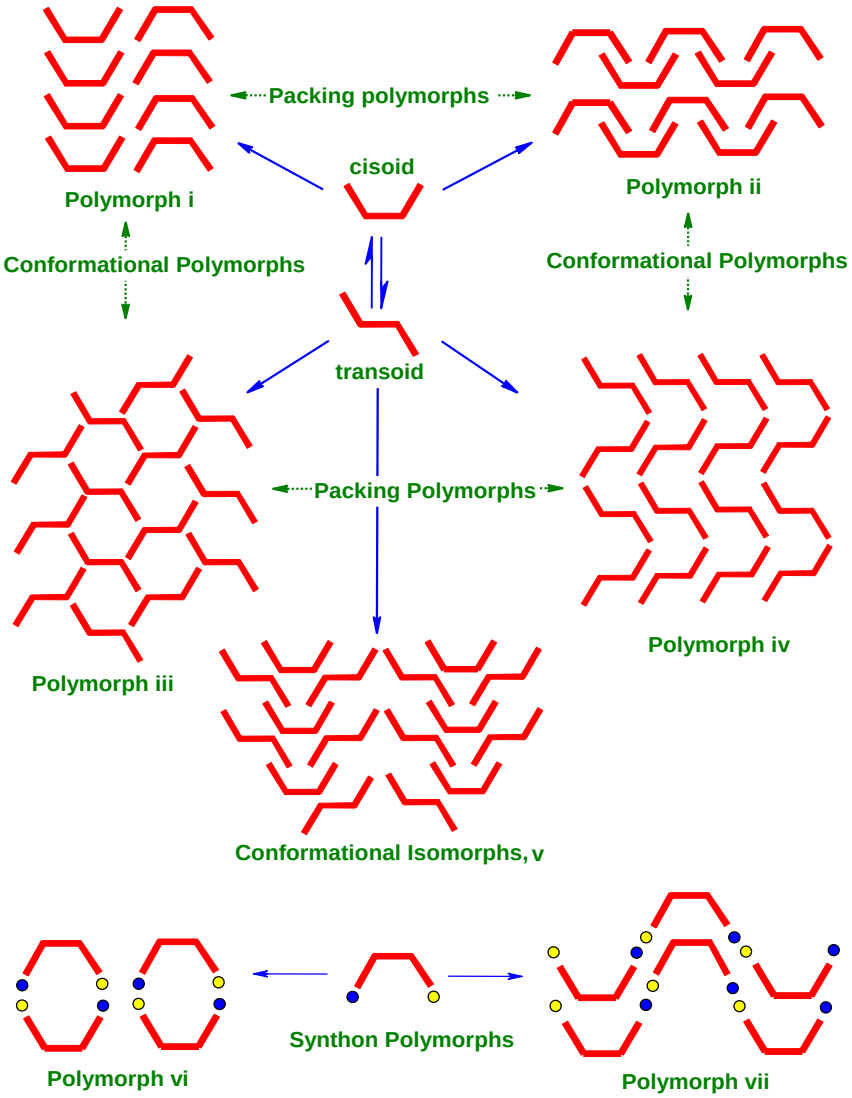

Figure 1.5 Schematic representation of different kinds of polymorphs (adapted from ref. 40a).

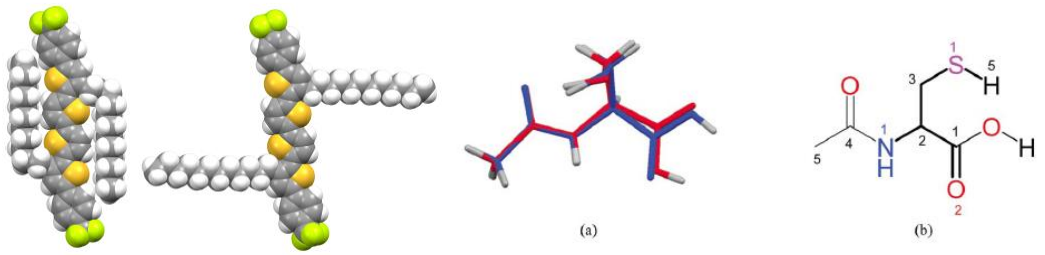

(a) (b)

Figure 1.6 (a) Oligothiophene derivative of conformational polymorphism (Adapted from ref. 83) (b) Overlay of molecular conformations (red form I and blue form II) of N-acetyl cysteine and main conformational difference are highlighted in bold single bonds (Adapted from ref. 84).

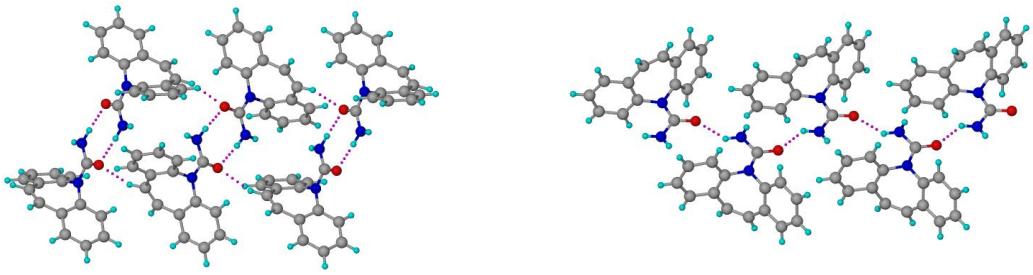

(a) (b)

Figure 1.7 a) Amide dimer in form IV of Carbamazepine, **b)** Amide catemer in Form V of Carbamazepine (adapted from ref. 86-87).

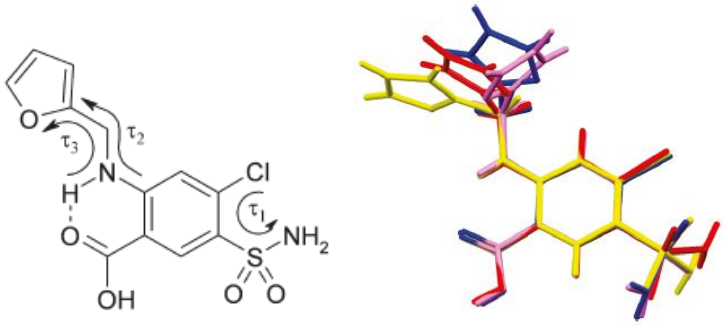

4 conformers in 3 polymorphs

(a)

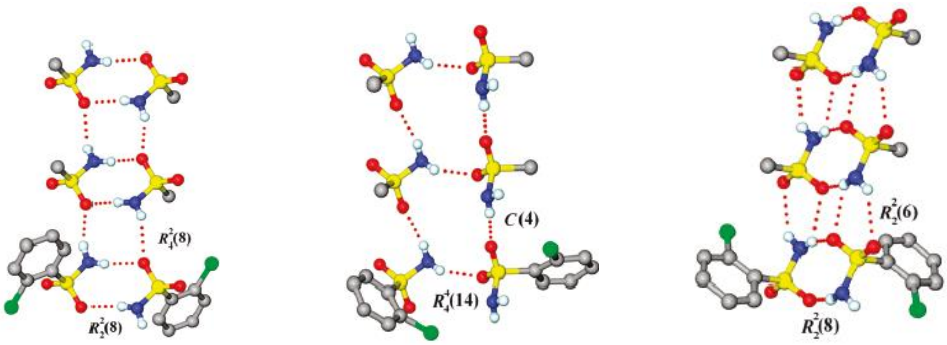

Form 1 **Form 2** **Form 3**

(b)

Figure 1.8 (a) Conformational polymorphism in Furosemide. The three torsion parameters in Furosemide: τ1=C-C-S-N, τ2=C-N-C-C, τ3=N-C-C-O. The anthranilic acid moiety is conformationally locked by intramolecular hydrogen bond but conformational flexibility in the furan and sulfonamide moieties resulted in four conformers (red, blue, pink and yellow) manifested in three polymorphs. (b) Synthon polymorphism in Furosemide. $R_2^2(8)$ N−H···O dimer and $R_4^2(8)$ motif in form 1, $C(4)$ catemer and $R_4^4(14)$ tetramer motif in form 2, $R_2^2(8)$ N−H···O motif and $R_2^2(6)$ rings in skewed dimer of form 3 (Adapted from ref. 88).

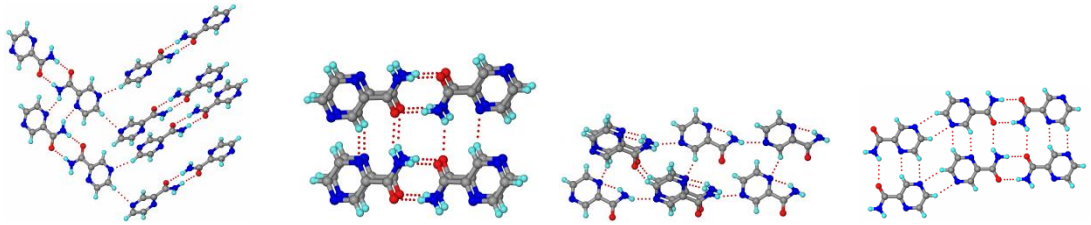

α β γ δ

Figure 1.9 Synthon and packing polymorphism in Pyrazinamide. In α polymorph, zigzag tapes formed by $R^2_2(8)$ N–H···O and $R^2_2(10)$ N–H···N hydrogen bonds are connected orthogonally to 2_1 screw related tapes through C–H···N interactions in a 3D arrangement. The *β* polymorph has non-planar $R^2_2(8)$ N–H···O dimers that make a helix along the *b*-axis through anti N–H···O and C–H···N interactions. In *γ* polymorph, 1D tapes assembled via N–H···N hydrogen bonds of $C(6)$ notation are connected through C–H···O and C–H···N

interactions. In δ polymorph, carboxamide tapes formed by $R^2_2(8)$ dimer and $C(4)$ catemer N–H···O synthons and $R^2_2(6)$ C–H···N synthons make 2D sheets (adapted from Ref. 89).

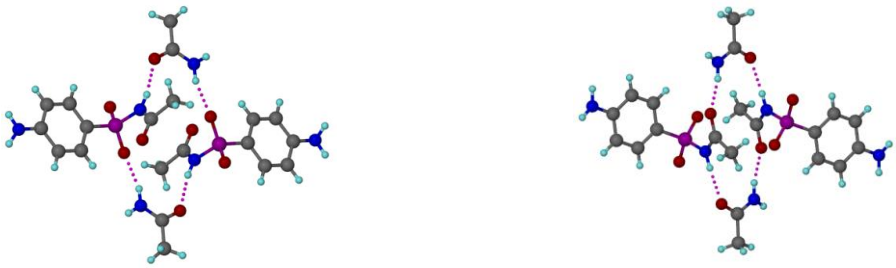

(a) (b)

Figure 1.10 Synthon and packing polymorphism of sulfacetamide-acetamide (SACT-ACT) cocrystal. (a) and (b) are SACT-ACT form I and II. In form I tetrameric ring motif connected through two each of one point N–H···$O_{sulfonamide}$ and N–H···$O_{carbonyl}$ hydrogen bonds and in form II tetrameric ring motif connected through four one point N–H···$O_{carbonyl}$ hydrogen bonds (Adapted from ref. 90)

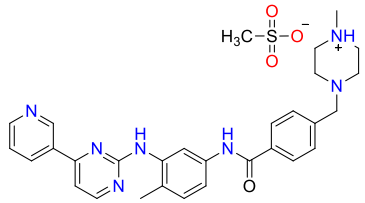

Imatinib mesylate salt

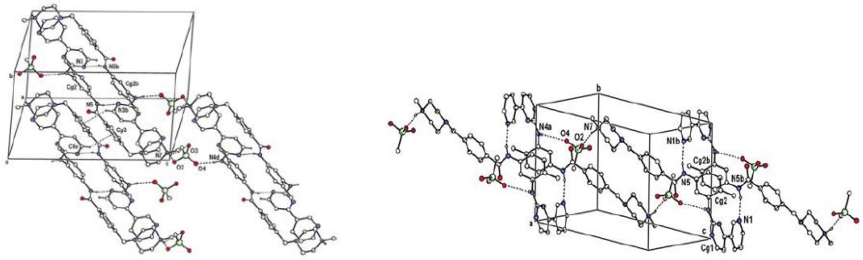

(a) (b)

Figure 1.11 Conformational polymorphism of imatinib mesylate. The conformational changes occurring part in crystal structures highlighted with red circle imatinib mesylate molecular structure and followed by crystal packing diagrams (a) α (b) β polymorphs of imatinib mesylate (Adapted from ref. 91)**.**

1.7.2.2 Generation of polymorphs

Solution crystallization has long been a popular approach for generating polymorphs. Solution crystallization conditions can be systematically changed by altering solvents (or solvent mixtures), temperature, stirring, cooling rate, slurrying, seeding, supersaturation, use of antisolvent etc. Recent approaches for polymorph generation include mechanical grinding[92], epitaxial growth[93], melting[94], sublimation[95], crystallization with structurally related additives[96], crystallization in capillaries[97], laser induced nucleation[98], using supercritical liquids[99] etc. Interestingly, many novel polymorphs of drug molecules and bioactive compounds have been discovered by serendipity during cocrystallization[100], as in the case of curcumin[101], where Form II crystals were discovered during an attempt to cocrystallize with 4-hydroxypyridine.

1.7.2.3 Kinetic Vs. Thermodynamic polymorph

Polymorphism results from the interplay of thermodynamic functions (enthalpy, entropy and free energy) and kinetic factors (supersaturation, temperature, activation energy, rate of evaporation etc.) that govern the crystallization process[68-70]. The role of nucleation governed by the Ostwald's law of stages is vital in predicting the nature of polymorphic outcome of a molecule,[100] which states that *"when leaving an unstable state, a system does not seek out the most stable state, but rather the nearest metastable state which can be reached with least loss of free energy"* (Figure 1.12). As a result, the structure with the lowest energy barrier is the one that crystallises first (highest energy, kinetically metastable). This form will transform in to the next lower energy polymorph until a thermodynamically stable state is reached, the so-called Ostwald's Law of Stages.

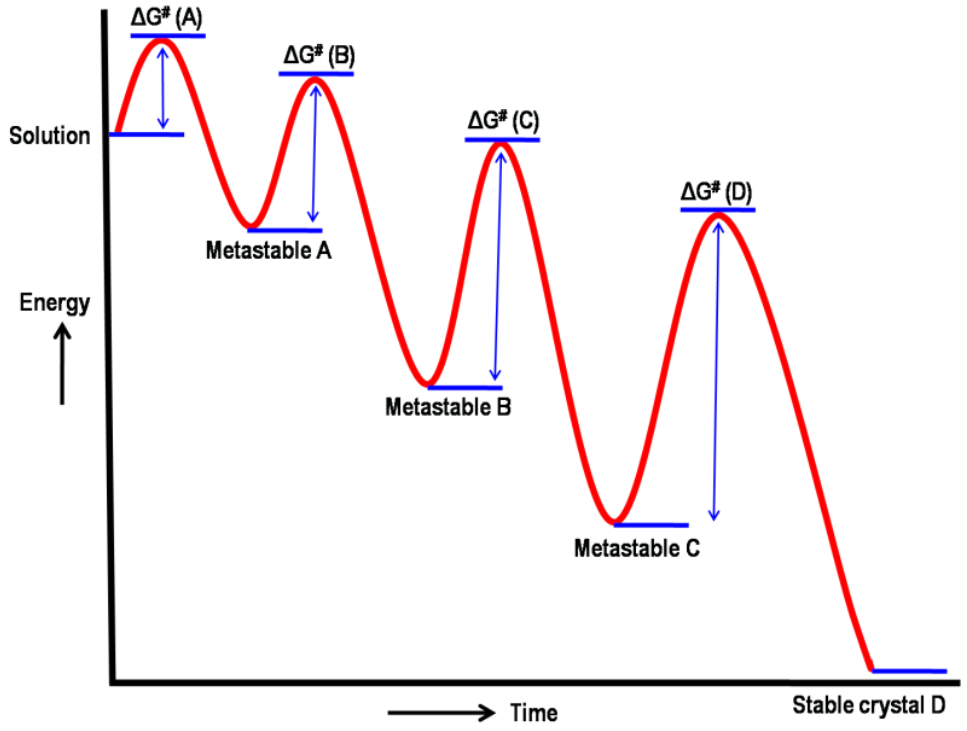

Figure 1.12 Ostwald's Rule of Stages. Initial high-energy state (metastable A) through minimal changes in free energy crystallizes first and is the one which has the lowest energy barrier. Metastable A form will then transform to the next lower energy polymorph (metastable B) and so on (metastable C) until thermodynamically stable crystal D. (Adapted from Ref. 100)

The Curtin-Hammett principle[102-103] states that "*for a pair of reactive intermediates or reactants that interconvert rapidly, each going irreversibly to a different product, the product ratio will depend both on the difference in the energy between the two conformers and the free energy of the transition state going to each product*". This definition also applies to the crystallisation process, where the kinetically favoured crystal forms faster due to lower activation energy requirement, whereas the thermodynamic polymorph forms later due to higher activation energy requirement. Nevertheless, the polymorph obtained at the end is the most stable because its thermodynamic state has the lowest energy. Polymorphism is less likely[103] if the same crystal structure is favoured both kinetically and thermodynamically. Close packing and intermolecular interactions are competing factors

that determine the polymorphic outcome at the molecular level. When close packing dominates intermolecular interactions, thermodynamic polymorph is preferred. Similarly, when the crystal nucleus is stabilised by intermolecular interactions, kinetic polymorph is preferred. On the other hand, the energy difference between polymorphs is typically less than 5 kcal mol^{-1},[71] Therefore, many polymorphs can crystallise at the same time if their nucleation rates are equal. This phenomenon is called '*concomitant polymorphism*'[104-109] in which both stable and metastable polymorphs crystallise in the same flask under identical crystal growth conditions using the same solvent. Concomitant polymorphs are generally 'isoenergitic' or 'near-energetic'.[104-109] For example, polymorphs of benzamide.[78] Tautomeric polymorphism[110-111] is a phenomenon that occurs when the tautomers of a compound rapidly interconvert in solution or melt but crystallize as polymorphs in the solidstate, for example, Omeprazole[110]. Tautomeric polymorphism is synonymous with the term Desmotropy[111].

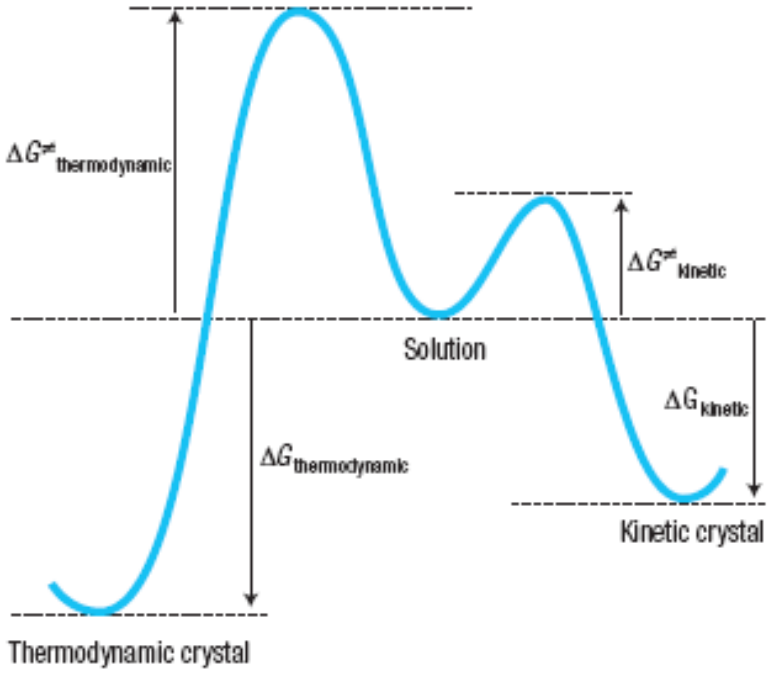

Scheme 1.13 Kinetic and thermodynamic outcome of crystallization reaction. This scheme is culled from Ref. 103.

Polymorphic pairs can be divided into monotropic and enantiotropic systems based on thermodynamic considerations.[112,89,68] Monotropic systems are those in which a single form is more stable regardless of temperature. Enantiotropic systems are those in which the relative stabilities of the two forms invert at a certain transition temperature. In other words, two forms are said to be enantiotropically related if their free energy curves cross below the melting point of the lower melting polymorph in the energy-temperature (E-T) diagram and they are said to be monotropically related[68] if the free energy curves do not cross below the lower melting polymorph.

1.7.2.4 Polymorphism in pharmaceutical industry

Polymorphism has gained a lot of attention in recent literature because of its importance in drug substances and pharmaceutical formulation[113]. Solubility and dissolution rate are key physicochemical properties that have a direct effect on a drug's physiological efficacy. Dissolution rate, in particular, is frequently the rate determining step that has a direct impact on drug bioavailability[68-70]. There are various examples of polymorphs whose bioavailability varies greatly. For example, 6-mercaptopurine[114] (6-MP) is an immunosuppressive drug. The plasma concentrations of form I and form III of 6-MP following intravenous injection of 50mg/kg to rabbits revealed that form III has a 1.5-fold better extended bioavailability than form I.

Polymorphs are patentable due to their different structures and properties.[115] If a generic pharmaceutical company discovers a novel crystal form of an already marketed drug, it will gain early access to the market; as a result, innovator companies must discover and patent all possible polymorphs of the drug in order to maintain their monopoly in the pharmaceutical industry and protect their product. Polymorphs of the anti-ulcer drug Ranitidine hydrochloride are a well-known example.[68-70] GlaxoSmithKline pharmaceutical company obtained a patent on the two polymorphs (I followed by II) of Ranitidine hydrochloride. Other pharmaceutical companies began preparing to offer cheaper, generic versions of form I in the mid-1990s, as the drug's patent (form I) was approaching expiration. However, generic manufacturers were unable to crystallise form I alone since it always crystallised as a mixture of forms I and II. This kept the generic companies' products off the market for several years, and GlaxoSmithKline pharmaceutical company was making

$10 million sales per day on this blockbuster drug during that period. Novopharm ultimately found a way to make form I exclusively with undetectable levels of form II, and won the struggle. Since then, generics have been introduced to the market. Similiarly, polymorphs of Ritonavir (Figure 1.14) from Abbott Laboratories removed from market after two years due to polymorphic conversion to the new form II.[116] This transformation was caused by a carbamate impurity, which is a hydrolytic product of Ritonavir. The form II with syn-confirmation is four times less soluble than the metastable form I with anti-conformation at the amide bond.[117] Other well-known patent disputes involving polymorphism include Cefadroxil, Terazosin hydrochloride, and Aspartame.[68-70]

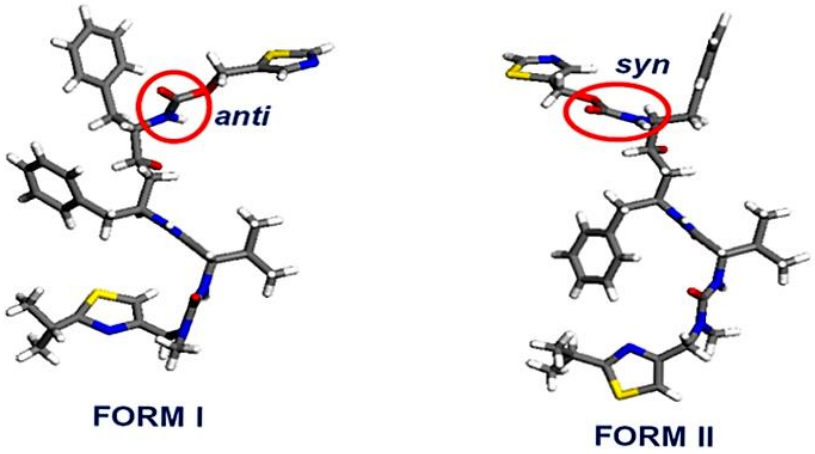

Figure 1.14 The *anti* and *syn* amide conformers of Ritonavir form I and II (Adapted from Ref. 117).

1.7.3. Solvates and Hydrates - Pseudopolymorphism

Pseudopolymorphism[115] is defined as a phenomenon in which a "*compound is obtained in crystalline forms that differ in the nature or stoichiometry of the included solvent molecules*" and the ensuing solid forms are known as pseudopolymorphs. Pseudopolymorphs are synonymous with terms such as hydrate, solvate, and solvatomorphs. A molecular solid can generate solvates with different stoichiometries of the same solvent[118-120]. For example, mono and 2/3 hydrate of the ergot alkaloid, Tergurid[118]. It can also produce a sequence of solvates with different solvent molecules, such as Sulfathiazole, which forms over a hundred

solvates with different solvents.[119] Moreover, polymorphs of a solvated structure can occur, such as α and β forms of Indantrione 1,2-dioxime[120] (IND) methanol solvate (Figure 1.15).

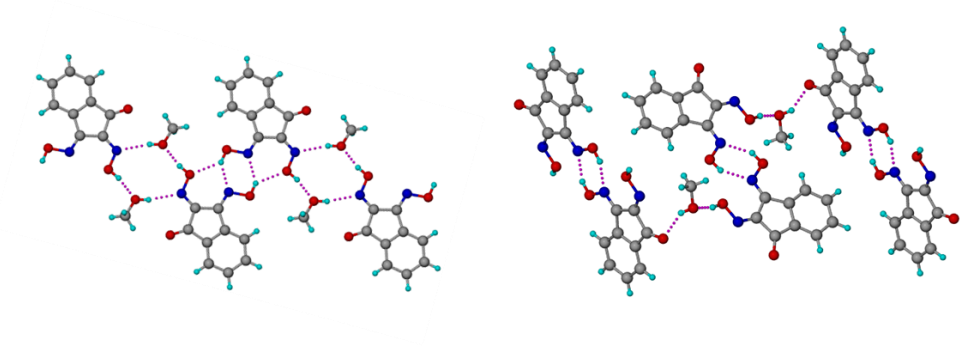

IND-MeOH solvate α form IND-MeOH solvate β form

Figure 1.15 In α form guest molecules bridge the dimeric units of IND through O–H···N and O–H···O hydrogen bonds resulting in the centrosymmetric cyclic assembly. In β form dimeric units of IND are linked by a single MeOH molecule extending the assembly through O–H···O hydrogen bonds (adapted from ref. 120).

The pharmaceutical properties of a drug, such as stability under various conditions, shelf life, and so on, will determine whether the solvated or unsolvated form of a drug suitable is formulation. Various drug molecules are presently sold as solvates/hydrates, such as Indinavir sulfate[121] is marketed as an ethanol solvate and Paroxetine hydrochloride[122] is marketed as a hemihydrate. Based on the effect of the solvent on the crystal lattice, solvated structures can be divided into two types: 1) Because these solvents have few interactions with the parent molecule in the crystal lattice, desolvation has no affect on the overall crystal structure, such as cephalosporine solvates[123]. 2) Solvent molecules are bound to the parent molecules in these crystal structures by strong intermolecular interactions. Therefore, their desolvation may result in new polymorphs of the guest free form. For example, Spironolactone[124] form I and II were prepared by altering the desolvation rates of its ethanol solvate. In essence, solvate/hydrate formation can have diverse applications in the pharmaceutical industry.

1.7.4 Pharmaceutical Salts

Salt formation is the most common and effective approach for enhancing the physicochemical properties of drug molecules[113,125-127]. The 'rule of three'[128-130] is a useful tool for predicting the formation of salts between organic acids and bases. According to Nangia and coworkers[128], who evaluated this hypothesis by forming salts and cocrystals between several acid and pyridine containing molecules, they concluded that the carboxylic acid–pyridine O–H···N interaction will be neutral when $\Delta pK_a < 0$ and it will have an intermediate H bond character, O–H···N and/or N^+–H···O^-, when the transition range $0 < \Delta pK_a < 3.75$. When pKa > 3.75, the interaction will be ionic N^+–H···O^-. Childs and Stahly[129] made similar findings in their study of 20 complexes of theophylline with COOH partners. The Orange Book database[130] contains information on various drugs approved by the US Food and Drug Administration, as well as the frequency of counterions utilised in salt formation over time. As a result, the orange page is a good source of information on counterions based on their usage.

Salt formation represents the traditional methodology for solid form development with diverse applications in pharmaceutical industry[131-135]. Salt formation provides enhanced solubility and thermal stability to drug molecules. For example, the antiulcer drug Ranitidine's poor solubility and low melting point were addressed by forming a hydrochloride salt of the drug, which had a much higher solubility (1g/mL) and an increased melting point (136°C). The wide range of counterions available gives plenty of options for creating the best solid formulation for maximum therapeutic efficacy[125-127]. Salts have been successfully applied as additives to discover metastable polymorphs of drug molecules. For example, Byrn and coworkers[136-139] reported the generation of metastable form V of Flufenamic Acid (FA) by dissolving FA in ammonium chloride (NH_4Cl) solution. This novel polymorph was obtained by a slow evaporation method with FA and NH_4Cl at a 1:2 stoichiometric ratio. Similarly several reports highlight the importance of ionic liquids (salt in liquid form) as media for discovering novel polymorphs[137-139]. For instance, An et. al.[137] reported a novel polymorph of Adefovir dipivoxil (AD) crystallized from 1-ally-3-ethylimidazolium tetrafluoroborate ($AEImBF_4$) ionic liquid. Apart from these notable

applications, salt formation is primarily used in the pharmaceutical industry for solubility modulation of drug molecules. The widespread use of salt formation for solubility enhancement of drug molecules is evidenced by about 50% of drug molecules marketed as salts. It is the most preferred approach for aqueous solubility enhancement of a liquid formulation for parenteral administration[140]. Numerous literature reports highlight this ability of salts through various criteria, comprising solubility and stoichiometry of the counter ion, polymorphism etc. Galcera et. al.[141] noted the effect of counter ion on the solubility of isostructural pharmaceutical salts of anticonvulsant drug Lamotrigine. They showed that the solubility of the salts varied linearly with the solubility of corresponding counterions. Puigjaner and coworkers[142] documented the importance of screening for polymorphs of pharmaceutical salts and their effect on the solubility of the parent molecule. They have reported three polymorphs of Ziprasidone maleate and showed that "form C" exhibited the highest solubility ever reported for Ziprasidone salts. Zaworotko and coworkers[143] went a step further in studying the pharmacokinetic behavior of salts apart from their solubility. They have obtained various solid forms of anticonvulsant drug Lamotrigine (LT). LT-saccharinate salt was shown to exhibit the highest solubility and the highest initial serum concentration (Figure 1.16). Numerous other reports highlight this solubility modulating ability of salts[144-146] for solid form development and better therapeutic efficacy. On the downside salts tend to be more hygroscopic and restricted to drugs with ionizable functional groups. The hygroscopic nature can cause loss of potency of drug, for example, the hygroscopicity of the anti-tuberculosis drug Ethambutol dihydrochloride salt has been reported to cause instability of the fixed dose combination of anti-TB drug (FDC, Pyrazinamide, Isoniazid, Rifampicin, and Ethambutol hydrochloride hydrate), resulting in less therapeutic efficacy and activity and thus becoming useless for treatment.[147-148] Furthermore, salts cannot be generated for APIs that are neutral or weakly ionizable. These issues warrant the need for other techniques for pharmaceutical solid form development. Of late, techniques like pharmaceutical cocrystals, polymorphs, solid dispersions, nanoparticles, inclusion complexes etc. seem to be very promising in addressing the poor physicochemical properties of drug molecules.

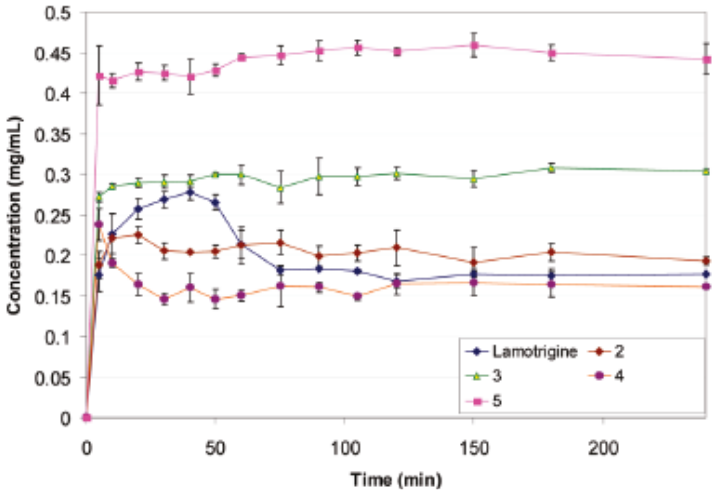

(a)

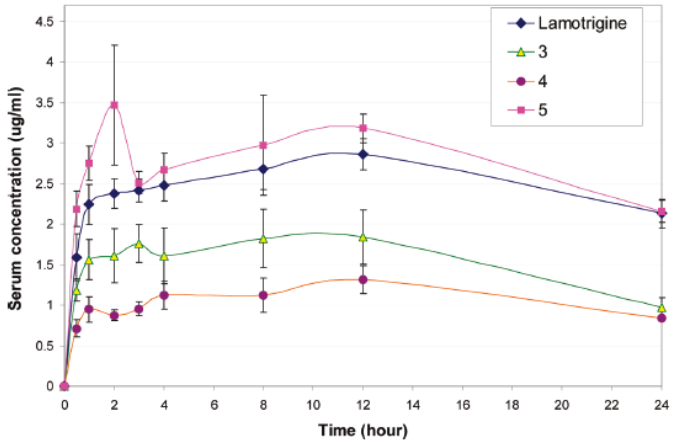

(b)

Figure 1.16 a) Aqueous Dissolution profiles for LT and crystal forms 2-5. **b)** Rat serum concentrations of LT, **3, 4,** and **5.** (Adapted from ref.143).

1.7.5 Pharmaceutical Cocrystals

Crystal engineering principles[9-11,13] and hydrogen bonding rules are the key design factors for cocrystal formation. A cocrystal[127] may be defined as "a stoichiometric multi-component system where the individual components are held together by heteromeric interactions like hydrogen bonds and are solids at room temperature". Although Krantz et al.[149] discovered

that a stoichiometric (1:1) cocrystal containing the sodium salt of theophylline and glycine increased the API's water solubility in 1946, it was not until about the year 2000 that its significance has been fully recognised in the current context and has been popularised as 'Pharmaceutical cocrystals'[150-155]. A pharmaceutical cocrystal is basically a cocrystal in which at least one of the molecular components is an API, while the other type of molecule is referred to as a cocrystal former. To be beneficial, the non-API component must be non-toxic and have no negative side effects. The co-crystal former should ideally be listed on the US FDA's "Everything Added to Food in the United States" (EAFUS) list, which includes over 3000 compounds that can be used as food additives, or designated as Generally Recognized as Safe (GRAS)[26]. Pharmaceutical cocrystals have sparked interest because, as crystal forms distinct from the pure API, they vastly enhance the spectrum of solid forms available for formulation. Cocrystals differ in physicochemical properties such as solubility, stability, compressibility, friability, melting point, hygroscopy, dissolution rate, habit, and bulk density. Cocrystals can be synthesized in a variety of ways, where the components are mixed together and subjected to solution crystallization, co-sublimation, co-melting, solid state grinding, solvent-drop grinding, slurry crystallization, reaction crystallization, spray drying, and so on[150-155]. Recently novel techniques such as inkjet printing[153] and crystallisation at the solvent-solvent interface[154] were used to form cocrystals. Conformers play a crucial role in influencing a cocrystal's physicochemical properties, which in turn affects the parent drug. With few exceptions, a high melting coformer invariably creates a high melting cocrystal, and a high soluble coformer confers greater solubility to a cocrystal[155].

In 2011, Nangia et al.[157] suggested a concept based on the 'spring and parachute' model of amorphous forms[158-159] to explain the effect of coformer in enhancing the solubility of cocrystals. According to the concept, a cocrystal containing a high solubility coformer can enable a low soluble component dissolve faster. This occurs when a high soluble coformer is rapidly released into an aqueous medium, causing the cocrystal to dissociate, leaving the low soluble component in an amorphous/randomized state. This, in turn, leads to an increase in the system's free energy, which, in turn, leads to an improvement in the low soluble component's solubility/dissolution (Figure 1.17). This model shows that a high-solubility coformer will produce a high-solubility cocrystal, and *vice-versa*. If a coformer has poor

water solubility, it does not easily dissociate from the lattice and hence can control the drug's solubility/dissolution of the drug, such as cocrystals of anti-lung cancer agent Hexamethylenebisacetamide[151] with sebacic acid and dodecanedioic acid. In some cases, cocrystal packing also regulates solubility independently of coformer solubility. For example, cocrystal packing and non-covalent interactions in sulfacetamide-caffeine cocrystal are stronger than sulfacetamide guest free form.[160] Thus, the cocrystal decreases the solubility of the sulfacetamide.

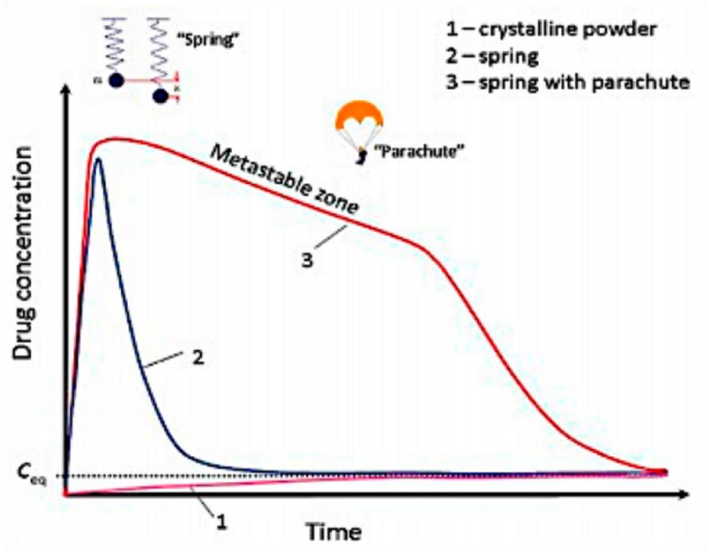

(a)

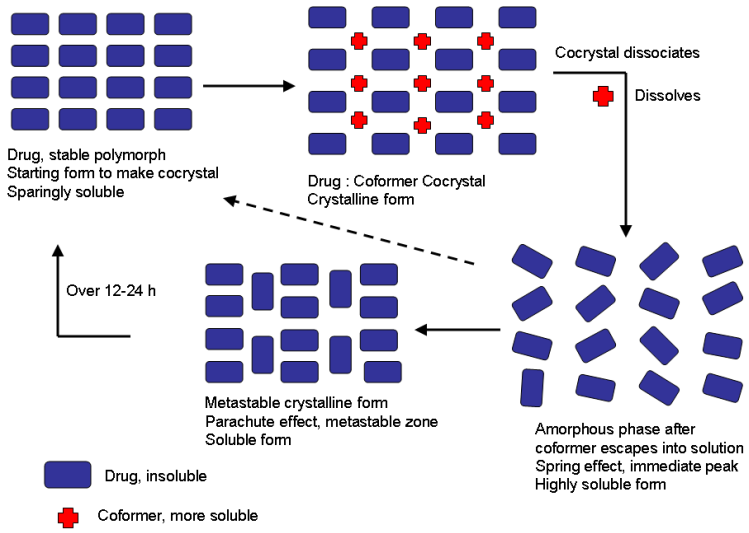

(b)

Figure 1.17 (a) The spring and parachute concept to achieve high apparent solubility for insoluble drugs (adapted from ref. 161). (1) The crystalline (stable) form has low solubility. (2) A short-lived metastable species (i.e., amorphous phase) shows peak solubility but quickly drops (within minutes to an hour) to the low solubility of the crystalline form. (3) Highly soluble drug forms manage to remain for a long enough time (usually hours) in the metastable zone. (b) Possible mechanisms of pharmaceutical cocrystals in dissolution medium (adapted from ref. 157).

Salts have traditionally been employed to increase the solubility of drug molecules, however cocrystals can alter the solubility of an API in either direction (increase or decrease). Numerous literature reports highlight the solubility enhancing ability of cocrystals. For example, Itraconazole-maleic acid[162] cocrystal has around 20 times higher solubility compared to the parent API which is comparable to that of the marketed amorphous form. In 1973, Higuchi[163] reported that the 1:1 and 1:2 complexes of caffeine with gentisic acid might limit caffeine dissolution rate, highlighting the solubility-lowering potential of cocrystals, which could be important in developing slow-release dosage forms. Polymorphism in cocrystals[154], as well as cocrystallization between organic compounds and an inorganic salt, commonly known as 'Ionic Cocrystals[164]', have recently gained popularity, not only for diversifying the structural landscape of an API, but also for conferring a solubility/dissolution benefit . Apart from solubility modulation, cocrystals have been used for a variety of other applications, as mentioned below[165-171] (Figure 1.18). Because of these properties, the US Food and Drug Administration (US-FDA) published 'Regulatory Classification of Pharmaceutical Cocrystals,' and the European Medicines Agency (EMA) recently published a reflection paper on the use of cocrystals that considers pharmaceutical cocrystals for edited applications. If the safety and efficacy of cocrystals are proven, they are designated as 'new active compounds' from the perspective of looking at them as intellectual property.[172-174] To our knowledge, till date, APIs of, Beta-Chlor (Chloral-betaine), Depakote (Sodium Valproate-Valproic acid), Cafcit (Caffeine-Citric acid), Lexapro (Escitalopram Oxalate), Odomzo (Sonidegib diphosphate), Suglat (Ipragliflozin L-proline), Steglatro

(Ertugliflozin L-pyroglutamic acid), and Entresto (Monosodium Sacubitril and Disodium Valsartan) cocrystal forms are in the market[56]. Entresto is the first multidrug cocrystal approved following the cocrystal gunidance by US-FDA.

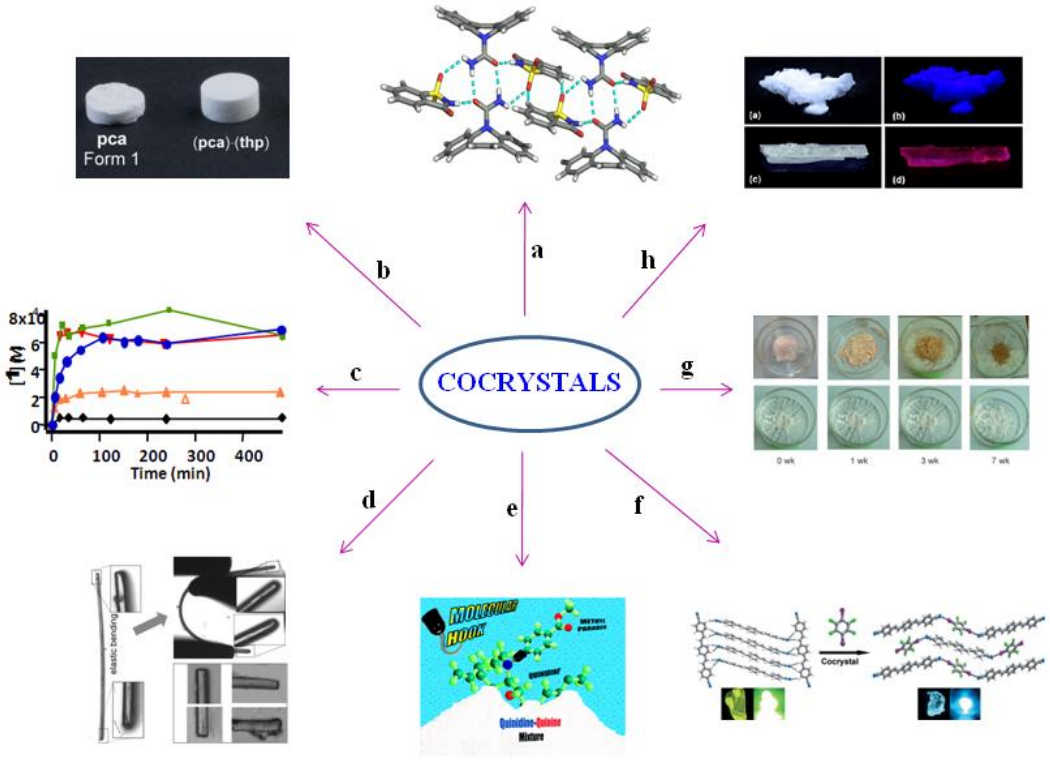

Figure 1.18 Some of the diverse applications of cocrystals **a)** unlike the parent drug carbamazepine, its cocrystal with saccharin was stable to hydration in a 24hrs slurry experiment, (ref. 166) **b)** Tabletability of paracetamol was improved by forming cocrystal with theophylline, (ref. 169) **c)** Cocrystal of itraconazole with maleic acid showed 20 times more solubility compared to parent drug. (ref.162) **d)** Highly flexible and elastically bendable cocrystal was formed on cocrystallizing caffeine with 4-chloro-3-nitrobenzoic acid (ref. 167) **e)** Methyl paraben acted as 'molecular hook by selectively forming cocrystal with quinidine from a mixture of quinidine-quinine stereoisomers. (ref. 168) **f)** Cocrystal strategy tuned the luminescent properties of stilbene type organic molecules (ref. 169) **g)** unlike temozolomide, its cocrystal with succinic acid showed good physical stability. (ref. 165) **h)** Cocrystallization turned on the phosphorescence of phenanthrene (ref. 170).

1.8 Conclusions

In this chapter we have briefly discussed the origin and evolution of crystal engineering as a primary design element in developing pharmaceutical solid forms. We have highlighted the importance of isotropic and anisotropic interactions in the synthesis of complex supramolecular architectures through various sections on intermolecular interactions and supramolecular synthons. This understanding is essential in the context of 'pharmaceutical solid form development', as it will allow the design of several solid forms with varying strengths of intermolecular interactions, such as polymorphs, cocrystals, salts, amorphous forms, and solid solutions/eutectics, for improved therapeutic effect.

An API can produce different types of crystal forms through solid form screening. In various sections of this chapter, a review of these solid forms was provided to highlight the inherent differences in structural aspects between these crystalline forms. Because of their uniqueness, these solid forms would have a wide range of physicochemical properties, which are essential for desirable solid form selection and development. As there is no single solution to the problems that arise from the physicochemical behaviour of various drug molecules, it is important to screen for all possible solid forms (polymorphs, cocrystals, salts, amorphous forms, hydrates/solvates, eutectics etc.), which would provide specific and desirable applications in various systems due to their unique physicochemical properties. In the subsequent chapters, chapter 2 discusses the novel cocrystals and cocrystal polymorphs of anti-TB drug Isoniazid and their stability studies, chapter 3 describes the stability enhancement of four-drug fixed dose combination of Rifampicin, Isoniazid, Ethambutol dihydrochloride and Pyrazinamide, chapter 4 investigates five color polymorphs and an amorphous phase along with configuration isomerism of aldose reductase inhibitor Epalrestat, chapter 4 describes the novel salt polymorphs form I and form II, salt-cocrystal hybrid and salt hydrate forms of Epalrestat with cytosine, chapter 7 explores the improved photostability of Epalrestat by making its cocrystals. In essence, this thesis is mainly focused on the use of crystal engineering principles in the design and discovery of various solid forms of drug molecules, as well as their application in addressing their poor physicochemical properties.

1.9 References

1. Wöhler, F. *Annalen der Physik und Chemie*, **1828**, **88**, 253-256.
2. Lehn, J. M. *Pure Appl. Chem.*, **1978**, *50*, 871-892.
3. Lehn, J. M. *Supramolecular Chemistry: Concepts and Perspectives*, VCH: Weinheim, **1995.**
4. Fischer, E. *Chem. Ber.*, **1894**, *27*, 2985-2993.
5. Palin, D. E.; Powell, H. M. *J. Chem. Soc.*, **1948**, 571-574.
6. Lehn, J. M. *Proc. Nat. Acad. Sci.*, **2002**, *99*, 4763-4768.
7. Lehn, J. M. *Angew. Chem. Int. Ed. Engl.*, **1988**, *27*, 1009-1020.
8. Lehn, J. M. *Angew. Chem. Int. Ed. Engl.*, **1990**, *29*, 1304-1319.
9. Desiraju, G. R. *Crystal Engineering: The Design of Organic Solids*, Elsevier, Amsterdam, **1989**.
10. Desiraju, G. R. *J. Chem. Sci*., **2010**, *122*, 667-675.
11. Desiraju, G. R.; Vittal, J. J.; Ramanan, A. *Crystal Engineering. A Textbook*, World Scientific Publishing, Singapore, **2011**.
12. Pepinsky, R. *Phys. Rev.*, **1955**, *100*, 52.
13. Tiekink, E. R. T.; Vittal J. J.; Zaworotko, M. J. *Organic Crystal Engineering: Frontiers in Crystal Engineering*, John Wiley & Sons, Ltd., West Sussex, **2010**.
14. Graetz, J. *Chem. Soc. Rev.*, **2009**, *38*, 73-82.
15. Bragg, W. H. *Proc. Phys. Soc. London*, **1921**, *34*, 1874-1925.
16. Robertson, J. M.; White, J. G. *J. Chem. Soc*. **1945**, 607.
17. Robertson, J. M. *Proc. R. Soc. London*, **1951**, ***A207***, 101-110.
18. Bernal, J. D.; Crowfoot, D. *J. Chem. Soc.* **1935**, 93.
19. Cohen, M. D.; Schmidt, G. M. J. *J. Chem. Soc*. **1964**, 1996
20. Schmidt, G. M. J. *J. Pure Appl. Chem*. **1971**, *27*, 647-678.
21. Biradha, K.; Santra, R. *Chemical Society Reviews*. **2013**, *42*, 950-67.
22. Dunitz, J. D. *Pure Appl. Chem*. **1991**, *63*, 177-185.
23. Kitaigorodskii, A. I. *Molecular crystals and molecules*, Academic Press, New York, **1973.**

24. Pertsin, A. J.; Kitaigorodskii, A. I. *The Atom-Atom Potential Method*, Springer-Verlag, **1987.**
25. Steiner, T. *Angew. Chem. Int. Ed.*, **2002**, *41*, 48-76.
26. Desiraju, G. R. *Acc. Chem. Res.*, **1991**, *24*, 290-296.
27. Jeffrey G. A.; Saenger, W. *Hydrogen Bonding in Biological Structures*, Springer-Verlag, Berlin, **1991**.
28. Werner, A. *Leibig's Annalen der Chemie*, **1902**, *322*, 261-97.
29. Hantzsch, A. *Chemische Berichte*, **1910**, *43*, 3049-76.
30. Latimer, W. M.; Rodebush, W. H. *J. Am. Chem. Soc.* **1920**, *42*, 1419-1433.
31. Pauling, L. *The Nature of the Chemical Bond,* Cornell University Press, **1939.**
32. Pauling, L. *The Nature of the Chemical Bond and the Structure of Molecules and Crystals: An Introduction to Modern Structural Chemistry,* Third edition, Ithaca, NY, Cornell University Press, **1960**.
33. Pimentel, G. C.; McClellan, A. L. *The Hydrogen Bond*. W. H. Freeman and Co., San Francisco, **1960**.
34. Steiner, T.; Saenger, W. *J. Am. Chem.Soc.* **1993**,*115*, 4540-4547.
35. Desiraju, G. R.; Steiner, T. *The Weak Hydrogen Bond in Structural Chemistry and Biology*, **1999**.
36. Arunan, E.; Desiraju, G. R.; Klein, R. A.; Sadlej, J.; Scheiner, S.; Alkorta, I.; Clary, D. C.; Crabtree, R. H.; Dannenberg, J. J.; Hobza, P.; Kjaergaard, H. G.; Legon, A. C.; Mennucci, B.; Nesbitt, D. J. *Definition of the Hydrogen Bond (IUPAC Recommendations 2011). Pure and Applied Chemistry,* **2011**, *83*.
37. Aakeröy, C. B.; Sinha, A. S. *Co-crystals: preparation, characterization and applications, Royal Society of Chemistry*, **2018.**
38. Corey, E. J. *Pure Appl. Chem*. **1967**, *14*, 19-38.
39. Corey, E. J. *Chem. Soc. Rev.*, **1988**, *17*, 111-133.
40. Seebach, D. *Angew Chem Int. Ed. Engl.*, **1990**, *29*, 1320-1367.
41. Smit, W.A.; Buchkov, A. F.; Cople, R. Organic Synthesis, the science behind the art. Royal Society of Chemistry. **1998.**
42. Desiraju, G. R. *Angew. Chem. Int. Ed. Engl.* **1995**, *34*, 2311-2327.

43. Aakeröy, C. B.; Beatty A. M.; Helfrich, B. A. *J. Am. Chem. Soc.* **2002**, 124, 14425-14432.
44. Walsh, R. D. B.; Bradner, M. W.; Fleishman, S.; Morales, L. A.; Moulton, B.; Rodríguez-Hornedo, N.; Zaworotko, M. J. *Chem Commun*, **2003**, 186.
45. Bhogala, B. R.; Basavoju S.; Nangia, A. *Cryst. Growth Des*., **2005**, *5*, 1683-1686.
46. Bis, J. A.; Zaworotko, M. J. *Cryst. Growth Des.*, **2005**, *5*, 1169.
47. Reddy, L. S.; Babu N. J.; Nangia, A. *Chem Commun*, **2006,** 1369.
48. Reddy, L. S.; Bhatt, P. M.; Banerjee, R.; Nangia A.; Kruger, G. J. *Chem. Asian J.* **2007**, *2*, 505-513.
49. Reddy, L. S.; Bhatt, P. M.; Banerjee, R.; Nangia, A.; Kruger, G. J. *Chem. Asian J.* **2007**, *2*, 505-513.
50. Goud, N. R.; Babu, N. J.; Nangia, A. *Cryst. Growth Des.*, **2011**, *11*, 1930-1939.
51. Vangala, V. R.; Mondal, R.; Broder, C. K.; Howard,,J. A. K.; Desiraju, G. R. *Cryst. Growth Des.*, **2005**, *5*, 99-104.
52. Etter, M. C. *J. Am. Chem. Soc*., **1982**, *104*, 1095-1096.
53. Etter, M. C. *Acc. Chem. Res*., **1990**, *23*, 120.
54. Etter, M. C. *J. Phys. Chem*., **1991**, *95*, 4601-4610.
55. Thayer, A. M. *Chem Eng News*, **2010**, *88*, 13-18.
56. Kavanagh, O. N.; Croker, D. M.; Walker, G. M.; Zaworotko, M. J. *Drug Discovery Today*, **2019,** *24*, 796-804.
57. Hilden, L. R.; Morris, K. R. *J. Pharm. Sci*., **2004**, *93*, 3-12.
58. Yu, L. *Adv. Drug Deliv. Rev*., **2001**, *48*, 27-42.
59. Thakuria, R.; Nangia, A. *CrystEngComm*, **2011**, *13*, 1759-1764.
60. Bahl, D.; Bogner, R. H. *Pharm. Res*., **2006**, *23*, 2317-2325.
61. Suresh, K.; Mannava, M. C.; Nangia, A. *Rsc Advances*, **2014**, *4*, 58357-58361.
62. Poole, P. H.; Grande, T.; Angell, C. A.; McMillan, P. F. *Science*, **1997**, *275*, 322-323.
63. Kieffer, J. *J. Phys. Chem., B* **1999**, *103*, 4153-4158.
64. Mishima, D.; Calvert L. E.; Whalley, E. *Nature*, **1984,** *310*, 393-395.
65. Johari, J. P.; Hallbrucker, A.; Mayer, E. *Nature*, **1987**, *330*, 552-553.
66. Bhatt, P. M.; Desiraju, G. R. *Chem. Commun*, **2007**, 2057-2059.

67. Chen, X.; Zhang, Y.; Wang, Y.; Zhou, W.; Knight, D. A.; Yisgedu, T. B.; Huang, Z.; Lingam, H. K.; Billet, B.; Udovic, T. J.; Brown, G. M.; Shore, S. G.; Wolverton, C.; Zhao, J. C. *Chem. Sci.,* **2012,** *3*, 3183-3191.
68. Bernstein, J. *Polymorphism in Molecular Crystals*; Clarendon, Oxford, U. K., **2002**.
69. Haleblian, J.; McCrone, W. *J. Pharm. Sci*., **1969**, *58*, 911-929.
70. Brittain, H. G. *Polymorphism in Pharmaceutical Solids*, Informa Health Care, New York, **2009**.
71. Mitscherlich, E. *Abhl. Akad. Berlin*, *43*, 1822-1823.
72. Berzelius, J. *Jahresbericht*, **1844**, *23*, 44-55.
73. http://en.wikipedia.org/wiki/Allotrope of carbon.
74. Stahly, G. P. *Crystal Growth Des.* **2007**, *7*, 1007.
75. Steed, J. W. *Trends in Pharmacological Sciences*, **2013**, *34*, 185-193.
76. Braga, D.; Grepioni, F. *Chem. Commun*. **2005**, 3635.
77. Rodrıguez-Spong, B.; Price, C. P.; Jayasankar, A.; Matzger, A. J. Rodrı´guez-Hornedo, N. *Adv. Drug Deliv. Rev.* **2004**, *56*, 241.
78. Wohler, F.; von Liebig, *J. Ann. Pharm*. **1832**, *3*, 249.
79. Porter III, W. W.; Elie, S. C.; Matzger, A. J. *Cryst. Growth Des*. **2008**, *8*, 14-16.
80. Braga, D.; Grepioni, F.; Maini, L. *Chem. Commun.* **2010**, 6232.
81. Nangia, A. *Acc. Chem. Res*. **2008**, *41*, 595-604.
82. Braun, D. E.; Gelbrich, T.; Kahlenberg, V.; Laus, G.; Wieser, J.; Griesser, U. J. *New J Chem.* **2008**, *32*, 1677-1685.
83. Cruz-Cabeza, A.; Bernstein, J. *Chem. Rev*. **2014**, *114*, 2170-2191.
84. Kumar, S.S.; Nangia, A. *CrystEngComm***, 2013**, *15*, 6498-6505.
85. Nath, N. K.; Nilapwar, S.; Nangia, A. *Cryst. Growth Des.* **2012**, *12*, 1613-1625.
86. Harris, R. K.; Ghi, P. Y.; Puschmann, H.; Apperley, D. C.; Griesser, U. J.; Hammond, R. B.; Ma, C.; Roberts, K. J.; Pearce, G. J.; Yates, J. R.; Pickard, C. J. *Org. Process Res. Dev.*, **2005**, *9*, 902-910.
87. Arlin, J-B.; Price, L. S.; Price S. L.; Florence, A. J. *Chem. Commun*., **2011,** *47*, 7074-7076.
88. Babu, N. J.; Cherukuvada, S.; Thakuria R.; Nangia, A. *Cryst. Growth Des*., **2010**, *10*, 1979-1989.

89. Cherukuvada, S.; Thakuria R.; Nangia, A. *Cryst. Growth Des.*, **2010,** *10*, 3931-3941.
90. Goud, N. R.; Nangia, A. *CrystEngComm*, **2013**, *15*, 7456-7461.
91. Thun, J.; Seyfarth, L.; Butterhof, C.; Senker, J.; Dinnebier, R. E.; Breu, J. *Angew. Chem. Int. Ed.* **2007,** *46*, 6729-6731.
92. Trask, A. V.; Shan, N.; Motherwell, W. D. S.; Jones, W.; Feng, S.;Tan R. B. H.; Carpenter K. J., *Chem. Commun.* **2005,** 880-882.
93. Mitchell, C. A.; Yu, L.; Ward, L. *J. Am. Chem. Soc.*, **2001**, *123*, 10830-10839.
94. Das, D.; Barbour, L. J. *J. Am. Chem. Soc.*, **2008**, *130*, 14032-14033.
95. Nath, N. K.; Aggarwal, H.; Nangia, A. *Cryst. Growth Des.*, **2011**, *11*, 967-971.
96. Thallapally, P. K.; Jetti, R. K. R.; Katz, A. K.; Carrell, H. L.; Singh, K.; Lahiri, K.; Kotha, S.; Boese, R.; Desiraju, G. R. *Angew. Chem. Int. Ed.*, **2004**, *43*, 1149-1155.
97. Hilden, J. L.; Reyes, C. E.; Kelm, M. J.; Tan, J. S.; Stowell J. G.; Morris, K. R. *Cryst. Growth Des.*, **2003**, *3*, 921-926.
98. Sun, X.; Garetz, B. A.; Myerson, A. S. *Cryst. Growth Des.*, **2006**, *6*, 684.
99. Bouchard, A.; Jovanović, N.; Hofland, G. W.; Mendes, E.; Crommelin, D. J. A.; Jiskoot W.; Witkamp, G. *Cryst. Growth Des.*, **2007**, *7*, 1432-1440.
100. Ostwald, W. F. *Z. Phys. Chem.*, **1897**, *22*, 289.
101. Sanphui, P.; Goud, N. R.; Khandavilli, U. B. R.; Bhanoth S.; Nangia, A. *Chem Commun*, **2011**, *47*, 5013-5015.
102. http://en.wikipedia.org/wiki/Curtin%E2%80%93Hammett_principle
103. Desiraju, G. R. *Nature Materials*, **2002,** *1*, 77.
104. Desiraju, G. R. (Ed.), *Crystal Design: Structure and Function, Perspectives in Supramolecular Chemistry*, Vol **7**. Wiley & Sons, **2003**.
105. Weber, E. (Ed.), *Design of Organic Solids*, Springer-Verlag, Berlin, **1998**.
106. Hollingsworth, M. D. *Science*, **2002**, *295*, 2410.
107. Kratochvil, B.; Novotny, J.; Husak, M.; Had, J.; Stuchlik, J.; Jogorov, A. *Collect. Czech. Chem. Commun.*, **1994**, *59*, 149.
108. Bingham, A. L.; Hughes, D. S.; Hursthouse, M. B.; Lancaster, R. W.; Travener S.; Threlfall, T. L. *Chem Commun.*, **2001**, 603.
109. Suzuki, M.; Kobayashi, K. *Cryst. Growth Des.*, **2011**, *11*, 1814.
110. Bhatt, P. M.; Desiraju, G. R. *Chem. Commun*, **2007**, 2057-2059.

111. Elguero, J. *Cryst. Growth Des.,* **2011**, *11*, 4731-4738.
112. Bernstein, J.; Davey R. J.; Henck, J. -O. *Angew. Chem., Int. Ed.*, **1999,** *38*, 3440.
113. Byrn, S. R.; Pfeiffer R. R.; Stowell, J. G. *Solid-State Chemistry of Drugs*; SSCI, West Lafayette, IN, **1999.**
114. Yokoyama, T.; Umeda, T.; Kuroda, K.; Kuroda, T.; Asada, S. *Chem Pharm Bull*, **1981**, *29*, 194-199.
115. Nangia A.; Desiraju, G. R. *Chem Commun.*, **1999,** 605-606.
116. Cruz-Cabeza, A, J.; Bernstein, J. *Chemical reviews* **2013**, *114*, 2170-2191.
117. Bauer, J.; Spanton, S.; Henry, R.; Quick, J.; Dziki, W.; Porter, W.; Morris, J. *Pharmaceutical research* **2001**, *18*, 859-866.
118. Kratochvil, B.; Novotny, J.; Husak, M.; Had, J.; Stuchlik J.; Jogorov, A. *Collect. Czech. Chem. Commun.*, **1994**, *59*, 149-158.
119. Bingham, A. L.; Hughes, D. S.; Hursthouse, M. B.; Lancaster, R. W.; Travener S.; Threlfall, T. L. *Chem Commun.*, **2001**, 603.
120. Suzuki, M.; Kobayashi, K. *Cryst. Growth Des.*, **2011**, *11*, 1814-1820.
121. Lin, J.; Ostovic D.; Vacca, J. *Pharm. Biotechnol.*, **1998**, *11*, 233-255.
122. http://www.gsk.com.au/resources.ashx/prescriptionmedicinesproductschilddataproinfo/1580/FileName/1FEC0F4C187D4D00DDE44D79CF7C72EA/Aropax_PI_007_approved.pdf
123. Pfeiffer, R. R. Yang and K. S. Tukker, M. A. *J. Pharm. Sci*., 1970, **59**, 1809.
124. Nicolai, B.; Espeau, P.; Ceolin, R.; Perrin, M.-A.; Zaske, L.; Giovannini, J.; Leveiller, F. *J. Therm. Anal. Calorim.*, **2007,** *90*, 337-339.
125. Qiu, Y.; Chen, Y.; Zhang, G. G. Z. Eds., *Developing Solid Oral Dosage Forms. Pharmaceutical Theory and Practice*, Academic Press, New York, **2009**.
126. Babu, N. J.; Nangia, A. *Cryst. Growth Des.*, **2011**, *11*, 2662.
127. Schultheiss, N.; Newman, A. *Cryst. Growth Des.*, **2009,** *9*, 2950.
128. Sarma, B.; Nath, N. K.; Bhogala B. R.; Nangia, A. *Cryst. Growth Des*. **2009**, *9*, 1546.
129. Childs, S. L.; Stahly G. P.; Park, A. *Mol. Pharmaceutics*, **2007**, *4*, 323.
130. Paulekuhn, G. S.; Dressman, J. B.; Saal, C. *J. Med. Chem*. **2007**, *50*, 6665.
131. Serajuddin, A. T. M. *Adv. Drug Delivery Rev*., **2007,** *59*, 603.
132. Berge, S. M.; Bighley L. D.; Monkhouse, D. C. *J. Pharm. Sci.*, **1977**, *66*, 1.

133. B. Sarma, R. Thakuria, N. K. Nath and A. Nangia, *CrystEngComm*, 2011, **13**, 3232-3240

134. Nanubolu, J. B.; Sridhar, B.; Ravikumar, K.; Cherukuvada, S. *CrystEngComm*, DOI: 10.1039/C3CE00022B

135. Ong, W.; Cheung, E. Y.; Schultz, K. A.; Smith, C.; Bourassa J.; Hickey, M. B. *CrystEngComm*, **2012**, *14*, 2428.

136. Lee, E. H.; Boerrigter, S. X. M.; Rumondor, A. F. C.; Chamarthy S. P.; Byrn, S. R. *Cryst. Growth Des.*, **2008,** *8*, 91-97.

137. An, J.; Kim, J.; Chang, S.; Kim, W. *Cryst. Growth Des.*, **2010**, *10*, 3044-3050.

138. Li, X. X.; Xu, X. D.; Den, Y. Y.; Feng, J.; Ge, L.; Zhang, L. M. *Cryst. Res. Technol.*, **2008**, *43*, 1062-1068.

139. Pusey, M. L.; Paley, M. S.; Turner, M. B.; Rogers, R. D. *Cryst. Growth Des.*, **2007**, *7*, 787-793.

140. Sweetana, S.; Akers, M. J. *J. Pharm. Sci. Tech*., **1996**, *50*, 330-342.

141. Galcera, J.; E. Molins. *Cryst. Growth Des.*, **2009**, *9*, 327-334.

142. Portell, A.; Barbas, R.; Font-Bardia, M.; Dalmases, P.; Prohens R.; Puigjaner, C. *CrystEngComm*, **2009**, *11*, 791-795.

143. Cheney, M. L.; Shan, N.; Healey, E. R.; Hanna, M.; Wojtas, L.; Zaworotko, M. J.; Sava, V.; Song, S.; Sanchez-Ramos, J. R. *Cryst. Growth Des*., **2010**, *10*, 395-405.

144. Goud, N. R.; Gangavaram, S.; Suresh, K.; Pal, S.; Manjunatha, S. G.; Nambiar, S.; Nangia, A. *J. Pharm. Sci.*, **2012**, *101*, 664-680.

145. Bolla, G.; Nangia, A. *Cryst. Growth Des.*, **2012,** *12*, 6250-6259.

146. Basavoju, S.; Bostrom, D.; Velaga, S. P. *Cryst. Growth Des.*, **2006**, *6*, 2699-2708.

147. Bhutani, H.; Singh, S.; Jindal, K. C.; Charkraborti, A. K. *J. Pharm. Biomed. Anal.*, **2005**, *39*, 892-899.

148. Singh, S.; Mohan, B. *Int. J. Tuberc. Lung Dis.*, **2003**, *7*, 298-303.

149. Krantz, J. C.; Holbert, J. M.; Iwamoto H. K.; Karr, C. J. *J. Am. Pharm. Assoc.*, **1947,** *36*, 248-250.

150. Vishweshwar, P.; McMahon, J. A.; Bis J. A.; Zaworotko, M. J. *J. Pharm. Sci*., **2006**, *95*, 499-516.

151. Aakeröy, C. B.; Forbes S.; Desper, J. *J. Am. Chem. Soc.*, **2009**, *132*, 17048-17049.

152. Alhalaweh A. and Velaga, S. P. *Cryst. Growth Des*., **2010,** *10*, 3302-3305.

153. Buanz, A. B. M.; Telford, R.; Scowen I. J.; Gaisford, S. *CrystEngComm*, 2013, **15**, 1031-1035.

154. Eddleston, M. D.; Sivachelvam S.; Jones, W. *CrystEngComm*, **2013,** *15*, 175-181.

155. Stanton, M. K.; Kelly, R. C.; Colletti, A.; Kiang, Y.-H.; Langley, M.; Munson, E. J.; Peterson, M. L.; Roberts J.; Wells, M. *J. Pharm. Sci.*, **2010**, *99*, 3769-3778.

156. Trask, A.V. (**2007**) An overview of pharmaceutical cocrystals as intellectual property. Mol. Pharmaceut. 4, 301–309.

157. Babu, N. J.; Nangia, A. *Cryst. Growth Des*., **2011**, *11*, 2662-2679.

158. Sanphui, P.; Goud, N. R.; Khandavilli, U. B. R.; Nangia, A. *Cryst. Growth Des.* **2011**, *11*, 4135-4145.

159. Shimpi, M. R.; Childs, S. L.; Boström D.; Velaga, S. P. *CrystEngComm*, **2014**, *16*, 8984-8993.

160. Goud, N. R.; Khan R. A.; Nangia, A. *CrystEngComm*, **2014**, *16*, 5859-5869.

161. Bavishi, D. D.; Borkhataria, C. H. *Prog. Cryst. Growth Charact. Mater*. **2016**, *62*, 1−8.

162. Remenar, J. F.; Morissette, S. L.; Peterson, M. L.; Moulton, B.; MacPhee, J. M.; Guzman, H. R.; Almarsson, O. *J. Am. Chem. Soc.*, **2003,** *125*, 8456-8457.

163. Higuchi, T.; Pitman, I. H. *J. Pharm. Sci.,* **1973,** *62*, 55-58.

164. Braga, D.; Grepioni, F.; maini, L.; Prosperi, S.; Gobetto R.; Chierotti, M. R. *Chem Commun.*, **2010**, *46*, 7715-7717.

165. Babu, N. J.; Sanphui P.; Nangia, A. *Chem. Asian J.*, **2012**, *10*, 2274-2285.

166. Hickey, M. B.; Peterson, M. L.; Scoppettuolo, L. A.; Morrisette, S. L.; Vetter, A.; Guzman, H.; Remenar, J. F.; Zhang, Z.; Tawa, M. D.; Haley, S.; Zaworotko M. J.; Almarsson, O. *Eur. J. Pharm. Biopharm.*, **2007,** *67*, 112-119.

167. Ghosh, S.; Reddy, C. M. *Angew. Chem. Int. Ed.*, **2012**, *51*, 10319-10323.

168. Khan, M.; Enkelmann, V.; Brunklaus, G. *J. Am. Chem. Soc.*, **2010**, *132*, 5254-5263.

169. Yan, D.; Delori, A.; Lloyd, G. O.; Friscic, T.; Day, G. M.; Jones, W.; Lu, J.; Wei, M.; Evans, D. G.; Duan, X. *Angew. Chem. Int. Ed.*, **2011**, *50*, 12483-12486.

170. Pang, X.; Wang, H.; Zhao, X. R.; Jin, W. J. *CrystEngComm*, **2013**, *15*, 2722-2730.

171. Karki, S.; Friščić, T.; Fábián, L.; Laity, P. R.; Day, G. M.; Jones, W. *Adv. Mater.*, **2009,** *21*, 3905-3909.

172. http://www.fda.gov/downloads/Drugs/.../Guidances/UCM281764.pdf

173. Mishima, D.; Calvert, L. E.; Whalley, E. *Nature*, **1984,** *310*, 393-395.

174. Johari, J. P.; Hallbrucker, A.; Mayer, E. *Nature*, 330**, 1987**, 552-553.

CHAPTER TWO

Cocrystals of the Tuberculosis Drug Isoniazid: Polymorphism, Isostructurality, and Stability

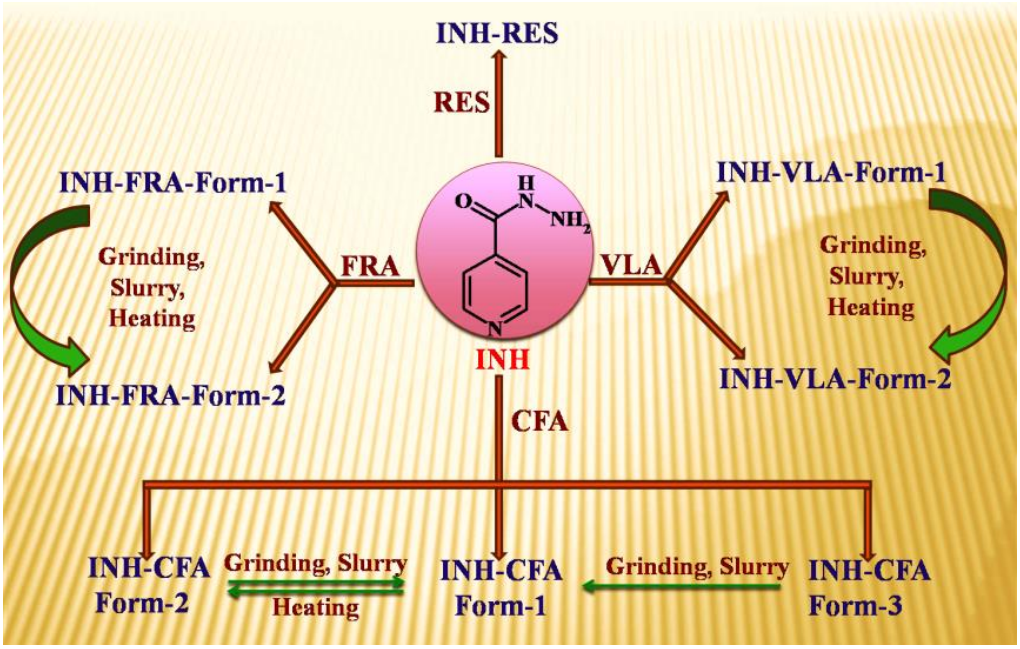

Isoniazid (INH) is a key active pharmaceutical ingredient used in the fixed dose combination Tuberculosis drug. Out of four cocrystals, INH–vanillic acid (VLA), INH–ferulic acid (FRA), INH–caffeic acid (CFA), and INH–resorcinol (RES), two cocrystals (INH-VLA and INH-FRA) are dimorphic, and INH-CFA is trimorphic. The cocrystal structures are sustained by the robust acid–pyridine synthon, except Form-1 of INH-VLA and INH-FRA, which has the hydroxyl–pyridine synthon. Slurry crystallization, powder grinding and stability experiments showed that Form-2 of INH-FRA and INH-VLA and Form-1 of INH-CFA potential cocrystals for a more stable INH solid form in the FDC.

2.1 Introduction

Several formulation strategies for improved drug delivery systems are currently under development, among which solid forms such as polymorphs,[1] salts,[2] cocrystals,[3] solvates/hydrates,[4] conjugate acid-base cocrystal,[5] etc. are considered to be promising for delivering improved physicochemical properties. Pharmaceutical cocrystals may be defined as molecular complexes comprising an active pharmaceutical ingredient (API) and one or more pharmaceutically acceptable cocrystal formers, usually selected from the list of US-FDA approved generally regarded as safe (GRAS)[6] chemicals, which are in the solid-state at ambient conditions. Akin to single component systems such as APIs, cocrystals and salts also exhibit polymorphism. Polymorphism is the existence of more than one crystalline modification of the same compound in the solid-state. Even though single molecule polymorphism is well known (e.g., barbital, benzamide, fuchsones, benzidine, pyridine, 1,3,5-Trinitrobenzene, etc.),[7] polymorphism in cocrystals is relatively recent (e.g., tetrachlorodicyanobenzene-hexamethylbenzene, triphenylsilanol-4,4′-bipyridyl, temozolomide- 4,4′-bipyridine-*N*,*N*′-dioxide, carbamazepine-saccharin, caffeine-glutaric acid, etc.).[8] A number of papers have appeared in the literature on structure-property relationships for cocrystal polymorphs.[9,8c-e] A recent review reported 114 neutral polymorphic cocrystals in the literature up to September 2013,[10] to which seven additional examples are updated from the May 2014 version of the CSD.[11] A few notable examples of pharmaceutical cocrystal polymorphs are those by Aitipamula et al. of ethenzamide-gentisic acid (trimorphic),[12] Ueto et al. described five polymorphs of furosemide-nicotinamide,[13] and Lemmerer et al. reported four dimorphic cocrystals.[14] A complementary phenomenon to polymorphism is Isostructurality,[15] wherein two or more structurally related molecules have the same or similar crystal packing and/ or space group (i.e., isostructurality and isomorphism). Investigating the polymorphic behavior of cocrystals is just as important as that of single component crystals and APIs, because of its influence on pharmaceutical properties, such as solubility, stability, bioavailability, melting point, density, etc.[1,16] The successful development of pharmaceutical cocrystals is expected to create patenting and novel intellectual property avenues.[17]

Some drug substances are known to exhibit physicochemical stability issues in the solid state during the manufacturing process and in different storage conditions, mainly under high humidity and/or high temperature conditions. The solid-state transformations can affect physicochemical properties like dissolution rate, solubility, compactability and

shelf-life, any of which could in turn impact drug product performance. Therefore, significant attention is given to the physicochemical stability of drug substances during preformulation development. Trask et al[18a]. reported four cocrystals of respiratory drug theophylline with oxalic, malonic, maleic and glutaric acids. The theophylline-oxalic acid cocrystal displayed superior stability to theophylline anhydrate upon storage at high relative humidity conditions, while the other cocrystals showed comparable stability to that of theophylline anhydrate. Nangia and coworkers[18b] have solved the chemical instability of bioactive agent andrographolide by preparing its cocrystals. Andrographolide-salicylic acid (AP-SLA) cocrystal has shown improved chemical stability and higher dissolution rate compare to the pure andrographolide (Figure 2.1).

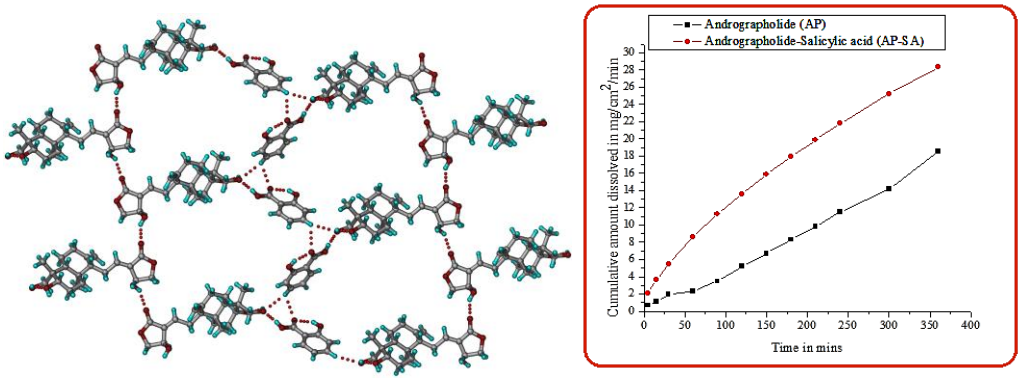

(a) **(b)**

Figure 2.1 (a) A layered section of AP–SLA cocrystal connected by O–H···O H bonds and C–H···O interactions. (b) Intrinsic dissolution rate curves of AP and AP-SLA cocrystal in 25% EtOH-water. (Adapted from ref. 18b).

In another article, Duggirala and coworkers[19] demonstrated ionic cocrystals (ICCs) of lithium drugs, lithium chloride (LIC) and lithium bromide (LIB) with α-D-glucose (GLU). Notably, LICGLU displayed improved physical stability when compared to its parent salt, LIC at 50% RH and 25°C stability conditions (Figure 2.2).

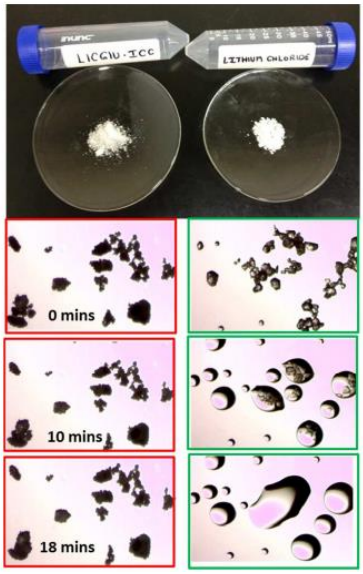

Figure 2.2 Qualitative observation of the physical stability of LICGLU versus LIC. Digital images of LIC and LICGLU were taken at 25°C and 50% RH after 0, 10, and 18 minutes[19].

These results suggest that the apply of pharmaceutical cocrystallization approach towards the avoid of hydrate formation and improvement in physical stability. Hence with this background of the study in this chapter we discussed cocrystals and cocrystal polymorphs of INH to address the stability issue of 4-drug fixed dose combination (FDC) formulations.

2.2 Literature reports on Isoniazid

Isoniazid (INH) is an important API used in combination with rifampicin, pyrazinamide (PZA), and ethambutol for the treatment of tuberculosis, referred to as fixed dose combinations (3FDC, 4FDC).[20] Tuberculosis (TB) is a major global health problem ranking as the second leading cause of death from a single infectious disease after HIV. According to WHO, an estimated 8.6 million people developed TB and 1.3 million died from the disease (including 320,000 deaths among HIV-positive people) in 2012.[21] The number of TB deaths are unacceptably large given that many are preventable. WHO recommended FDCs against TB over six to nine months of treatment for better patient compliance and fewer chances of developing drug resistance. However, serious concerns have been raised about the utility of these products due to quality problems such as stability and bioavailability of the formulation.[22] Pure INH is stable over long time periods at ambient (25-30 °C, 30-40% RH, for Hyderabad) as well as in accelerated

stability ICH conditions (40 °C, 75% RH),[23] whereas in the FDC tablet formulations INH undergoes degradation due to drug-drug interactions.[22e,24] The exposure to light and the presence of other drug compounds (pyrazinamide, ethambutol) also increase the level of INH degradation.[25] Since INH is susceptible to hydrolysis and oxidation, and interacts with excipients particularly reducing sugars to form hydrazones, the incompatibility of INH drug and lactose (milk) is well documented.[26] Generally combinations of anti-TB drugs are prescribed due to drug resistance, and hence there is an immediate urgency to develop stable FDC formulations. There are no reports on polymorphs, hydrates, and solvates of INH. Cocrystals of INH with various coformers were reported by Lemmerer et al.,[27] and Desiraju et al. reported a multidrug cocrystal of INH and another anti-TB drug 4-aminosalicylic acid,[28] and Aitipamula et al. reported polymorphic cocrystals of INH with p-hydroxybenzoic acid, fumaric acid, and ternary cocrystals of INH, nicotinamide and fumaric acid or succinic acid.[29] Sarcevica et al. reported cocrystals of INH with a series of carboxylic acids,[30] and our group has reported binary and ternary eutectic compositions of INH and PZA with pharmaceutically acceptable dicarboxylic acids.[31]

2.3 Preparation of INH cocrystals

We performed a cocrystal screen of INH with several GRAS coformers to address the stability issue, including vanillic acid (VLA), ferulic acid (FRA), caffeic acid (CFA), and resorcinol (RES) (Scheme 2.1). All the solid forms were fully characterized by spectroscopic, thermal, X-ray diffraction techniques, and their structural details and pharmaceutical properties such as stability, hygroscopicity were evaluated.

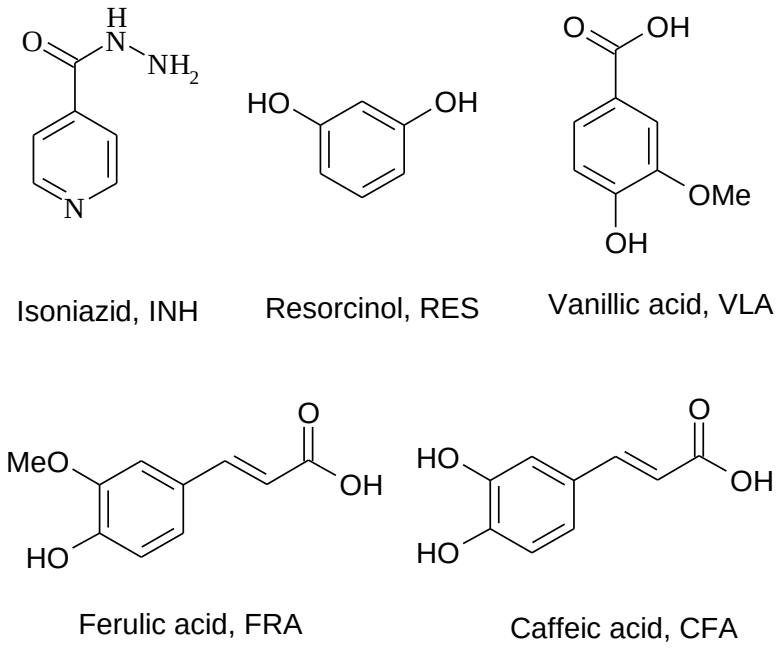

Scheme 2.1 Chemical Structure of INH and Coformers Used in This Study.

2.4 Results and Discussion

Isoniazid is highly soluble in water[32] and stable over a long period at ambient temperature and even at accelerated conditions (40 °C, 75% RH) in pure form. However, INH undergoes degradation in the FDC.[22e,24] The cocrystal approach to improve the stability of anti-TB drug INH was examined in this study by expanding the diversity of multicomponent crystal structures. In INH, the principal functional groups are hydrazide and pyridine ring. The pyridine N atom is an excellent hydrogen bond acceptor from the acidic OH donors in the acid−pyridine heterosynthon.[33] The hydrazide group has good hydrogen bond acceptor atoms (O and N) as well as donors (3 Hs). Both homosynthon (hydrazide N−H···O) and heterosynthon (acid−pyridine O−H···N) are expected in the crystal structure. In this background, we performed liquid-assisted grinding (LAG)[34] of INH with pharmaceutically acceptable GRAS coformers to prepare cocrystals. Novel crystalline multicomponent forms were obtained with VLA, FRA, CFA, and RES. Except for INH-RES, the other cocrystals of INH-VLA, INH-FRA and INH-CFA are polymorphic. In order to obtain single crystals of these solid forms, we used solution crystallization. Crystallization from different solvent mixtures afforded diffraction quality single crystals of all the solid forms except that of INH-CFA-Form-2 and INH-FRA-Form-2, which did not give diffraction quality single crystals even after several

attempts. All cocrystals were found to be 1:1 (API/coformer) stoichiometry by X-ray diffraction. The composition of all the cocrystals was confirmed from the crystal structure, except that for INH-FRA-Form-2 and INH-CFA-Form-2 which were confirmed through ^{1}H NMR and ^{13}C ss-NMR. Structural analysis revealed that all the cocrystal structures containing acidic coformers are stabilized by the robust acid–pyridine synthon (COOH···N_{arom}). The occurrence of this heterosynthon is in accordance with the hydrogen bond hierarchy rule,[35] except in INH-VLA-Form-1 and INH-FRA-Form-1 in which the hydroxyl–pyridine synthon (OH···N_{arom}) was observed. Interestingly, INH-VLA-Form-1 and INH-FRA-Form-1, which do not follow the hydrogen bond hierarchy rule, are two-dimensional (2D) isostructural. Further, analysis of all the structures revealed that eight different kinds of supramolecular synthons (four homosynthons and four heterosynthons) were observed in the cocrystals of INH with acid and hydroxyl functionality conformers (Scheme 2.2). All the novel cocrystal forms were characterized by spectroscopic (FT-IR, FT-Raman, ^{13}C ss-NMR), thermal (differential scanning calorimetry (DSC), hot-stage microscopy (HSM)), X-ray diffraction (powder X-ray diffraction (PXRD), single crystal XRD) techniques. In order to understand the stability of these novel cocrystals, their polymorphs were characterized and stability relationships were established. The crystallographic information is given in Table 2.1, and hydrogen bonds are presented in Table 2.2.

Table 2.1 Crystallographic Parameters of Isoniazid Cocrystals.

	INH-VLA-Form-1	INH–VLA-Form-2	INH–CFA-Form-1	INH–CFA-Form-3	INH–FRA-Form-1	INH–RES
Chemical formula	C28 H30 N6 O10	C14 H15 N3 O5	C15 H15 N3 O5	C15 H15 N3 O5	C16 H17 N3 O5	C12 H13 N3 O3
Formula weight	610.58	305.29	317.30	317.30	331.33	247.25
Crystal system	Triclinic	Monoclinic	Monoclinic	Triclinic	Triclinic	Monoclinic
Space group	$P\bar{1}$	$C2/c$	$P2_1/c$	$P\bar{1}$	$P\bar{1}$	$P2_1/c$
***T* [K]**	298(2)	298(2)	100(2)	100(2)	298(2)	298(2)
***a* [Å]**	7.3139(5)	25.379(3)	7.2470(12)	7.4051(16)	7.3931(8)	5.0623(5)
***b* [Å]**	7.4461(6)	4.9943(6)	20.694(4)	9.733(2)	7.5175(10)	16.119(2)
***c* [Å]**	14.2942(9)	22.281(3)	9.6836(16)	10.384(2)	15.0471(16)	14.6266(15)
***α* [°]**	101.678(6)	90	90	74.183(3)	82.133(10)	90
***β* [°]**	91.124(5)	91.741(12)	100.974(3)	84.064(4)	77.444(9)	96.618(10)
***γ* [°]**	109.433(7)	90	90	78.944(3)	73.205(10)	90

Z	2	8	4	2	2	4
***V* [Å^3]**	715.72(9)	2822.8(6)	1425.7(4)	705.7(3)	779.00(15)	1185.6(2)
D_{calc} [g cm^{-3}]	1.417	1.437	1.478	1.493	1.413	1.385
M [mm^{-1}]	0.109	0.111	0.113	0.114	0.107	0.102
Reflns. collected	4909	5440	14546	8017	5720	4690
Unique reflns.	2380	1056	2799	2400	2646	2427
Observed reflns.	2925	2879	2125	1980	2085	1451
R_1 [I>2(I)]	0.0396	0.0621	0.0507	0.0492	0.0443	0.0535
wR_2 (all)	0.1056	0.0737	0.1069	0.1289	0.1026	0.0957
Goodness-of-fit	1.039	0.890	1.041	1.024	1.027	1.015
Diffractometer	Oxford CCD	Oxford CCD	Bruker SMART Apex	Bruker SMART Apex	Oxford CCD	Oxford CCD

Table 2.2 Hydrogen Bond Metrics of Isoniazid Crystal Structures.

interaction	H···A (Å)	D···A (Å)	D–H···A (º)	symmetry code
INH-VLA-Form-1				
N2–H2A···N3	2.08	2.997(2)	148	–x+1, –y, –z
N3–H3A···N1	2.60	3.299(1)	125	–x+1, –y+1, –z
N3–H3A···O2	2.23	3.182(2)	153	–x, –y, –z
N3–H3B···O1	2.03	3.022(2)	162	–x, –y, –z
O3–H3···N1	1.89	2.760(1)	154	x–1,+y–1,+z
C11–H11···O4	2.48	3.421(1)	145	x–1,+y,+z
C12–H12···O5	2.43	3.436(1)	155	–x, –y+2, –z+1
INH-VLA-Form-2				
N2–H2A···O1	1.85	2.876(2)	176	x,+y+1,+z
N3–H3B···O3	2.38	3.108(2)	128	–x+1/2,+y–1/2, z+1/2
O3–H3···N3	1.97	2.851(1)	157	–x+1/2,+y–1/2, z+1/2
O5–H5A···N1	1.75	2.679(1)	174	–x+1, –y+2, –z+1
C1–H1···O2	2.50	3.480(1)	150	x, –y+2,+z+1/2
C4–H4···O4	2.30	3.219(2)	143	x,+y–1,+z
C11–H11···O3	2.45	3.482(1)	162	–x+1/2,+y+1/2, z+1/2
C13–H13A···N1	2.59	3.649(1)	167	x, –y+1,+z–1/2
C13–H13C···O5	2.42	3.394(1)	150	–x+1,+y, –z+1/2
INH-CFA-Form-1				
N2–H2A···O1	1.77	2.792(2)	176	x, –y+1/2,+z+1/2
N3–H3B···O5	2.00	3.000(3)	164	–x,+y–1/2, –z+1/2+1
O2–H2B···N3	1.80	2.711(2)	164	–x+1, –y+1, –z+2
O3–H3C···O2	2.02	2.818(2)	142	–x+1, –y+1, –z+2
O4–H4A···N1	1.68	2.604(2)	172	x,+y+1,+z
C1–H1···O4	2.48	3.318(2)	134	–x+1, –y+1, –z+2

C2–H2···O1	2.48	3.172(3)	121	x, –y+1/2,+z+1/2
C4–H4···O5	2.33	3.176(2)	134	–x, –y+1, –z+1
INH-CFA-Form-3				
N2–H2A···O5	1.86	2.885(2)	179	–x+2, –y, –z+1
N3–H3A···O3	2.47	2.975(2)	110	x+1,+y–1,+z
N3–H3B···O3	2.65	2.975(2)	98	x+1,+y–1,+z
N3–H3A···O5	2.25	3.143(2)	144	x,y,z
N3–H3B···O4	2.44	3.333(2)	145	x+1,+y,+z
O2–H2B··· O1	1.74	2.668(2)	170	–x+1, –y, –z+2
O3–H3C ··· O2	1.96	2.747(2)	141	–x, –y+1, –z+2
O4–H4A··· N1	1.68	2.618(2)	177	x,+y–1,+z
C2–H2··· O5	2.24	3.249(2)	156	–x+2, –y, –z+1
C4–H4··· O1	2.58	3.269(2)	122	–x+2, –y, –z+2
C8–H8···O1	2.48	3.204(2)	124	–x+1, –y, –z+2
INH-FRA-Form-1				
N2–H2A···N3	2.10	3.014(3)	146	–x, –y, –z+2
N3–H3A···N1	2.65	3.328(2)	123	–x, –y+1, –z+2
N3–H3A···O3	2.19	3.164(2)	158	–x+1, –y, –z+2
N3–H3B···O1	2.02	3.034(2)	170	–x+1, –y, –z+2
O2–H2B···N1	1.90	2.779(2)	154	x+1,+y–1,+z
O4–H4A···O5	1.67	2.605(2)	174	–x, –y+2, –z+1
C15–H15···O5	2.33	3.396(2)	168	–x+1, –y+2, –z+1
INH-RES				
N2–H2A···O1	2.03	2.932(2)	145	x+1,+y,+z
N3–H3A···O1	2.05	3.009(3)	154	–x+1, –y+1, –z+1
N3–H3B···O3	2.13	3.106(3)	158	x,y,z
O2–H2B···N1	1.83	2.756(3)	169	x–1,+y,+z–1
O3–H3C···N3	1.90	2.837(3)	174	x–1,+y,+z
C2–H2···O2	2.55	3.290(3)	125	–x, –y+1, –z+1

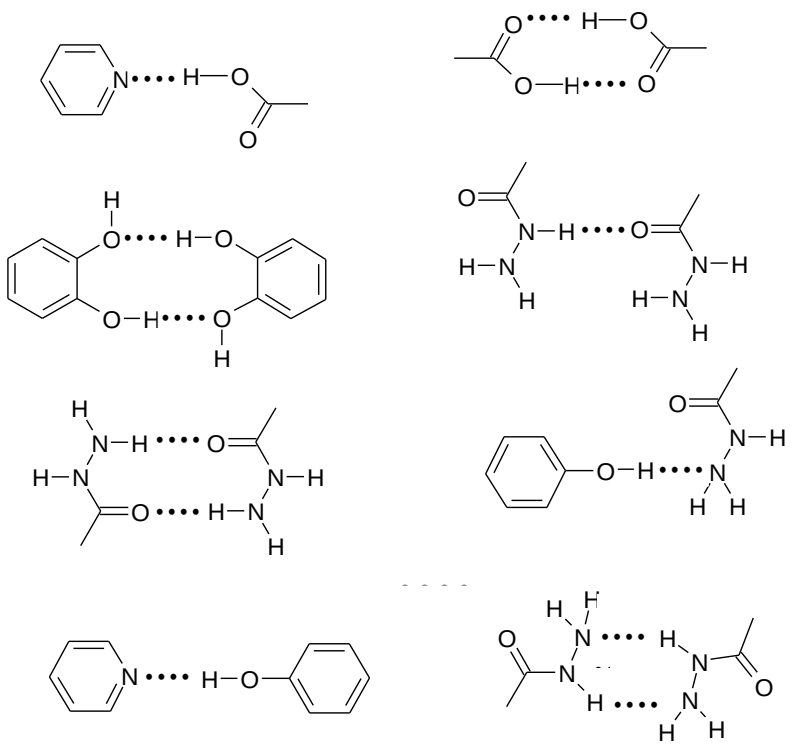

Scheme 2.2 Various Hydrogen Bonding Synthons (Homo and Hetero) in INH Cocrystal Structures.

2.4.1 Crystal Structure Description

Isoniazid-Ferulic acid cocrystal form-1 (INH-FRA-Form-1): Crystallization of the ground material INH and ferulic acid in CH_3CN : $CHCl_3$ afforded block-shaped crystals which was solved and refined in the triclinic space group $P\bar{1}$ with one molecule of INH and FRA in the asymmetric unit. INH molecules form a head-to-head hydrazide···hydrazide homosynthon through N–H···O (2.02 Å, 170º) hydrogen bonds in $R_2^2(10)$ dimer,[36] and FRA molecules form a carboxylic acid $R_2^2(8)$ dimer synthon. The dimers of INH and FRA were connected through hydroxyl-pyridine synthon (O–H···N, 1.90 Å, 154º) in a zigzag chain. Surprisingly, here there is no hydrogen bond between the best donor (carboxylic acid) and the best acceptor (pyridine N) in the supramolecular system. The infinite chains of molecules extend in the crystallographic [100] direction through N–H···N (2.10 Å, 146º) hydrogen bonds in a 2D sheet. Such neighboring sheets are connected through N–H···O (2.19 Å, 158º) hydrogen bonds parallel to the $(0\bar{1}4)$ plane (Figure 2.3). The INH-FRA cocrystal exists in two forms, but we could not

harvest the crystals of INH-FRA-Form-2 even after numerous crystallization experiments.

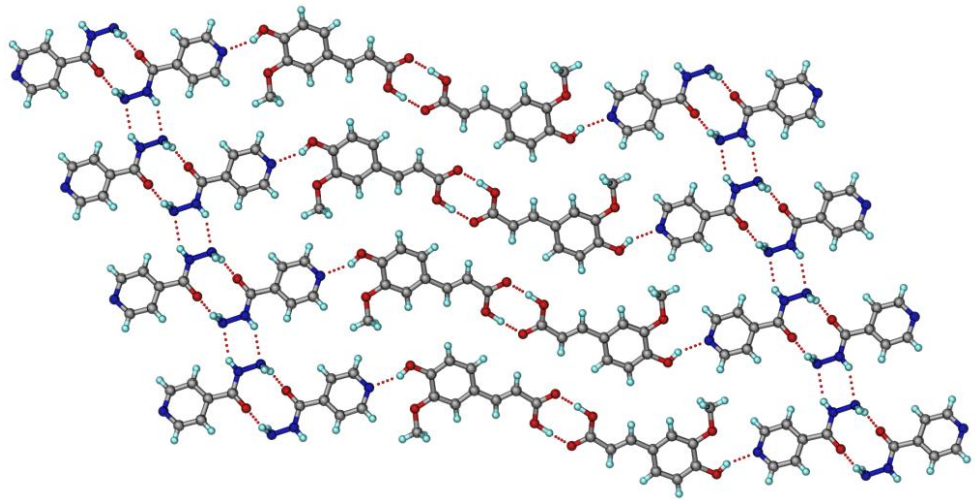

Figure 2.3 Sheet structure of INH-FRA-Form-1 mediated by acid ⋯acid, hydrazide⋯hydrazide homosynthons, and hydroxyl⋯pyridine heterosynthon.

Isoniazid-Vanillic acid cocrystal form-1 (INH-VLA-Form-1): Crystallization of the ground material INH and VLA in EtOAc : CH_3NO_2 afforded block crystals which was solved in $P\bar{1}$ space group with one INH and one VLA molecule in the asymmetric unit. INH molecules form a head-to-head hydrazide⋯hydrazide homosynthon through N–H⋯O (2.03 Å, 162º) hydrogen bonds in R_2^2 (10) dimeric motif, and VLA molecules form a carboxylic acid R_2^2 (8) dimer synthon. The dimers of INH and VLA are connected through the hydroxyl-pyridine synthon, just as in INH-FRA-Form-1, to result in an infinite zig-zag chain. Such chains extend in the crystallographic [100] direction through N–H⋯N hydrogen bond (2.08 Å, 148º) to form a 2D sheet. Such adjacent sheets are connected through N–H⋯O (2.23 Å, 153º) hydrogen bonds parallel to the $(0\bar{1}4)$ plane (Figure 2.4). Interestingly, INH-VLA-Form-1 was found to be isostructural with INH-FRA-Form-1. Isostructurality is more common in multicomponent systems such as solvent inclusion compounds, molecular complexes, cocrystals, etc.[37,15c-e] From XPac analysis, a closer placement of the (δa, δp) points to the origin of the system indicates a better match between INH-FRA-Form-1 and INH-VLA-Form-1 pair (Figure 2.5). The XPac dissimilarity index[38, 15a] (X = 4.5) is indicative of a supramolecular construct with a

degree of similarity, and also 2D isostructurality between INH-FRA-Form-1 and INH-VLA-Form-1 was noted (Figure 2.6). Their unit cell similarity index (Π = 0.031, a value close to zero)[38, 15a] indicates that the two unit cells being compared have practically the same shape and volume.

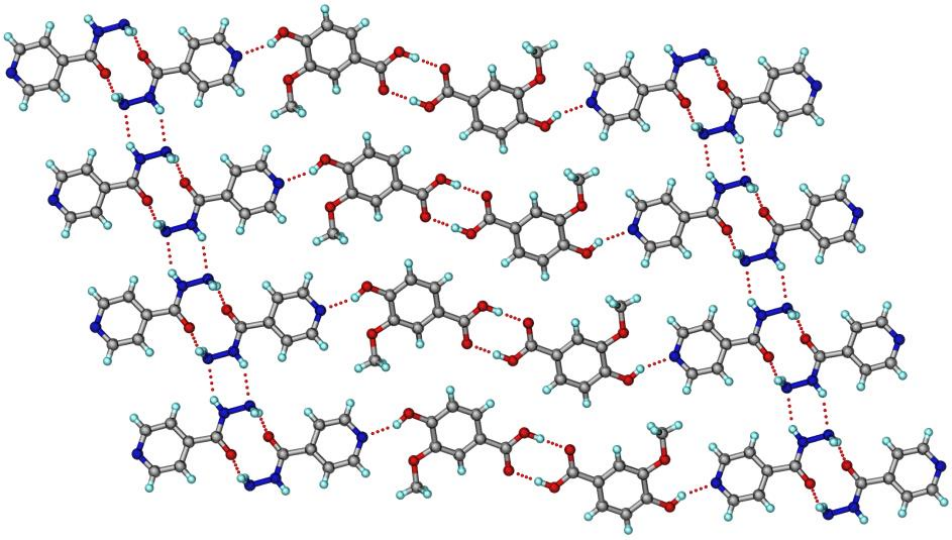

Figure 2.4 Sheet structure of INH-VLA-Form-1 mediated by acid ⋯acid, hydrazide homosynthons, and hydroxyl⋯ heterosynthons. pyridine ⋯hydrazide

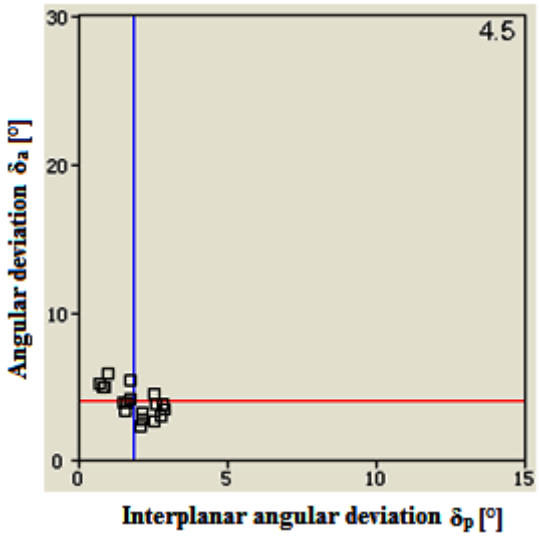

Figure 2.5 XPac plot of δ_p vs. δ_a (in °) for INH–FRA-Form-1 and INH–VLA-Form-1 pair illustrating the degree of similarity (top right corner value indicates dissimilarity index).

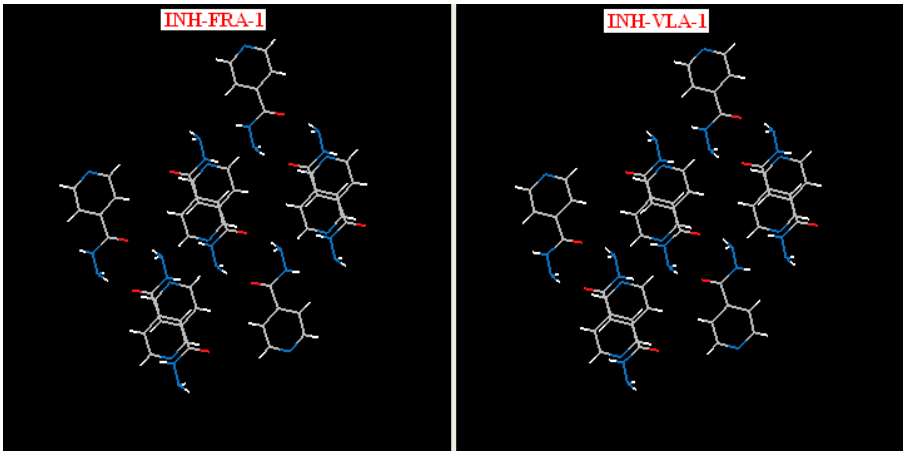

Figure 2.6 2D supramolecular constructs in INH–FRA-Form-1 and INH–VLA-Form-1.

Isoniazid-Vanillic acid cocrystal form-2 (INH-VLA-Form-2): Crystallization of the ground material INH and VLA from anisole : isopropanol afforded needle-shaped crystals which was solved and refined in the monoclinic space group *C*2/*c* with one molecule of INH and VLA in the asymmetric unit. The carboxylic acid group of VLA forms an O–H···N hydrogen bond to the pyridine nitrogen atom of INH to result in an acid-pyridine heterosynthon, whereas in Form-1 the carboxylic acid homosynthon was observed. Further the hydroxyl group of VLA forms O–H···N (1.97 Å, 157º) hydrogen bond to give a one-dimensional (1D) zigzag tape, whereas in Form-1 it is H-bonded to pyridine N atom. These tapes extend in the crystallographic [010] direction as a 2D sheet through N–H···O (1.85 Å, 176º) and N–H···O (2.38 Å, 128º) hydrogen bonds thereby forming a R_3^3 (10) motif.[36] These sheets extend parallel to the $(0\bar{1}4)$ plane through auxiliary C–H···O interactions (2.30 Å, 143º; 2.45 Å, 162º) interactions (Figure 2.7). INH-VLA-Form-1 and INH-VLA-Form-2 were classified as synthon and packing polymorphs.[8d,14]

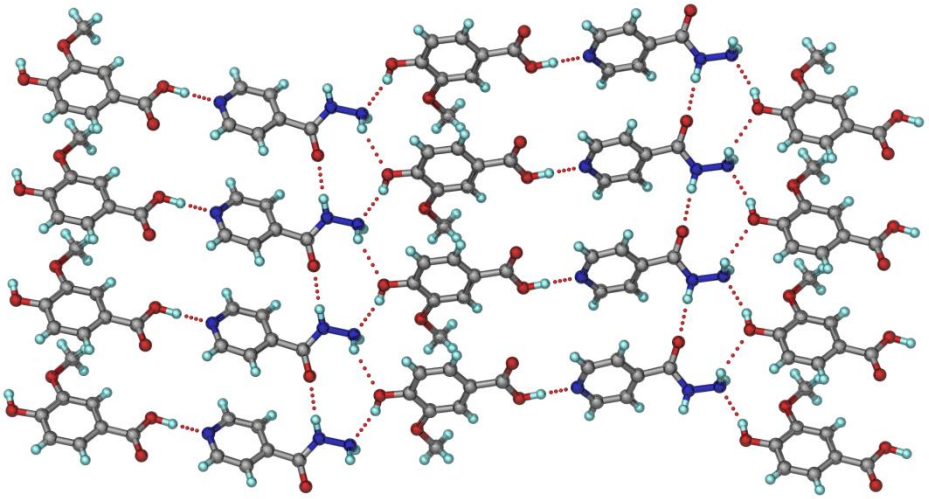

Figure 2.7 Sheet structure of INH-VLA-Form-2 assembled via N–H···O, O–H···N hydrogen bonds, and acid···pyridine heterosynthon.

Isoniazid-Caffeic acid cocrystal form-1 (INH-CFA-Form-1): Crystallization of ground INH and caffeic acid from THF : n-heptane afforded plate crystals, which were solved and refined in monoclinic space group $P2_1/c$ with one molecule of INH and CFA in the asymmetric unit. CFA molecules are connected by O–H···O (2.02 Å, 142º) hydrogen bonds in a $R_2^2(10)$ type dimeric motif reminiscent of catechol crystal structure. INH molecules are hydrogen bonded to the catechol dimer through O–H···N (1.80 Å, 164º) H-bond. The carboxylic acid group of CFA forms an O–H···N (1.68 Å, 172º) hydrogen bond to the pyridine nitrogen atom of INH via the robust acid–pyridine heterosynthon (strongest donor–strongest acceptor pairing)[33] in a linear tape motif. Adjacent tapes are connected through C–H···$O_{carbonyl}$ (2.33 Å, 134º) interactions in a 2D sheet (Figure 2.8a), which are connected through N–H···O hydrogen bonds (1.77 Å, 176º; 2.00 Å, 164º) (Figure 2.8b) from the amine NH donor.

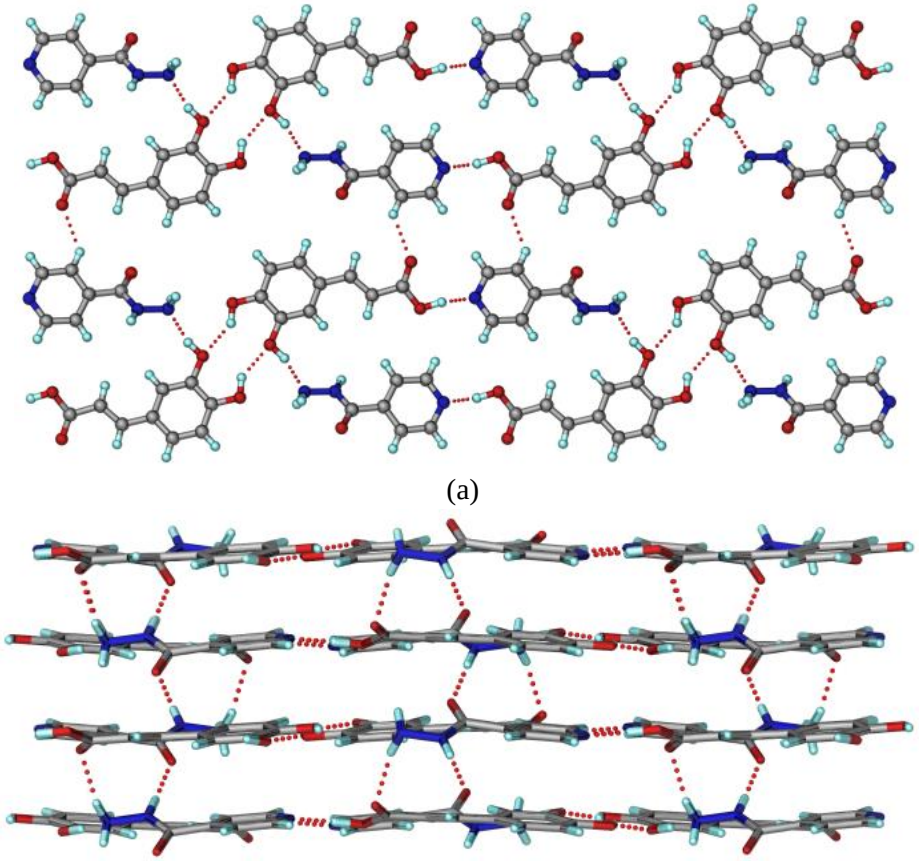

(a)

(b)

Figure 2.8 (a) Sheet structure of INH-CFA stabilized by the hydroxyl homodimer, acid-pyridine synthon and auxiliary C–H···O interactions. (b) The sheets were connected through N–H···O interactions.

Isoniazid-Caffeic acid cocrystal form-3 (INH-CFA-Form-3): The X-ray crystal structure of INH-CFA-Form-2 could not be solved because single crystals could not be harvested. A third polymorph of INH-CFA cocrystal was obtained upon crystallizing ground INH and CFA in a xylene/methanol solvent mixture, and its X-ray crystal structure was solved and refined in space group $P\bar{1}$ with one molecule of INH and CFA. CFA molecules are connected through O–H···O (1.96 Å, 141º) hydrogen bonds resulting in an R_2^2 (10) catechol-like dimer motif, similar to that in the structure of INH-CFA-Form-1. INH molecules are H-bonded to this catechol dimer through N–H···O (2.47 Å, 110º) and O–H···O (1.74 Å, 170º) H-bonds resulting in a R_3^3 (9) motif. The carboxylic acid group of CFA forms an O–H···N (1.68 Å, 177º) hydrogen bond to the pyridine N of INH (acid–pyridine synthon) leading to a linear tape, as in the structure of Form-1. These

tapes are linked through secondary amine NH of hydrazide to the carboxylic C=O of CFA (1.86 Å, 179º) (Figure 2.9a). The 2D sheets are connected via N–H···O (2.25 Å, 144º; 2.44 Å, 145º) H-bonds (Figure 2.9b). INH-CFA-Form-1 and Form-3 may be classified as synthon polymorphs.

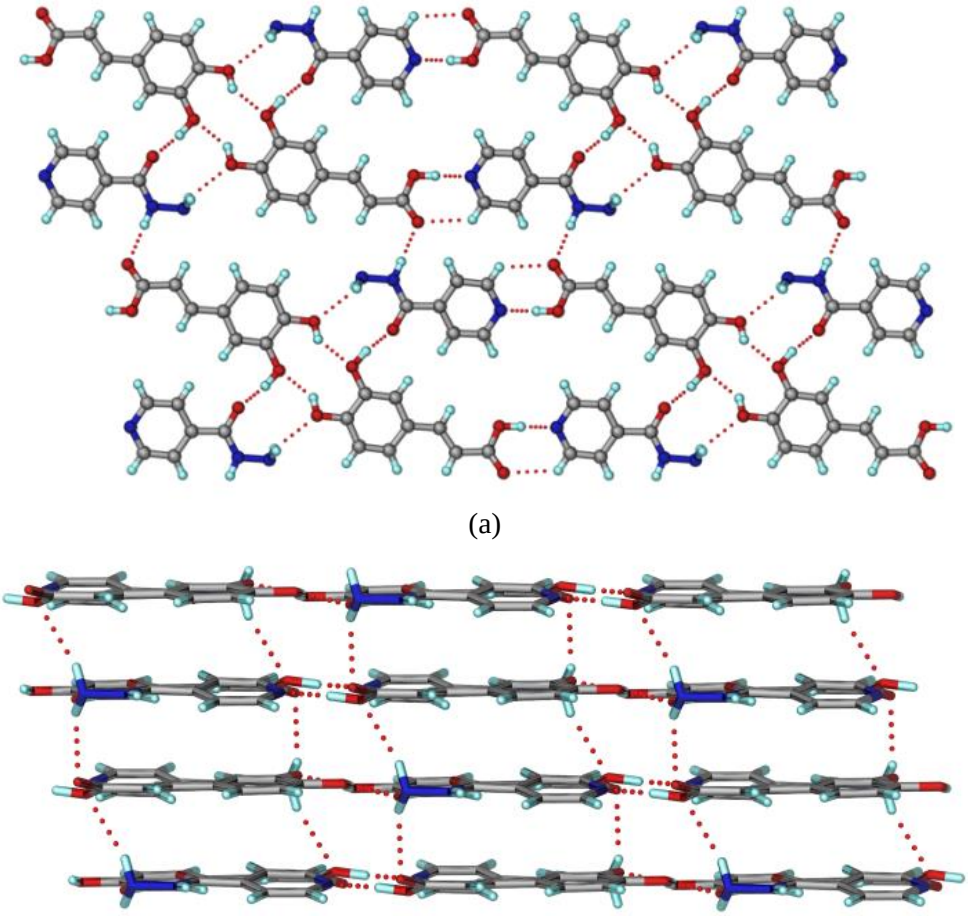

(a)

(b)

Figure 2.9 (a) Sheet structure of INH-CFA-Form-3 formed through hydroxyl homodimer, acid-pyridine synthon and C–H···O interactions. (b) The sheets are stacked through N–H···O H-bonds.

Isoniazid-Resorcinol cocrystal (INH-RES): The cocrystal of INH-RES was crystallized from CH_3NO_2 and the bulk material was obtained by liquid assisted grinding (LAG) using the same solvent. INH-RES cocrystal structure in the monoclinic space group $P2_1/c$ contains one molecule of INH and RES each. INH molecules form a head-to-head hydrazide homosynthon via N–H···O (2.05 Å, 154º) hydrogen bonds resulting in a $R_2^2(10)$ motif. The hydroxyl group of RES forms an O–H···N (1.83 Å, 169º) H-bond to the pyridine N of INH. The other phenolic O–H of RES interacts with the terminal

nitrogen atom of hydrazide through O–H···N (1.90 Å, 174º) hydrogen bond in a tape along the [001] direction (Figure 2.10a). Such zigzag tapes were connected by N–H···O=C (2.03 Å, 145º) H-bonds (Figure 2.10b).

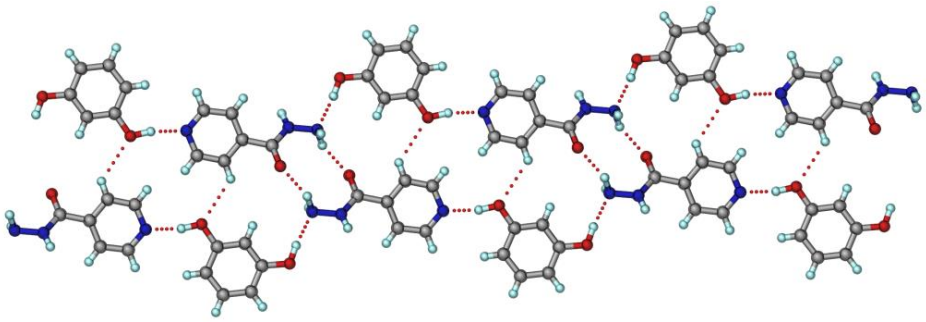

(a)

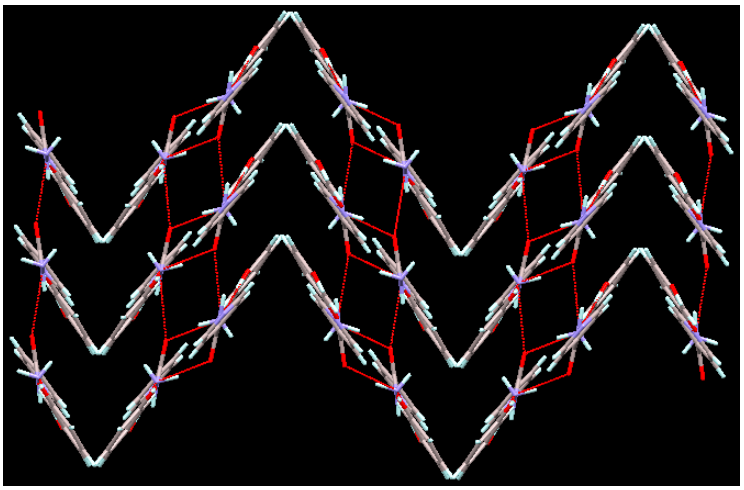

(b)

Figure 2.10 (a) Linear tapes in INH-RES cocrystal of hydrazide homosynthon and hydroxyl-pyridine heterosynthon. (b) Linear tapes were connected by N–H···O H-bonds in a zigzag chain.

2.4.2 Powder X-ray Diffraction

Powder X-ray diffraction is the most preferred characterization method to establish the formation of novel crystalline forms.[39] It can distinguish the resulting new solid phases from the starting materials by the unique diffraction line pattern. There are no reported polymorphs for INH except a guest-free crystal structure. The experimental powder diffraction pattern of INH commercial material showed a good match with the calculated powder lines of the reported crystal structure confirming polymorphic identity. In the present study all the cocrystals were found to exhibit polymorphic: INH-VLA is dimorphic, INH-CFA trimorphic, and INH-FRA dimorphic, the exception being INH-

RES. All the novel cocrystal forms were prepared in bulk by liquid-assisted grinding (LAG) or by heating in a programmable oven (120-150 ºC). The unique powder line pattern for each solid product was different from the starting components INH and coformer. The experimental PXRD pattern of the crystalline products showed an excellent match with the calculated diffraction line pattern from the crystal structure, thereby confirming identity and homogeneity of the crystalline phases (Figure 2.11). Numerous experiments to obtain single crystals of INH-FRA-Form-2 and INH-CFA-Form-2 were unsuccessful, and their unique powder XRD is the signature pattern. When INH-FRA-Form-1 was kept at 130 °C in a programmable oven for 30 min, the product did not match the calculated powder XRD lines of Form-1, which suggested a polymorphic modification upon heating. The transition was confirmed by VT-PXRD measurement which showed transition from INH-FRA-Form-1 to 2 at 125-130 ºC (Figure 2.12). Similarly, heating INH-CFA-Form-1 at 145 ºC in a salt bath for 15 min gave Form-2 product analyzed by PXRD (Figure 2.13)

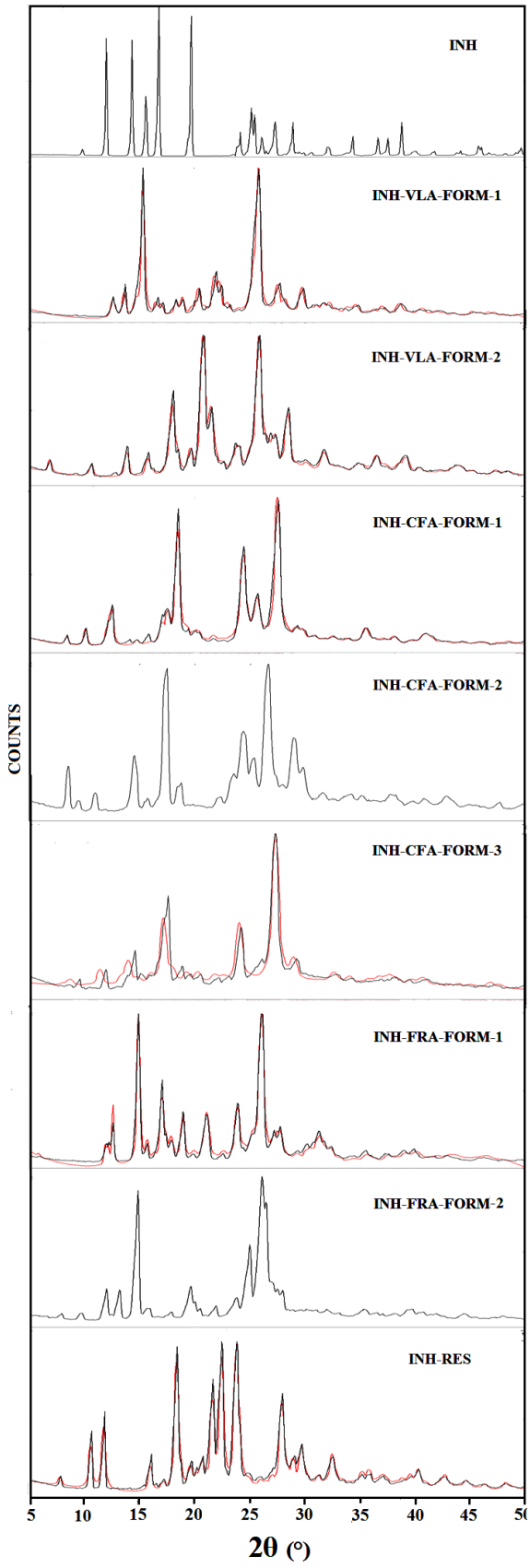
INH
INH-VLA-FORM-1
INH-VLA-FORM-2
INH-CFA-FORM-1
INH-CFA-FORM-2
INH-CFA-FORM-3
INH-FRA-FORM-1
INH-FRA-FORM-2
INH-RES
COUNTS
5
10
15
20
25
30
35
40
45
2θ (°)

Figure 2.11 Overlay of experimental PXRD (black) of INH cocrystals shows excellent match with the calculated powder XRD lines from the crystal structure (red).

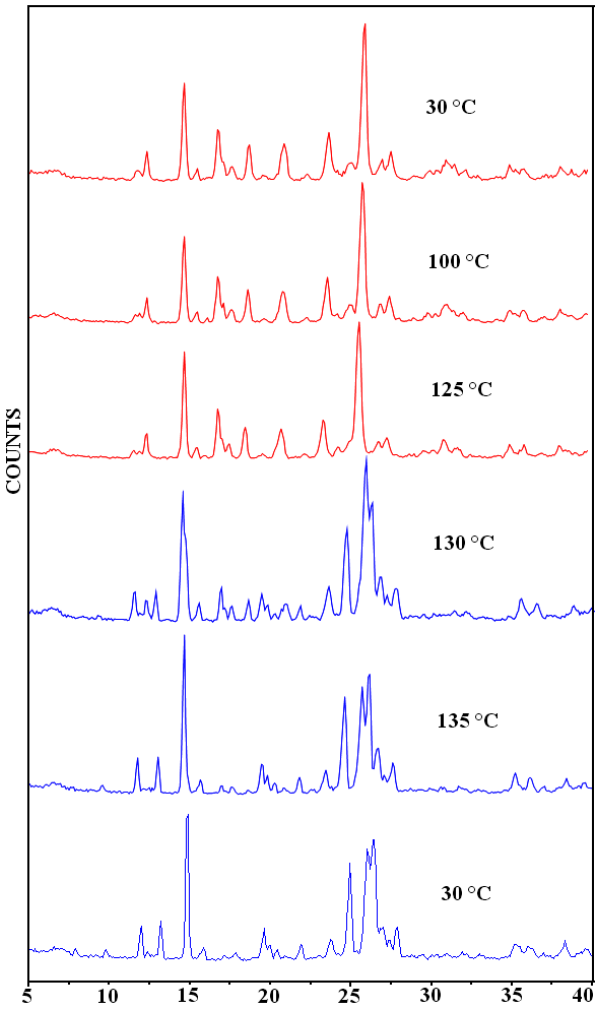

Figure 2.12 VT-PXRD of INH-FRA-Form-1 (top) shows transformation to INH-FRA-Form-2 (bottom) upon heating. Form-2 is stable upon cooling.

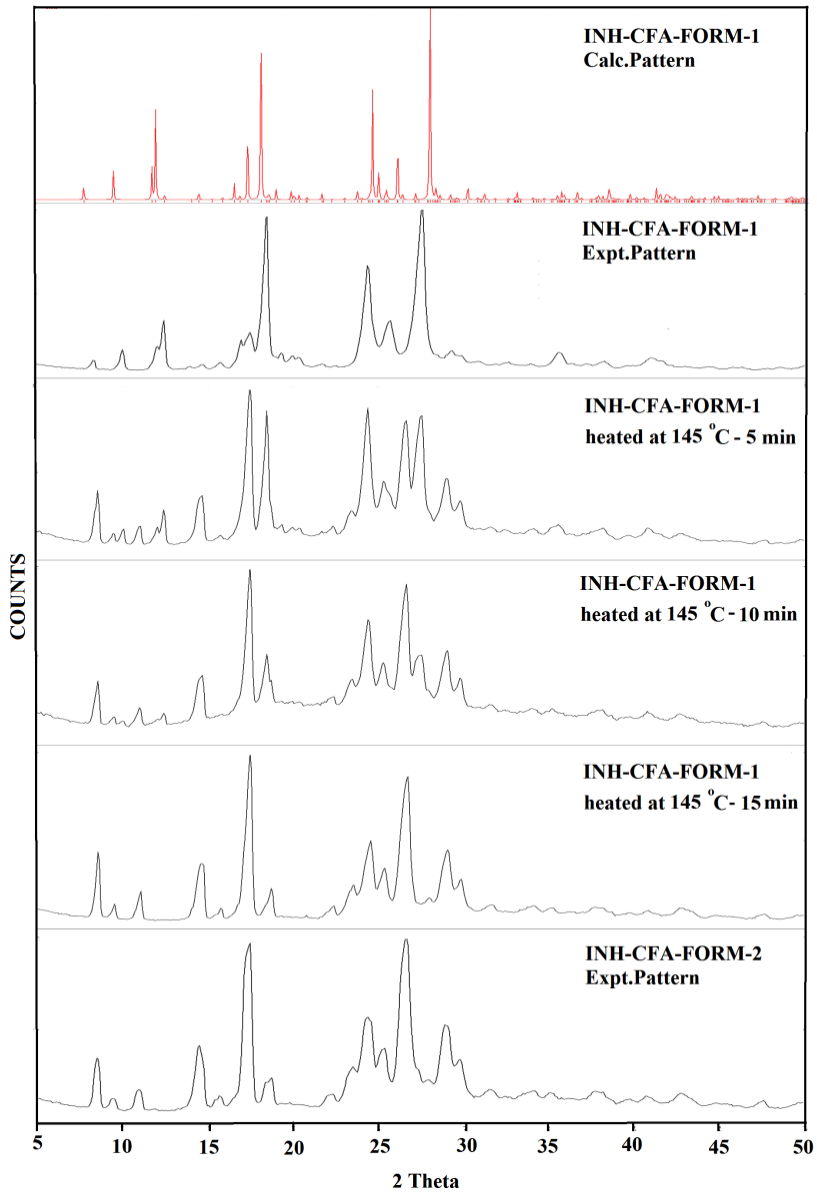

Figure 2.13 Overlay of PXRD patterns to show the conversion of INH-CFA-Form-1 to Form-2 upon heating. The calculated XRD line pattern of Form-1 (top) and the experimental profile of Form-2 are shown for comparison (bottom).

2.4.3. Spectroscopic Characterization

Spectroscopy (FT-IR and FT-Raman) is a quantitative tool for the characterization and identification of solid-state forms.[40] Generally IR spectroscopy is used as a first-hand tool which is informative about hydrogen bonding in the structure. These spectra are based on the vibrational modes of a compound and are extremely sensitive to the structure, hydrogen bonding, molecular conformations, and environment of the API. The

functional groups in this system such as amide C=O, primary and secondary NH, and pyridine N exhibit IR stretching frequencies at 3303.8 cm^{-1}, 3211.2 cm^{-1} (1° NH stretch), 3111.1 cm^{-1} (2° NH stretch), 1667.6 cm^{-1} (amide C=O stretch), and 1334.8 cm^{-1} (C=N pyridine ring). On the basis of the changes in the frequency of these functional groups, we ascertained the formation of novel solid forms. Carboxylic acids were selected as conformers, and the difference in stretching frequency observed from the pure carboxylic acid to the cocrystal was observed. The carbonyl stretch C=O of carboxylic acid (COOH) normally displays an intense band at 1750-1680 cm^{-1}, whereas the carboxylate anion (COO^-) has two characteristic coupled carbonyl absorption bands at 1600 cm^{-1} for asymmetric and 1400 cm^{-1} for symmetric stretch. The FT-IR stretching frequencies of carbonyl C=O stretch of COOH appeared at 1674.9 cm^{-1}, 1693.6 cm^{-1} in INH-VLA-Form-1, Form-2, at 1674.9 cm^{-1}, 1670.7 cm^{-1}, 1670.8 cm^{-1} in INH-CFA-Form-1, Form-2, Form-3, at 1683.2 cm^{-1}, 1673.0 cm^{-1} in INH-FRA-Form-1, Form-2. The cocrystals exhibited shift in C=O stretching frequency (5-30 cm^{-1}), O–H stretching frequency (4-50 cm^{-1}), and N–H stretch shift of 3-50 cm^{-1}. FT-IR spectra and stretching frequency values are shown Figure 2.14 and Table 2.3. Further, all the cocrystals were characterized by FT-Raman spectroscopy which showed the expected changes in the products compared to the starting materials. The characteristic Raman stretching frequency of INH is at 3090.1 cm^{-1}, 3063.7 cm^{-1} (1° NH stretch), 1669.1 cm^{-1} (amide C=O stretch) and 1322.8 cm^{-1} (C=N pyridine ring). The formation of cocrystals was established by changes in the stretching frequency of functional groups (Figure 2.15 and Table 2.4). Solid state-NMR spectroscopy provides information about the differences in hydrogen bonding, molecular environment, and short-range order in crystalline and amorphous solids.[41] The solid-state ^{13}C ss-NMR spectra of all the cocrystals showed the peaks for INH drug plus the coformer, but the chemical shifts were moved upfield/ downfield relative to the pure components because differences in short-range aggregation and shielding/deshielding in the molecular environments. ^{13}C ss-NMR analysis of all the cocrystals showed clear differences in chemical shifts as compared to starting components (Figure 2.16, see Table 2.5 for chemical shift values).

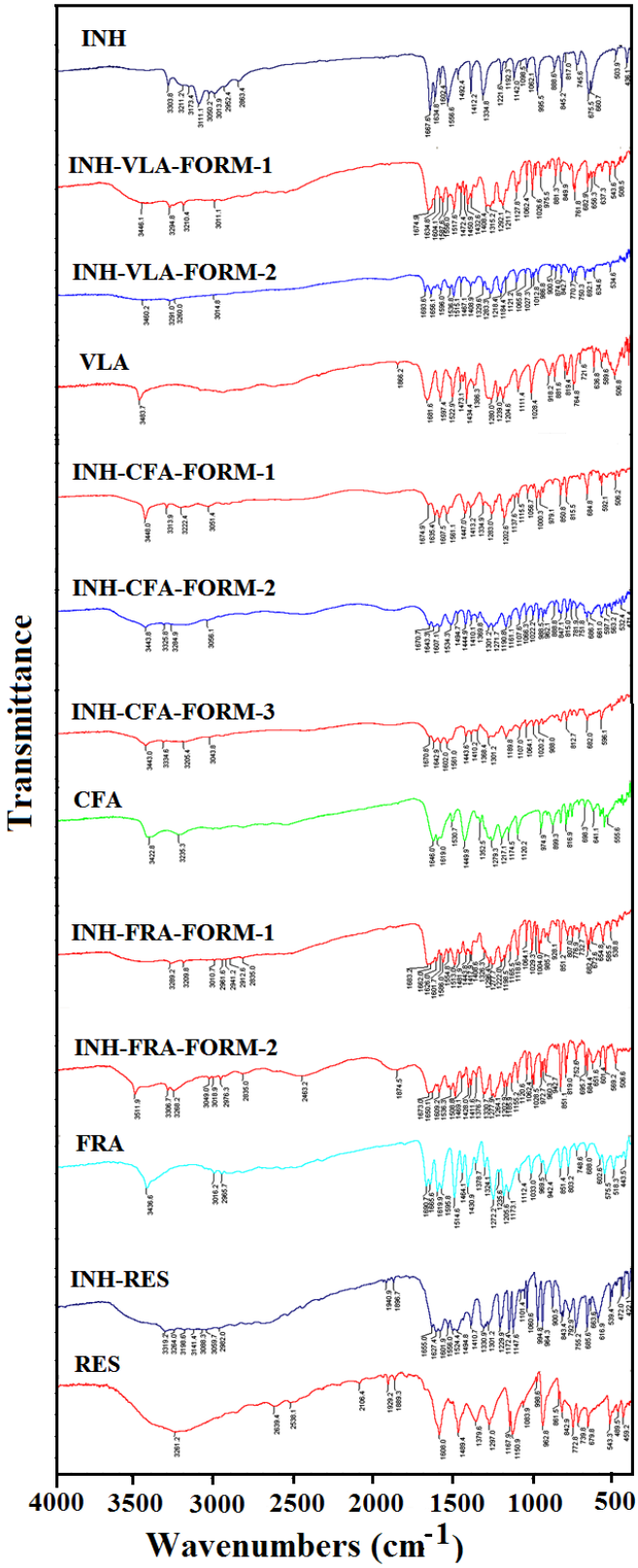

Figure 2.14 FT-IR spectra of INH cocrystals.

Table 2.3 List of IR stretching frequencies of INH cocrystals and the starting materials.

Compound	NH (stretch) 1°	NH (stretch) 2°	Carboxylic C=O (stretch)	Amide C=O (stretch)	O–H (stretch)	C-N (stretch)
INH	3303.8 3211.2	3111.1	-	1667.6	-	1334.8
INH-VLA-Form-1	3294.8 3210.4	3011.1	1674.9	1634.8	3446.1	1315.2
INH-VLA-Form-2	3291.0 3260.0	3014.8	1693.6	1656.1	3460.2	1312.1
VLA	-		1684.0	-	3483.5	-
INH-CFA-Form-1	3313.9 3222.4	3051.4	1674.9	1635.4	3448.0	1334.9
INH-CFA-Form-2	3325.8 3284.9	3056.1	1670.7	1643.3	3443.8	1301.2
INH-CFA-Form-3	3334.6 3205.4	3043.8	1670.8	1642.9	3443.0	1368.4
CFA	-		1646.0	-	3422.8	-
INH-FRA-Form-1	3289.2 3209.8	3010.7	1683.2	1662.0	2961.6	1326.3
INH-FRA-Form-2	3306.7 3268.2	3049.0	1673.0	1650.1	3018.9	1330.7
FRA	-		1690.7	-	3016.2	-
INH-RES	3319.2 3264.0	3088.3	-	1655.0	3141.4	1330.9
RES	-		-	-	3261.2	-

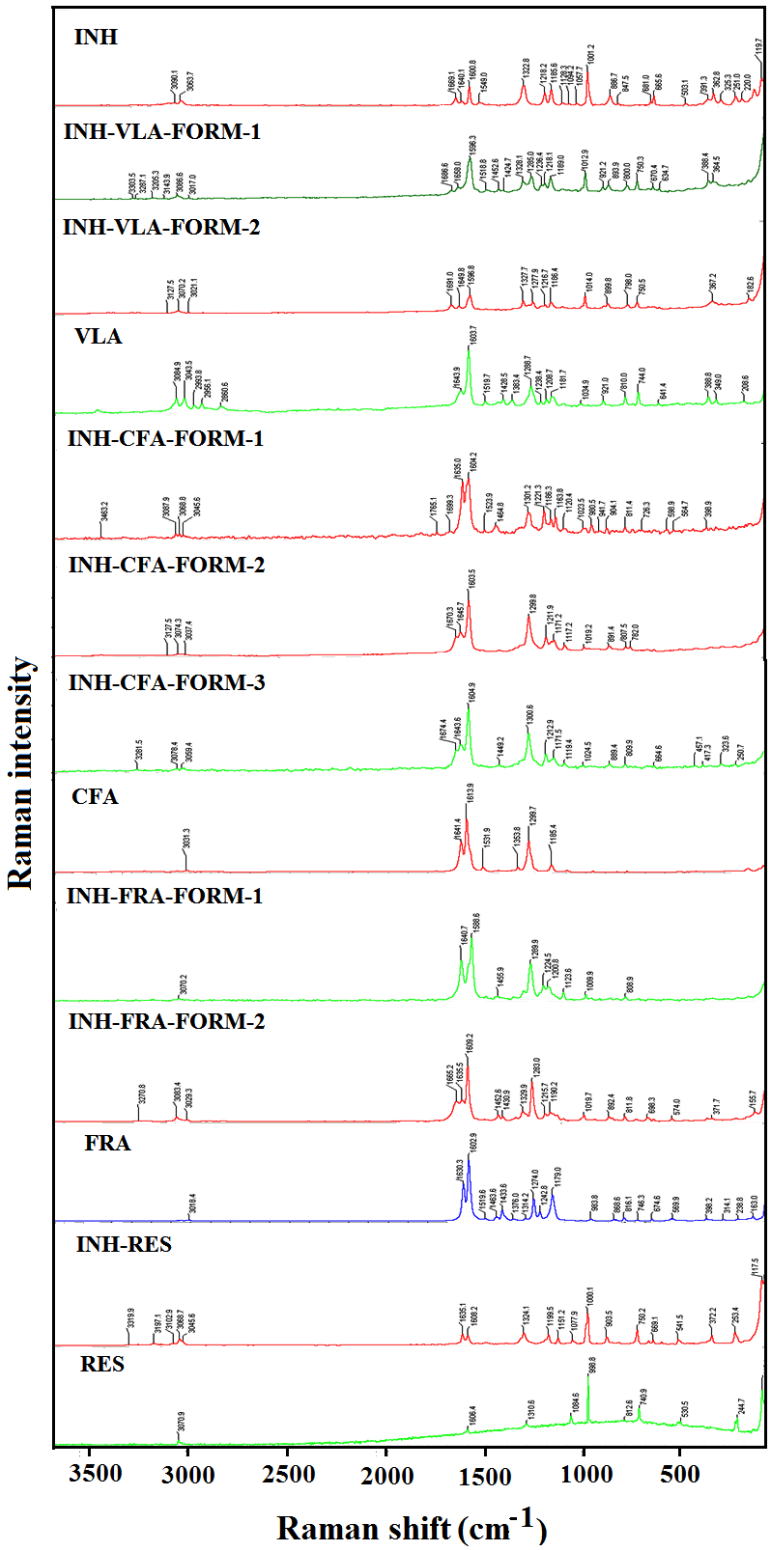

Figure 2.15 FT-Raman spectra of INH cocrystals.

Table 2.4 List of Raman stretching frequencies of INH cocrystals and the starting materials.

Compound	NH (stretch) 1°	Carboxylic C=O (stretch)	Amide C=O (stretch)	O–H (stretch)	C-N (stretch)
INH	3090.1 3063.7	-	1669.1	-	1322.8
INH-VLA-Form-1	3086.6 3017.0	1658.0	1686.6	-	1328.1
INH-VLA-Form-2	3070.2 3021.1	1649.8	1691.0	-	1327.7
VLA	-	1643.9	-	2993.8	-
INH-CFA-Form-1	3087.9 3068.8	1635.0	1699.3	3045.6	1301.2
INH-CFA-Form-2	3074.3 3037.4	1645.7	1670.3	-	1299.8
INH-CFA-Form-3	3078.4 3059.4	1643.6	1674.4	-	1300.6
CFA	-	1641.4	-	3031.3	-
INH-FRA-Form-1	3071.2 -	1640.7	-	-	1289.9
INH-FRA-Form-2	3083.4 3029.3	1635.5	1665.2	-	1329.9
FRA	-	1630.3	-	3018.4	-
INH-RES	3102.9 3068.7	-	1635.1	3045.6	1324.1
RES	-	-	-	3070.9	-

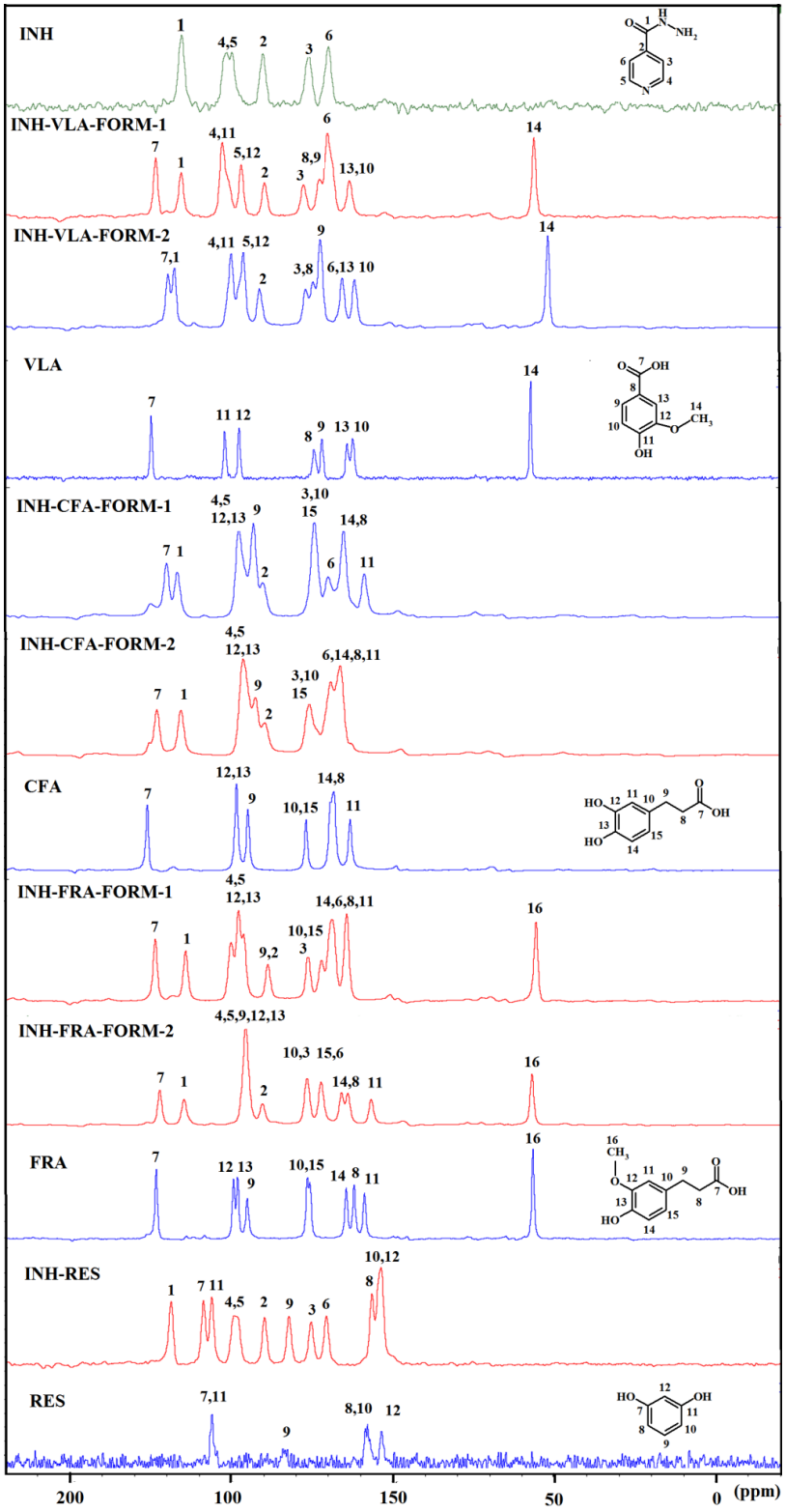

Figure 2.16 ^{13}C ss-NMR spectra of INH cocrystals compared to the API and the coformers.

Carbon No.	INH	INH-VLA-Form-1	VLA	INH-VLA-Form-2	INH-CFA-Form-1	CFA	INH-CFA-Form-2	INH-FRA-Form-1	FRA	INH-FRA-Form-2	INH-RES	RES
1	163.5	163.7	-	166.5	166.6	-	165.0	164.0	-	164.5	168.5	-
2	138.8	138.4	-	140.4	140.1	-	139.1	138.6	-	140.3	139.6	-
3	124.7	126.4	-	124.0	124.1	-	125.3	126.2	-	126.4	125.2	-
4	149.8	151.2	-	149.1	147.5	-	145.8	146.1	-	145.4	149.0	-
5	148.2	145.4	-	145.4	147.5	-	145.8	146.1	-	145.4	149.0	-
6	118.7	119.1	-	115.1	119.9	-	118.7	118.8	-	122.1	120.5	-
7	-	171.5	173.5	168.5	169.9	175.4	172.5	173.4	173.1	172.0	158.5	155.8
8	-	122.5	123.4	126.3	115.1	117.8	118.7	118.8	111.9	113.8	106.4	108.4
9	-	122.5	121.0	121.8	143.0	144.3	142.0	138.6	144.9	145.4	132.1	133.3
10	-	112.4	111.5	111.3	124.1	126.3	125.3	126.2	126.4	126.4	103.6	107.7
11	-	151.2	151.0	149.1	108.7	112.7	115.8	114.2	108.7	106.6	155.9	155.8
12	-	145.4	146.4	145.4	147.5	147.8	145.8	150.0	149.2	145.4	103.6	103.4
13	-	112.4	113.2	115.1	147.5	147.8	145.8	147.7	147.9	145.4	-	-
14	-	56.0	56.8	52.1	115.1	118.7	118.7	122.0	114.3	115.8	-	-
15	-	-	-	-	124.1	126.3	125.3	126.2	125.6	122.1	-	-
16	-	-	-	-	-	-	-	55.6	56.5	56.8	-	-

Table 2.5 ^{13}C ss-NMR chemical shifts (δ, ppm) of INH cocrystals.

2.4.4 Thermal Analysis

Differential scanning calorimetry (DSC) is the most widely used method for thermal analysis. DSC of INH commercial material showed a single melting endotherm at 171 °C without any phase transition. All the novel solid phases were prepared by LAG, and the resulting bulk material was used for DSC analysis (recorded from 30 to 300 °C) to observe phase transitions and melting point. The melting point of the cocrystal was different from that of the starting components (Table 2.6). The ground material of INH and RES (INH-RES cocrystal as confirmed by single crystal XRD) shows a unique melting endotherm by DSC at 114.4 °C, a value that is intermediate between the API and the coformer (110 °C). We did not observe any polymorphic behavior of this cocrystal. DSC of INH-VLA-Form-1 showed melting endotherm at 144.4 °C and immediately followed by recrystallization to the second polymorph (Form-2) which melts at 152.3 °C. It is difficult to say whether an enantiotropic or monotropic relationship is present between polymorphs of INH-VLA which exhibit a melting followed by crystallization behavior[42a] for Form-1 by applying the classic Burger-Ramburger rules.[42b,42c] The recent tutorial by Threlfall[42a] is an excellent cautionary note on overinterpretation of thermal data to deduce stability relationship of polymorphs. In a separate experiment on INH-VLA-Form-2, a single melting endotherm was observed at 153.2 °C. Further to visualize whether the conversion of Form-1 to 2 is a solid-to-solid or solid-liquid-solid transformation, we performed Hot-stage microscopy (HSM) measurements on Form-1 (Figure 2.17). The microscopy images show morphological changes and then melting at 140 °C, which means that the first endotherm in DSC for Form-1 is associated with melting, and then crystallization to Form-2 at 142-144 °C, and last immediate melting of Form-2 at 147 °C. The DSC of INH-FRA-Form-1 showed a endothermic transition at 129 °C which was ascribed to phase transformation of Form-1 to Form-2, and the melting endotherm at 154 °C corresponds to that for Form-2. However, the heating curve of INH-FRA-Form-2 did not show any phase transition before melting at 153.1 °C. This form conversion was also supported by VT-PXRD experiments in which INH-FRA-Form-1 converts to Form-2 at 125-130 °C (Figure 2.12). HSM experiments on Form-1 (Figure 2.18) showed a solid-to-solid phase transition at 126-127 °C, and conversion to Form-2, and then melting of the latter polymorph at 148 °C, similar to the observations in DSC. On the basis of the Burger and Ramberger's heat of transition rule,[37] there is an

endothermic phase transition before melting, and hence INH-FRA polymorphs are enantiotropically related. DSC measurements show that as Form-1 undergoes endothermic phase transition to Form-2, it is the stable phase below the transition point, and Form-2 is the stable modification above the transition point. Similar to INH-FRA-Form-1, DSC on INH-CFA-Form-1 also exhibited an endothermic phase transition at 150.1 °C and then conversion to Form-2, and melting of the latter solid at 168.4 °C. Since the transition endotherm is very close to the melting endotherm, we could not visualize the phase changes by HSM of Form-1, which instead showed direct melting. DSC of Form-2 did not show any phase transition before melting at 168.0 °C. Hence both Form-1 and 2 of INH-CFA are enantiotropically related by the heat of transition rule. In a separate experiment on Form-3, a melting endotherm was observed at 165.8 °C without any phase transition as in the case of Form-2. The higher melting Form-2 has the higher heat of fusion, and hence by the heat of fusion rule Form-2 and -3 are monotropically related. The characteristic melting profiles of all the cocrystals are shown in DSC thermograms (Figure 2.19).

Table 2.6 Melting Point of INH Cocrystals.

drug/ coformer	Mp of coformer (°C)	cocrystal/ cocrystal polymorphs	M.p. of cocrystal/ cocrystal polymorph (°C)
INH	171	-	-
VLA	210–213	INH-VLA-Form-1	144.4
VLA	210–213	INH-VLA-Form-2	153.2
CFA	223–225	INH-CFA-Form-1	-
CFA	223–225	INH-CFA-Form-2	168.0
CFA	223–225	INH-CFA-Form-3	165.8
FRA	168–172	INH-FRA-Form-1	-
FRA	168–172	INH-FRA-Form-2	153.1
RES	110	INH-RES	114.4

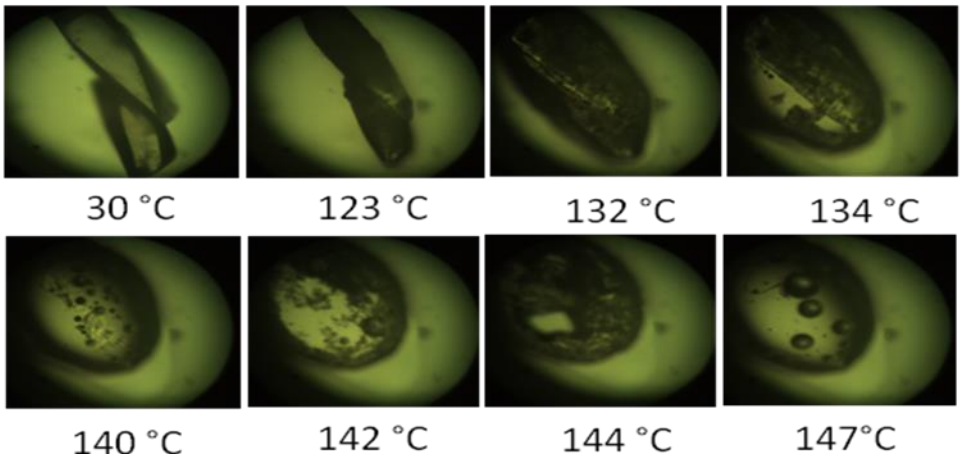

Figure 2.17 HSM snapshot of INH-VLA-Form-1 shows significant morphological changes in which melting of Form-1 (at 140 °C) and recrystallization to Form-2 (at 142-144 °C) is seen.

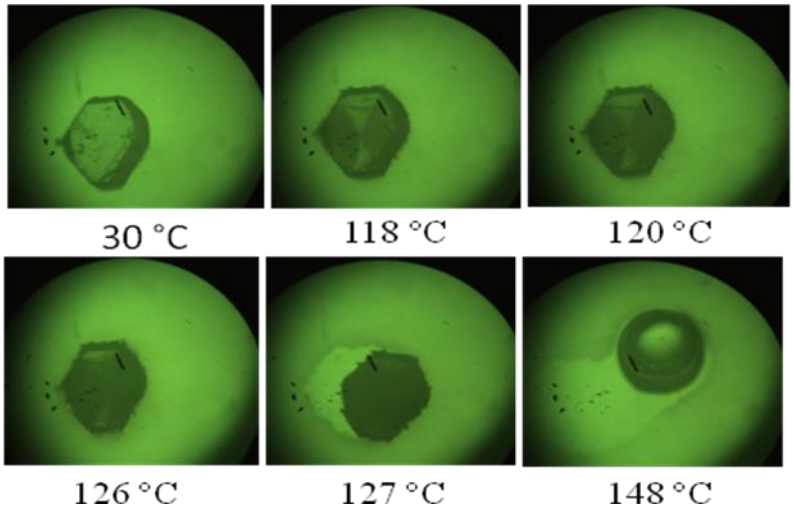

Figure 2.18 HSM snapshots of INH-FRA-Form-1 shows phase transition at 126–127 °C to Form-2. The morphological changes are seen in the images.

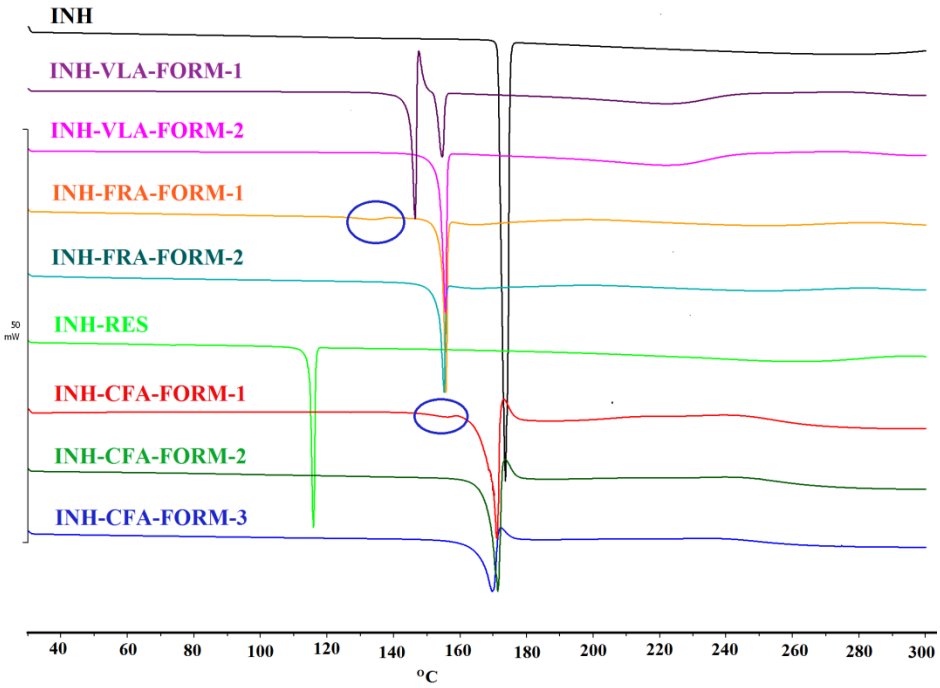

Figure 2.19 DSC heating curves of INH and its cocrystals exhibit unique melting behavior. The blue circles indicate phase transition associated with the very minor endotherm peak.

2.4.5 Slurry and Grinding

The stability of the cocrystals was first verified in selected solvent systems because phase stability studies on polymorphs can be carried out only if the cocrystal is stable in that medium. In most cases, slurry grinding of the cocrystal in a particular solvent system resulted in the precipitation of the less soluble component of the cocrystal (usually the API) due to incongruent solubilities of the components. The same was observed for INH cocrystals when slurry grinding was attempted in water. Several solvents from non-polar to polar solvent systems were screened for cocrystal stability by slurring. These experiments suggested that INH-FRA and INH-VLA are stable in MeOH/EtOAc solvent medium for slurry grinding and competition experiments. The pure polymorphs were exposed to the slurry conditions as well as a mixture of Form 1 and 2 in 1:1 ratio. Pure Form-1 completely converted to Form-2 for both cocrystals INH-VLA and INH-FRA after 24 h, and in competitive slurry experiments the transformation was slightly faster (Figure 2.20 and 2.21). In contrast, pure Form 2 was stable under the same slurry conditions for both cocrystals in separate experiments for up to 3 days. Thus, Form-2 is the stable modification and the thermodynamic phase of INH-VLA and INH-

FRA. Similarly, slurry experiments on trimorphs of INH-CFA in the EtOH/THF solvent medium showed the conversion of pure Form-2 and Form-3 in separate batches to Form-1 after 5 days and 1 day, respectively. Competitive slurry of Form-1 and -2 (1:1 mixture) also converted to Form-1 after 4 days, and Form-1 and Form-3 mixture (1:1) converted to pure Form-1 after 8 h (Figures 2.22 and 2.23). Lastly, the slurry of Form-1 did not show any phase change, confirming that INH-CFA-Form-1 is the thermodynamic state.

The stability relationship found in slurry experiments was cross-checked by performing mechanochemical grinding experiments. Neat grinding (NG)/LAG of INH and FRA in a 1:1 stoichiometric ratio initially resulted in metastable Form-1 after 45 min (Figure 2.27). Further grinding of Form-1 completely converted it to Form-2 (monitored by PXRD). Such polymorphic transformations are reported,[43] and in accordance with Ostwald's law of stages:[44] the metastable polymorph appears first followed by the stable polymorph which grows at the expense of the transient species. Extended NG/LAG on INH-FRA-Form-2 and INH-VLA-Form-2 did not show any effect, but under similar experimental conditions INH-VLA-Form-1 completely converted to Form-2 (Figure 2.24). Hence, Form-1 of both cocrystals INH-FRA and INH-VLA are metastable and Form-2 is the stable polymorph. Crystal structure analysis also shows that the stability of the Form-2 compared to Form-1 may be a result of the hydroxy-pyridine heterosynton between INH and VLA in Form-1 compared to the stronger acid-pyridine O–H···N H-bond in Form-2. Similarly, NG/LAG of INH-CFA cocrystal (Form-2 and -3) converted them to Form-1 (Figures 2.25 and 2.26), whereas extended grinding under similar conditions did not show any effect on Form-1. Hence, from slurry and grinding experiments the stability order of cocrystals follows Form-1 < Form-2 (for INH-FRA), Form-1 < Form-2 (INH-VLA), and Form-3 < Form-2 < Form-1 (INH-CFA).

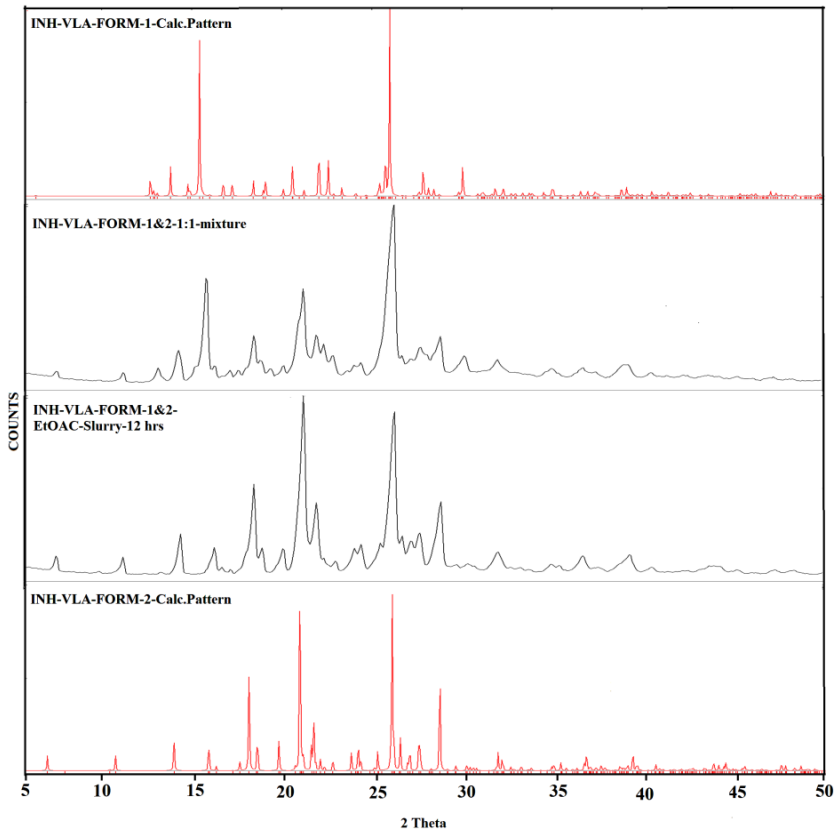

Figure 2.20 Overlay of the experimental PXRD of 1:1 mixture of INH-VLA-Form-1 and Form-2 (2nd from top) along with the experimental PXRD of Form-2, obtained after slurry grinding the mixture in EtOAC for 12 hrs (3rd from top). The calculated patterns of Form-1 and Form-2 are shown for comparison.

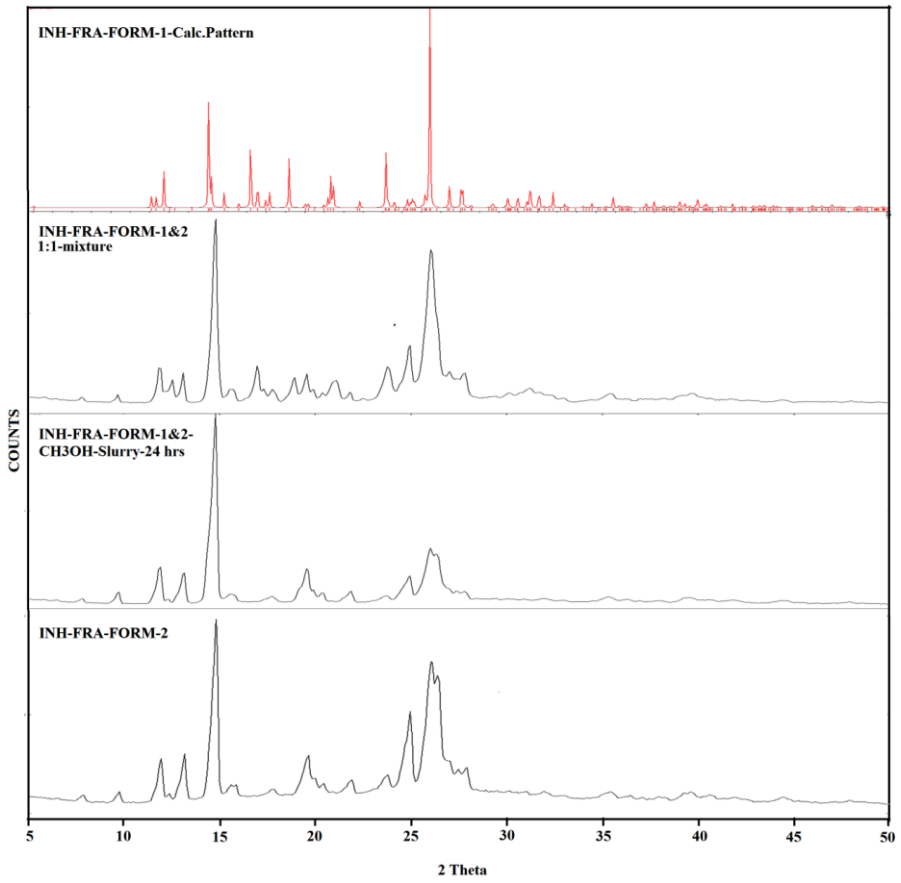

Figure 2.21 Overlay of experimental PXRD pattern of 1:1 mixture of INH-FRA-Form-1 and Form-2 (2nd from top) with the experimental PXRD of Form-2, obtained after slurry grinding the mixture in MeOH for 24 h (3rd from top). The calculated pattern of Form-1 (top) and the experimental pattern of Form-2 (bottom) for comparison.

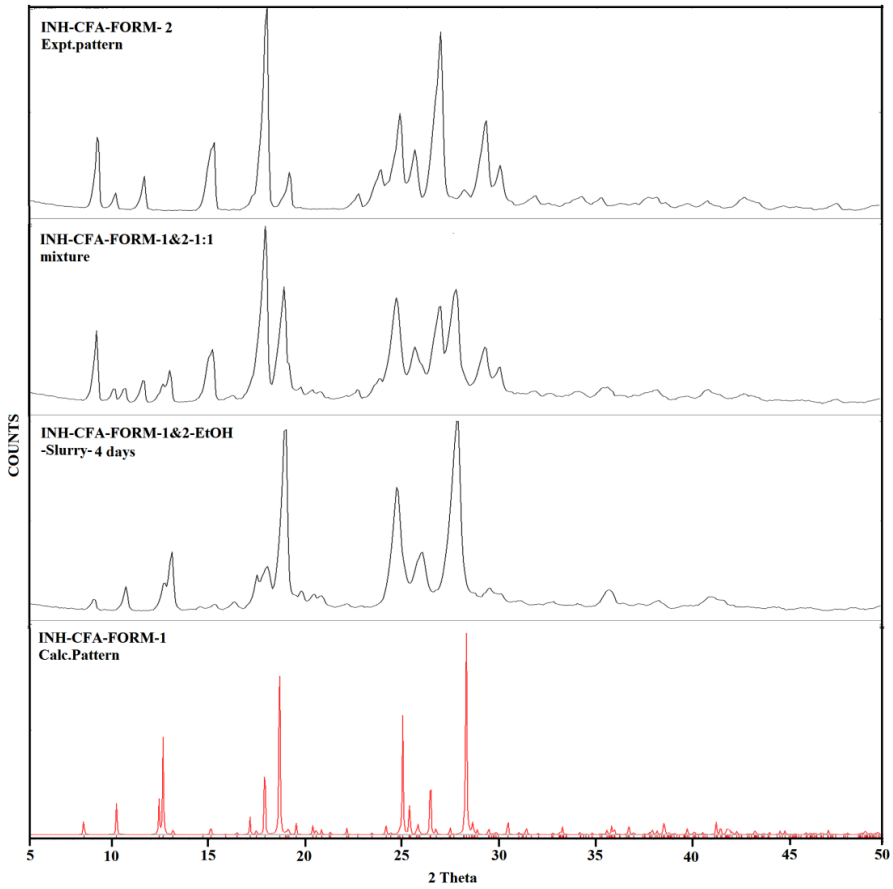

Figure 2.22 Overlay of the experimental PXRD of 1:1 mixture of INH-CFA-Form-1 and Form-2 (2nd from top) with the experimental PXRD of Form-1, obtained after slurry grinding the mixture in EtOH for 5 days (3rd from top). The experimental pattern of Form-2 (top) and the calculated pattern of Form-1 are shown for comparison (bottom).

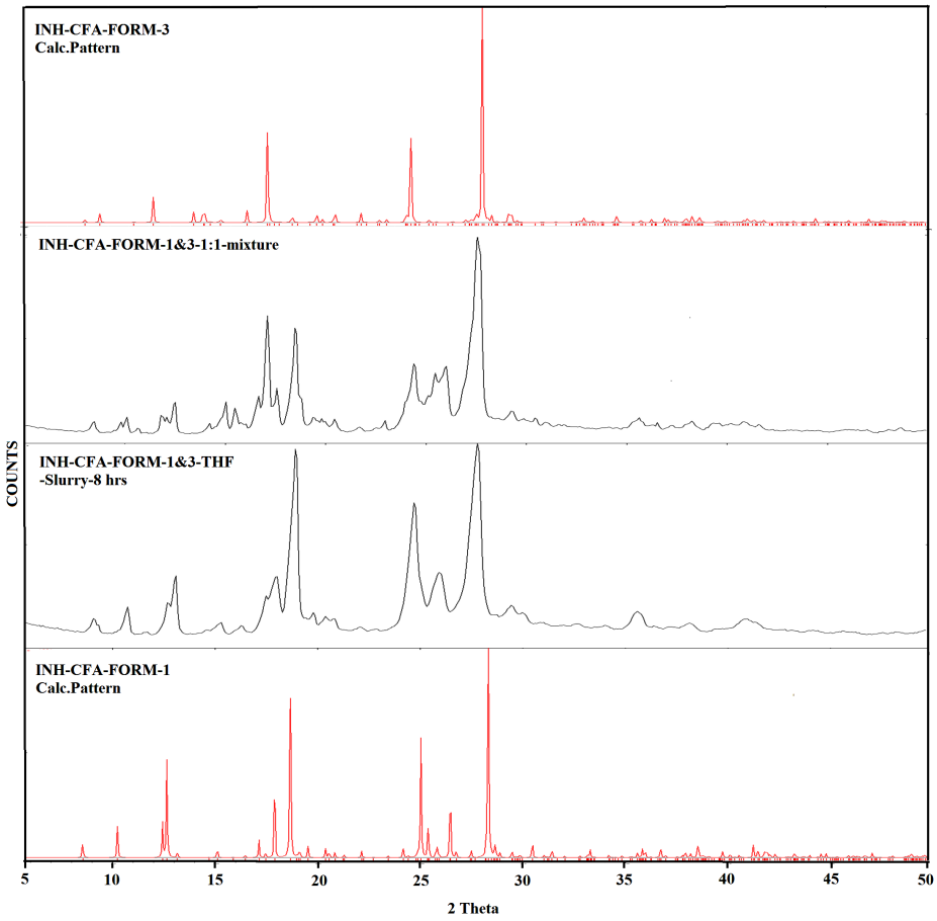

Figure 2.23 Overlay of experimental PXRD pattern of 1:1 mixture of INH-CFA-Form-1 and Form-3 (2nd from top) with the experimental PXRD of Form-1, obtained after slurry grinding the mixture in THF for 8 h (3rd from top). The calculated line pattern of Form-3 and Form-1 are shown for comparison.

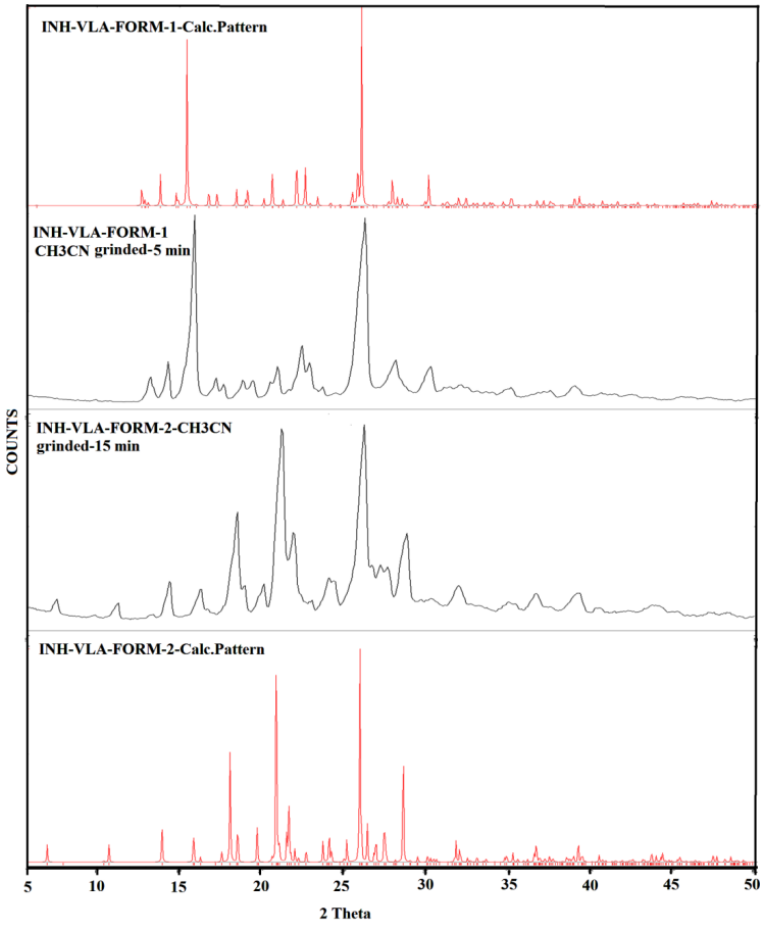

Figure 2.24 Overlay of calculated PXRD pattern of INH-VLA-Form-1 (top) with the experimental PXRD matching with Form-2 obtained after CH_3CN assisted-grinding of Form-1 for 15 min (3rd from top). The calculated patterns of Form-1 and Form-2 are shown for comparison.

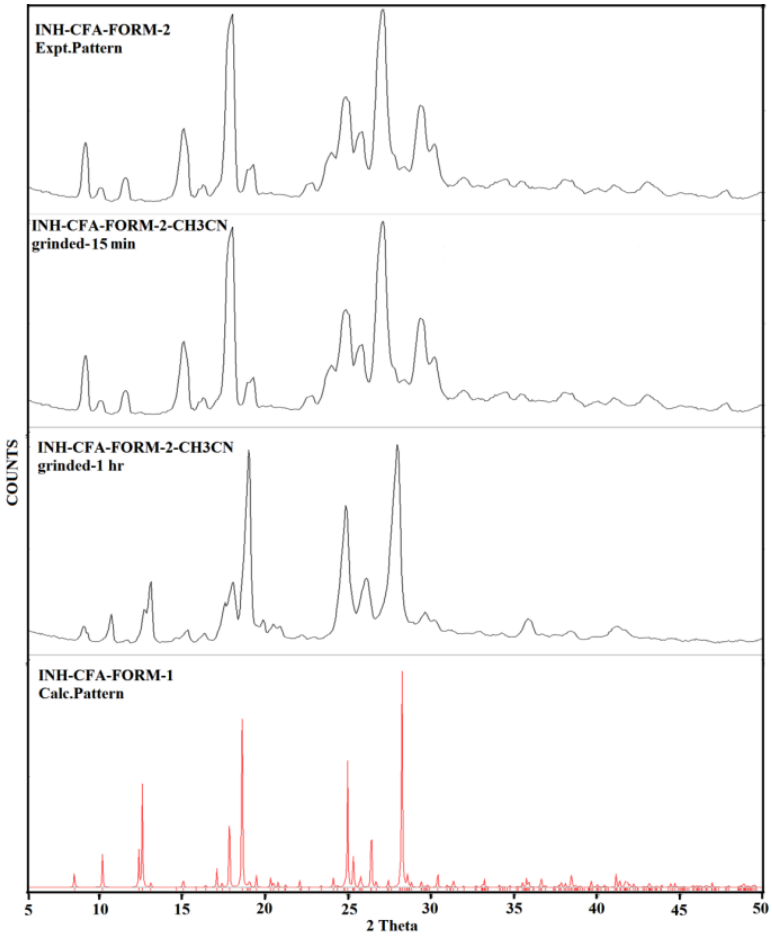

Figure 2.25 Overlay of experimental PXRD pattern of INH-CFA-Form-2 (top) with the experimental PXRD of Form-1 obtained after CH_3CN assisted grinding of Form-2 for 1 h (3rd from top). The experimental pattern of Form-2 (top) and the calculated pattern of Form-1 (bottom) are shown for comparison.

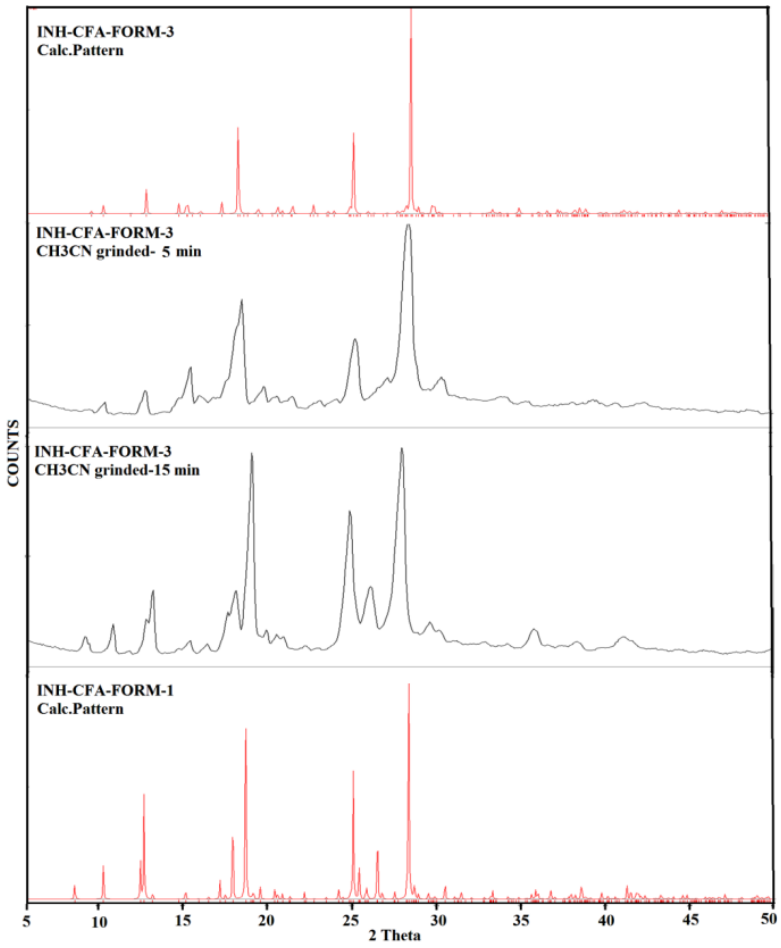

Figure 2.26 Overlay of calculated PXRD pattern of INH-CFA-Form-3 (top) with the experimental PXRD of Form-1 obtained after CH_3CN assisted grinding of Form-3 for 15 min (3^{rd} from top). The calculated patterns of Form-3 and Form-1 are shown for comparison.

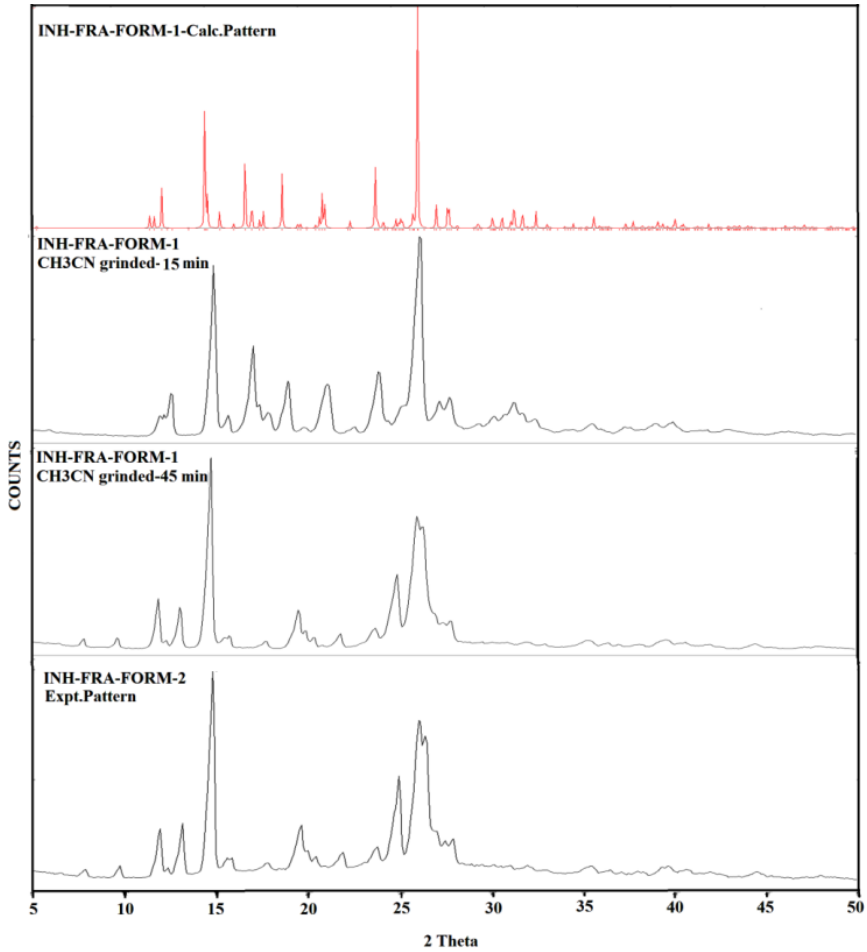

Figure 2.27 Overlay of calculated PXRD pattern of INH-FRA-Form-1 (top) with the experimental PXRD of Form-2 obtained after CH_3CN assisted grinding of Form-1 for 45 min (3rd from top). The calculated pattern of Form-1 (top) and the experimental pattern of Form-2 (bottom) are shown for comparison.

2.4.6 Polymorph Stability

All the APIs used in the FDC are individually stable at ambient conditions, but in the combination the stability of the INH is a serious problem. In view of the chemical degradation of INH, stability of the cocrystals was studied in our work by slurry, grinding, and storage of the cocrystals at accelerated ICH conditions. Cocrystals have the potential in tuning not only solubility, dissolution, and bioavailability of APIs but also stability, color, and tableting.[45,18,19] The cocrystals were found to be stable in ambient conditions of Hyderabad (35 °C and 40% RH) for more than one year. Further, they were tested for form stability in accelerated conditions of 40 °C and 75% RH.[46] The cocrystals did not exhibit any polymorphic change or hydrate formation in the test period of six

months. The only exception was INH–RES which dissociated to its staring materials after one month (see PXRD in Figure 2.28). The results are summarized in Table 2.7.

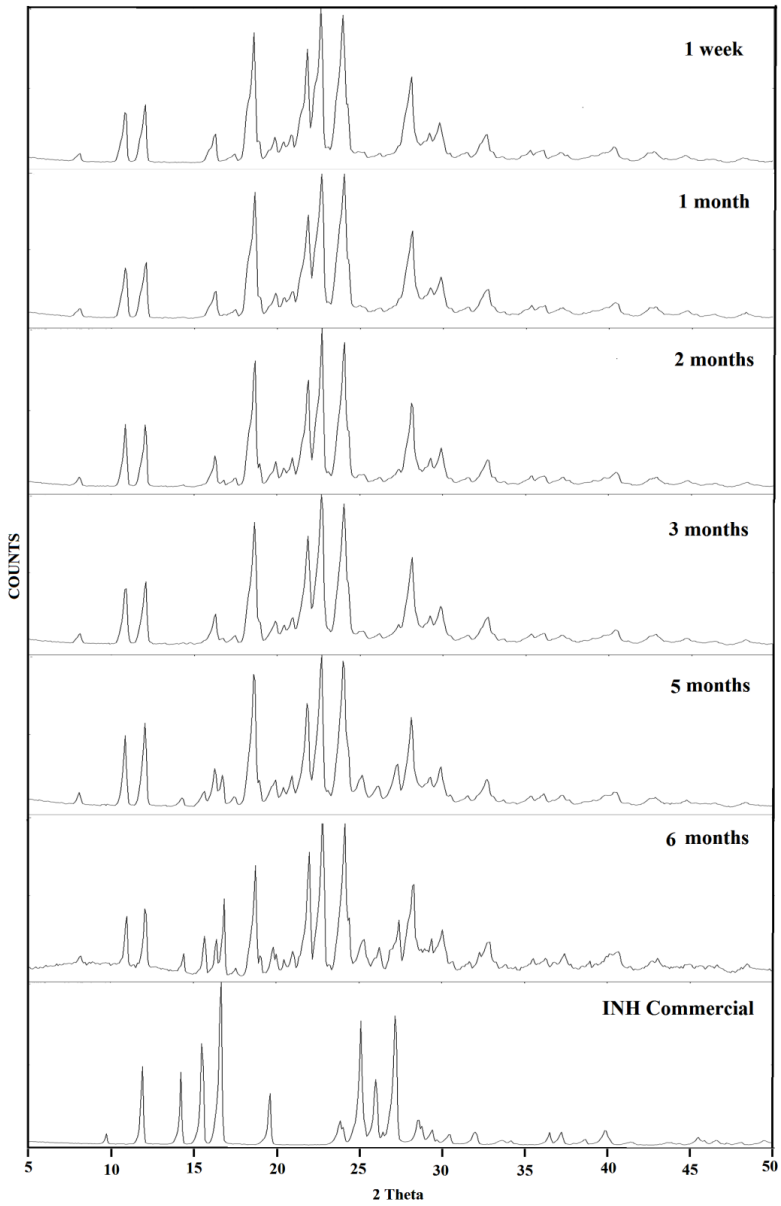

Figure 2.28 Stability study at 40 °C and 75% RH of INH-RES cocrystal. Peaks corresponding to INH start appearing after 2 months and the cocrystal is not stable in accelerated ICH conditions.

Table 2.7 Stability of Isoniazid cocrystal forms under ICH Conditions of 40 °C and 75% RH[a].

compound	1 M	2 M	3 M	4 M	5 M	6 M
INH	√	√	√	√	√	√
INH-VLA-Form-1	√	√	√	√	√	√
INH-VLA-Form-2	√	√	√	√	√	√
INH-CFA-Form-1	√	√	√	√	√	√
INH-CFA-Form-2	√	√	√	√	√	√
INH-CFA-Form-3	√	√	√	√	√	√
INH-FRA-Form-1	√	√	√	√	√	√
INH-FRA-Form-2	√	√	√	√	√	√
INH-RES	√	×	×	×	×	×

[a]M = month, √ = no phase change/no hydrate formation, × = dissociation.

2.5 Conclusions

Isoniazid is one of the key APIs used in fixed-dose combination FDC to treat tuberculosis. In this chapter we have reported novel cocrystal forms of INH with pharmaceutically acceptable coformers. The main goal of this work was to obtain stable solid forms of INH, because the stability of INH in the FDC is one of the major concerns in the current-day formulation. Hence novel solid forms of INH were prepared using conventional screening techniques such as LAG and solvent evaporative crystallization with selected GRAS coformers which resulted in four cocrystals (INH-VLA, INH-FRA, INH-CFA and INH-RES). All the cocrystals (INH-VLA dimorphic; INH-FRA dimorphic; INH-CFA trimorphic) exhibited polymorphic behavior except INH-RES in our study. The cocrystal forms were characterized by thermal, spectroscopic and X-ray diffraction techniques. Structural comparison shows significant differences in the hydrogen bonding patterns and all the cocrystals were sustained the by robust acid–pyridine synthon, except INH-VLA-Form-1 and INH-FRA-Form-1 in which hydroxyl–pyridine synthon was observed. Single crystal X-ray diffraction and XPac analysis showed 2D isostructurality between INH-VLA-Form-1 and INH-FRA-Form-1. On basis of slurry and grinding techniques, we established that Form-2 of INH-FRA and INH-VLA and Form-1 of the INH-CFA is the thermodynamic form of that cocrystal. These cocrystal forms were stable in ambient temperature and humidity conditions for up to one year. Further these solid forms were tested in accelerated ICH conditions of 40 ºC and 75% RH, and it was found that all the solid forms were stable for a test period of six months except INH-RES cocrystal which was found to dissociate into the starting

components after one month. Slurry crystallization, powder grinding, and stability experiments suggest that Form-2 of INH-FRA and INH-VLA and Form-1 of INH-CFA are potential cocrystals for a stable INH solid form. These screening results suggest that to obtain the optimal solid form of an API for improved pharmaceutical formulation, a comprehensive polymorph screen on the cocrystals should be as broad as that one would generally perform on single component crystals.

2.6 Experimental Section

Materials and Methods

Isoniazid was purchased from Sigma-Aldrich and used without further purification. The coformers (purity >99.8%) also were purchased from Sigma-Aldrich. All other chemicals were of analytical or chromatographic grade. Water purified from a deionizer-cum-mixed-bed purification system (AquaDM, Bhanu, Hyderabad, India) was used in the experiments.

Preparation of Isoniazid Cocrystals

INH-FRA-Form-1 (1:1)

This form was obtained upon grinding about 100 mg of a 1:1 stoichiometric ratio of INH and FRA for 30 min by CH_3CN liquid-assisted grinding. The formation of cocrystal was confirmed by FT-IR, FT-Raman, ^{13}C ss-NMR, PXRD, and DSC. 30 mg of the ground material was dissolved in 6 Ml of hot CH_3CN: $CHCl_3$ (1:1, v/v) and left for slow evaporation at room temperature. Light yellow colour block crystals suitable for X-ray diffraction were obtained after 3-4 days upon solvent evaporation.

INH-FRA-Form-2 (1:1)

INH–FRA-Form-2 was obtained upon extended grinding of INH-FRA-Form-1 for 45 min by liquid-assisted grinding (CH_3CN solvent). Bulk material of Form-2 can also be obtained upon heating of Form-1 at 130 °C for 30 min. The formation of Form-2 was confirmed by FT-IR, FT-Raman, ^{13}C ss-NMR, PXRD, DSC, and ^{1}H NMR. Attempts to crystallize the compound in ethanol, CH_3CN, THF, nitromethane, toluene, acetone, and also a mixture of solvents gave polycrystalline powders, but no diffraction quality single

crystals were obtained. Stoichiometry of the cocrystal was confirmed through ^{1}HNMR recorded in DMSO-d6 solvent.

^{1}H NMR (DMSO-d_6, 400MHz) δ ppm: 9.5 (1 H, s), 8.7 (2 H, dd, *J* 1.6Hz, *J* 4.4Hz), 7.7 (2 H, dd, *J* 1.6Hz, *J* 4.4Hz), 7.5 (1 H, d, *J* 16Hz), 7.3 (1 H, d, *J* 2Hz), 7.1 (1 H, dd, *J* 1.6Hz, *J* 8Hz), 6.8 (1 H, d, *J* 8Hz), 6.3 (1 H, d, *J* 15.6Hz), 3.8 (3 H, s).

INH-VLA-Form-1 (1:1)

This form was obtained upon grinding about 100 mg of a 1:1 stoichiometric ratio of INH and VLA for 30 min with CH_3CN liquid-assisted grinding. The formation of cocrystal was confirmed by FT-IR, FT-Raman, ^{13}C ss-NMR, PXRD, and DSC. 30 mg of the ground material was dissolved in 6 mL of hot EtOAc: CH_3NO_2 and left for slow evaporation at room temperature. Light brown colour block crystals suitable for X-ray diffraction were obtained after 3-4 days upon solvent evaporation.

INH-VLA-Form-2 (1:1)

INH-VLA-Form-2 was obtained upon further grinding of INH-VLA-Form-1 for 15 min with CH_3CN liquid-assisted grinding. The formation of Form-2 was confirmed by FT-IR, FT-Raman, ^{13}C ss-NMR, PXRD and DSC. 30 mg of the ground material was dissolved in 6 Ml of hot anisole: isopropanol and left for slow evaporation at room temperature. Colorless needle crystals suitable for X-ray diffraction were obtained after 3-4 days upon solvent evaporation.

INH-CFA-Form-1 (1:1)

The bulk material of INH-CFA-Form-1 was obtained upon extensive grinding of INH-CFA-Form-2 for 1-2 h by adding catalytic amount of CH_3CN solvent. The formation of cocrystal was confirmed by FT-IR, FT-Raman, ^{13}C ss-NMR, PXRD, and DSC. 30 mg of the ground material was dissolved in 8 mL of hot THF: n-heptane (1:1, v/v) and left for slow evaporation at room temperature. Colorless plate crystals suitable for X-ray diffraction were obtained after 3-4 days upon solvent evaporation.

INH-CFA-Form-2 (1:1)

INH-CFA-Form-2 was obtained upon grinding about 100 mg of a 1:1 stoichiometric ratio of INH and CFA for 40 min by liquid-assisted grinding (CH_3CN solvent). The formation of cocrystal was confirmed by FT-IR, FT-Raman, ^{13}C ss-NMR, PXRD, and DSC. Numerous crystallization experiments in ethanol, CH_3CN, THF, nitromethane, toluene, acetone, and also a mixture of solvents gave polycrystalline powders, but no diffraction quality single crystals were obtained. Stoichiometry of the cocrystal was confirmed through ^1H NMR recorded in DMSO-d_6 solvent.

^1H NMR (DMSO-d_6, 400MHz) δ ppm: 9.5 (1 H, s), 9.1 (1 H, s), 8.7 (2 H, dd, *J* 1.6Hz, *J* 4.4Hz), 7.7 (2 H, dd, *J* 1.6Hz, *J* 4.4 Hz), 7.4 (1 H, d, *J* 15.6 Hz), 7.0 (1 H, d, *J* 1.6Hz), 6.9 (1 H, dd, *J* 2Hz, *J* 8Hz), 6.7 (1 H, d, *J* 8Hz), 6.1 (1 H, d, *J* 15.6 Hz).

INH-CFA-Form-3 (1:1)

INH-CFA-Form-3 was serendipitously obtained upon crystallizing the ground material of INH and CFA in 8 mL of hot xylene: methanol (1:1, v/v) solvent mixture. Light brown color block crystals suitable for X-ray diffraction were obtained after 3-4 days upon solvent evaporation. Form-3 bulk material was obtained upon slow evaporation of 1:1 stoichiometric ratio of INH and CFA from chlorobenzene: methanol (1:1, v/v) solvent mixtures after 3-4 days. The formation of INH-CFA-form-3 was confirmed by FT-IR, FT-Raman, PXRD, and DSC.

INH-RES (1:1)

INH–RES cocrystal was obtained upon grinding about 100 mg of a 1:1 stoichiometric ratio of INH and RES for 30 min by CH_3CN liquid-assisted grinding. The formation of cocrystal was confirmed by FT-IR, FT-Raman, ^{13}C ss-NMR, PXRD, and DSC. 30 mg of the ground material was dissolved in 8 mL of hot CH3NO2 (1:1, v/v) and left for slow evaporation at room temperature. Light yellow colour needle-shape crystals suitable for X-ray diffraction were obtained after 3-4 d upon solvent evaporation.

Vibrational Spectroscopy

Thermo-Nicolet 6700 Fourier transform infrared spectrophotometer with NXR-Fourier transform Raman module (Thermo Scientific, Waltham, Massachusetts) was used to record IR and Raman spectra. IR spectra were recorded on samples dispersed in KBr

pellets. Raman spectra were recorded on samples contained in standard NMR diameter tubes or on compressed samples contained in a gold-coated sample holder. Data were analyzed using the Omnic software (Thermo Scientific, Waltham, Massachusetts).

Solid-State NMR Spectroscopy

Solid-state ^{13}C NMR (ss-NMR) spectroscopy provides structural information about differences in hydrogen bonding, molecular conformations, and molecular mobility in the solid state.[40] The solid-state ^{13}C NMR spectra were obtained on a Bruker Ultrashield 400 spectrometer (Bruker BioSpin, Karlsruhe, Germany) utilizing a ^{13}C resonant frequency of 400 MHz (magnetic field strength of 9.39 T). Approximately 100 mg of crystalline sample was packed into a zirconium rotor with a Kel-F cap. The crosspolarization, magic angle spinning (CP-MAS) pulse sequence was used for spectral acquisition. Each sample was spun at a frequency of 5.0 ± 0.01 kHz, and the magic angle setting was calibrated by the KBr method. Each data set was subjected to a 5.0 Hz line broadening factor and subsequently Fourier transformed and phase corrected to produce a frequency domain spectrum. The chemical shifts were referenced to TMS using glycine (δglycine = 43.3 ppm) as an external secondary standard.

Differential Scanning Calorimetry (DSC)

DSC was performed on a Mettler Toledo DSC 822e module. Samples were placed in crimped but vented aluminum sample pans. The typical sample size was 3-4 mg, and the temperature range was 30-300 °C @ 5 °C min^{-1}. Samples were purged by a stream of dry nitrogen flowing at 80 mL min^{-1}.

X-ray Crystallography

X-ray reflections for all the cocrystal forms of INH were collected at 298 K on Oxford Xcalibur Gemini Eos CCD diffractometer using Mo−Kα radiation (λ = 0.7107 Å) except INH-CFA-Form-1 and INH-CFA-Form-3. Data reduction was performed using CrysAlisPro (version 1.171.33.55),[47] and OLEX2-1.0[48] was used to solve and refine the structures. X-ray reflections for both INH-CFA-Form-1 and INH-CFA-Form-3 cocrystal forms were collected at 100 K on Bruker SMART-APEX CCD diffractometer equipped with a graphite monochromator and Mo-Kα fine-focus sealed tube (λ = 0.71073 Å). Data

reduction was performed using Bruker SAINT Software.[49] Intensities were corrected for absorption using SADABS,[50] and the structure was solved and refined using SHELX-97.[51] All non-hydrogen atoms were refined anisotropically. Hydrogen atoms on heteroatoms were located from difference electron density maps, and all C−H hydrogens were fixed geometrically. Hydrogen bond geometries were determined in Platon.[52] X-Seed[53] was used to prepare packing diagrams.

Powder X-ray Diffraction

Powder X-ray diffraction of all the samples were recorded on Bruker D8 Advance diffractometer (Bruker-AXS, Karlsruhe, Germany) using Cu-Kα X-radiation (λ = 1.5406 Å) at 40 kV and 30 mA power. X-ray diffraction patterns were collected over the 2θ range 5-50° at a scan rate of 1º min^{-1}. Powder Cell 2.4[54] was used for Rietveld refinement of experimental PXRD and calculated lines from the X-ray crystal structure.

2.7 References

1. (a) Bernstein, J. *Polymorphism in Molecular Crystals*; Clarendon, Oxford, U. K., **2002**. (b) Fabbiani, F.; Allan, D.; Parsons, S.; Pulham, C. *CrystEngComm* **2005**, *7*, 179–186. (c) Sanphui, P.; Goud, N. R.; Khandavilli, U.; Bhanoth, S.; Nangia, A. *Chem. Commun.***2011**, *47*, 5013–5015. (d) Haleblian, J.; McCrone, W. *J. Pharm. Sci.* **1969**, *58*, 911–929.
2. (a) Serajuddin, A. T. M. Adv. *Drug Delivery Rev.* **2007**, *59*, 603–616. (b) Berge, S. M.; Bighley, L. D.; Monkhouse, D. C. *J. Pharm. Sci.* **1977**, *66*, 1–19. (c) Bhatt, P. M.; Ravindra, N. V.; Banerjee, R.; Desiraju, G. R. *Chem. Commun.* **2005**, 1073–1075. (d) Thakuria, R.; Nangia, A. *CrystEngComm* **2011**, *13*, 1759–1764.
3. (a) Remenar, J. F.; Morissette, S. L.; Peterson, M. L.; Moulton, B.; MacPhee, J. M.; Guzmán, H. R.; Almarsson, Ö. *J. Am. Chem. Soc.* **2003**, *125*, 8456–8457. (b) Sanphui, P.; Goud, N. R.; Khandavilli, U. B. R.; Nangia, A. *Cryst. Growth Des.* **2011**, *11*, 4135–4145.(c) Almarsson, Ö.; Zaworotko, M. J. *Chem. Commun.* **2004**, 1889–1896. (d) Good, D. J.; Rodríguez-Hornedo, N. *Cryst. Growth Des.* **2009**, *9*, 2252–2264.

4. (a) Khankari, R. K.; Grant, D. J. W. *Thermochimica Acta* **1995**, *248*, 61–79. (b) Banerjee, R.; Bhatt, P. M.; Desiraju, G. R. *Cryst. Growth Des.* **2006**, *6*, 1468–1478. (c) Roy, S.; Goud, N. R.; Babu, N. J.; Iqbal, J.; Kruthiventi, A. K.; Nangia, A. *Cryst. Growth Des.* **2008**, *8*, 4343–4346.
5. (a) Sequeira, A.; Berkebile, C. A.; Hamilton, W. C. *J. Mol. Struct.* **1968,** *1*, 283–294. (b) Grimvall, S.; Wengelin, R. F. *J. Chem. Soc. A.* **1967**, 968–970. (c) Perumalla, S. R.; Sun, C. C. *CrystEnggComm* **2013,** *15*, 5756–5759. (d) Perumalla, S. R.; Sun, C. C. *CrystEngComm*, **2012,** *14*, 3851–3853. (e) Brittain, H. G. *Cryst. Growth Des.* **2010,** *10*, 1990–2003.
6. US-FDA GRAS chemical list, http://www.fda.gov/Food/IngredientsPackagingLabeling/FoodAdditivesIngredients/ucm091048.htm (accessed on 31 July, 2014).
7. (a) Craven, B. M.; Vizzini, E. A.; Rodrigues, M. M. *Acta Crystallogr., Sect. B* **1969,** *25*, 1978–1993. (b) David, W.I.F.; Shankland, K.; Pulham, C.R.; Blagden, N.; Davey, R.J.; Song, M. *Angew. Chem. Int. Ed.* **2005,** *44*, 7032 –7035. (c) Chandran, S. K.; Nath, N. K.; Roy, S.; Nangia, A. *Cryst. Growth Des.* **2008,** *8*, 140–154. (d) Thallapally, P. K.; Jetti, R. K.R.; Katz, A. K.; Carrell, H. L.; Singh, K.; Lahiri, K.; Kotha, S.; Boese, R.; Desiraju, G. R. *Angew. Chem. Int. Ed.* **2004,** *43*, 1149 –1155. (e) Rafilovich, M.; Bernstein, J. *J. Am. Chem. Soc.* **2006,** *128*, 12185–12191. (f) Crawford, S.; Kirchner, M. T.; Bläser, D.; Boese, R.; David, W. I. F.; Dawson, A.; Gehrke, A.; Ibberson, R. M.; Marshall, W. G.; Parsons, S.; Yamamuro, O. *Angew. Chem. Int. Ed.* **2009,** *48*, 755–757.
8. (a) Britton, D. Acta Cryst. *Acta Crystallogr., Sect. B* **2002,** *58*, 553–563. (b) Bowes, K. F.; Ferguson, G.; Lough, A. J.; Glidewell, C. *Acta Crystallogr., Sect. B* **2003,** *59*, 277–286. (c) Trask, A. V.; Motherwell, W. D. S.; Jones, W. *Cryst. Growth Des.* **2005,** *5*, 1013–1021. (d) Porter III, W. W.; Elie, S. C.; Matzger, A. J. *Cryst. Growth Des.* **2008,** *8*, 14–16. (e) Babu, N. J.; Reddy, L. S.; Aitipamula, S.; Nangia, A. *Chem. Asian. J.* **2008,** *3*, 1122–1133.
9. (a) Braga, D.; Palladino, G.; Polito, M.; Rubini, K.; Grepioni, F.; Chierotti, M. R.; R. Gobetto, R. *Chem. – Eur. J,* **2008**, *14*, 10149−10159. (b) Childs, S. L.; Hardcastle, K. I. *Cryst. Growth Des*, **2007**, *7*, 1291−1304. (c) Aitipamula, S.; Chow, P. S.; Tan, R. B. H. *Cryst. Growth Des*. **2010**, *10*, 2229−2238.
10. (a) Aitipamula, S.; Chow, P. S.; Tan, R. B. H. *CrystEngComm* **2014**, *16*, 3451–3465.

11. (a) McKellar, S. C.; Kennedy,A. R.; McCloy, N. C.; McBride, E.; Florence, A. J. *Cryst. Growth Des.* **2014,** 14, 2422−2430. (b) Seliger, J.; Žagar, V. *J. Phys. Chem. B,* **2014**, *118*, 996−1002. (c) Jung, S.; Ha, J.-M.; Kim, I. W. *Polymers* **2014**, *6*, 1−11. (d) Bevill, M. J.; Vlahova, P. I.; Smit, J. P. *Cryst. Growth Des*. **2014,** *14*, 1438−1448. (e) Madusanka, N.; Eddleston, M. D.; Arhangelskis, M.; Jones, W. *Acta Crystallogr*. **2014**, *B70*, 72−80.
12. Aitipamula, S.; Chow, P. S.; Tan, R. B. H. *CrystEngComm* **2009**, *11*, 1823–1827.
13. Ueto, T.; Takata, N.; Muroyama, N.; Nedu, A.; Sasaki, A.; Tanida, S.; Terada, K. *Cryst. Growth Des.* **2011**, *12*, 485–494.
14. Lemmerer, A.; Adsmond, D. A., Esterhuysen, C.; Bernstein, J. *Cryst. Growth Des.* **2013**, *13*, 3935–3952.
15. (a) Kálmán, A.; Párkányi, L.; Argay, G. *Acta. Cryst.* **1993,** *B49*, 1039–1049. (b) Saha, B. K.; Nangia, A. *Heteroatom Chemistry* **2007,** 18, 185–194. (c) Fábián, L.; Argay, G.; Kálmán, A.; Báthori, M. *Acta. Cryst.* **2002,** *B58*, , 710–720. (d) Cinčić, D., Friščić, T., Jones, W. *Chem. –Eur. J.* **2008**, *14*, 747–753.(e) Kitaigorodskii, A. I., *Molecular Crystals and Molecules*, Academic Press, New York, **1973**.
16. (a) Grant, D. J. W. In Polymorphism in Pharmaceutical Solids; Brittain, H. G., Ed.; Marcel Dekker, Inc.: New York, 1999; Vol. 95, pp 1−33. (b) J. Bernstein, Polymorphism in Molecular Crystals, Clarendon, Oxford, 2002. (c) Davey, R. J. *Chem. Commun*. **2003**, 1463−1467. (d) López-Mejías, V.; Kampf, J. W.; Matzger, A. J. *J. Am. Chem. Soc.*, **2012**, *134*, 9872–9875. (b) Cruz-Cabeza, A. J.; Bernstein, J. *Chem. Rev.* **2014**, *114*, 2170−2191.
17. (a) Almarsson, Ö.; Peterson, M. L.; Zaworotko, M. J. *Pharmaceutical Patent Analyst* **2012,** *1*, 313−327. (b) Trask, A. V. *Mol. Pharmaceutics* **2007**, *4*, 301−309. (c) Guidance for Industry: Regulatory Classification of Pharmaceutical Co-Crystals; U.S Department of Health and Human Services, FDA, Center for Drug Evaluation and Research (CDER): Silver Spring, MD, **2013**, http://www.fda.gov/downloads/Drugs/Guidances/UCM281764.pdf.
18. (a) Trask, A. V.; Motherwell, W. D. S.; Jones, W. *Int. J. Pharm.* **2006,** *320*, 114-123. (b) Suresh, K.; Goud, N. R.; Nangia, A. *Chem. Asian J.* **2013**, *8*, 3032 – 3041.

19. Duggirala, N. K.; Smith, A. J.; Wojtas, L.; Shytle, R. D.; Zaworotko, M. J. *Cryst. Growth Des.* **2014**, *14*, 6135–6142.

20. (a) Catalani, E. *Int. J. Tuberc. Lung Dis.* **1999**, *3*, S289–291. (b) Iseman, M. D. *Eur. Respir. J.* **2002**, *20*, 87S–94S. (c) USP DI1, *Drug Information for the Health Care Professional*, Vol. I, 15th edn, 1995, p. 1627.
21. World Health Organization (WHO) report **2013**, http://www.who.int/tb/publications/factsheet_global.pdf
22. (a) Singh, S.; Mohan, B. *Int. J. Tuberc. Lung Dis.***2003**, *7*, 298–303. (b) Bhutani, H.; Mariappan, T. T.; Singh, S. *Int. J. Tuberc. Lung Dis.* **2004**, *8*, 1073–1080. (c) Laing, R.; Vrakking, H.; Fourie, B. Int. *J. Tuberc. Lung Dis*. **2004**, *8*, 1043–1044. (d) Laserson, K. F.; Kenyon, A. S.; Kenyon, T. A.; Layloff, T.; Binkin, N.J. *Int. J. Tuberc. Lung Dis.* **2001**, *5*, 448–454. (e) Bhutani, H.; Singh, S.; Jindal, K. C.; Chakraborti, A. K. *J. Pharma. Biomed. Anal.* **2005**, *39*, 892–899.
23. (a) Haywood, A.; Mangan, M.; Grant, G.; Glass, B., *J. Pharm. Pract. Res.* **2005**, *35*, 181−182. (b) Bhutani, H.; Mariappan, T. T.; Singh, S., *Drug Dev. Ind. Pharm.* **2004**, *30*, 667−672.
24. (a) Bhutani, H.; Singh, S.; Jindal, K. C. *Pharm. Dev. Technol*. **2005**, *10*, 517–524. (b) Singh, S.; Mariappan, T. T.; Sharda, N.; Singh, B. *Pharm. Pharmacol Commun.* **2000**, *6*, 491–494.
25. (a) Bhutani, H.; Mariappan, T. T.; Singh, S. *Int. J. Tuberc. Lung Dis*. **2004**, *8*, 1073−1080.
26. (a) Bailey L. C.; Abdou, H. *J. Pharm. Sci.*,**1977**, *66*, 564–567. (b) Lund W. The pharmaceutical codex. 12th ed. London: The Pharmaceutical Press, **1994**, 928–930.
27. Lemmerer, A.; Bernstein, J.; Kahlenberg, V. *CrystEngComm* **2010**, *12*, 2856–2864. (b) Lemmerer, A.; Bernstein, J.; Kahlenberg, V. *CrystEngComm* **2011**, *13*, 55–59. (c) Lemmerer, A.; Bernstein, J.; Kahlenberg, V. *J. Chem. Crystallogr*. **2011**, *41*, 991–997.
28. Grobely, P.; Mukherjee, A.; Desiraju, G. R. *CrystEngComm* **2011**, *13*, 4358–4364.
29. Aitipamula, S.; Wong, A. B. H; Chow, P. S.; Tan, R. B. H. *CrystEngComm* **2013**, *15*, 5877–5887.

30. Sarcevica, I.; Orola, L.; Veidis, M. V.; Podjava, A.; Belyakov, S. *Cryst. Growth Des.* **2013**, *13*, 1082–1090.
31. Cherukuvada, S.; Nangia, A. *CrystEngComm* **2012**, *14*, 2579–2588.
32. Becker, C.; Dressman, J. B.; Amidon, G. L.; Junginger, H. E.; Kopp, S.; Midha, K. K.; Shah, V. P.; S. Stavchansky, S.; Barends, D. M. *J. Pharm. Sci.* **2007**, *96*, 522–531
33. (a) Walsh, R. D. B.; Bradner, M. W.; Fleischman, S.; Morales, L. A.; Moulton, B.; Rodriguez-Hornedo, N.; Zaworotko, M. J. *Chem. Commun.* **2003**, *2*, 186–187. (b) Desiraju, G. R. *Angew. Chem., Int. Ed. Engl*. **1995**, *34*, 2311–2327. (c) Allen, F. H.; W. D. S. Motherwell, W. D. S.; Raithby, P. R.; Shields, G. P.; Taylor, R. *New J. Chem.* **1999**, *23*, 25–34.
34. (a) Shan, N.; Toda, F.; Jones, W. *Chem. Commun*. **2002**, 2372–2373. (b) Trask, A. V.; Haynes, D. A.; Motherwell, W. D. S.; Jones, W. *Chem. Commun.* **2006**, 51–53. (c) Friščić, T.; Trask, A. V.; Jones, W.; Motherwell, W. D. S. *Angew. Chem. Int. Ed*. **2006**, *45*, 7546–7550. (d) Weyna, D. R.; Shattock, T.; Vishweshwar, P.; Zaworotko, M. J. *Cryst. Growth Des.* **2009**, *9*, 1106–1123.
35. (a) Etter, M. C. *J. Phys. Chem*. **1991**, *95*, 4601–4610. (b) Etter, M. C. *Acc. Chem. Res*. **1990**, *23*, 120–126.
36. Bernstein, J.; Davis, R. E.; Shimoni, L.; Chang, N. L. *Angew. Chem., Int. Ed. Engl.* **1995**, *34*, 1555–1573.
37. (a) Clarke, H. D.; Hickey, M. B.; Moulton, B.; Perman, J. A.; Peterson, M. L.; Wojtas, Ł.; Almarsson, Ö.; Zaworotko, M. J. *Cryst. Growth Des.* **2012**, *12*, 4194–4201. (b) Thakuria, R.; Nangia, A. *Cryst. Growth Des.* **2013**, *13*, 3672–3680. (c) Cinčić, D.; Friščić, T.; Jones, W. *New J. Chem.* **2008**, *32*, 1776–1781.(d) Desiraju, G. R.; Anthony, A.; Nangia, A.; Jaskólski, M. *Chem. Commun.*, **1998**, 2537–2538.(e) Csöregh, I.; S. Hirano, S.; Toyota, S.; Bombicz, P.; Toda, F. *CrystEngComm* **2004**, *6*, 60–69. (f) Cruz Cabeza, A. J.; Day, G. M.; Motherwell, W. D. S.; Jones, W. *J. Am. Chem. Soc.*, **2006**, *128*, 14466–14467.
38. (a) Gelbrich, T.; Hursthouse, M. B. *CrystEngComm* **2005**, *7*, 324–336; (b) Gelbrich, T.; Hursthouse, M. B. *CrystEngComm* **2006**, *8*, 448–460; (c) Gelbrich, T.; Threlfall, T. L.; Hursthouse, M. B. *CrystEngComm* **2012**, *14*, 5454–5464.
39. (a) Remenar, J. F.; Peterson, M. L.; Stephens, P. W.; Zhang, Z.; Zimekov, Y.; Hickey, M. B. *Mol. Pharmaceutics* **2007**, *4*, 386. (b) Karki, S.; Friščić, T.; Fábián, L.; Jones, W. *CrystEngComm* **2010**, *12*, 4038–4041.

40. (a) Silverstein, R. M. *Spectrometric Identification of Organic Compounds*. 6th Ed.; John Wiley & Sons, Inc.: New York, **2002**. (b) E. Smith, E.; Dent, G. *Modern Raman Spectroscopy, A Practical Approach*, John Wiley: New York, **2005**.
41. (a) Vogt, F. G.; Clawson, J. S.; Strohmeier, M.; Edwards, A. J.; Pham, T. N.; Watson, S. A. *Cryst. Growth Des.* **2008**, *9*, 921–937.(b) Aliev, A. E.; Harris, K. D. (2004). *Supramolecular Assembly via Hydrogen Bonds I,* **2004**, 1–53. (c) Newman, A. W.; Childs, S. L.; Cowans, B. A. Salt Cocrystal Form Selection, In *Preclinical Development Handbook*; John-Wiley, Hoboken, **2008**; pp. 455–481
42. (a) Threlfall,T.L. *Org. Process Res. Dev*. **2009**, *13*, 1224–1230. (b) Burger, A.; Ramberger, R. *Mikrochim. Acta II* **1979**, 259–271. (c) Burger, A.; Ramberger, R., *Microchim. Acta II*, **1979**, 273–316.
43. (a) Aitipamula, S.; Chow, P. S.; Tan,R. B. H. *CrystEngComm* **2009**, *11*, 889–895.(b) Childs, S. L.; Hardcastle, K. I. *CrystEngComm* **2007**, *9*, 364–367. (c) Halasz, I.; Rubčić, M.; Užarević, K.; Đilović, I.; Meštrović, E. *New J. Chem*. **2011**, *35*, 24–27. (d) Goud, N. R.; Nangia, A. *CrystEngComm* **2013**, *15*, 7456–7461.
44. Ostwald, W. *Z. Phys. Chem.* **1987**, *22*, 289–302.
45. (a) Karki, S.; Friščić, T.; Fábián, L.; Laity, P. R.; Day, G. M.; Jones, W. *Adv.Mater.* **2009**, *21*, 3905–3909. (b) Cherukuvada, S.; Babu, N. J.; Nangia, A. *J. Pharm. Sci.* **2011,** *100*, 3233–3244. (c) Babu, N. J.; Sanphui, P.; Nangia, A. *Chem. Asian J.* **2012,** *7*, 2274 – 2285.
46. http://www.ich.org/fileadmin/Public_Web_Site/ICH_Products/Guidelines/Quality/Q1F/Stability_Guideline_WHO.pdf (accessed 31 July, 2014).
47. *CrysAlis CCD and CrysAlis RED*, Ver. 1.171.33.55; Oxford Diffraction Ltd: Yarnton, Oxfordshire, UK, **2008**.
48. Dolomanov, O. V.; Blake, A. J.; Champness, N. R.; Schröder, *M. J. Appl. Crystallogr*. **2003**, *36*, 1283–1284.
49. *SAINT-Plus*, version 6.45; Bruker AXS Inc.: Madison, Wisconsin, U.S.A., **2003**.
50. SADABS, *Program for Empirical Absorption Correction of Area Detector Data*; Sheldrick, G. M. University of Göttingen: Göttingen, Germany, **1997**.
51. (a) *SMART*, version 5.625 and *SHELX-TL*, version 6.12;, Bruker AXS Inc.: Madison, Wisconsin, USA, **2000**. (b) Sheldrick, G. M. *SHELXS-97* and *SHELXL-97*; University of Göttingen: Göttingen, Germany, **1997**.

52. Spek, A. L. *PLATON, A Multipurpose Crystallographic Tool*; Utrecht University: Utrecht, Netherlands, **2002**.
53. Barbour, L. J. *X-Seed, Graphical Interface to SHELX-97 and POV-Ray, Program for Better Quality of Crystallographic Figures*; University of Missouri-Columbia, Missouri, U.S.A., **1999**.
54. Powder Cell, *A Program for Structure Visualization, Powder Pattern Calculation and Profile Fitting*, http://www.ccp14.ac.uk/index.html (accessed 31 July, 2014).

CHAPTER THREE

Improved Stability of Tuberculosis Drug Fixed-Dose Combination Using Isoniazid-Caffeic acid and Vanillic acid Cocrystal

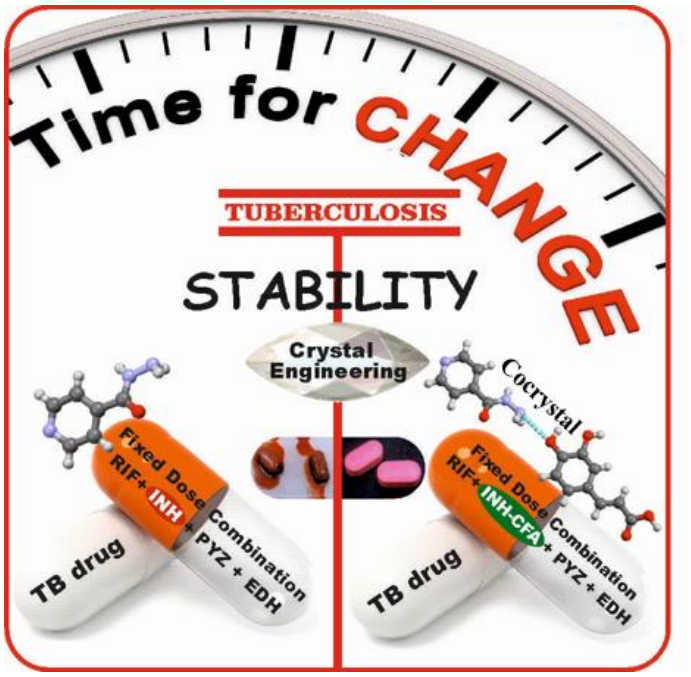

The fixed dose combination of tuberculosis drugs, namely Rifampicin (RIF), Isoniazid (INH), Pyrazinamide (PZA) and Ethambutol Dihydrochloride (EDH) has the twin issues of physical stability and rifampicin cross-reaction in the 4FDC. Pharmaceutical cocrystals of INH with caffeic acid and vanillic acid are able to stabilize the FDC formulation compared to the reference batch. FDC-INH-CFA cocrystal batch exhibited greater stability compared to FDC-INH-VLA cocrystal and FDC reference drug. The superior stability of INH-CFA cocrystal is attributed to the presence of stronger hydrogen bonds and cyclic O–H···O synthon in the crystal structure.

3.1 Introduction

A cocrystal is a multi-component crystal in which two or more molecules that are solids under ambient temperature coexist through non-covalent interactions such as hydrogen bonds, halogen bonds, π–π stacking, van der Waals interactions, etc.[1-2] The cocrystal approach has been used to construct functional organic solids for pharmaceuticals, high energy materials, optical and electronic applications, as well as for stereoselective organic synthesis.[3-7] Pharmaceutical cocrystals are a sub-class of cocrystals made from an active pharmaceutical ingredient (API) and one or more pharmaceutically acceptable coformers (U.S. Food and Drug Administration-approved generally regarded as safe compounds) to manipulate the physicochemical properties of the API, such as stability, processability, solubility, dissolution rate, and bioavailability, without changing the drug molecular structure and its pharmacological profile.[3,8,9] Physicochemical stability is a major problem in several of the marketing drugs.[10] The supramolecular synthon approach to cocrystal design can improve the stability of such drugs.[11] For example, Nangia et al. reported significant improvement in the hydrolytic stability of anticancer drug Temozolomide (TMZ) by forming cocrystals with oxalic acid (OA) and succinic acid (SA).[12a] They highlighted that, hydrolytic degradation of temozolomide in the solidstate started within a week during stability studies at accelerated ICH conditions of 40°C and 75% RH whereas its cocrystals with succinic acid and oxalic acid were intact for 28 weeks (Figure 3.1).

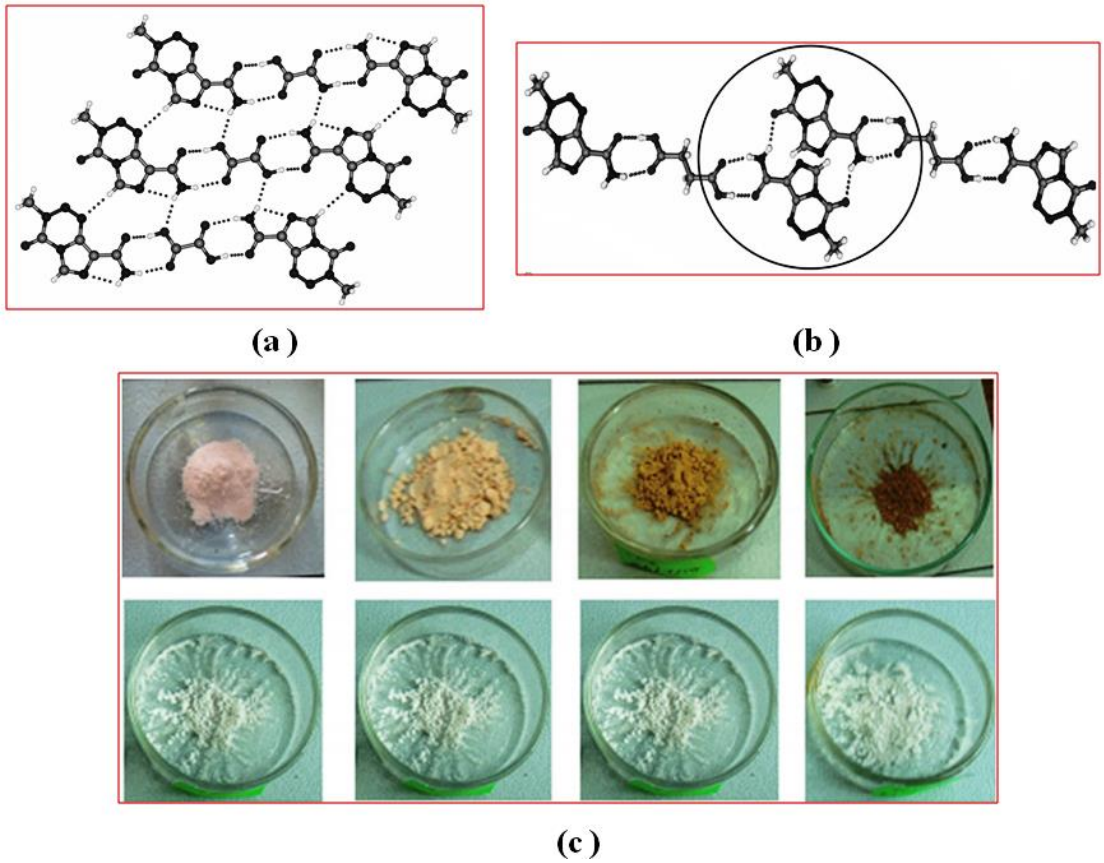

Figure 3.1 (a) Amide-acid heterosynthon of N–H···O and O–H···O hydrogen bonds in TMZ-oxalic acid cocrystal (1:0.5). (b) Amide–acid heterosynthon of N–H···O and O–H···O hydrogen bonds in TMZ–succinic acid cocrystals (1:0.5). (c) Physical stability and color comparison of pure TMZ (top panel) and TMZ–SA cocrystal (bottom panel) under accelerated ICH conditions. The TMZ– SA cocrystal shown greater stability than pure TMZ (Adapted from Ref. 12a).

In another report, A. V. Trask and coworkers[12b] reported cocrystals of caffeine with dicarboxylic acids such as oxalic acid, malonic acid, maleic acid, and glutaric acid to address the hydration problem of caffeine. Caffeine-glutaric acid cocrystal showed superior stability towards hydration over a period of several weeks (Figure 3.2). Z. Z Wang and coworkers[12c] enhanced the hygroscopic stability of the nootropic drug S-oxiracetam via cocrystallization with gallic acid. Furthermore L. Wang and coworkers[12d] improved the hydration stability of antifungal drug 5-fluorocytosine by forming conjugate acid-base cocrystal with acesulfame. Based on these literature reports, in this chapter we highlight the cocrystallization of pharmaceutically active molecules represents a viable means of enhancing stability of fixed dose combination of tuberculosis drugs.

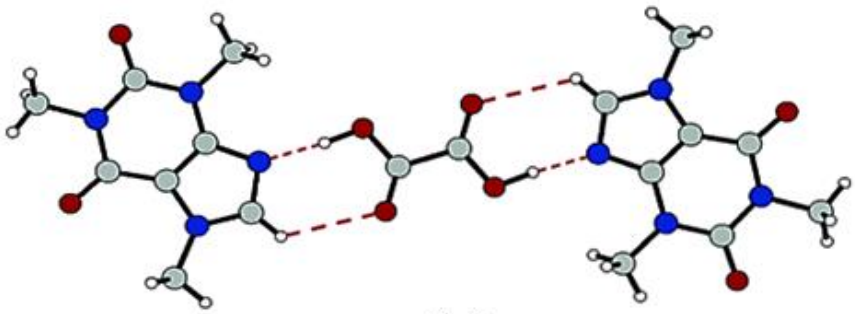

(a)

Material	Condition (% RH)	Observed Relative Humidity Stability*			
		1 day	3 days	1 week	7 weeks
Caffeine	0	✓	✓	✓	✓
	43	✓	✓	✓	✓
	75	✓	✓	✓	✓
	98	×	×	×	×
caffeine-oxalic acid cocrystal	0	✓	✓	✓	✓
	43	✓	✓	✓	✓
	75	✓	✓	✓	✓
	98	✓	✓	✓	✓

(b)

Figure 3.2 (a) Caffeine and oxalic acid are associated via O–H···N and C–H···O hydrogen bonds in the crystal structure. (b) Improved hydration stability of caffeine-oxalic acid cocrystal compared to pure caffeine (Adapted from Ref.12b).

3.2 Literature reports on Tuberculosis drugs

Tuberculosis (TB) is an airborne infectious disease caused by organisms of the Mycobacterium Tuberculosis complex. [13] It is one of the top 10 leading causes of death worldwide. According to the World Health Organization (WHO) an estimated 10.4 million people developed TB and 1.8 million died from the disease (including 0.4 million deaths among HIV-positive people) in 2015.[14] The first-line drugs recommended by WHO for the treatment of TB include Rifampicin (RIF), Isoniazid (INH), Pyrazinamide (PZA), and Ethambutol dihydrochloride (EDH) (Scheme 1).[15] Since 1994, The WHO and International Union Against Tuberculosis and Lung Disease (IUATLD) recommended the use of fixed dose combination (2-drug, 3-drug and 4-drug FDCs) of these drugs for the treatment for tuberculosis over single-drug monotherapy tablets, for preventing the emergence of multidrug-resistant tuberculosis, and for better patient/

doctor compliance, simpler treatment and management of drug supply.[16] In 1999 a 4-drug FDC tablet was included in the WHO Model List of Essential Drugs which comprises a combination of four anti-tuberculosis drugs namely, Rifampicin (RIF), Isoniazid (INH), Pyrazinamide (PZA), and Ethambutol dihydrochloride (EDH).[17] Despite its numerous advantages, the 4-FDC tablet is known to exhibit quality and stability problems, including poor bioavailability of rifampicin and instability of anti-TB drugs during storage.[18] When marketed FDC tablets in packed and unpacked state containing RIF, INH, PZA and EDH were stored under ICH (International Conference on Harmonisation of Technical Requirements for Registration of Pharmaceuticals for Human Use) accelerated stability conditions of 40 °C and 75% RH, extensive physical changes such as color fading, red bleeding and significant decomposition of RIF was observed.[19,20] Isonicotinyl hydrazone (HYD) is the major degradation product in the mixture, which is formed by the interaction of the imino group of 3-formyl rifampicin of RIF with the hydrazine group of isoniazid under acidic conditions.[21,22] Due to the hygroscopic nature of EDH, it attracts moisture and creates acidic environment in the formulation and thereby increases the rate of decomposition of RIF.[23] Discoloration and conversion of the solid tablet to sticky, gummy mass is a common problem (Figure 3.3).[19] Treatment of tuberculosis with poor-quality drugs, will result in treatment failures and development of drug resistance. With this background, WHO and IUATLD gave a joint statement that only FDC tablets of good quality and proven bioavailability of RIF should be used.[24] In this regard, cocrystals of INH with several GRAS conformers were reported from our group previously where INH-CFA-form 1 and INH-VLA form 2 cocrystals showed good stability compared to the reference drug. [25] In the present study, we replaced INH with stable cocrystals of INH in the 4-drug FDC formulation to improve the stability and prepared FDC INH-VLA and FDC INH-CFA cocrystal batches and compared their stability with FDC reference batch (containing pure INH) after storage at accelerated conditions of 40 °C/ 75% RH for a period of one month.

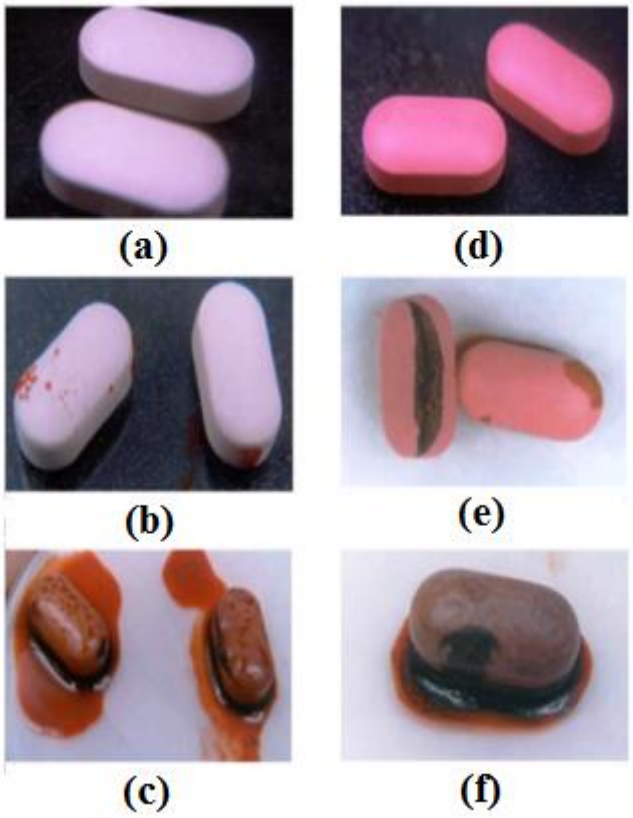

Figure 3.3 Decomposition of 4-FDC tablets (a, d) on the shelf after storage at accelerated conditions of 40 °C/ 75% RH for a period of 2 days (b, e) and 5 days (c, f).[19]

3.2.1 Decomposition of Rifampicin in the presence of Isoniazid

The formation of isonicotinyl hydrazone by-product due to the reaction of INH with reducing sugars under acidic conditions has been reported.[26] Based on this known reaction, Singh et al. isolated, synthesized and confirmed the chemical structure of isonicotinyl hydrazone and they proposed a mechanism for the increased decomposition of RIF in the presence of INH (Scheme 3.2).[27] RIF is first converted to 3-formyl rifamycin through first order reaction under acidic conditions, later it reacts with INH to form isonicotinyl hydrazone (HYD) through a fast second order step. The unstable hydrazine by-product regenerates isoniazid and 3-formyl rifamycin by a pseudo first-order reaction under acidic conditions. As the second-order forward reaction is faster than the preceding reaction (rifampicin to 3-formyl rifamycin) and the following first-order reaction (hydrazone to 3-formyl rifamycin and isoniazid), the overall reaction is favored toward the formation of hydrazone. The decomposition of rifampicin to 3-formylrifamycin is pushed forward and an overall increase in the degradation of

rifampicin is observed in the presence of isoniazid. This reaction pathway also explains the reason for the loss of smaller amount of INH compared with RIF. This is because INH is recovered during the reversible process.

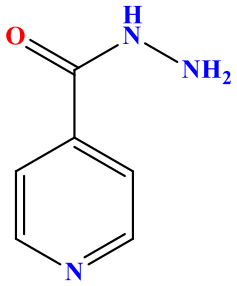

Isoniazid, INH

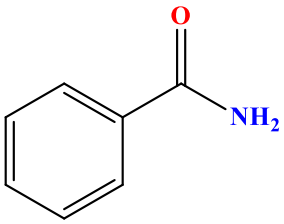

Pyrazinamide, PZA

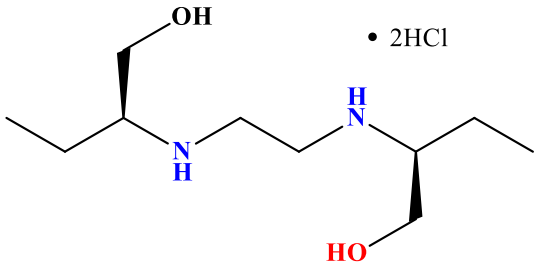

(S,S)-Ethambutol dihydrochloride, EDH

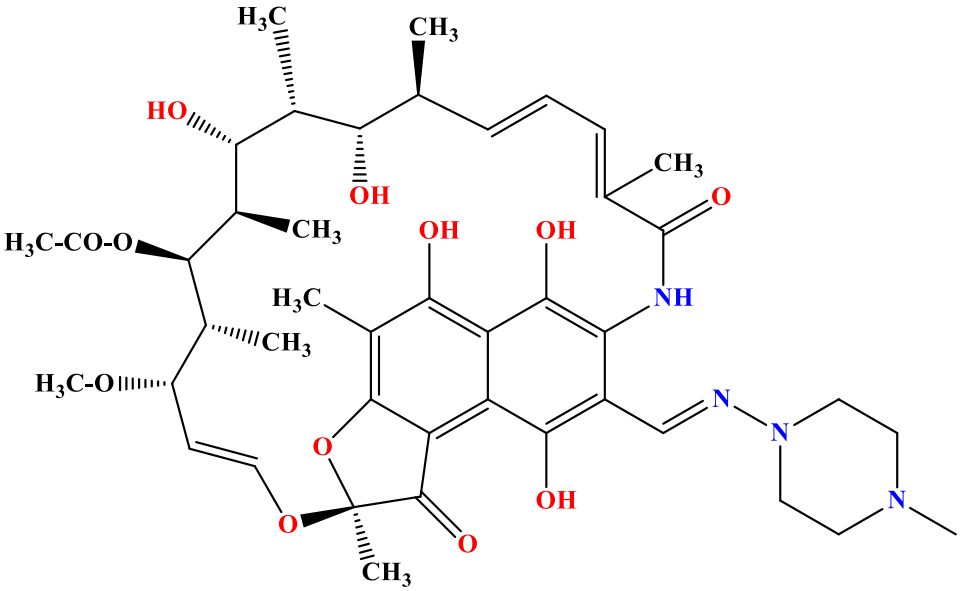

Rifampicin, RIF

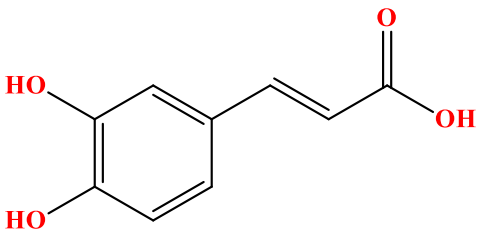

Caffeic acid, CFA

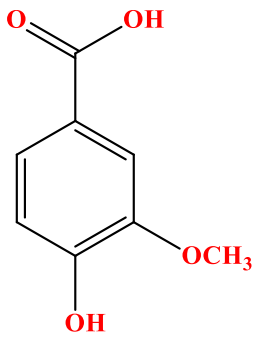

Vanillic acid, VLA

Scheme 3.1 Chemical structures of first-line anti-TB drugs and coformers used in this study.

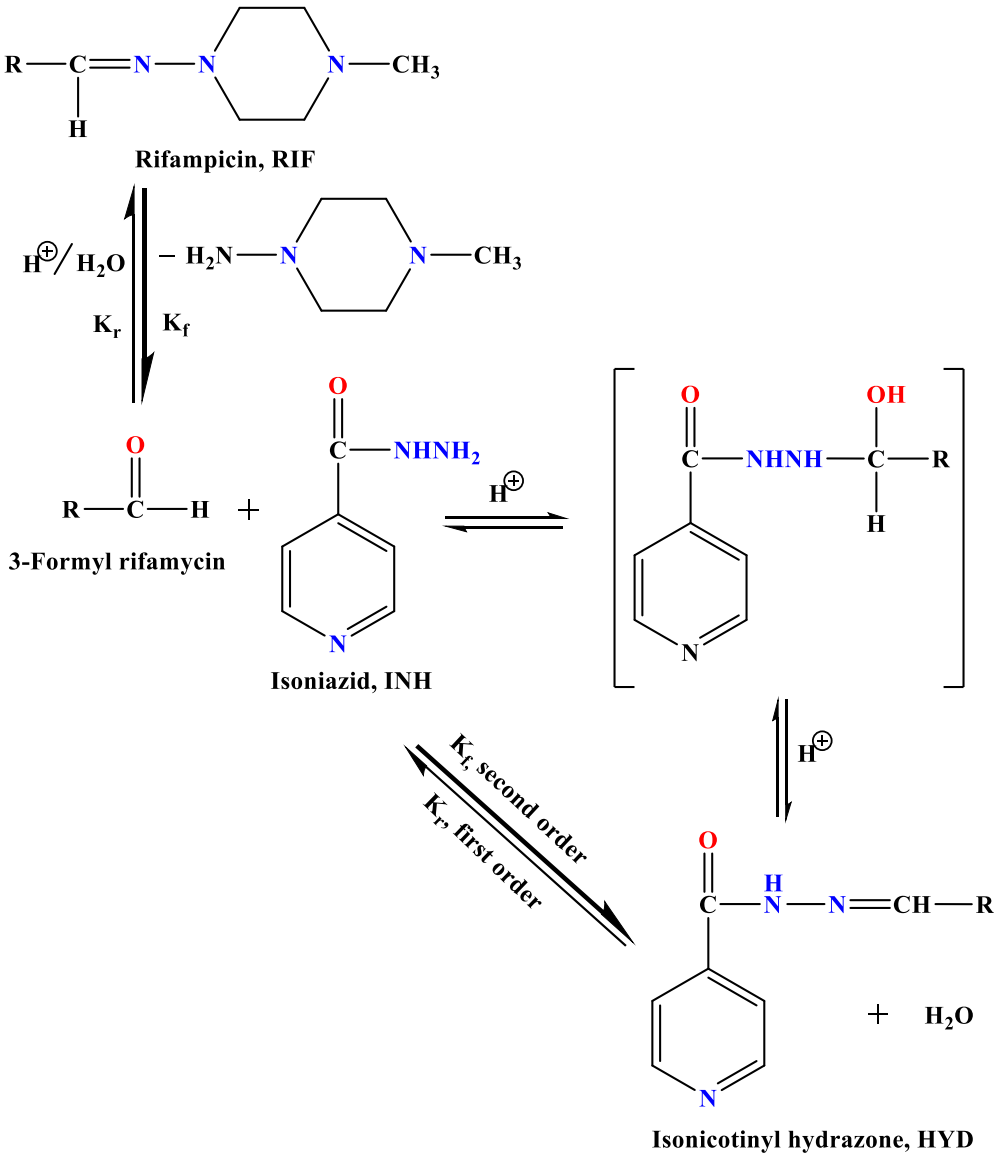

Scheme 3.2 Proposed pathway for decomposition of rifampicin in the presence of isoniazid[27].

3.3 Results and Discussion

The poor bioavailability of rifampicin, particularly when the anti-TB drugs are present in fixed-dose combination (FDC) product, is a matter of serious concern. There is the potential of failure of therapy in patients with an active disease. It contributes to the increasing resistance to anti-tubercular drugs. The change in physical state from solid to semi-solid/ liquid-like due to cross reactions not only destroys the shelf-life of the drug

but also causes concern for patients with limited access to drugs in the tropical/ developing world. Hence there is an immediate urgency to develop stable FDC formulations. The present investigation was carried out to develop solid-state forms (cocrystals) of the individual drugs by crystal engineering to improve the physical and chemical stability of fixed dose combination (FDC). To address the reactivity of isoniazid we prepared its cocrystals. The stability studies were carried out on the novel cocrystal combinations at accelerated humidity conditions of 40 °C and 75% RH over one month. The samples were prepared of the reference FDC and that with cocrystals INH-VLA-form 2 and INH-CFA-form 1, and tested for both physical and chemical stability during the period of storage through different techniques such as PXRD, photographic images, SEM and HPLC analysis.

3.3.1 Crystal Structures

Form 2 of INH-VLA and form 1 of INH-CFA cocrystals from our previous study of INH cocrystals[25] were used in this study because they are the more stable forms and their X-ray crystal structures are known. A summary of the cocrystals prepared and stability of their polymorphs is summarized in Table 1. In the crystal structure of INH-VLA-Form-2, the carboxylic acid group of VLA forms an O–H···N hydrogen bond with the pyridine nitrogen atom of INH via the acid-pyridine heterosynthon. Further the hydroxyl group of VLA forms O–H···N hydrogen bond to give a 1D zigzag tape. These tapes extend in the crystallographic [010] direction as make a 2D sheet through N–H···O hydrogen bonds thereby forming a R_3^3 (10) ring motif. These sheets extend parallel to the $(0\bar{1}4)$ plane through auxiliary C–H···O interactions (Figure 3.4).

Table 1 Criteria to select cocrystals of INH for the FDC stability study (based on data from ref. 25).

Cocrystal polymorph	X-ray crystal structure	Stability order	Selected/ Not suited, and reason
INH-VLA F1	determined	metastable	not suited, metastable
INH-VLA F2	**determined**	**stable**	**selected, stable and crystal structure known**
INH-CFA F1	**determined**	**stable**	**selected, stable and crystal**

			structure known
INH-CFA F2	not available	intermediate	not suited, metastable and crystal structure not known
INH-CFA F3	determined	least stable	not suited, metastable
INH-FRA F1	determined	metastable	not suited, metastable
INH-FRA F2	not available	stable	not selected, crystal structure not known

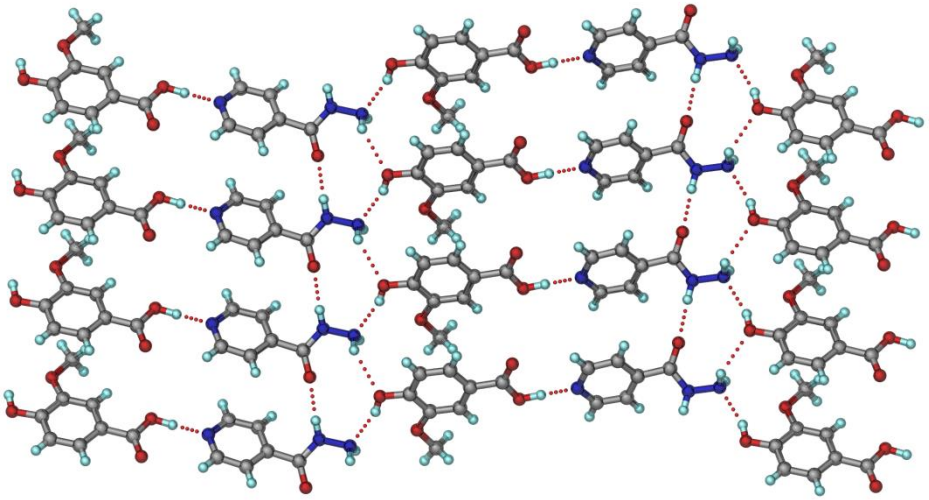

Figure 3.4 Sheet structure of INH-VLA-Form-2 assembled via N–H···O, O–H···N hydrogen bonds and acid···pyridine heterosynthon (Adapted from ref. 25).

In the crystal structure of INH-CFA-Form-1, CFA molecules are connected by O–H···O hydrogen bonds in a R_2^2 (10) type dimeric motif reminiscent of catechol crystal structure. INH molecules are hydrogen bonded to the catechol dimer through O–H···N H-bond. The carboxylic acid group of CFA forms an O–H···N hydrogen bond to the pyridine nitrogen atom of INH via the robust acid–pyridine heterosynthon in a linear tape motif. Adjacent tapes are connected through C–H···$O_{carbonyl}$ interactions in flat 2D sheets (Figure 3.5), which are connected through N–H···O hydrogen bonds of the amine NH donor.

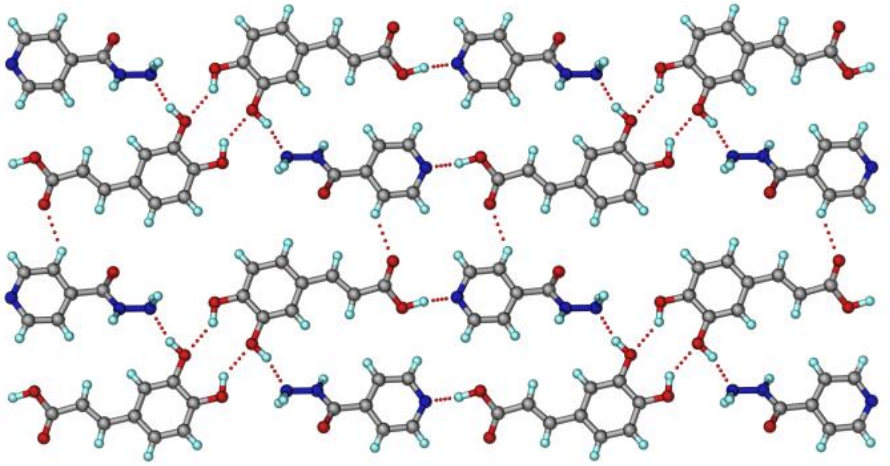

Figure 3.5 Sheet structure of INH-CFA-Form 1 stabilized by the hydroxyl homodimer, acid-pyridine synthon, N–H···O and auxiliary C–H···O interactions (Adapted from ref. 25).

These two crystal structures were selected for the FDC stability study because they are the stable polymorphs (INH-VLA-Form-2 and INH-CFA-Form 1) and their hydrogen bonding and molecular packing are known from the X-ray crystal structure. The present study was performed with three objectives: (1) to find out if the stability of the pure cocrystal survives in the multifunctional group FDC environment; (2) to understand whether the cyclic catechol O–H···O synthon in the layered structure of INH-CFA-Form 1, or the extended hydrogen bond network of INH-VLA-Form-2 is superior one in stabilizing the 4-FDC drug combination; (3) if the NH_2 group of hydrazide is engaged in hydrogen bonding in the cocrystal, then will it reduce cross reactivity with rifampicin aldehyde to minimize the undesired hydrazone by-product? The reference to the stable polymorph number (F1, F2) is omitted for brevity in the remaining paper.

The layered structure of INH-CFA form 1 appears to have stronger and tighter network of hydrogen bonds. The layer structure assembled via catechol type O–H···O synthon are in turn connected via amide and hydrazide N–H···O=C hydrogen bonds to build a strong 3D network (Figure 3.5). This should reduce the reactivity of hydrazide NH group as a nucleophile with RIF-CHO electrophilic fragment. On the other hand, the hydrazine NH in INH-VLA form 2 is not so tightly bound by hydrogen bonds (Figure 3.4) and perhaps able to react as a nucleophile. In comparison the NH_2 group of the pure drug INH would be the most reactive with rifampicin in 4-FDC. The crystal structures and hydrogen bonding are detailed in ref. 25.

3.3.2 Physical stability

The three cocrystal batches of FDC reference, FDC INH-VLA and FDC INH-CFA were kept under accelerated conditions of 40 °C/ 75% RH for a period of one month and their physical stability was checked through powder X-ray diffraction (PXRD) lines, photographic images, and scanning electron microscopy (SEM).

Photographic images of the powder materials of FDC reference, FDC INH-VLA and FDC INH-CFA cocrystal batches were taken at 0 h and then during storage under accelerated conditions of 40 °C/ 75% RH samples were withdrawn from the humidity chamber after 1, 2, 3 and 4 week intervals and their photographs were compared (Figure 3.6). FDC reference batch turned to complete liquid-like state within one week due to degradation of RIF. For FDC with INH-VLA cocrystal batch, slight color change was observed after one week and the product turned to dark brown color after 4 weeks of storage. The FDC INH-CFA cocrystal batch showed slight color change after one week and remained in solid form for up to 4 weeks, which indicates excellent stability.

Compound	**FDC INH ref**	**FDC INH-VLA cocrystal**	**FDC INH-CFA cocrystal**
0 h		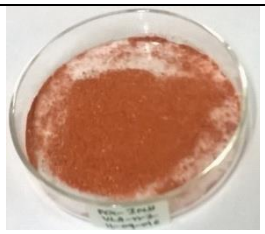	
7 days	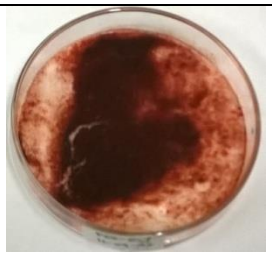		
14 days	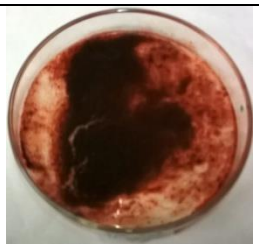		

21 days			
28 days			

Figure 3.6 Images of FDC samples after keeping at accelerated conditions of 40 °C and 75% RH for 1, 2, 3 and 4 weeks. Left, middle and right side petridishes corresponds to FDC reference, FDC-INH-VLA and FDC-INH-CFA cocrystal batches.

Scanning electron microscopy (SEM) provides detailed information about the morphology and particle size at the nm and μm scale[28] for powdered pharmaceutical samples.[29] During storage under accelerated stability conditions, samples were drawn after 1, 2, 3 and 4 weeks intervals and SEM images were recorded (Figure 3.7). There are no clear particles in the SEM image of FDC reference batch after one week of storage which is consistent with the sample turning to a pasty material (as seen in the visual images) due to immediate reaction between INH and RIF. Similarly, SEM image of FDC-INH-VLA cocrystal batch showed aggregated particles after 2 weeks. SEM image of FDC-INH-CFA cocrystal batch shows that particles are clear and well separated compare to FDC reference and FDC-INH-VLA cocrystal batches. Therefore, FDC-INH-CFA cocrystal batch is the more stable combination.

Compound	FDC INH ref	FDC INH-VLA	FDC INH-CFA
Day 0	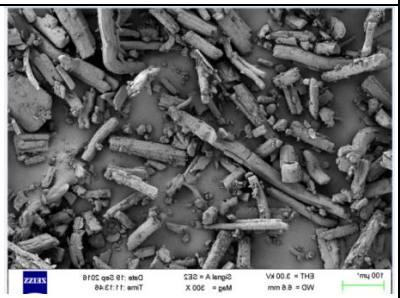		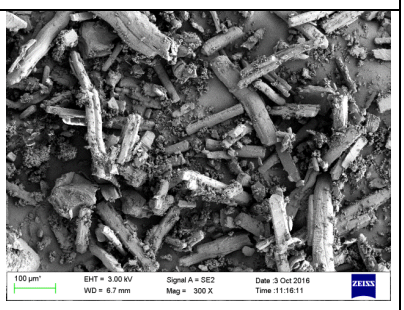
Week 1	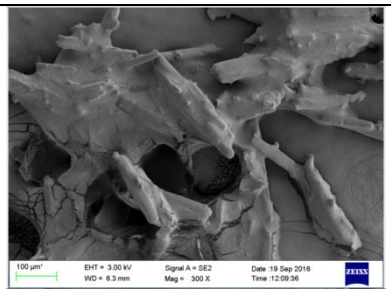	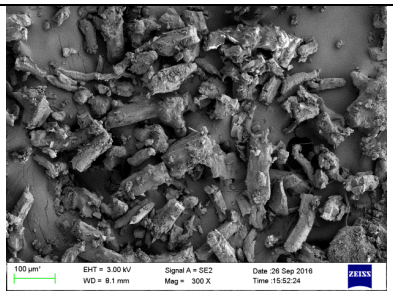	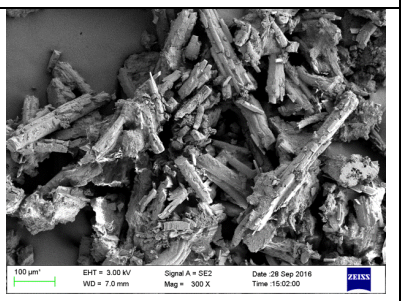
Week 2	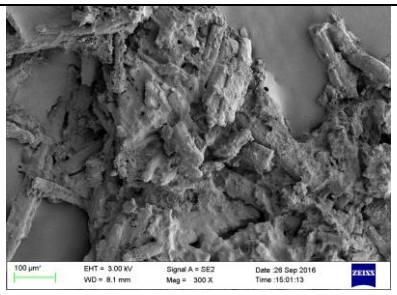	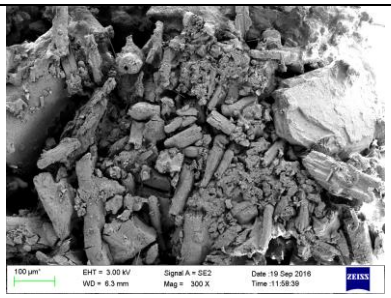	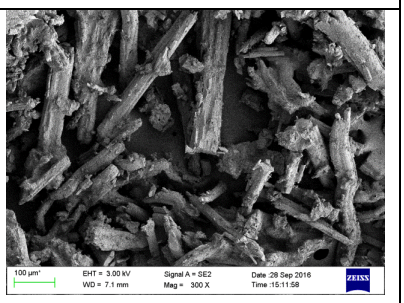
Week 3	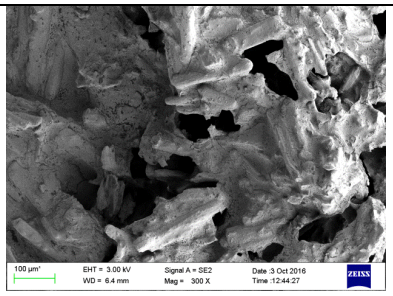	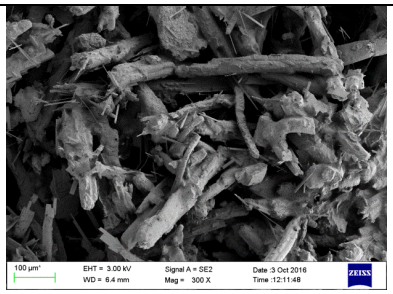	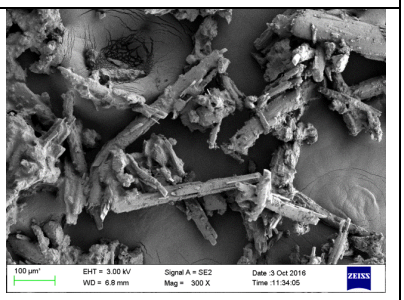
Week 4	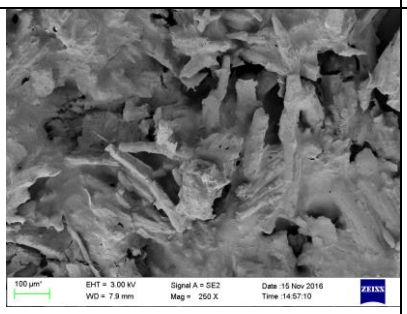	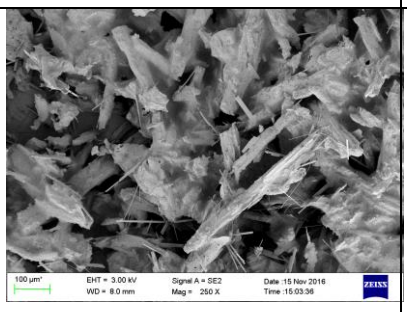	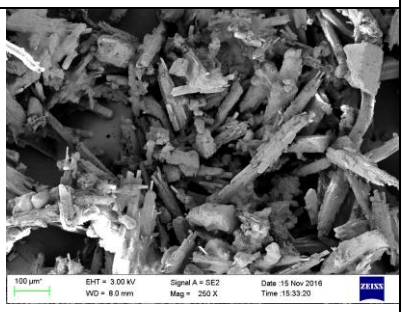

Figure 3.7 SEM Images of FDC samples after keeping at accelerated conditions of 40 °C and 75% RH for 1, 2, 3 and 4 weeks. Left, middle and right side SEM images corresponds to FDC reference, FDC-INH-VLA and FDC-INH-CFA cocrystal batches, respectively. The well separated particles distribution is clear for FDC-INH-CFA at the end of 1 month.

Powder X-ray diffraction technique (PXRD) is a standard method for the characterization of solid-state forms. PXRD is vital to study polycrystalline materials, and is often suited for characterization and to monitor phase changes in solid-state materials.[30] The freshly prepared material exhibits prominent lines at $2\theta \approx 8°$, 13-14°, 15°, 18° for all three batches. After 1 day PXRD of FDC reference, FDC-INH-VLA and FDC-INH-CFA exhibit two additional peaks at 26-28° which persist up to 28 days, except that there is some line broadening, due to loss of crystallinity with time. A comparison of the PXRD pattern showed significant differences in powder XRD lines of the FDC reference batch at 0 h, after 1, 2, 3, and 4 weeks. The disappearance of certain peaks indicated degradation of the reference batch. The missing powder XRD lines in the PXRD pattern were majorly from RIF, INH and EDH.HCl by peak profile comparison with the standard line pattern. After 24 h in ICH conditions there was a drastic reduction in the intensity of the powder pattern lines for the reference batch, from about 16-18,000 counts to 2-3,000 counts (mid-level intensity of peaks) for the same amount of sample taken on the holder (Figure 3.8). The transformation from solid, crystalline to liquid-like state of the sample noted visually and in SEM images is reflected in the PXRD as well. The liquefying of the sample and the color change is due to the hygroscopic nature of the EDH, and the subsequent cross reaction between isoniazid and rifampicin. Under similar experimental conditions the FDC INH-CFA and FDC INH-VLA cocrystal batches exhibited similar peaks profile of low intensity peaks between 30-45°, but with the difference that FDC INH-CFA has fewer interfering peaks than FDC INH-VLA and FDC INH (Figure 3.9 and 3.10). Moreover, the much superior solid-state crystallinity of cocrystal FDCs (notably of FDC INH-CFA) is seen in the higher peak intensity counts after 24 h at 7-8,000 (starting batches have similar intensity at 16-18,000 counts). The sample size for PXRD analysis was similar for all measurements about 50 mg. PXRD analysis confirms the superior nature of FDC INH-CFA in terms of crystallinity and solid-state nature semi-quantitatively over a 1 month stability study. Overall, the petri dish images, SEM micrographs and PXRD profile together show that INH-CFA is the superior cocrystal for a stable FDC of Rifampicin, Isoniazid, Pyrazinamide and Ethambutol Dihydrochloride.

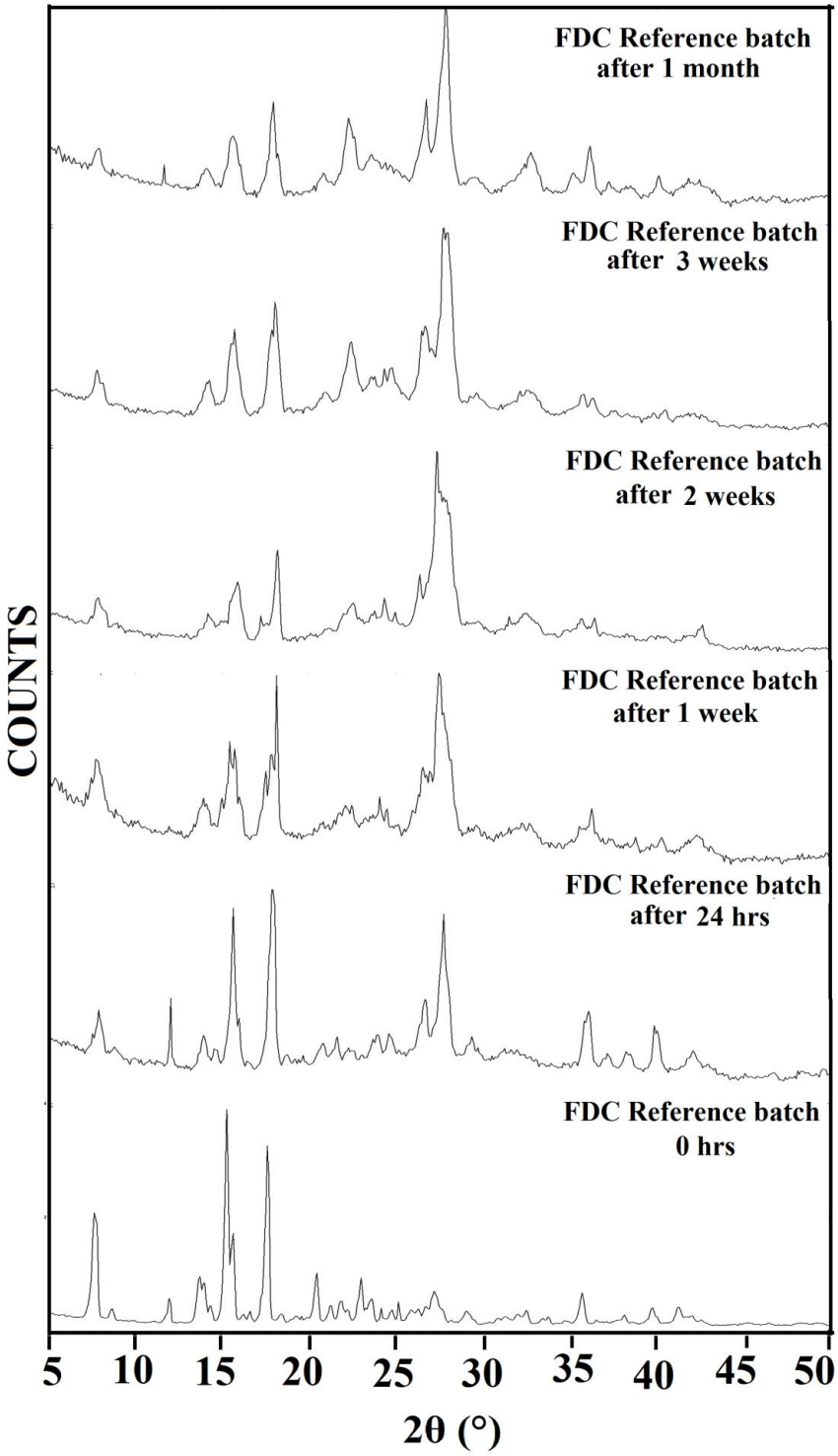

Figure 3.8 Comparison of PXRD pattern of FDC reference batch (RIF+INH+PZA+EDH) kept at 40 °C and 75% RH for 30 days shows the degradation of the product at 30 days. Peak intensity counts are not shown for the stacked plots. The value was about 16,000-18,000 at T = 0 and 2,000-3,000 after 24 h which reduced marginally with slight line broadening at 1 month.

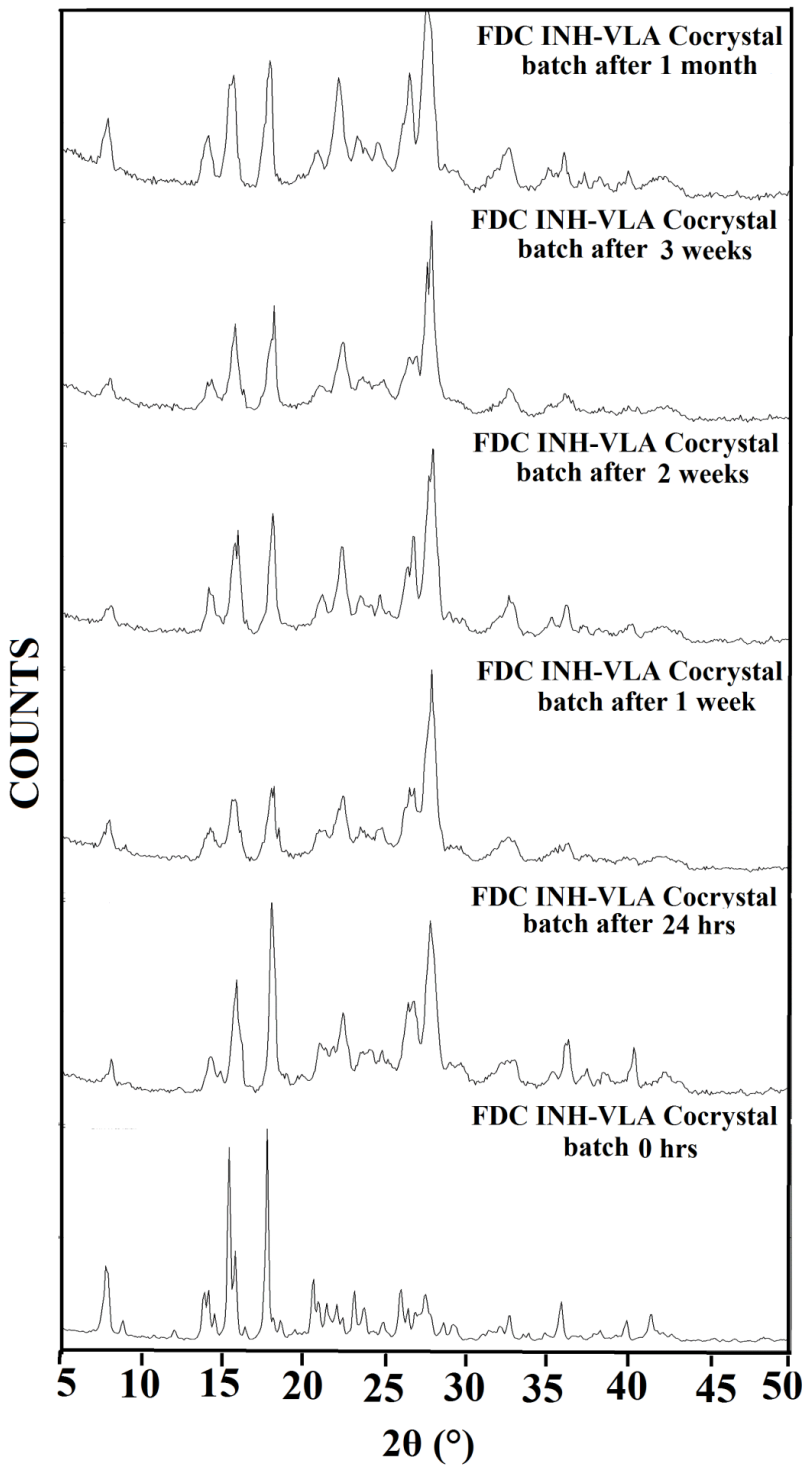

Figure 3.9 Comparison of PXRD pattern of FDC INH-VLA cocrystal batch (RIF+INH-VLA+PZA+EDH) kept at 40 °C and 75% RH for 30 days shows degradation of the product. The value was about 16,000-18,000 at T = 0 and 2,000-3,000 after 24 h which reduced marginally with slight line broadening at 1 month.

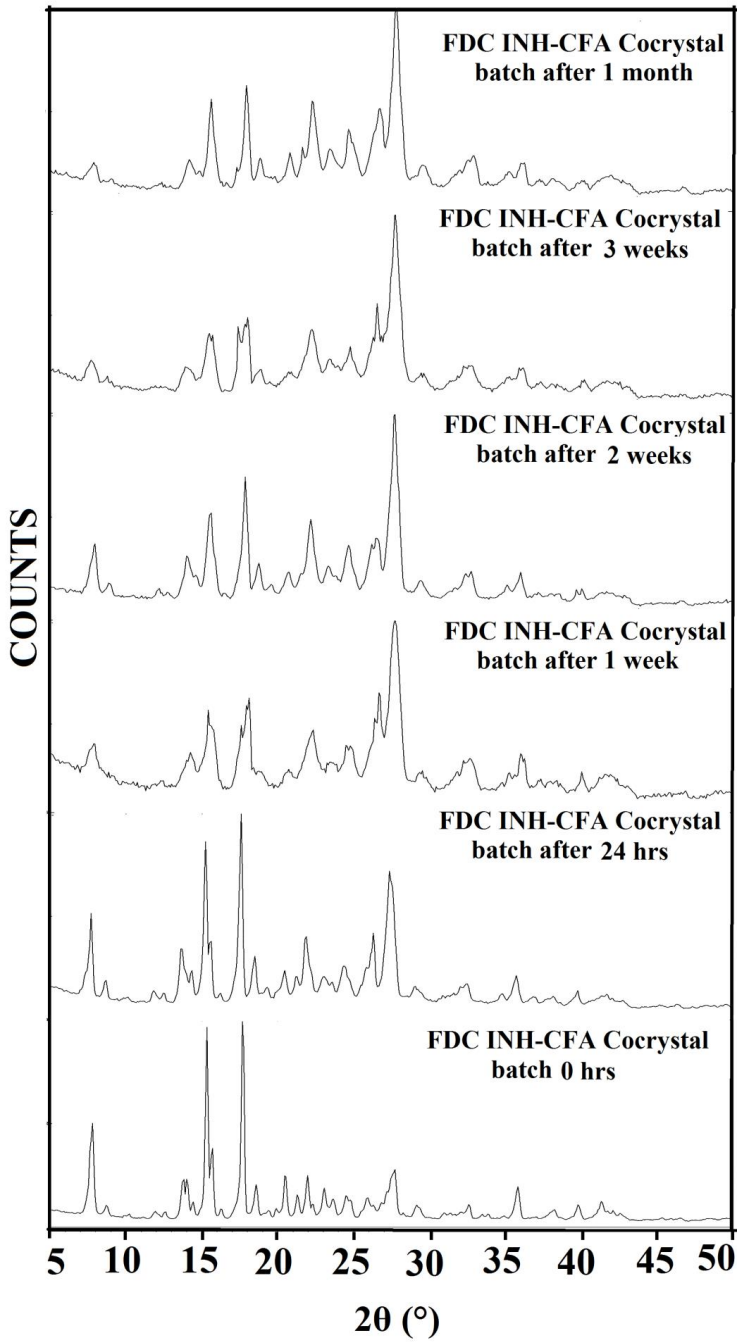

Figure 3.10 Comparison of PXRD pattern of FDC INH-CFA cocrystal batch (RIF+INH–CFA+PZA+EDH) kept at 40 °C and 75% RH for 30 days to show better stability. The value was about 16,000-18,000 at T = 0 and 7,000-8,000 after 24 h which reduced marginally to 3,000-4,000 counts with slight line broadening at 1 month.

3.3.3 Chemical stability by HPLC analysis

Chemical stability of all the three FDC batches was analyzed by HPLC (Figure 3.11-3.13). HPLC method of analysis for the stability of FDC drugs was developed by Mariappan et al.[31] who found that new peaks appeared in the HPLC chromatogram during decomposition of RIF in the presence of INH, PZA and EDH as HYD, based on the known reaction of INH with reducing sugars.

The extent of decomposition of RIF, INH and PZA in the three FDC batches stored under 40°C/ 75% RH conditions was determined as the percent fall in drug concentration relative to the initial drug strength. Table 2 gives the data of the mean area percent values pertaining to HYD.

Table 2 Percent drug remaining after storage of FDC reference, FDC-INH-VLA and FDC-INH-CFA cocrystal batches to accelerated conditions of temperature and humidity (40 °C/ 75% RH) for 0 h, day 3, 6, 9, 12, 15 and day 30.

Compound	Time interval	% of INH remaining[a] (n=3)	% of PZA remaining[a] (n=3)	% of RIF remaining[a] (n=3)
FDC-Ref	0 h	100	100	100
FDC-INH-VLA cocrystal	0 h	100	100	100
FDC-INH-CFA cocrystal	0 h	100	100	100
FDC ref	Day 3	94.40	93.29	75.80
FDC-INH-VLA cocrystal	Day 3	94.85	93.43	66.18
FDC-INH-CFA cocrystal	Day 3	97.21	94.88	63.64
FDC ref	Day 6	73.56	90.07	52.07
FDC-INH-VLA cocrystal	Day 6	83.13	91.02	47.97
FDC-INH-CFA cocrystal	Day 6	90.07	91.56	62.24
FDC ref	Day 9	71.50	89.01	40.67
FDC-INH-VLA cocrystal	Day 9	77.99	90.29	33.81
FDC-INH-CFA cocrystal	Day 9	79.22	90.78	59.36
FDC ref	Day 12	69.08	85.99	37.26
FDC-INH-VLA cocrystal	Day 12	76.14	86.53	31.52
FDC-INH-CFA cocrystal	Day 12	76.89	86.75	56.74

FDC ref	Day 15	66.79	84.47	35.57
FDC-INH-VLA cocrystal	Day 15	72.96	85.11	28.68
FDC-INH-CFA cocrystal	Day 15	75.42	85.35	54.52
FDC ref	Day 30	33.94	42.49	23.12
FDC-INH-VLA cocrystal	Day 30	42.61	47.70	15.86
FDC-INH-CFA cocrystal	Day 30	48.86	52.99	43.55

[a] Calculated on the basis of decrease in the amount of a particular drug with respect to the mean area of a particular peak in HPLC chromatogram of the initial sample and after storage under accelerated conditions for a specified time. Ethambutol could not be determined in the same HPLC measurements due to lack of a chromophore.

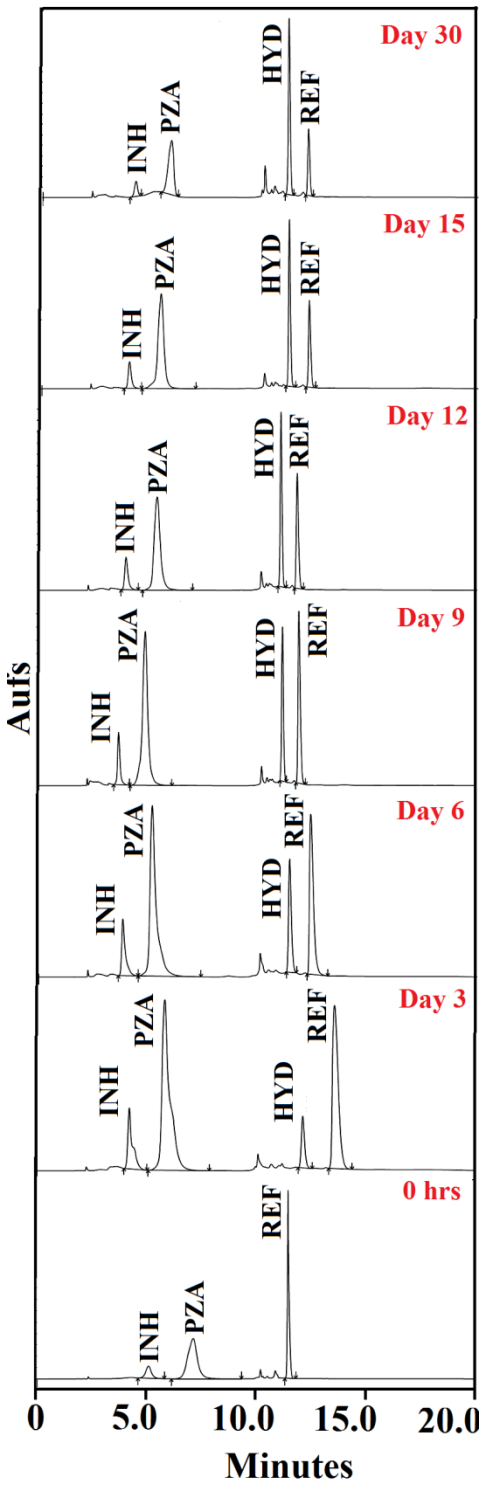

Figure 3.11 HPLC Chromatograms showing changes in the purity of drugs and formation of by-products on storage of the FDC reference batch (RIF+INH+PZA+EDH) at accelerated conditions of temperature and humidity (40 °C, 75% RH) for 0, 3, 6, 9, 12, 15 and 30 d.

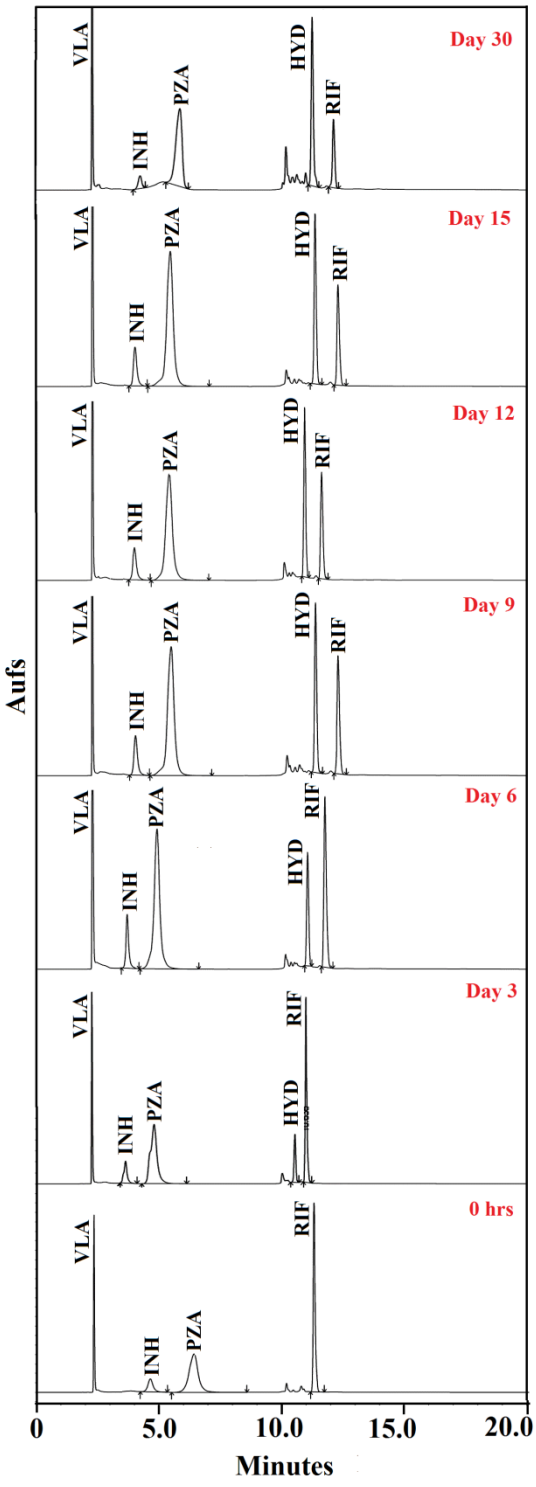

Figure 3.12 HPLC Chromatograms showing changes in the purity of drugs and formation of by-products on storage of the FDC INH-VLA cocrystal batch (RIF+INH-VLA+PZA+EDH) at accelerated conditions of temperature and humidity (40 °C, 75% RH) for 0, 3, 6, 9, 12, 15 and 30 d.

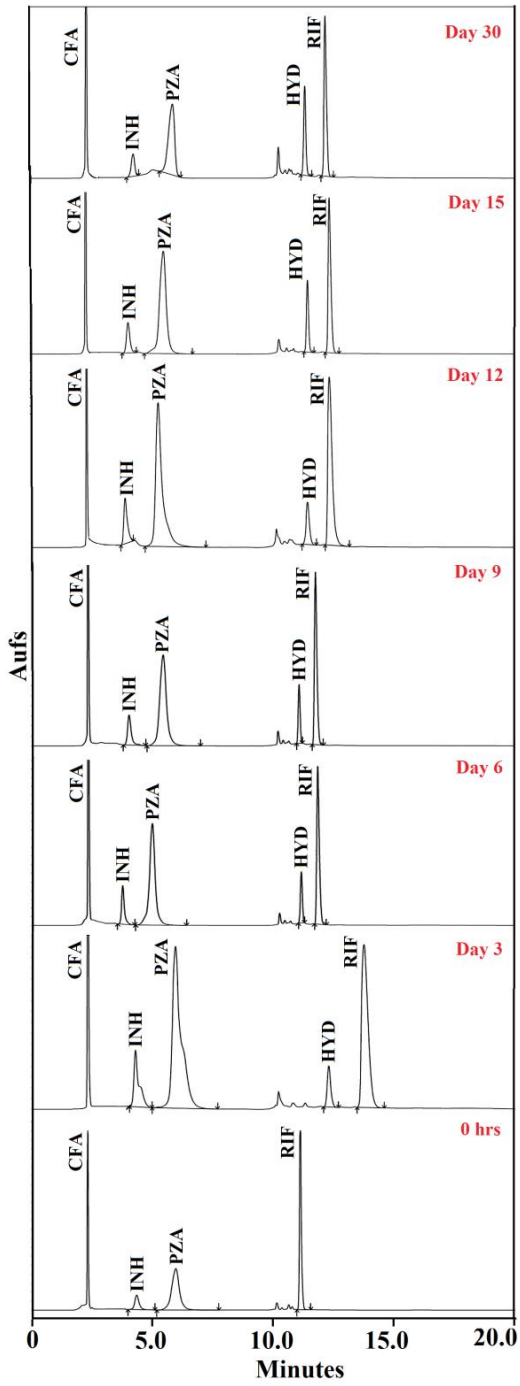

Figure 3.13 HPLC Chromatograms showing changes in the purity of drugs and formation of by-products on storage of the FDC INH-CFA cocrystal batch (RIF+INH-CFA+PZA+EDH) at accelerated conditions of temperature and humidity (40 °C, 75% RH) for 0, 3, 6, 9, 12, 15 and 30 d.

The slight movement in the retention time of the same compound from one HPLC run to another was due to the changes in the mobile phase composition, the lag in the column from previous runs, and pH of the solvent phase buffers and pressure not being strictly possible to maintain constant over the extended study period of several weeks. The sharp peaks and near match of the peak position confirm the chemical identity and purity of components at different time points. Overall, the HPLC plots shows the superior quality of drugs concentration being present in FDC INH-CFA. The percentage of rifampicin was higher in FDC INH than that for FDC INH-VLA.

3.4 Conclusions

Cocrystals have been used to control the hygroscopicity and to improve the bioavailabilty and dissolution rate of TB drugs.[32-33] Eutectics of EDH has been reported with greater hygroscopic stability.[34] Ethambutol oxalate was found to be remarkably non-hygroscopic in a recent study.[32] In this study, we used pharmaceutical cocrystals of INH (INH-Caffeic acid and INH-Vanillic acid) to improve the stability of 4 drug FDC and stability studies were carried out under accelerated temperature and humidity conditions of 40 °C and 75% RH. The physical stability was tested by PXRD and SEM analysis, and chemical purity was analyzed by HPLC. Our study shows that the 4FDC-INH-CFA cocrystal batch (PZA + EDH + RIF + INH-CFA cocrystal) exhibits superior stability compared to 4FDC-INH-VLA cocrystal (PZA + EDH + RIF + INH-VLA cocrystal and 4FDC reference (PZA + EDH + RIF + INH) is unstable. We show for the first time the improved stability of anti-TB 4FDC drugs using cocrystals of INH in a fixed dose formulation.

3.5 Experimental Section

Materials and Methods

RIF, INH, PZA and EDH (purity >99.8%) were purchased from Sigma-Aldrich, Hyderabad, India. Sodium phosphate dibasic was purchased from Sisco Research Laboratories Pvt. Ltd, Mumbai, India. High pressure liquid chromatographic (HPLC) grade acetonitrile, methanol and water solvents were procured from Merck Life Science Pvt. Ltd, Mumbai, India.

Preparation of FDC batches

INH-CFA cocrystal (1:1)

The bulk material of INH-CFA cocrystal was obtained upon extensive grinding of INH-CFA-Form-2 for 1-2 h by adding catalytic amount of CH_3CN solvent. The formation of cocrystal was confirmed by FT-IR, FT-Raman, PXRD and Differential Scanning Calorimetry (DSC).

INH-VLA cocrystal (1:1)

The bulk material of INH-VLA cocrystal was obtained upon extensive grinding of INH-VLA-Form-1 for 30 min by adding catalytic amount of CH_3CN solvent. The formation of cocrystal was confirmed by FT-IR, FT-Raman, PXRD and DSC.

FDC reference batch (RIF+INH+PZA+EDH)

Pure drugs were taken in prescribed amounts given by WHO 4-FDC formulation,[17] i.e. Rifampicin 150 mg, Isoniazid 75 mg, Pyrazinamide 400 mg, Ethambutol dihydrochloride 275 mg. The drugs were mixed uniformly and used for further studies.

FDC cocrystal batch (RIF+INH-CFA cocrystal +PZA+EDH)

Pure drugs were taken in prescribed amounts given by WHO, i.e. Rifampicin 150 mg, Pyrazinamide 400 mg, Ethambutol dihydrochloride 275 mg, and Isoniazid-Caffeic acid cocrystal (173 mg, equiv. to 75 mg of isoniazid). The 4-FDC of INH-CFA was used for further studies after proper mixing.

FDC cocrystal batch (RIF+INH–VLA cocrystal +PZA+EDH)

Pure drugs were taken in prescribed amounts given by WHO, i.e. Rifampicin 150 mg, Pyrazinamide 400 mg, Ethambutol dihydrochloride 275 mg, and Isoniazid-Vanillic acid cocrystal (167 mg, equiv. to 75 mg of isoniazid). The 4-FDC of INH-VLA was used for further studies after proper mixing.

The powder sample batches were ground to a uniform particle size distribution of 80-120 μm in a mortar-pestle and sorted by sieving. Extensive grinding was avoided to minimize any cross reactivity in the solid-state.

Storage of FDC batches

All the three FDC batches were prepared in triplicate and transferred to separate petri dishes. The petri dishes were charged in open state to the Thermolab T-908 stability chamber (Thermolab Scientific Equipments Pvt. Ltd., Maharashtra, India) set at accelerated stability test conditions of 40±1°C and 75±2% RH. Both physical and chemical changes were checked in the samples drawn after 7, 15, 22, and 30 days of storage in comparison with 0 day samples.

HPLC analysis for drug concentration

FDC reference batch (RIF+INH+PZA+EDH), FDC-INH-CFA cocrystal batch (RIF+INH-CFA cocrystal +PZA+EDH) and FDC-INH-VLA cocrystal batch (RIF+INH-VLA cocrystal +PZA+EDH) were taken in an open petri dish and exposed to accelerated ICH conditions of 40 °C and 75% RH. Samples were drawn after 3, 6, 9, 12, 15 and 30 d time intervals and dissolved in methanol solvent. 20 µl of the resultant solution was injected to HPLC for analysis. A previously reported validated RP-HPLC method[35] for the determination of RIF, INH and PZA in the presence of degradation products of RIF was used for the analysis of the sample composition. The mobile phase and the gradient program are described in Table 1. HPLC conditions of flow rate 1.2 mL/min, detection λ 238 nm were used. It was possible to analyze Rifampicin, Isoniazid, Pyrazinamide and HYD using this procedure. The difference in area under the peaks at 3, 6, 9, 12, 15 and 30 d as compared to 0 time was used for calculating the percent degradation of a particular drug. For HYD, direct peak area percent was taken for quantitation, because of its absence in the initial samples. We were unable to analyze ethambutol dihydrochloride due to lack of UV chromophore in this molecule.

Table 1 Gradient program for HPLC analysis.

Time (min)	Solution A (%)	Solution B (%)
0	100	0
0-5	100	0
5-18	0	100
18-25	100	0

Solution A = Buffer: ACN (96: 4)

Solution B = Buffer: ACN (55: 45)

Buffer composition: 1.4 g of dibasic sodium phosphate (Na_2HPO_4) in 1 L water (pH 6.8)

ACN: acetonitrile

The HPLC system consisted of a solvent delivery unit (LC-20AD), an on-line degasser (DGU-20A3), a PDA detector (SPD-M20A), and LC solution software for data acquisition and processing (All from Shimadzu, Japan). Separation was achieved on a Zodiac C18 column (250 X 4.6 mm, 5 µm, purchased from Zodiac Life Sciences, Hyderabad, India).

Scanning Electron Microscope (SEM)

The shape and morphology of the FDC batches were examined on a Carl Zeiss model Merlin Compact 6027 FESEM with a beam voltage of 3.0 kV. The sample was spread on a carbon-coated copper grid. Prior to SEM imaging, an ultrathin layer of gold was coated in order to enhance the conductivity of the sample.

Powder X-ray diffraction

Powder X-ray diffraction of all the samples were recorded on Bruker D8 Advance diffractometer (Bruker-AXS, Karlsruhe, Germany) using Cu-Kα X-radiation (λ= 1.5406 Å) at 40 kV and 30 mA power. X-ray diffraction patterns were collected over the 2θ range 5-50° at a scan rate of 1º/ min. Powder Cell 2.4[36] (Federal Institute of Materials Research and Testing, Berlin, Germany) was used for Rietveld refinement of experimental PXRD and calculated lines from the X-ray crystal structure.

3.6 References

1. Remenar, J. F.; Morissette, S. L.; Peterson, M. L.; Moulton, B.; MacPhee, J. M.; Guzmán, H. R.; Almarsson, Ö. *J. Am. Chem. Soc.* **2003**, *125*, 8456-8457.
2. Tothadi, S.; Desiraju, G.R.; *Chem. Commun*. **2013**, *49*, 7791-7793.
3. Steed, J. W. *Trends Pharmacol. Sci.* **2013,** *34*, 185-193.
4. Bolton, O.; Simke, L. R.; Pagoria, P. F.; Matzger, A. J.; *Cryst. Growth Des.* **2012**, *12*, 4311-4314.
5. Morimoto, M.; Kobatake, S.; Irie, M. *Chem. Commun*. 2008(3):335-337.

6. Sokolov, A. N.; Friščić, T.; MacGillivray, L. R. *J. Am. Chem. Soc*. **2006**, *128*, 2806-2807.
7. MacGillivray, L. R.; Papaefstathiou, G. S.; Friščić, T.; Hamilton, T. D.; Bučar, D. K.; Chu, Q.; Varshney, D. B.; Georgiev, I. G.; *Acc. Chem. Res*. **2008**, *41*, 280-291.
8. Schultheiss, N.; Newman, A. *Cryst. Growth Des.* **2009,** *9*, 2950-2967.
9. Duggirala, N. K.; Perry, M. L.; Almarsson, Ö.; Zaworotko, M. J. *Chem. Commun*. **2016**, *52*, 640-655.
10. Cherukuvada, S.; Babu, N. J.; Nangia, A. *J. Pharm. Sci*. **2011,** *100*, 3233-3244.
11. Suresh, K.; Goud, N. R.; Nangia, A. *Chem. –Asian J*. **2013**, *8*, 3032-41.
12. (a) Babu, N. J.; Sanphui, P.; Nangia, A. *Chem. –Asian J.* **2012,** *7*, 2274-2285. (b) Trask, A.V.; Motherwell, W. S.; Jones, W. *Cryst. Growth Des*. **2005**, *5*, 1013-1021. (c) Wang, Z. Z.; Chen, J. M.; Lu, T.B.; *Cryst. Growth Des.* **2012**, *12*, 4562-4566 (d) Wang, L.; Wen, X.; Li, P.; Wang, J.; Yang, P.; Zhang, H.; Deng, Z. *CrystEngComm* **2014**, *16*, 8537-8545.
13. Pai, M.; Behr1, M. A.; Dowdy, D.; Dheda, K.; Divangahi, M.; Boehme, C. C.; Ginsberg, A.; Swaminathan, S.; Spigelman, M.; Getahun, H.; Menzies, D.; Raviglione, M. *Tuberculosis. Nature Reviews Disease Primers.* **2016,** *2*, 1-23.
14. World Health Organization (WHO) report **2016**, http://www.who.int/tb/publications/factsheet_global.pdf
15. Yee, D.; Valiquette, C.; Pelletier, M.; Parisien, I.; Rocher, I.; Menzies, D. *American Journal of Respiratory and Critical Care Medicine*. **2003**, *167*, 1472-1477.
16. Blomberg, B.; Spinaci, S.; Fourie, B.; Laing, R. *Bulletin of the World Health Organization*. **2001,** *79*, 61-68.
17. World Health Organization. The Use of Essential Drugs: Ninth report of the WHO Expert Committee (including the revised Model list of essential drugs). Geneva, World Health Organization, 2000 (WHO Technical Report Series, No. 895).
18. Zwolska, Z.; Niemirowska-Mikulska, H.; Augustynowicz-Kopec, E.; Walkiewicz, R.; Stambrowska, H.; Safianowska, A.; Grubek-Jaworska, H. *Int. J. Tuberc. Lung Dis*. **1998**, *2*, 824-830.
19. Singh, S.; Mohan, B. *Int. J. Tuberc. Lung Dis.* **2003**, *7*, 298-303.

20. Bhutani, H.; Mariappan, T. T.; Singh, S. *Int. J. Tuberc. Lung Dis.* **2004**, *8*, 1073-1080.
21. Singh, S.; Mariappan, T. T.; Sharda, N.; Singh, B. *Pharmacy and Pharmacology Communications*. **2000**, *6*, 491-494.
22. Bhutani, H.; Singh, S.; Jindal, K. C.; Chakraborti, A. K. *J. Pharm. Biomed. Anal.* **2005,** *39*, 892-899.
23. Singh, S.; Bhutani, H.; Mariappan, T. T.; Kaur, H.; Bajaj, M.; Pakhale, S. P. *International Journal of Pharmaceutics.* **2002**, *245*, 37-44.
24. WHO, IUATLD, The promise and reality of fixed-dose combinations with rifampicin. *Int. J. Tuberc. Lung Dis.* **1994**, *75*, 180-181.
25. Swapna, B.; Maddileti, D.; Nangia, A. *Cryst. Growth Des.* **2014**, *14*, 5991-6005.
26. Devani, M. B.; Shishoo, C. J.; Doshi, K. J,; Patel, H. B. *J. Pharm. Sci.* **1985,** *74*, 427-432.
27. Singh, S.; Mariappan, T. T.; Sharda, N.; Kumar, S.; Chakraborti, A. K. *Pharmacy and Pharmacology Communications.* **2000**, *6*, 405-410.
28. Reichelt, R. Scanning electron microscopy. In: Hawkes PW, Spence JCH. (eds) Science of Microscopy. Springer. New York. **2007,** 133-272.
29. Maddileti, D.; Swapna, B.; Nangia, A. *Cryst. Growth Des.* **2015**, *15*, 1745-1756.
30. Swapna, B.; Suresh, K.; Nangia, A. *Chem. Commun*. **2016,** *52*, 4037-4040.
31. Mariappan, T. T.; SINGH, B.; SINGH, S. *Pharmacy and Pharmacology Communications.* **2000,** *6*, 345-349.
32. Diniz, L. F.; Carvalho Jr, P. S.; de Melo, C. C.; Ellena, J. *Cryst. Growth Des*. **2017**, *17*, 2622-2630.
33. Mannava, M. C.; Suresh, K.; Nangia, A. *Cryst. Growth Des*. **2016**, *16*, 1591-1598.
34. Cherukuvada, S.; Nangia, A. *Chem. Commun*. **2014**, *50*, 906-923.
35. Mohan, B.; Sharda, N.; Singh, S. *Journal of Pharmaceutical and Biomedical Analysis.* **2003,** *31*, 607-612.
36. Kraus, W.; Nolze, G. Powder Cell, A Program for Structure Visualization, Powder Pattern Calculation and Profile Fitting, Available at: http://www.ccp14.ac.uk/ccp/web-mirrors/powdcell/a_v/v_1/powder/e_cell.html

CHAPTER FOUR

Color Polymorphs of Aldose Reductase Inhibitor Epalrestat: Configurational, Conformational and Synthon Differences

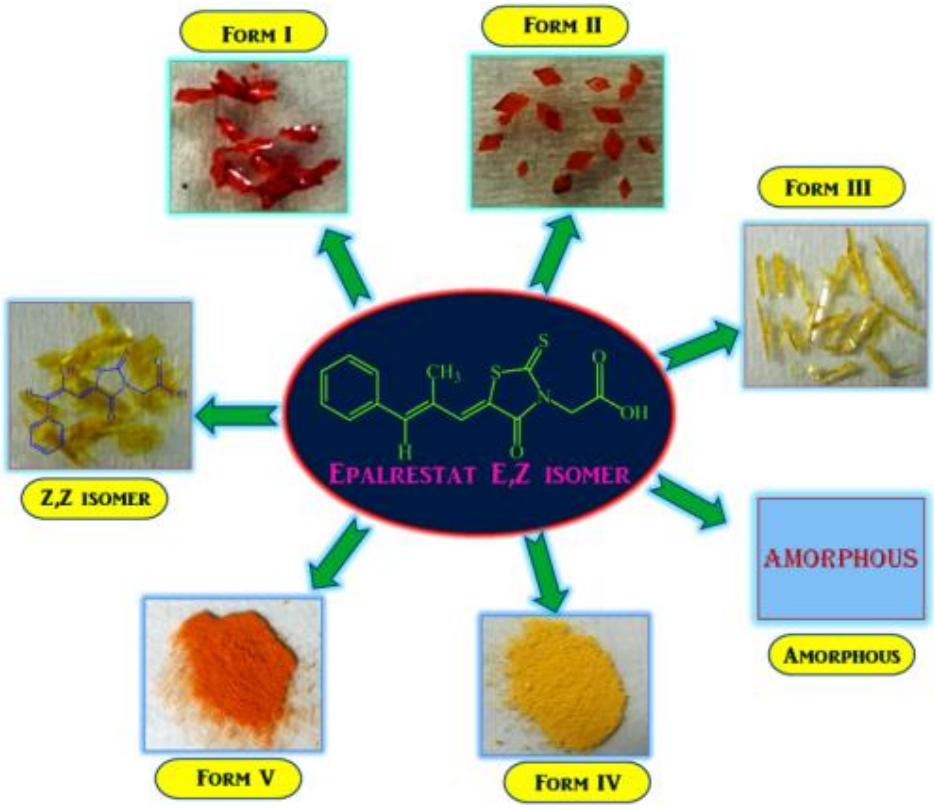

Color polymorphs of aldose reductase inhibitor Epalrestat exhibit configurational, conformational and synthon differences. Form I (deep red), form II (deep orange), form III (bright yellow), form IV (yellow), form V (orange) are in the E,Z configuration of the drug, and a Z,Z isomer (bright yellow). The stability of polymorphs was established by grinding, solvent slurry and thermal conditions as Form I (thermodynamic) > Form II > Form V > Form III > Form IV (least stable).

4.1 Introduction

Polymorphism (supramolecular isomers) and configurational isomers (R/S, cis-trans, diastereomers) are related phenomena which can influence the structure and property of molecules.[1,2] Polymorphism is the ability of a chemical substance to exist in multiple crystal structures which have different packing arrangements and/or conformations of molecules in the solid state. Configurational isomerism may be stated as the compounds with the same molecular formula exhibiting different orientation of groups in space (stereoisomers) or about double bond (geometric isomers). Configurational isomers are considered to be stable and not inter convertible at room temperature (possible to isolate), in contrast to conformers which are interconvertible readily at room temperature. Whereas isomerism is a molecular feature, polymorphism is about the supramolecular arrangements of molecules in the solid state.

Polymorphism of crystalline materials, especially for drugs, is an area of immense interest and value to the pharmaceutical industry because polymorphs can exhibit different physicochemical properties, such as solubility, dissolution rate, chemical and physical stability, melting point, color, filterability, density, flow properties and bioavailability.[3,4] For example, Chloramphenicol, a broad spectrum antibiotic is marketed as its prodrug, palmitate ester which converts to the active compound in the small intestine[5a]. Chloramphenicol palmitate exists in three polymorphic forms, form A, form B, and form C. Form C is highly unstable and form A is practically insoluble and has low biological activity as it is slowly hydrolyzed to the active component. Form B is metastable and more soluble. Therefore, Form B is an active form. Thus, maximum blood levels attained with 100% form B is about 7 times greater than with 100% form A and that with mixtures of A and B the blood levels varies according to the percentage of form B in suspension[5b,c] when the same dose was administered (Figure 4.1). Another example is furosemide, whose metastable forms II and III are not preferred despite being more soluble, because they are chemically unstable compared to the stable polymorph I[6]. In addition, the unfortunate withdrawal of the HIV drug Ritonavir[7] from the market by Abbott laboratories because of the spontaneous appearance of the more stable polymorph (and so less soluble), which compromised the drug bioavailability. In essence, the above literature reports highlight the study of all polymorphs of a drug and establishing their stability relationships is as an obligatory step in solid form development.[8,9] Since

polymorphs occur at different levels on the 'free energy' surface, inter-conversions are possible and lead to changes in the properties of bulk drugs which in result affect drug efficacy.[8] Therefore, it is important to gain adequate understanding of their properties so as to optimize conditions for a desired polymorph and avoid accidental transformations (polymorphic transformations, hydration etc.).[8]

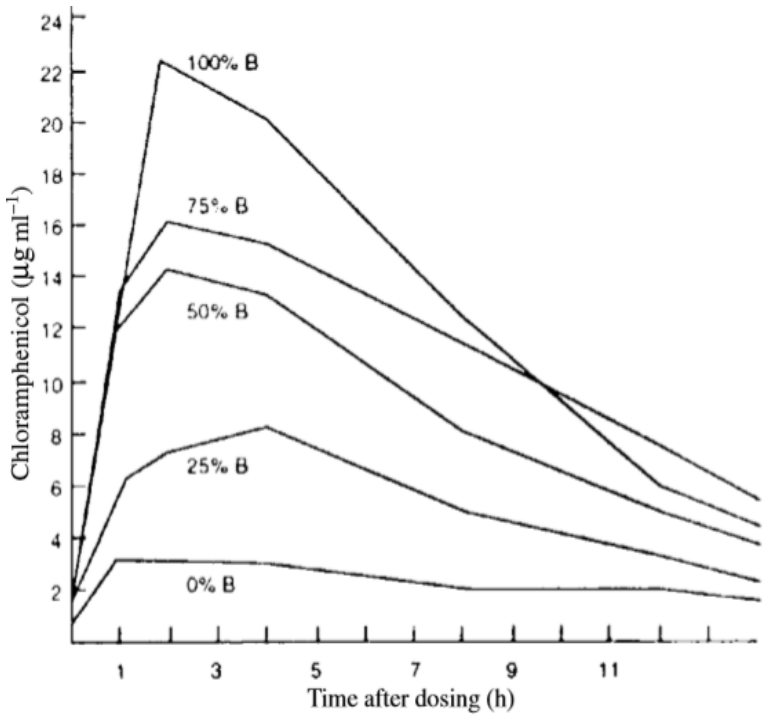

Figure 4.1 Comparison of serum levels (μg cm^{-3}) obtained with suspensions of Chloramphenicol palmitate after oral administration of a dose equivalent to 1.5g of Chloramphenicol (Adapted from ref. 5c).

4.2 Literature Reports on Epalrestat

Epalrestat (EPR, hereafter) 5-[(1Z,2E)-2-methyl-3-phenylpropenylidene]-4-oxo-2-thioxo-3-thiazolidineacetic acid is an anti-diabetic drug which acts by inhibiting aldose reductase enzyme. Igarashi et al.[10a] reported the crystal structure of EPR form I and the ethanol solvate was reported by Ishida et al.[10b] Other reported solvates are methanol[10c], tetrahydrofuron[11a], acetone[11b], dimethyl formamide[12], and dimethyl sulfoxide[12]. A cocrystal[12] of EPR is also reported. EPR is stable in the dark but undergoes isomerisation by photoirradiation to give four isomers[13] (E,Z, Z,Z, E,E and Z,E isomers). Spectroscopic evidences (^{1}H NMR and HPLC) suggest the structures for these

photoisomers (Scheme 4.1). In this chapter we report five polymorphs, an amorphous phase, and the Z, Z isomer of EPR. Crystal form I, II, III (E,Z isomer) and Z,Z isomer structures were established by X-ray diffraction, and the remaining forms IV, V and amorphous state were characterized by spectroscopic (FT-IR, Raman, ^{13}C ss-NMR), thermal (DSC, HSM), and powder XRD techniques. Phase transformations were studied by VT-PXRD, DSC and HSM analysis.

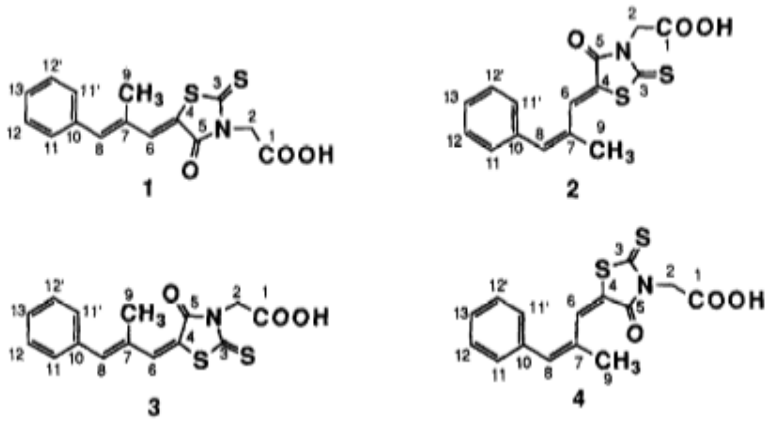

Scheme 4.1 Molecular structures of EPR photoisomers.

4.3 Results and Discussion

Polymorphism screening of anti-diabetic drug Epalrestat has resulted in five anhydrous polymorphs E,Z isomer, amorphous form and Z,Z isomer. The amorphous form was prepared by rapidly cooling the EPR melt by liquid nitrogen. Heating the amorphous form at 85 °C resulted in form IV. Form V was obtained by heating form IV at 170 °C. Forms I to III and Z,Z isomer were prepared by slow evaporation/ crystallization from various solvents. Interesting feature of EPR is color polymorphism i.e; form I exhibits a red color, form II, V are light orange in color and form III, IV and Z,Z isomer exhibits a yellow color. Different crystal colors can be explained through conformational polymorphism. Conformational polymorphism refers to the existence of different molecular conformations in different polymorphs. In the case of EPR, the conformational difference is most pronounced in the torsional angle (C12-N1-C14-C15). Other remarkable feature of EPR is geometrical isomerism. When Z,Z isomer was heated at 180 °C for 30 min in programmable oven, it resulted in form I of E,Z isomer. Crystal structures of form I, II, III and Z,Z isomer were determined form single crystal X-ray diffraction techniques. Crystal structure analysis of form I and II has revealed that both

crystal structures have O–H···O and C–H···O hydrogen bonding interactions and differ in molecular packing. Therefore form I and II can be classified as packing polymorphs. Polymorphic pairs form I, III and II, III significantly differ in molecular conformation and acid···acid dimer synthon was observed in the crystal structure of form III. Therefore they can be classified as synthon and conformational polymorphs. The stability relationships between the EPR polymorphs were investigated by thermal methods such as DSC (differential scanning calorimetry), HSM (hot-stage microscopy) experiments and VT-PXRD (variable-temperature powder x-ray diffraction), grinding and solvent slurry experiments. From thermal data, we found that form I is enantiotropically related to form II and form V, monotropically related to form III and IV. The thermodynamic stability of EPR polymorphs at RT can be given as (stable) form I>form II>form V>form III>form IV> amorphous (meta stable).

A flowchart (Scheme 4.2) shows the different solution crystallization and temperature conditions which gave the different polymorphs of EPR and their conversion. The different colors of these polymorphs are displayed in Figure 4.2 (see crystallographic data in Table 4.1 and hydrogen bonds in Table 4.2).

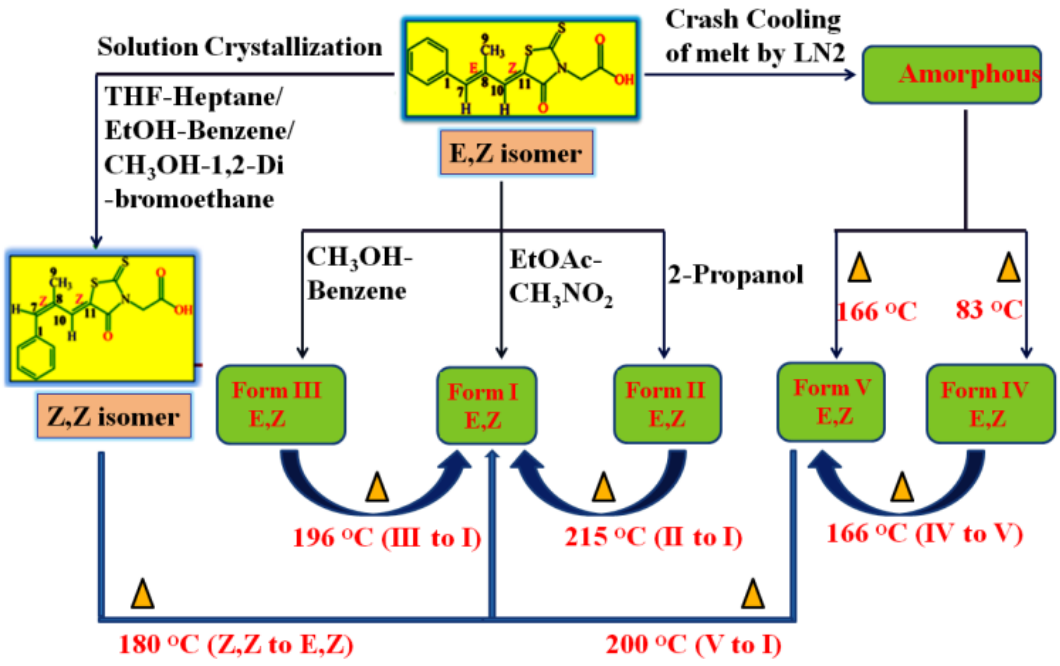

Scheme 4.2 Preparation and phase transformations of EPR polymorphs.

Figure 4.2 Photographs of different colored EPR polymorphs: deep red – form I, deep orange – form II, orange – form V; bright yellow – form III, yellow – form IV, and bright yellow – Z,Z isomer.

Table 4.1 Cystallographic parameters of EPR forms.

	Form I This study	**Form I Reported[a]**	**Form II This study**	**Form III This study**	**Z,Z isomer This study**
Chemical formula	C15 H13 N O3 S2	C15 H13 N O3 S2	C15 H13 N O3 S2	C15 H13 N O3 S2	C15 H13 N O3 S2
Crystal system	Triclinic	Triclinic	Monoclinic	Monoclinic	Monoclinic
Formula weight	319.38	319.39	319.38	319.38	319.38
Space group	$P\bar{1}$	$P\bar{1}$	*C2/c*	$P2_1/n$	$P2_1/c$
***T* [K]**	298	298	298	298	298
***a* [Å]**	8.1399(10)	8.20888(15)	13.7384(4)	14.7831(13)	11.4252(5)
***b* [Å]**	11.5584(14)	11.6639(2)	9.1063(3)	5.6288(5)	6.9479(3)
***c* [Å]**	16.1506(19)	16.3107(3)	24.1429(7)	18.2621(16)	19.4673(9)
***α* [°]**	96.721(10)	96.5985(8)	90	90	90
***β* [°]**	93.818(10)	93.8393(8)	100.747(3)	98.364(8)	102.898(5)
***γ* [°]**	104.724(10)	104.6780(8)	90	90	90
Z	4	4	8	4	4
***V*[Å^3]**	1452.2(3)	1493.22(5)	2967.44(16)	1503.5(2)	1506.35(12)
D_{calc} [g cm^{-3}]	1.461	1.421	1.430	1.411	1.408
Reflns. collected	9766	16752	10378	6015	5273
Unique reflns.	5131	5319	2625	2654	2663

Observed reflns.	2548	5319	2441	1989	1910
R_1 **[I>2(I)]**	0.0632	0.0460	0.0558	0.0427	0.0543
wR_2 **(all)**	0.1084	0.1315	0.1550	0.0996	0.1603
Goodness-of-fit	0.983	1.081	1.087	1.026	1.036
Diffractometer	Oxford CCD	Rigaku RAXIS-RAPID II	Oxford CCD	Oxford CCD	Oxford CCD

[a] Reported crystal structure in ref. 10.

Table 4.2 Hydrogen bond metrics in the crystal structures.

Interaction	H···A (Å)	D···A (Å)	D–H···A (º)	Symmetry Code
EPR form I				
O3–H3A···O4	1.98	2.751(6)	174	x,1+y,z
O6–H6A···O1	1.80	2.664(5)	147	1-x,-y,-z
C4–H4···O2	2.56	3.419(8)	154	1-x,-y,-z
C7–H7···O5	2.40	3.301(6)	164	1-x,-y,-z
C10–H10···O5	2.39	3.284(6)	161	1-x,-y,-z
C24–H24C···S4	2.86	3.796(5)	165	2-x,-y,1-z
C29–H29B···O2	2.30	3.212(6)	157	x,-1+y,z
C19–H19···S2	2.82	3.616(6)	130	x-1,+y,+z
C21–H21···S3	2.84	3.908(4)	168	x-1,+y,+z
C9–H9A···S1	2.39	3.161(6)	137	Intra
C10–H10···O1	2.51	2.876(6)	104	Intra
C14–H14B···O1	2.41	2.773(6)	101	Intra
C24–H24A···S3	2.54	3.087(5)	116	Intra
C25–H25···O4	2.53	2.874(6)	102	Intra
C29–H29B···O4	2.47	2.812(5)	100	Intra
EPR form II				
O3–H3A···O1	1.97	2.780(3)	168	1/2-x,-1/2+y,1/2-z
C14–H14B···O2	2.38	3.330(4)	165	1/2-x,1/2+y,1/2-z
C10–H10···S2	2.74	3.819(2)	175	x+1/2,+y-1/2,+z
C4–H4···O2	2.60	3.389(4)	129	-x+2,-y+2,-z+1
C9–H9A···S1	2.56	3.128(3)	118	Intra
C10–H10···O1	2.54	2.883(3)	102	Intra
C14–H14B···O1	2.46	2.839(3)	103	Intra
EPR form III				
O3–H3A···O2	1.85	2.670(3)	177	2-x,2-y,1-z
C10–H10···O1	2.46	3.345(3)	159	3/2-x,-1/2+y,1/2-z
C9–H9A···S1	2.59	3.198(2)	122	Intra
C10–H10···O1	2.46	3.345(3)	159	Intra
C14–H14A···S2	2.74	3.095(3)	102	Intra
EPR form *Z,Z* isomer				
O3–H3A···O2	1.84	2.658(3)	177	2-x,1-y,1-z
C9–H9C···S1	2.80	3.107(5)	100	Intra
C10–H10···O1	2.57	2.903(5)	102	Intra
C14–H14B···O1	2.43	2.815(5)	103	Intra

4.3.1 Crystal Structure Analysis

Epalrestat form I: Block morphology crystals of EPR form I were obtained from EtOAc : CH_3NO_2 solvent mixture (1:1) in triclinic space group $P\bar{1}$ with two molecules (Z'=2) in the asymmetric unit. Two symmetry-independent molecules are connected via O–H···O and C–H···O hydrogen bonds (O3–H3A···O4, 1.98 Å, 174°, C29–H29B···O2, 2.30 Å, 157°) in a $R_2^2(9)$ dimeric motif. Such motifs are held together by O–H···O (O6–H6A···O1, 1.80 Å, 147°) hydrogen bonds in a tetrameric $R_4^4(22)$ motif (Figure 4.3a), and such tetrameric motifs extend through weak C–H···S interactions (C21–H21···S3, 2.84 Å, 168°; C24–H24C···S4, 2.86 Å, 165°) (Figure 4.3b). The importance of auxiliary C–H···O interactions from acidic C–H donors,[14-16] such as phenyl, cubane, and adjacent to C=O, in fortifying the O–H···O synthons of carboxylic acids was first identified by Desiraju.[14,15]

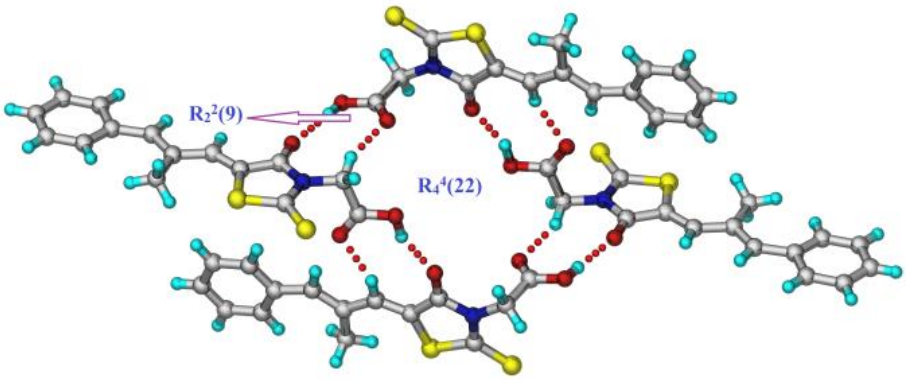

(a)

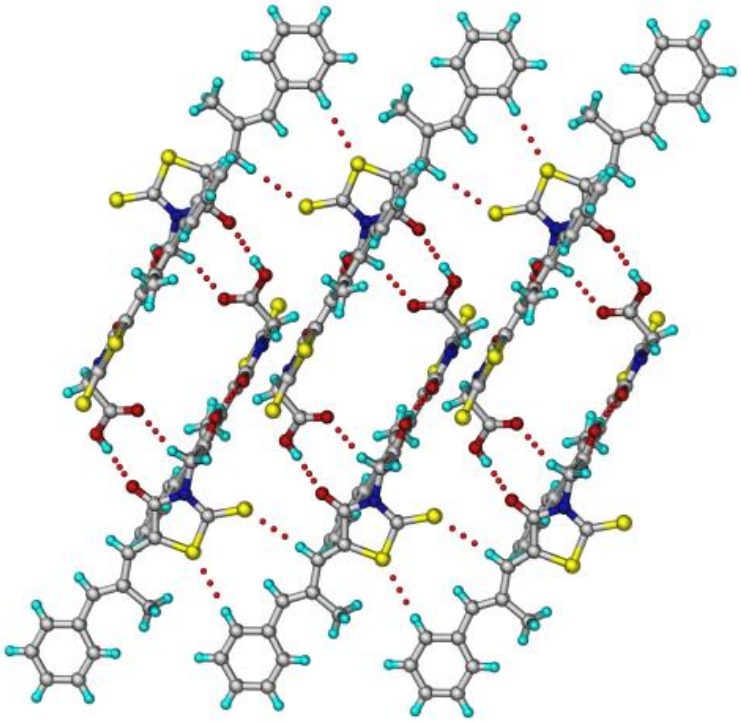

(b)

Figure 4.3 (a) $R_2^2(9)$ dimeric and $R_4^4(22)$ tetrameric assembly of EPR molecules via O–H···O and C–H···O hydrogen bonds. (b) Tetrameric motif EPR molecules were extend in to a chain through C–H···S interactions in the crystal structure of form I

Epalrestat form II: Diamond shaped crystals of EPR form II were obtained from i-PrOH in monoclinic space group *C2/c* (*Z′*=1). A $R_2^2(9)$ dimeric motif similar to Form I (O3–H3A···O1, 1.97 Å, 168º, C14–H14B···O2, 2.38 Å, 165º) arranges the molecules in a 1D zigzag chain, with such chains being assembled via π···π and C–H···O (C4–H4···O2, 2.60 Å, 129º) interactions (Figure 4.4). Form I and II have the same primary synthon but exhibit differences in their molecular packing.

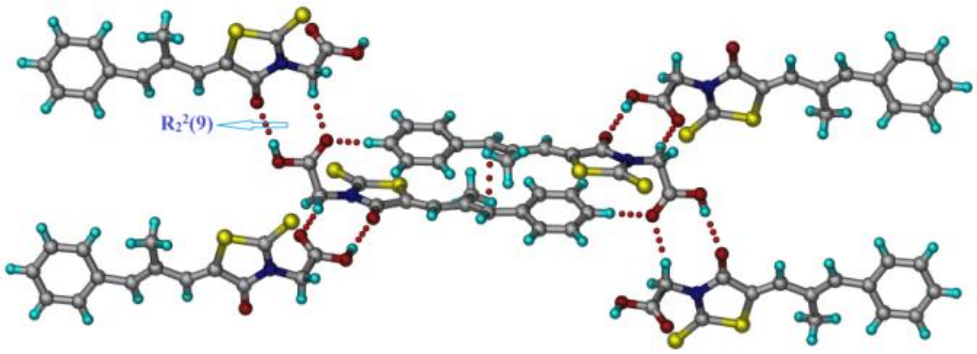

Figure 4.4 $R_2^2(9)$ dimeric motif in Form II EPR together with π stacking and C–H···O interactions.

Epalrestat form III: Needle morphology crystals of EPR form III were obtained from methanol : benzene (1:1) in $P2_1/n$ space group (Z'=1). The molecules are connected through the common carboxylic acid homosynthon $R_2^2(8)$ through O–H···O hydrogen bonds (O3–H3A···O2, 1.85 Å, 177°), which are connected via an auxiliary C–H···O (C10–H10···O1, 2.46 Å, 159°) (Figure 4.5). Polymorphic pairs I, III and II, III differ in hydrogen bond synthons[17] and molecular conformation.[18]

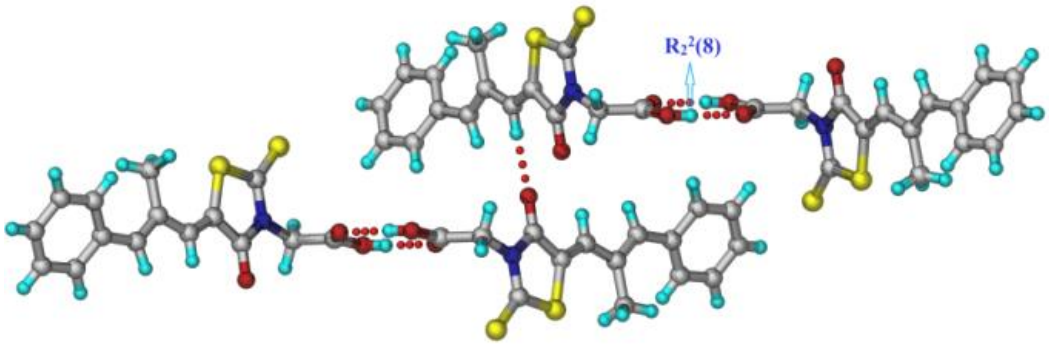

Figure 4.5 Acid-acid dimer homosynthon ring motif between molecules connected through C–H···O interactions in form III crystal structure.

Epalrestat Z,Z isomer: Plate morphology crystals of the Z,Z-isomer of EPR were obtained from different solvent mixtures, e.g. THF : heptane, ethanol : benzene, methanol : 1,2-dibromoethane (1:1) in $P2_1/c$ space group (Z'=1). The crystal structure exhibits the acid dimer homosynthon (O3–H3A···O2, 1.84 Å, 177°) and S···O chalcogen type II interaction[19] (S···O, 2.65 Å, 177°) (Figure 4.6).

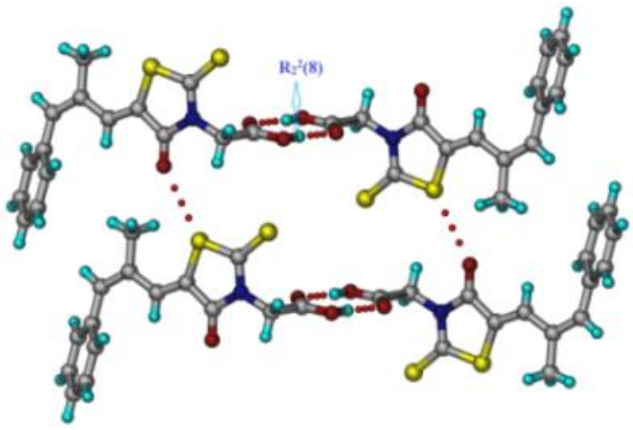

Figure 4.6 Corrugated sheet structure in EPR Z,Z-isomer sustained by COOH dimer and chalcogen S···O interactions.

4.3.2 Conformational analysis and color polymorphism

Molecular structures of EPR E,Z and Z,Z isomers are shown in Scheme 4.2. It consists of carboxy methyl rodhanine and methyl phenyl propenylidene moieties. Polymorphs I to V adopts an E,Z configuration along C(7)=C(8) and C(10)=C(11) bonds while Z,Z isomer adopts an Z,Z configuration. The configurational isomers E,Z and Z,Z are differ in the τ_1 (C1-C7-C8-C9) torsion angle. The difference in the overall geometry is mostly caused by the rotation of the benzene ring around the C(7)=C(8) bond. Polymorphic pairs form I and III; form II and III exhibit conformational polymorphism and they differ in the torsion angle τ_2 (C12-N1-C14-C15). The conformational difference arises because of the free rotation of the acetic acid group along the C(14)-C(15) bond. Form II exhibits different torsion angles compared to forms I and III. The two crystallographically non-equivalent molecules of form I (red and green) have distinct torsion angles which are also different from the forms II and III. Torsion angles of some selected EPR conformers are shown in Table 4.3 and Figure 4.7 presents an overlay diagram of ERR conformers which shows the extent of conformational diversity found in the different forms of EPR molecule.

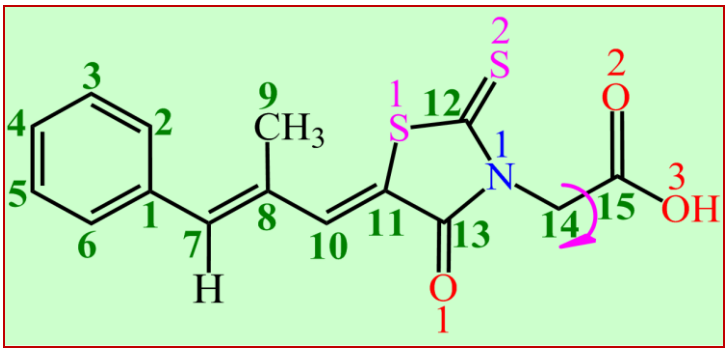

τ_1 (C1-C7-C8-C9), τ_2 (C12-N1-C14-C15), τ_3(S2-C12-N1-C14), τ_4 (C13-N1-C14-H14B), τ_5 (N1-C14-C15-O3)

Crystal Forms	τ_1(°)	τ_2(°)	τ_3(°)	τ_4(°)	τ_5(°)
EPR form I (molecule A)	-2.12	-77.14	0.59	-21.75	159.07
EPR form I (molecule B)	-1.07	-80.12	0.48	-22.98	167.30
EPR form II	4.96	-72.50	-3.77	-15.98	167.82
EPR form III	0.65	84.50	2.90	31.08	-162.77
EPR Z,Z isomer	176.85	74.33	1.32	17.97	-157.84

Table 4.3 Torsion angles in EPR molecule in different polymorphs and Z, Z isomer

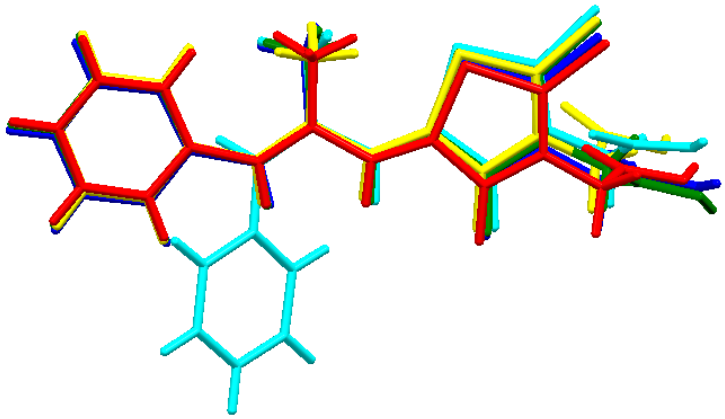

Figure 4.7 An overlay diagram of the conformers found in the EPR forms. Color codes: Red–molecule A of EPR form I, Green–molecule B of EPR form I, Yellow–EPR form II, Blue–EPR form III, Cyan EPR Z,Z isomer

Interestingly different polymorphs of EPR display color polymorphism (Figure 4.2). The archetype color polymorphism in ROY (red, orange, yellow colors) was ascribed to conformational differences between polymorphs.[20] The conformations of EPR polymorphs are different (Figure 4.7) as well as hydrogen bonding and molecular packing. Solid-state UV-Vis spectra (Figure 4.8) show differences in λ_{max} due to torsion angle changes and varying degrees of π-electron delocalization between the rhodanine, phenyl propenylidene and acetic acid groups, resulting in color polymorphism. The absorption band due to n → π* transition appears at λ_{max} = 467 nm (red) for Form I, 462 nm (orange) in Form II and Form V, and at 437 nm (yellow) for Form IV and III, and 456 nm (yellow) for the Z,Z isomer.

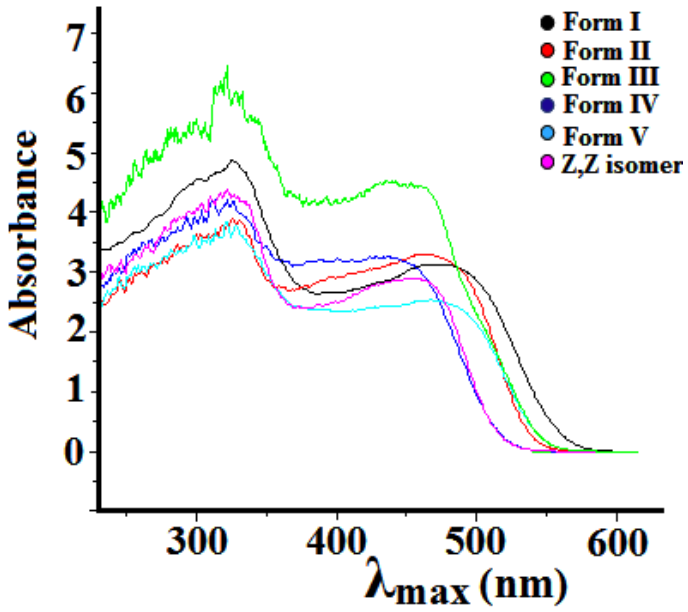

Figure 4.8 Solid-state UV−Vis spectra of EPR forms.

4.3.3 Spectroscopic Analysis

Spectroscopic techniques such as FT-IR and FT-Raman are often used to obtain information pertaining to the differences in molecular conformation and hydrogen bonding in the solid state[21]. FT-IR spectra and stretching frequency values of EPR forms is shown in Figure 4.9 and Table 4.4. The carbonyl stretching vibrations of keto and carboxylic acid functional groups are observed at 1677.5, 1746.5 cm^{-1} for form I; 1686.3, 1747.3 cm^{-1} form II; 1677.1, 1745.6 cm^{-1} for form V; 1702.4, 1726.9 cm^{-1} for Z,Z isomer. Whereas forms III and IV showed only one peak in this region at 1708.5 cm^{-1}, 1710.4 cm^{-1} owing to the overlapping between keto and acid carbonyl stretching vibrations and as mentioned above, in the case of Z,Z isomer these two stretching vibrations are very closer. The significant differences in the vibrational modes of forms are due to the differences in the hydrogen bonding patterns in the polymorphs, that is, in the crystal structures of forms I and II, keto and carboxylic acid functional groups makes O–H···O and C–H···O H-bonds. But in the case of form III and Z,Z isomer acid group forms acid-acid dimer synthon and keto group makes C–H···O (form III) and S···O (Z,Z isomer) interactions. Because of this hydrogen bonding differences, we also observed O–H stretching frequencies only for forms I, II, V at 3240.9 cm^{-1}, 3249.3 cm^{-1} and 3235.3 cm^{-1} which are absent in forms III, IV and Z,Z isomer. We observed aromatic C–H stretching vibrations at 2994.8 cm^{-1} in form I, at 3007.0 cm^{-1} in form II, 2962.1 cm^{-1} in

form III, 3023.4 cm^{-1} in form IV, at 3056.1 cm^{-1} in form V, and 2966.2 cm^{-1} for Z,Z isomer. Similar vibrational patterns were observed for the amorphous form and crystalline modifications form III, form IV and Z,Z isomer indicating that they exhibit same hydrogen bonding interactions.

We also observed significant differences in the FT-Raman spectra of all forms for the carbonyl stretching vibrations that involved in hydrogen bonding (Figure 4.10 and Table 4.5). The carbonyl stretching vibrations of keto and carboxylic acid functional groups are observed at 1593.8, 1555.0 cm^{-1} for form I; 1596.2, 1561.1 cm^{-1} for form II; 1597.9, 1566.3 cm^{-1} for form III; 1599.5, 1566.7 cm^{-1} for form IV, 1594.8, 1555.2 cm^{-1} for form V, 1599.1, 1571.5 cm^{-1} for Z,Z isomer and 1594.9, 1568.1cm^{-1} for amorphous form.

Solid-state NMR spectroscopy is a sensitive probe of molecular conformations, hydrogen bonding and short-range order in solids[22]. There are two well resolved peaks in the ss-NMR spectrum (Figure 4.11 and Table 4.6) representing the thiocarbonyl region at 191.8 and 193.9 ppm, methyl peak at 17.8 and 14.9 ppm, propenyl carbons at 117.4 and 120.8 ppm; the doubled peaks are due to two non-equivalent crystallographic molecules in the asymmetric unit of form I. Similar to form I, two peaks (and sometime three) were observed in the thiocarbonyl, methyl, propenyl and methylene regions of form V. Since PXRD and DSC (Figure 4.12 and 4.18) suggest that form V is not a mixture of polymorphs, it is likely that there are multiple molecules in the crystal structure (a surmise in the absence of single crystal X-ray structure). There are significant differences in the chemical shift values of form II, III and IV, due to different molecular conformations, hydrogen bonding and molecular packing. The ss-NMR of the Z,Z isomer of EPR is dramatically distinct from all other polymorphs of the E,Z isomer, particularly in the phenyl propenylidene group carbon region, in which there is a downfield shift of the methyl resonance of the phenyl propenylidene group, 20 ppm versus approximately 17 ppm in all other forms. The amorphous form exhibited broader and less resolved peaks due to absence of long-range molecular order and packing in the solid-state.

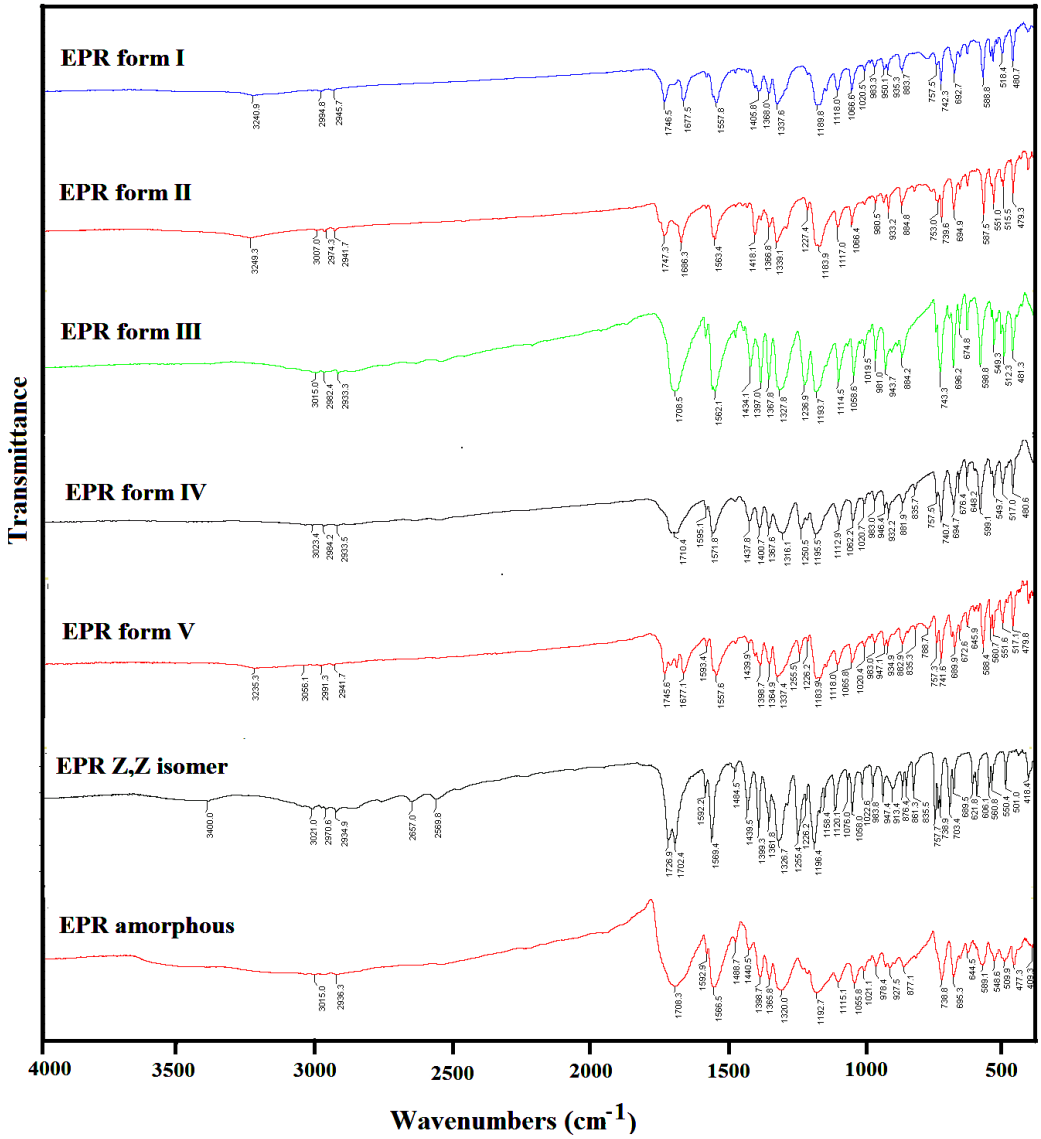

Figure 4.9 FT-IR spectral overlay of EPR forms.

Table 4.4 List of FT-IR stretching frequencies of EPR forms (in cm^{-1}).

Form	Aromatic C–H stretch	Ketone C=O stretch	Carboxylic C=O stretch	O–H Stretch	C–N stretch
Form I	2994.8	1677.5	1746.5	3240.9	1337.6
Form II	3007.0	1686.3	1747.3	3249.3	1339.1
Form III	3015.0	1708.5	-	-	1327.8
Form IV	3023.4	1710.4	-	-	1316.1
Form V	3056.1	1677.1	1745.6	3235.3	1337.4
Z,Z isomer	3021.0	1702.4	1726.9	-	1326.7
amorphous	3015.0	1708.3	-	-	1320.0

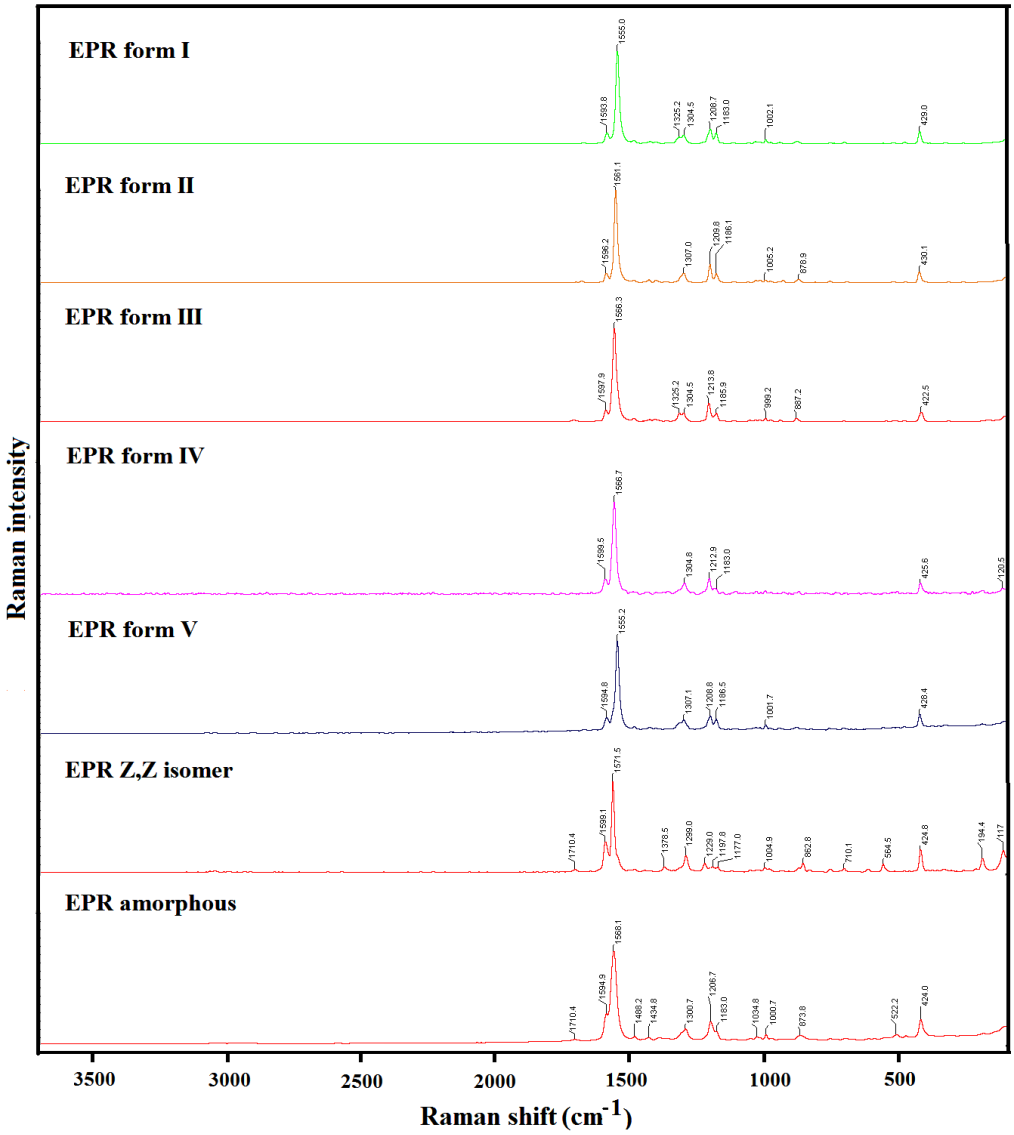

Figure 4.10 FT-Raman spectral overlay of EPR forms.

Table 4.5 List of FT-Raman stretching frequencies of EPR forms (in cm^{-1}).

Form	C–N stretch	Ketone C=O stretch	Carboxylic C=O stretch	C=C–C=C asymmetric stretch
Form I	1208.7	1555.0	1593.8	1304.5
Form II	1209.8	1561.1	1596.2	1307.0
Form III	1213.8	1566.3	1597.9	1304.5
Form IV	1212.9	1566.7	1599.5	1304.8
Form V	1208.8	1555.2	1594.8	1307.1
Z,Z isomer	1229.0	1571.5	1599.1	1299.0
amorphous	1206.7	1568.1	1594.9	1300.7

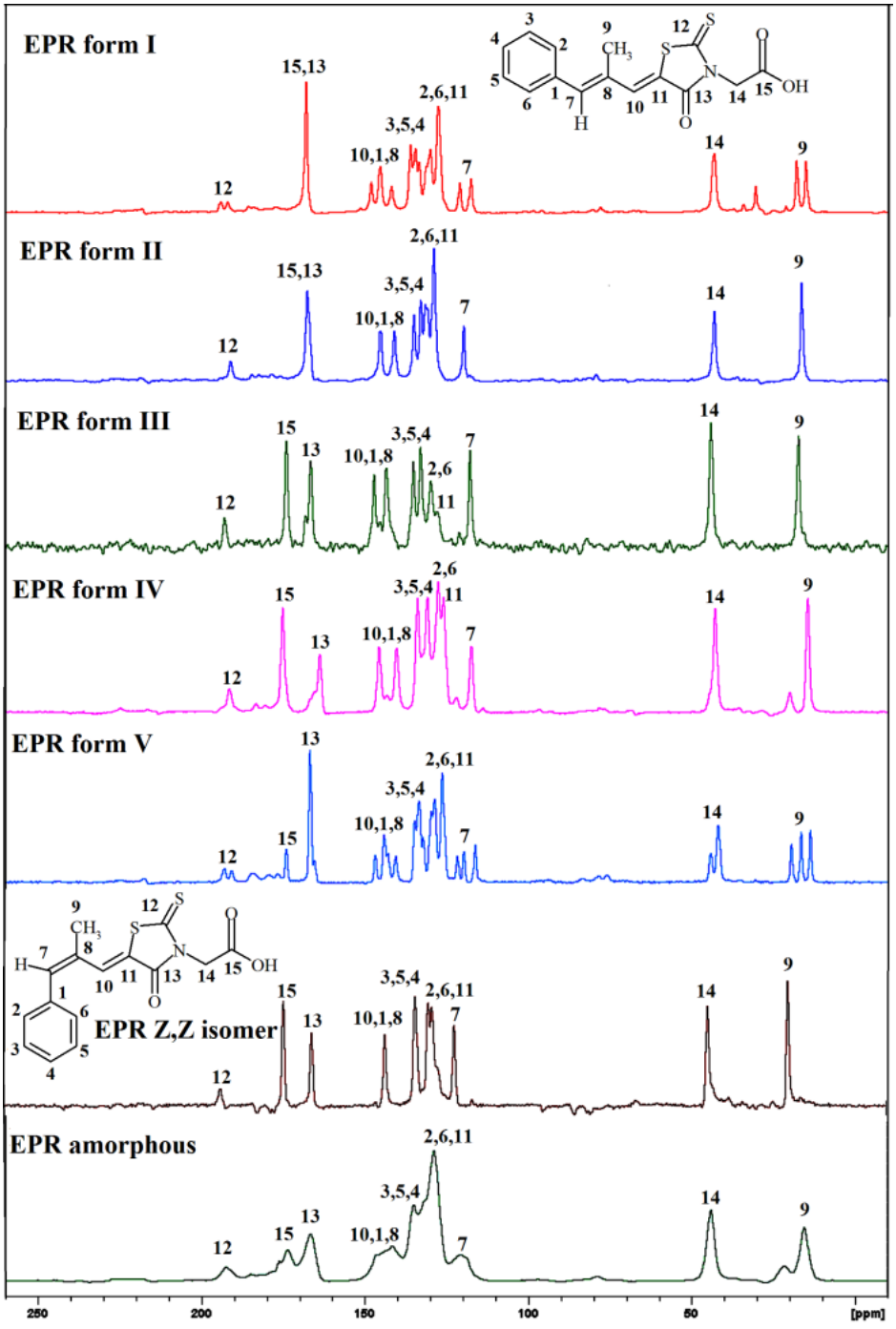

Figure 4.11 ^{13}C ss-NMR spectrum of EPR forms to show differences in chemical shifts.

Table 4.6 ^{13}C ss-NMR chemical shifts (δ, ppm) of EPR forms.

Carbon No.	EPR form I	EPR form II	EPR form III	EPR form IV	EPR form V	EPR Z,Z isomer	EPR Amorphous
1	141.7	140.9	143.1	140.2	140.7	143.3	141.4
2	129.8	131.4	129.4	127.6	128.8, 129.8	130.0	128.7
3	134.4, 135.9	134.9	134.8	133.9	133.6, 134.9	134.0	134.9
4	133.3	132.8	132.6	130.8	132.3	134.0	134.9
5	134.4, 135.9	134.9	134.8	133.9	133.6, 134.9	134.0	134.9
6	129.8	131.4	129.4	127.6	128.8, 129.8	130.0	128.7
7	117.4, 120.8	119.7	117.5	117.4	116.4, 119.9, 121.8	122.0	120.6
8	141.7	140.9	143.1	140.2	140.7	143.3	141.4
9	17.8, 14.9	16.3	17.0	14.5	14.0, 16.9, 19.8	20.0	15.4
10	145.2, 147.9	145.2	146.8	145.6	144.2, 146.9	143.3	141.4
11	127.4	130.9	127.6	125.9	126.5	128.9	128.7
12	191.8, 193.9	191.0	192.6	191.5	190.9, 193.0	193.6	192.2
13	167.8	167.6	166.3	163.7	166.8	165.7	166.4
14	43.0	43.0	43.7	42.8	42.2, 44.4	44.6	43.9
15	167.8	167.6	173.7	175.1	174.0	174.3	173.4

4.3.4 Powder X-ray Diffraction Analysis

Powder X-ray diffraction is the most fundamental tool for the study of polycrystalline materials and is eminently suited for the characterization of polymorphs[23]. The powder X-ray diffraction patterns for the EPR forms shows major differences throughout their diffraction patterns(Figure 4.12). PXRD pattern of commercial EPR matches with the powder XRD pattern of EPR form I. The experimental PXRD pattern of the form I, form II, form III and Z,Z isomer showed excellent match with the calculated diffraction line pattern from the crystal structure, thereby confirming identity and homogeneity of the crystalline phases (Figure 4.13). Several experiments to get single crystals of form IV and form V were unsuccessful and their unique powder XRD is the signature pattern. The amorphous form of EPR was prepared by quench cooling of EPR melt by liquid nitrogen and it shows one broad PXRD maxima, indicating that there is a very low degree of order. At ambient conditions, amorphous form was stable for 3 days and after this period it was converted to form I (Figure 4.14). VT-PXRD is ideally suited for the study of solid-state phase transformations in polymorphs and amorphous phases. Form IV was prepared by heating the amorphous form at 85 °C in programmable oven for 30 min and it was confirmed through VT-PXRD (variable-temperature PXRD) (Figure 4.15a). Similarly, form V was prepared by heating form IV at 170 °C for 30 min. Form

V was transformed to form I by heating at 200 °C for 30 min. The phase transformations from form IV to V and form V to I were confirmed through VT-PXRD studies (Figure 4.16a and 4.15b). Similarly, The phase transformations from form II to I and form III to I were confirmed through VT-PXRD studies (Figure 4.16b and 4.17a). Interestingly, when Z,Z isomer of EPR was heated at 180 °C in programmable oven for 30 min form I of E,Z isomer was obtained. In order to prove this configurational isomerism we have done VT-PXRD studies on Z,Z isomer where diffraction peaks corresponding to Z,Z isomer were disappeared after 180 °C and new peaks corresponding to form I of E,Z isomer were observed (Figure 4.17b). Form I exhibits characteristic peaks at 2θ = 7.8°, 12.5°, 17.2°, 22.7°, and 25.3°. Form II was found to possess peaks at 2θ = 7.4°, 14.5°, 21.6°, 25.4°, and 27.1°. Form III has peaks at 2θ = 8.2°, 9.6°, 14.9°, 21.2°, and 22.8°.Form IV shows peaks at 2θ = 7.7°, 14.2°, 15.1°, 19.9°, and 25.1°. Form V has characteristic peaks at 2θ = 7.7°, 9.0°, 16.2°, 22.5°, and 26.8°.Z,Z isomer was found to be distinct from forms I to V by the presence of peaks at 2θ = 7.7°, 9.1°, 16.6°, 21.5°, and 26.7°.

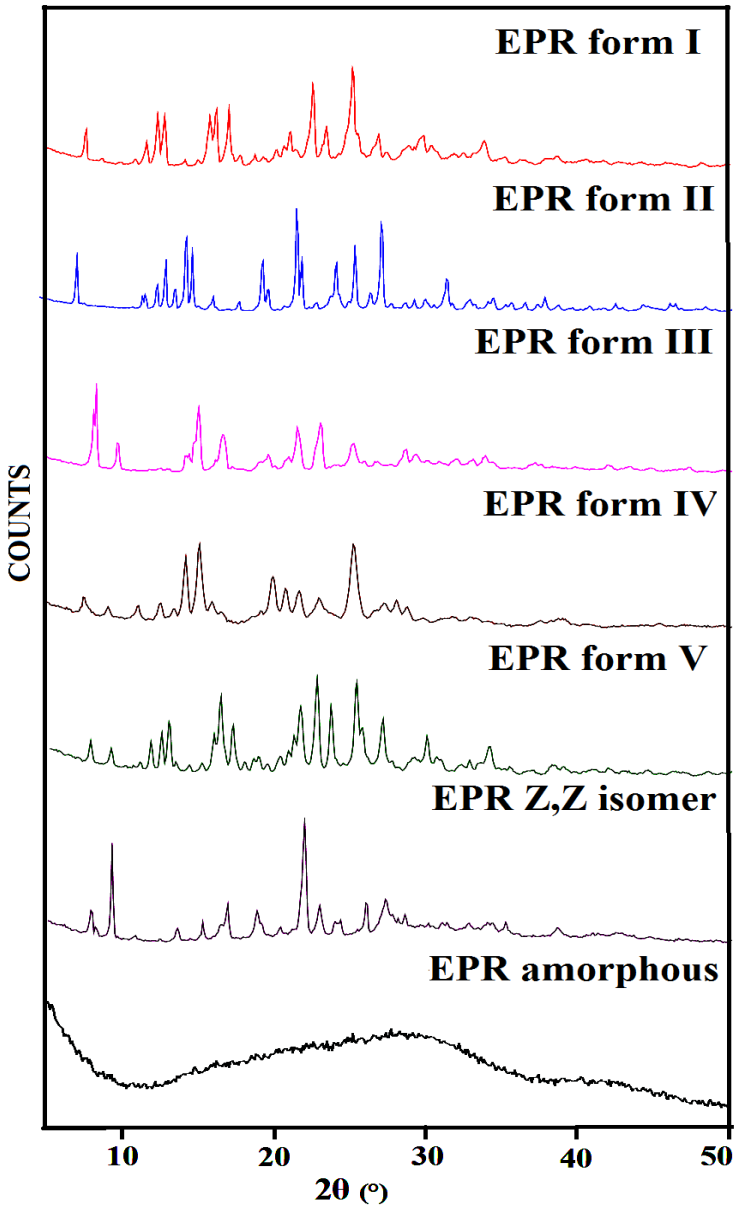

Figure 4.12 Experimental PXRD pattern of EPR forms.

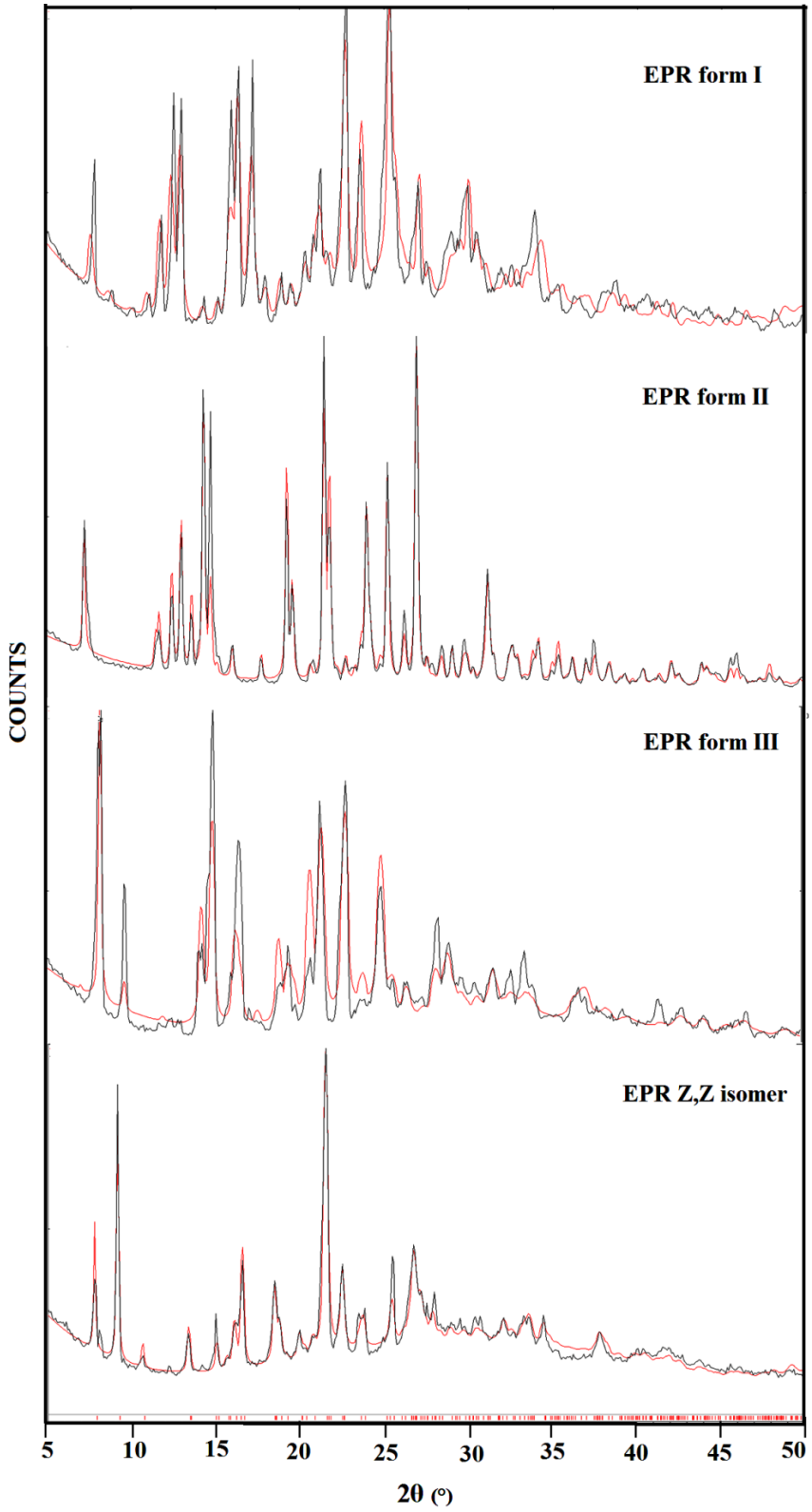

Figure 4.13 Overlay of experimental PXRD (black) of EPR forms I, II, III and Z,Z isomer match with the calculated lines from the crystal structure (red).

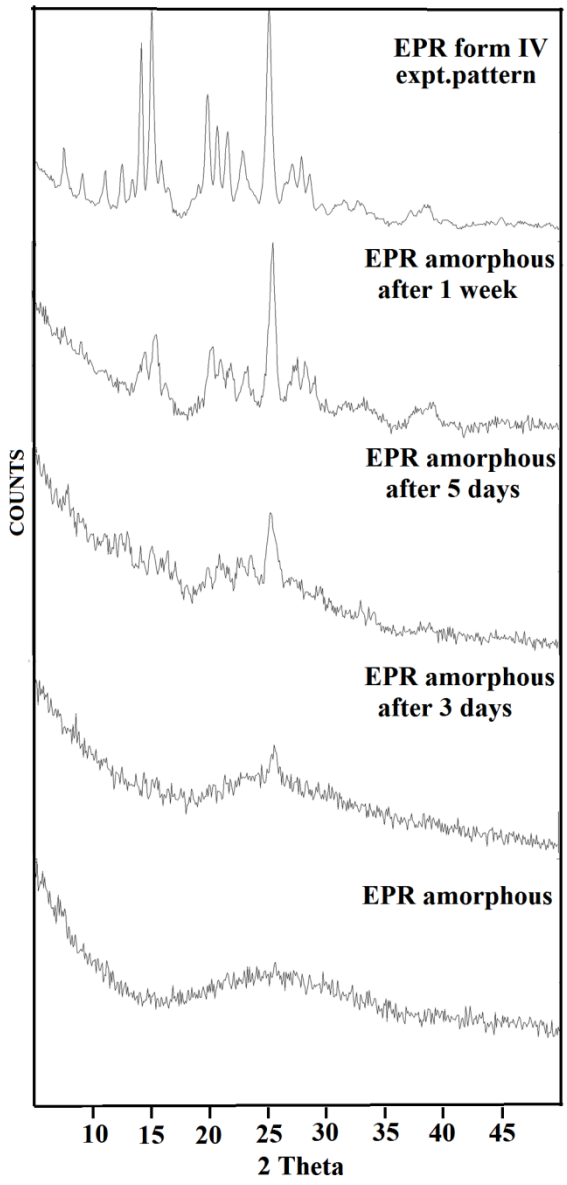

Figure 4.14 Stability of EPR amorphous form at ambient conditions shows that after 3 days it transforms to form IV.

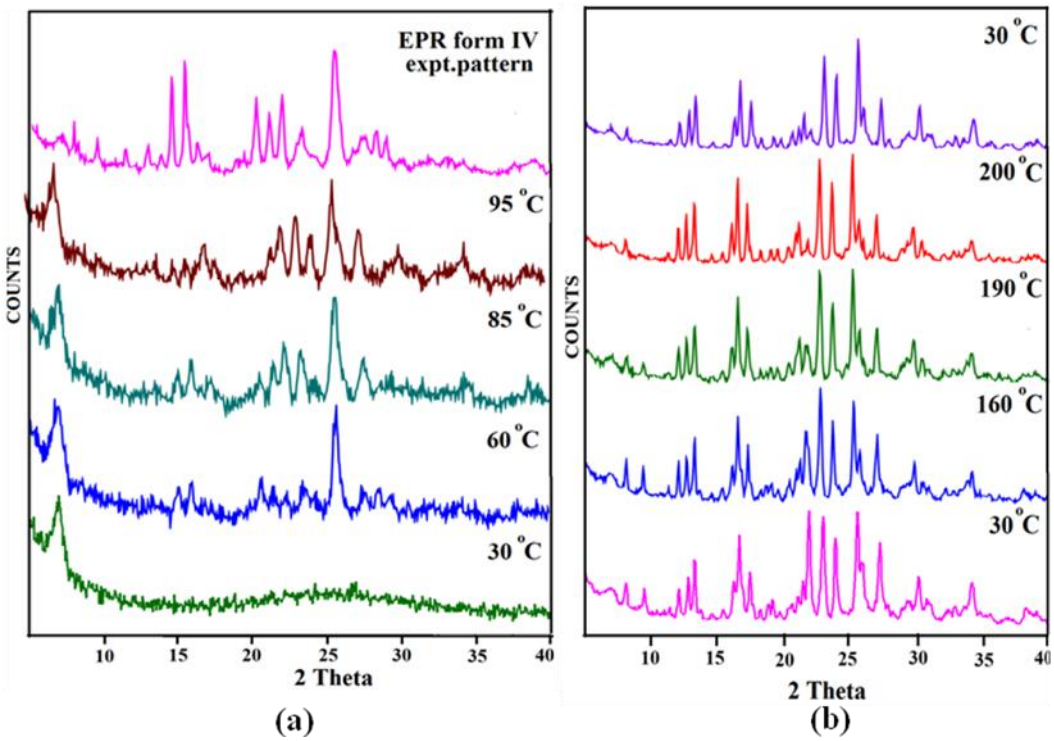

Figure 4.15 (a) VT-PXRD of EPR amorphous form (green) shows transformation to form IV upon heating. **(b)** VT-PXRD of EPR form V (pink) shows transformation from form V to form I started at 190 ºC (green) and completed at 200 ºC (red) and form I is stable upon cooling.

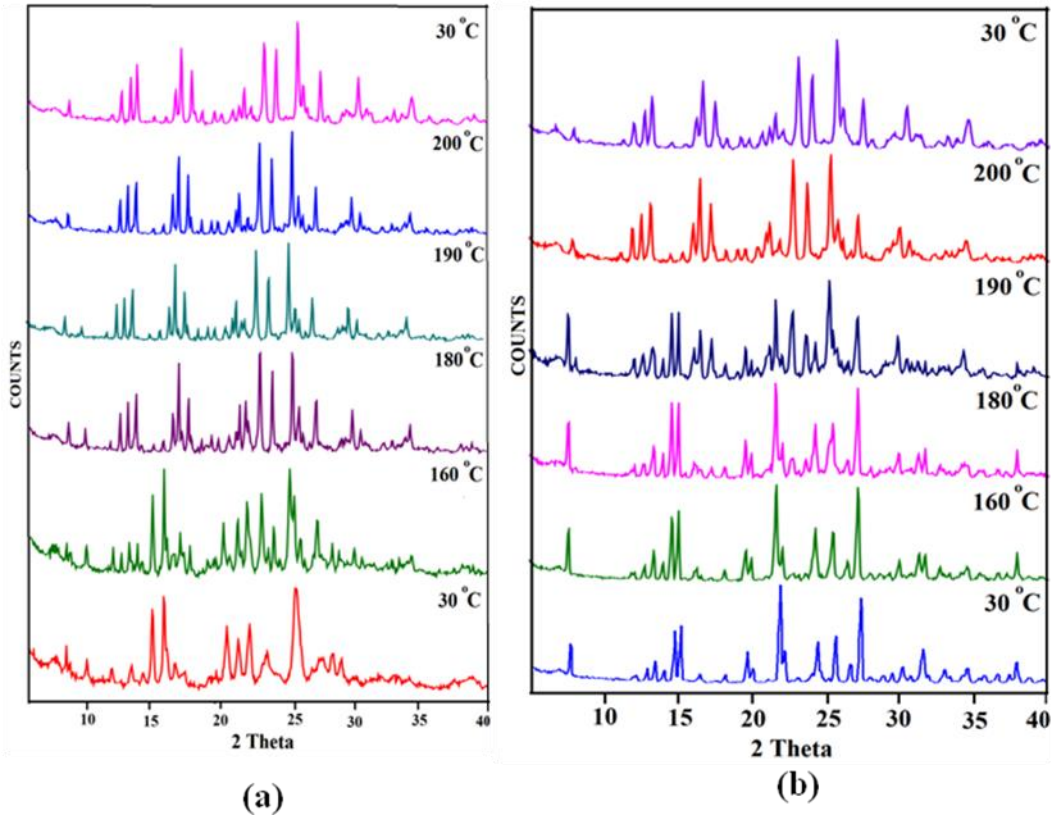

Figure 4.16 (a) VT-PXRD of EPR form IV (red) shows transformation from form IV to form V started at 160 ºC (green) and completed at 180 º (purple) and form V is stable upon cooling. (b) VT-PXRD of EPR form II (blue) shows transformation from form II to form I started at 190 ºC (dark blue) and completed at 200 ºC (red) and form I is stable upon cooling.

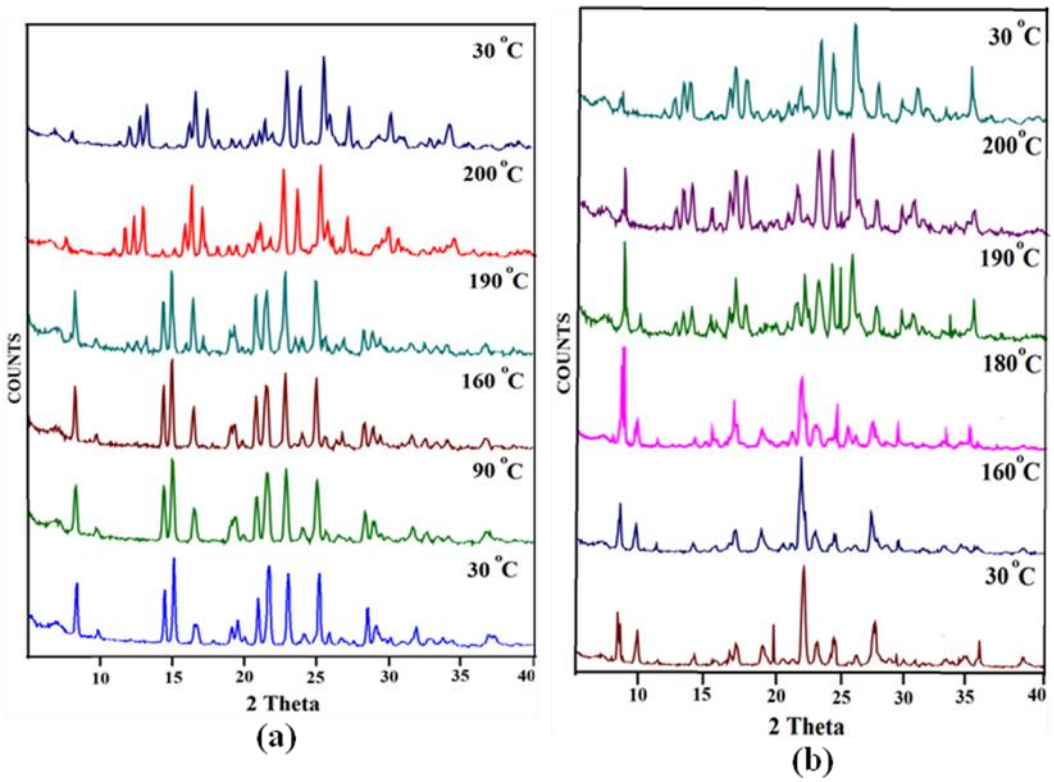

Figure 4.17 (a) VT-PXRD of EPR form III (blue) shows transformation from form III to form I started at 190 ºC (cyan) and completed at 200 ºC (red) and form I is stable upon cooling. (b) VT-PXRD of EPR Z,Z isomer (brown) shows transformation to form I of E,Z isomer upon heating at 190 ºC (green) and form I is stable upon cooling.

4.3.5 Phase Transformations in EPR Polymorphs

Form I showed no phase change and a single melting endotherm in DSC at high T_{onset} of 221.94 °C (Figure 4.18) and form II showed two endothermic peaks, one at 215.83 °C corresponding to phase transformation of II to I and then melting at 227.76 °C. Form III exhibited an exotherm (phase transition to I) and then endotherm (melting of form I). Initial heating of the amorphous form starting at 30 °C resulted in a second-order glass transition to a supercooled liquid (Figure 4.19). A second-order transition is characterized by a change in the heat capacity with no heat absorbed or evolved, and is recorded as a lowering of the baseline. The resulting unstable supercooled liquid crystallized spontaneously upon heating, yielding the sharp exotherm corresponding to a metastable phase form IV, in accord with Ostwald's Law of Stages.[8f] Further heating of form IV showed an exothermic solid-solid transition to form V at 166.09 °C, which

underwent an endothermic transition at 200.18 °C resulting in the stable modification I, which then melts at 222.72 °C (Figure 4.18). The Z,Z isomer exhibited two endothermic peaks, the first one at T_{onset} 178.97 represents the transformation of Z,Z isomer to the configurational E,Z isomer (form I) and the second endotherm corresponds to melting of form I at 216.93 °C (Figure 4.20).

We carried out hot stage microscopy (HSM) measurements on single crystals of EPR polymorphs to investigate the nature of phase transformations. Form I, II, III and Z, Z isomer crystals were taken separately on glass slides and heated from 30 °C to 300 °C on hot stage microscope. We observed that form I started melting at 220 °C and completely melted at 230 °C (Figure 4.21a). During this heating period form I did not showed any morphological changes. Orange color crystals of form II started darkening at 183 °C and completely tuned to red at 190 °C followed by melting at 238 °C (Figure 4.21b). This color change from orange to red indicates solid–solid phase transformation from form II to I. Yellow crystals of form III turn red between 168 – 170 °C as a result of a solid–solid phase transformation from form III to form I and latter was melted completely at 228 °C (Figure 4.21c). Similarly, yellowish Z, Z isomer crystal was turned to red around 177 – 182 °C indicating its transformation to form I of E, Z isomer (Figure 4.21d) and the resulted form I crystal melted at 190 °C.

A combination of DSC, HSM, and VT-PXRD established the transformations summarized in Scheme 2 (see Figure 4.22 for a possible mechanism on the intermediacy of ZZ-isomer), and that polymorph I of epalrestat is the thermodynamic modification. Thermodynamic relationships between polymorphs, i.e. enantiotropic or monotropic,[24-26] may be assigned based from DSC curves. Form I has the highest melting form and its enthalpy of fusion is higher than that of form III, but lower than form II and form V. Based on the heat of fusion rule[27], form I is enantiotropically related to form II and V, but monotropically related to form III (Table 4.7).

On the basis of thermal analysis (DSC and HSM), the melting point of form I is higher than that all other forms. We believe that this highest melting form I is the most stable thermodynamic polymorph of EPR, consistent with the Ostwald's law of stages. The thermodynamic stability of EPR polymorphs at RT can be given as (more stable) form I > form II > form V > form III > form IV (least stable) and the kinetic stability of EPR polymorphs at -273°C is form V > form IV > form II > form I > form III (least stable).

Burger and Ramberger's famous density rule[27] states that if one form of a molecular crystal has a higher density than other forms, it may be assumed to be more stable at RT. Here the calculated density of form I is higher than that of the density of form II and III (form I, 1.461g cm^{-3}; form II, 1.430g cm^{-3}; form III, 1.411g cm^{-3}). Therefore, this is in agreement with the observation that form I is stable form at room temperature.

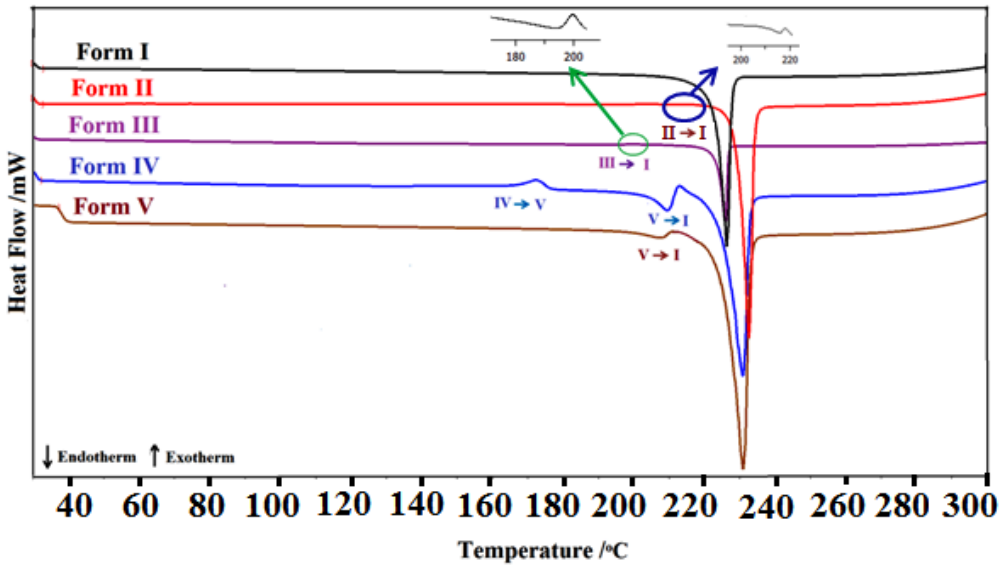

Figure 4.18 DSC thermogram of EPR polymorphs at heating rate 10 °C min^{-1}. A close up of the phase transition is shown in insert. Phase transition from II to I and V to I is endothermic, and transformation from III to I and IV to V is exothermic.

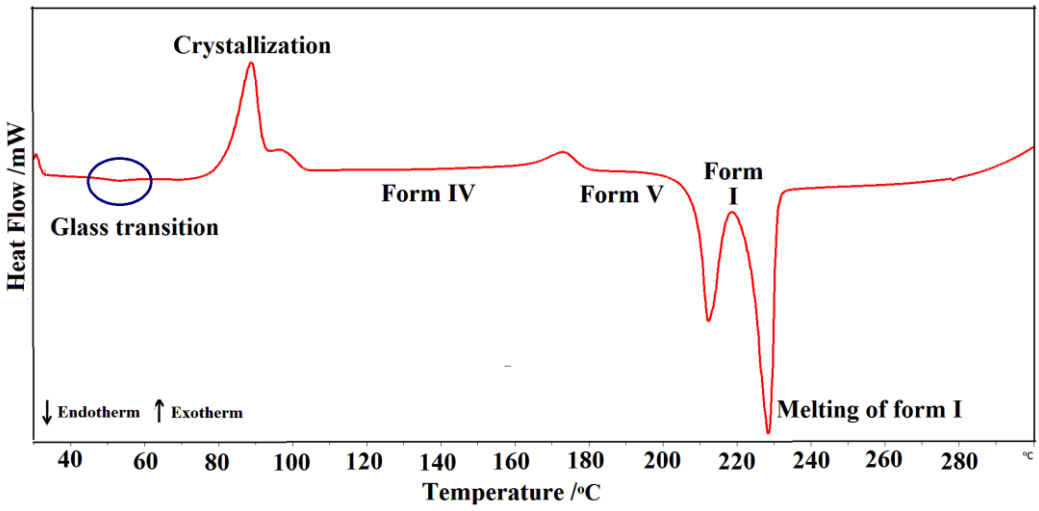

Figure 4.19 DSC thermogram of EPR amorphous form showing phase transformations.

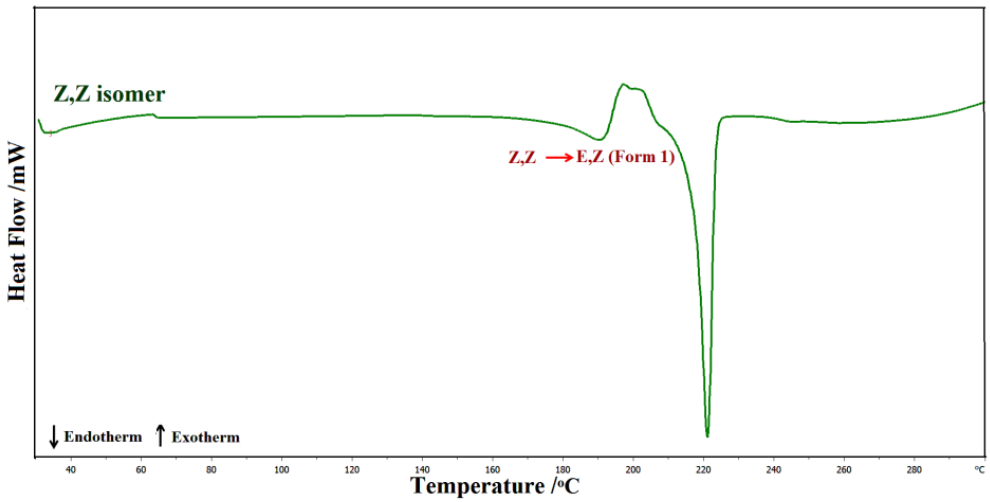

Figure 4.20 DSC thermogram of EPR Z,Z isomer.

	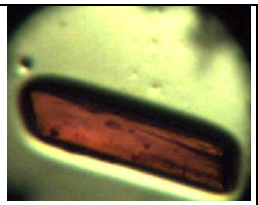	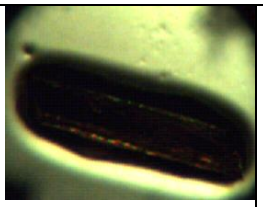	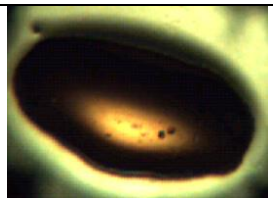
30 ˚C	220 ˚C	226 ˚C	230 ˚C

(a)

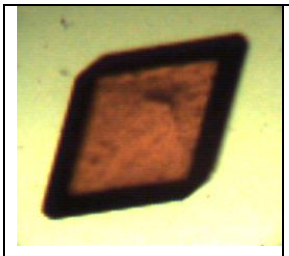	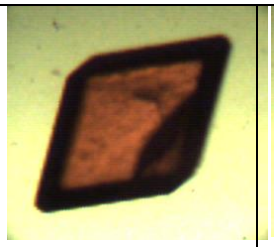	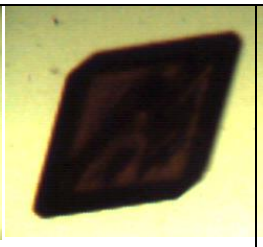	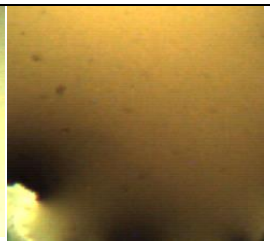
30 ˚C (orange)	183 ˚C	190˚C (dark red)	238 ˚C

(b)

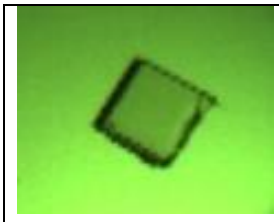	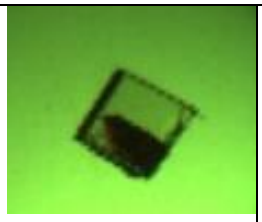	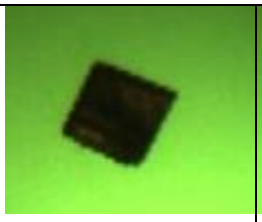	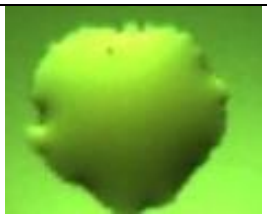
30 ˚C (yellow)	168 ˚C	170 ˚C (red)	228 ˚C

(c)

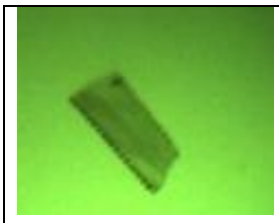	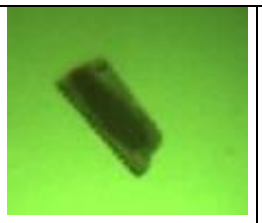	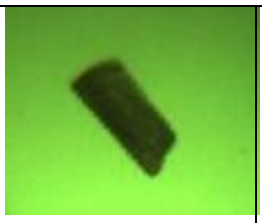	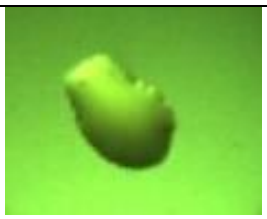
30 ˚C (yellow)	177 ˚C	182 ˚C (red)	190 ˚C

(d)

Figure 4.21 HSM snapshots of EPR polymorphs. a) No changes were observed in crystal morphology of form I. b) Orange color crystals of form II darkened between 183-190°C indicating phase transition. c). Yellow color of form III crystals turned to red between 168-170°C indicating phase transition. d) Yellow color of Z,Z isomer crystals turned to red between 177-182°C indicating its conversion to form I of E,Z isomer.

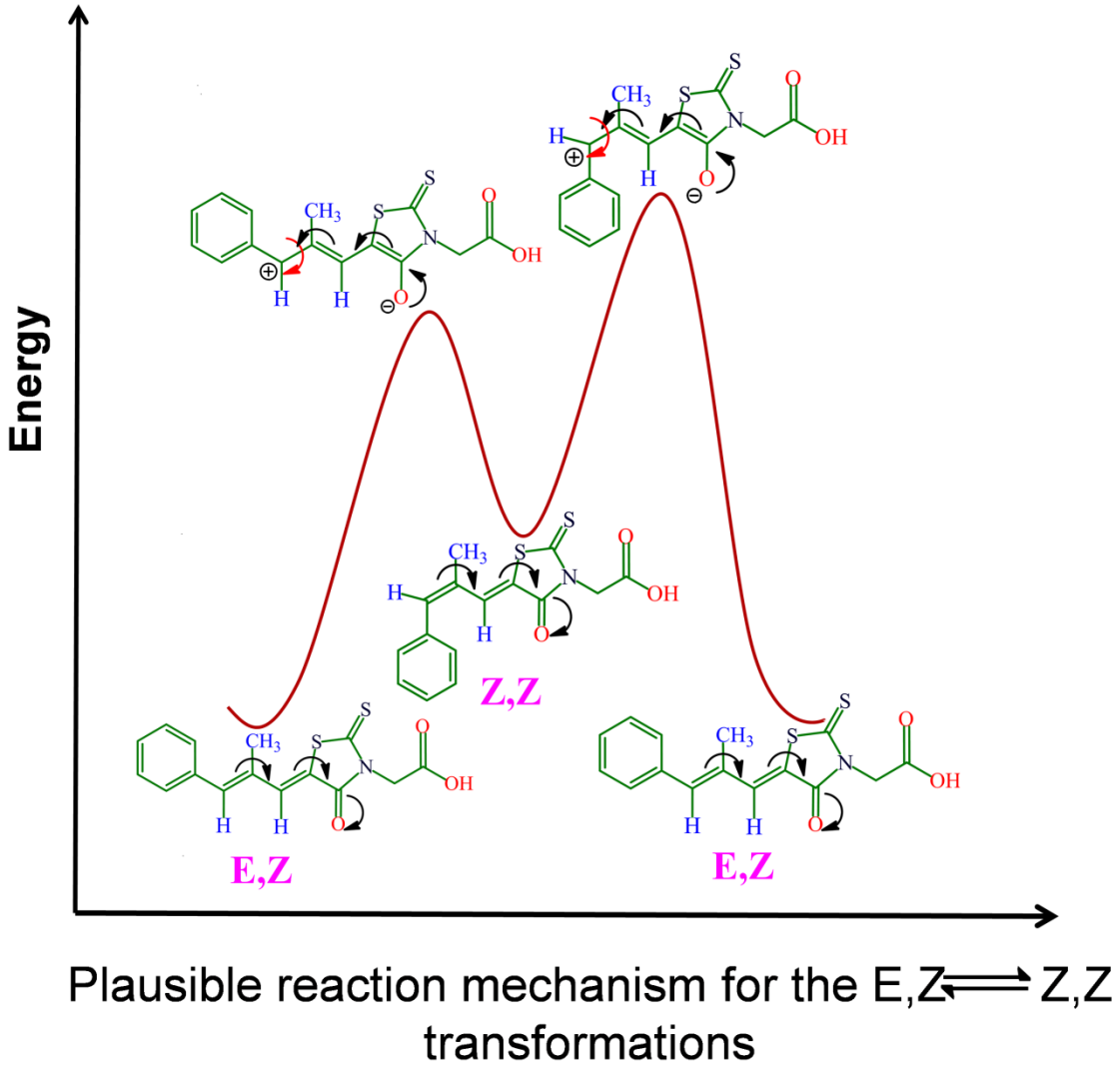

Figure 4.22 Possible reaction mechanism and qualitative energy diagram to show the transformation of E,Z-EPR to ZZ-EPR and then EZ-EPR polymorph.

Table 4.7 Transition temperature and enthalpy values of EPR forms.[a]

Drug Forms	$T_{trs/fus}$ (°C) T_{onset}/ T_{peak}	ΔH_{fus} kJ/mol	ΔH_{trs} kJ/mol	Stability relation
Form I	221.94/224.40	42.96	-	-
Form II	215.83/218.11	43.34	+0.38, (II→I)	enantiotropic

Form III	196.53/199.60	42.29	−0.67, (III→I)	monotropic
Form IV	166.09/172.42	46.75	−2.17, (IV→V)	monotropic
Form V	200.18/207.08	48.92	+5.96, (V→1)	enantiotropic
Amorphous	82.20/88.92	-	-	-
Z,Z isomer	178.97/190.82	-	-	-

[a] T_{fus} = melting point; T_{trs} = transition temperature; ΔH_{fus} = enthalpy of fusion; ΔH_{trs} = enthalpy of transition.
Enthalpy of fusion (ΔH_{fus}) of form I was determined directly from DSC, since it doesn't show any phase transformation.

ΔH_{fus} values of remaining forms were calculated as follows.

$$\Delta H_{fus\ (form\ 2)} = \Delta H_{fus\ (form\ 1)} + \Delta H_{trs}$$

$$\Delta H_{fus\ (form\ 3)} = \Delta H_{fus\ (form\ 1)} + \Delta H_{trs}$$

$$\Delta H_{fus\ (form\ 5)} = \Delta H_{fus\ (form\ 1)} + \Delta H_{trs}$$

$$\Delta H_{fus\ (form\ 4)} = \Delta H_{fus\ (form\ 5)} + \Delta H_{trs}$$

Phase transitions from II to I and V to I are endothermic (DSC), while transitions from III to I and IV to V are exothermic and there is no direct phase transformation from form IV to I.

In accordance with the heat of transition rule[27], form I is enantiotropically related to forms II, V, and monotropically related to forms III, IV; Form IV and V also monotropically related.

Based on T_{onset} in DSC (ºC), the stability of polymorphs may be ordered as Form I (221.94, most stable) > Form II (215.83) > Form V (200.18) > Form III (196.53) > Form IV (166.09, least stable).

4.3.6 Polymorphic Stability under ICH Conditions

EPR polymorphs were found to be stable in ambient conditions of Hyderabad (35 °C and 40% RH) for more than one year. Polymorphs will undergo phase transformations or hydrate formation on exposure to humidity[28]. Therefore EPR polymorphs were tested for form stability in accelerated conditions of 40 °C and 75% RH. EPR polymorphs I to V did not exhibit any polymorphic change or hydrate formation in the test period of six months (Figure 4.23 to 4.25 and Table 4.8).

Table 4.8 Stability of Epalrestat Polymorphs under ICH Conditions of 40 °C and 75% RH.

Polymorph	1 M	2 M	3 M	4 M	5 M	6 M
EPR form I	√	√	√	√	√	√
EPR form II	√	√	√	√	√	√
EPR form III	√	√	√	√	√	√
EPR form IV	√	√	√	√	√	√
EPR form V	√	√	√	√	√	√

M = month, √ = no phase change/no hydrate formation

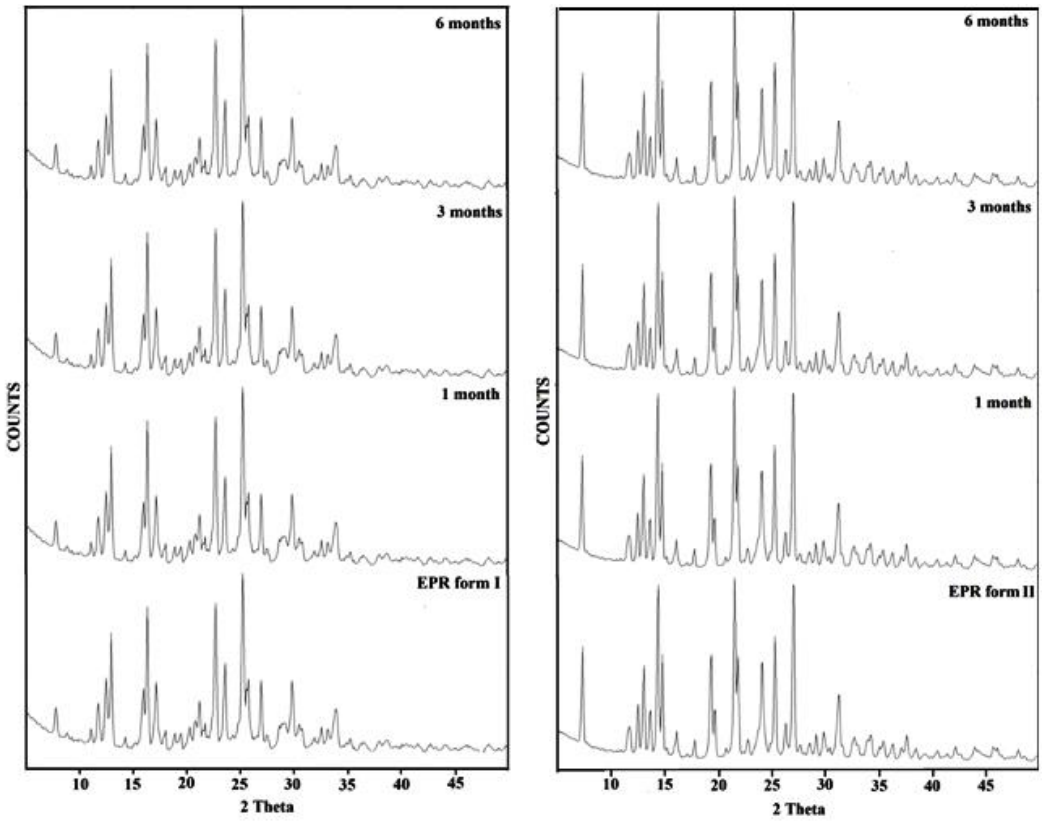

Figure 4.23 Stability study at 40 °C and 75% RH of EPR form I and form II. There is no form change up to 6 months.

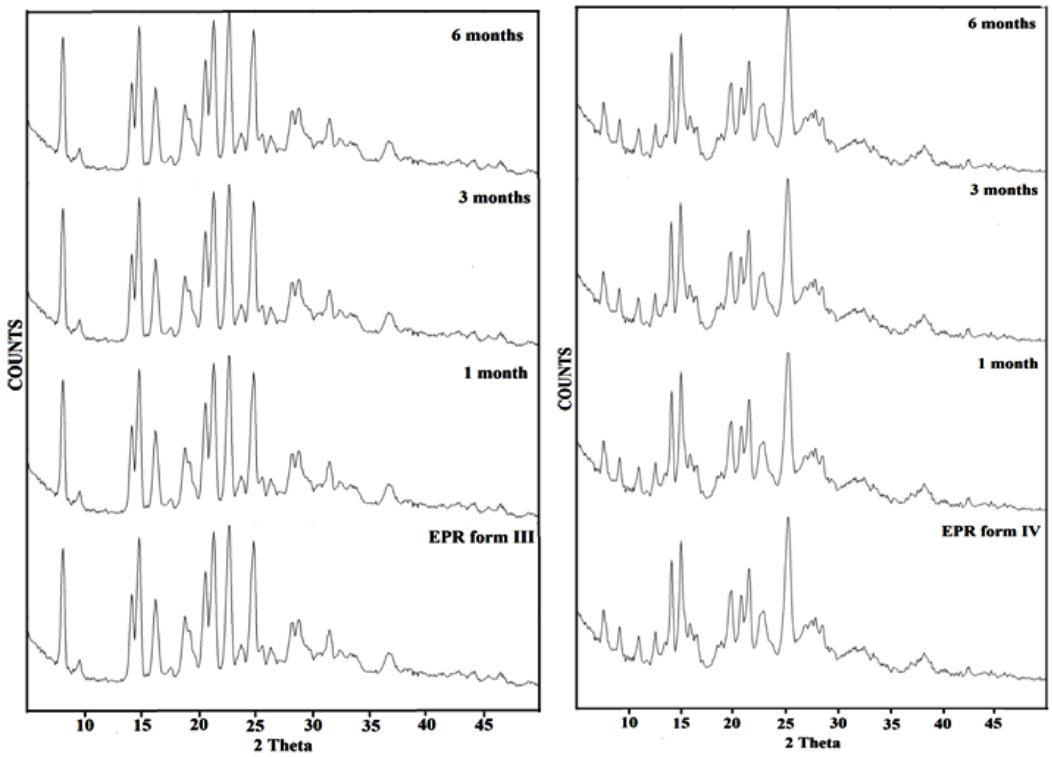

Figure 4.24 Stability study at 40 °C and 75% RH of EPR form III and form IV shows that form III is stable up to 6 months.

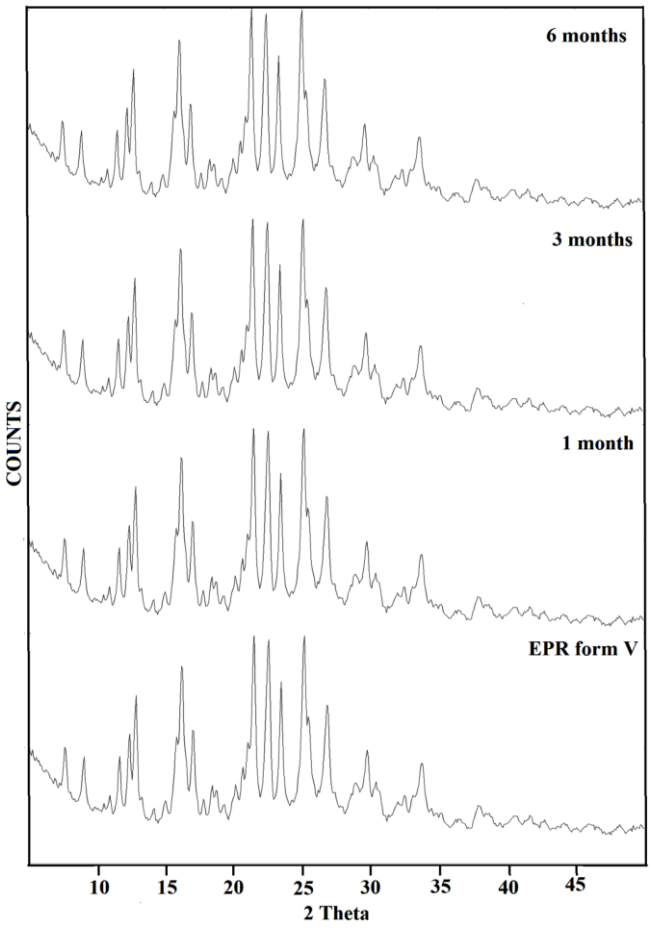

Figure 4.25 Stability study at 40 °C and 75% RH of EPR form V. There is no form change up to 6 months.

4.3.7 Grinding and Slurry experiments

Phase stability studies at ambient conditions are very important in order to establish the thermodynamic modification of polymorphs at ambient conditions. The stable phase at room temperature was determined by subjecting both the forms to slurry and grinding experiments[29]. EPR forms I, II, and V did not exhibit any phase transformation even after 2 h of solid-state grinding, whereas form IV was converted to form I after 20 min and form III was transformed to form I in 30 min. Slurry experiments were also performed at 100 mg scale. Water (5 mL in each experiment) was used as solvent in slurry experiments. The slurry was stirred at 800 rpm using a magnetic stirrer at 30 °C. After 5 d, the suspension was filtered through Whatman's filter paper No. 1 and the dried material was characterized by PXRD. No phase transformations of form I, II, IV and V were observed even after 5 d, but form III converted to form I after 24 h (Table 4.9).

Based on the grinding and slurry experiments as well as thermal analysis, EPR polymorphs are ranked in the following stability order: Form I (thermodynamic) > Form II > Form V > Form III > Form IV (least stable).

Table 4.9 Stability of Epalrestat Polymorphs under mechanical grinding and slurry experiments.

Solid form	Mechanical grinding (dry grinding, 2 hours)	Slurry grinding (in water, 5 days)
Form I	Stable	Stable
Form II	Stable	Stable
Form III	Transformed to form I (30 min)	Transformed to form I (after 24 hrs)
Form IV	Transformed to form I (20 min)	Stable
Form V	Stable	Stable

Based on the thermal analysis and VT-PXRD, a semi-schematic Energy vs Temperature (E-T) diagram was constructed (Figure 4.26), in which the relative thermodynamic stability of all polymorphs may be visualized in the temperature range from 0 K (–273 °C) up to their melting point. Since form V is the stable form at low temperature (highest ΔH_{fus}, Table 4.7), the G-isobar (free energy) of form V runs below that of all other polymorphs. The E–T diagram shows that the G-isobars of forms III and IV do not intersect with any of the other G-isobars and hence III and IV are monotropically related to the other polymorphs. The G-isobars of form II and V intersect with that of form I, indicating their enantiotropic relationship. The transition points at 215.8 °C and 200.1 °C are due to the conversion of form II and form V to form I during the heating stage. Form I is the stable phase above 215.8 °C and up to its melting temperature at 221.9 °C.

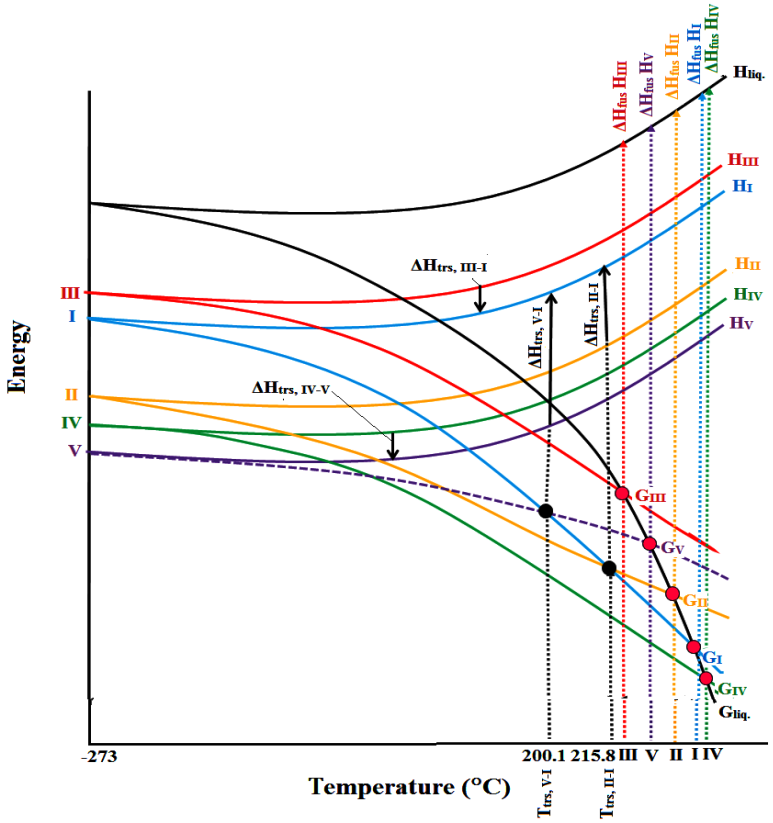

Figure 4.26 Semi-schematic Energy–Temperature diagram of the five polymorphs of EPR. Dotted line G-isobar of form V indicates that it is enantiotropically related to form I but monotropically related to form II and IV, and its heat of fusion value is higher than all polymorphs of EPR.

4.3.8 Photostability Study of EPR polymorphs

E,Z to Z,Z isomerization of EPR is reported in the literature[13]. Therefore, photostability studies of novel EPR polymorphs were carried out in this study. Novel EPR forms obtained in this work were dissolved in DMSO-d_6 and subjected to normal sunlight for 4 h, and then the ^{1}H NMR spectrum was recorded immediately. However, polymorphs did not stop the transformation of E,Z to Z,Z isomer. E,Z to Z,Z isomerization was visualized from the appearance of new peaks which corresponds Z,Z isomer and similar in all cases (Figure 4.27).

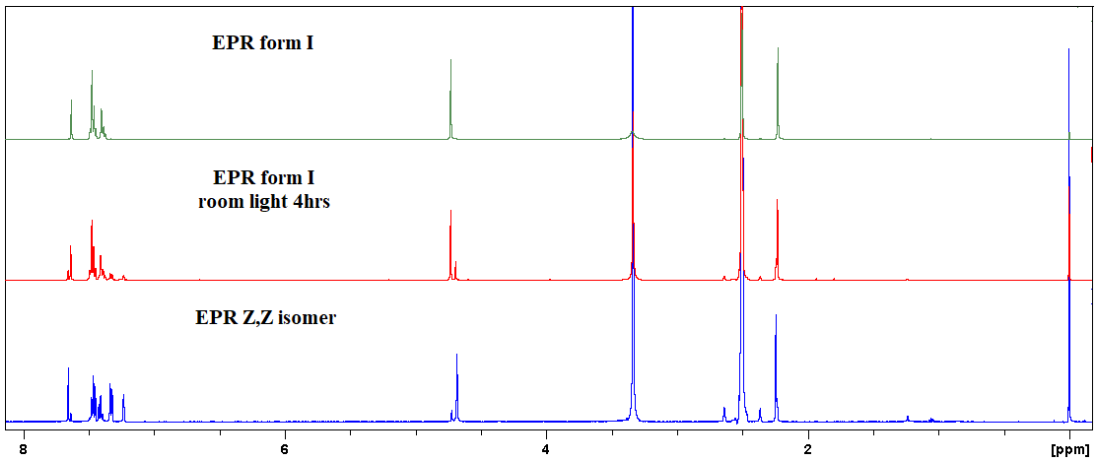
EPR form I
EPR form I
room light 4hrs
EPR Z,Z isomer
8
6
4
2
[ppm]

(a)

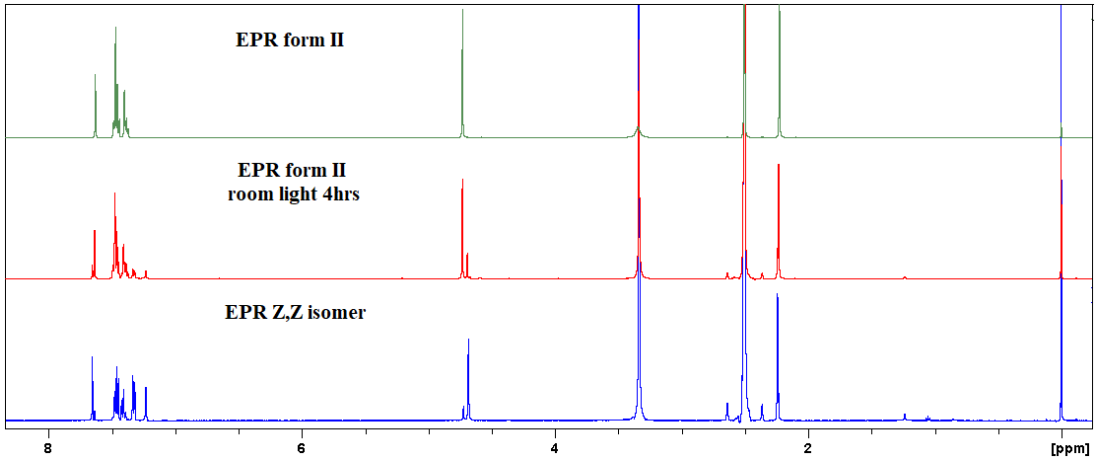
EPR form II
EPR form II
room light 4hrs
EPR Z,Z isomer
8
6
4
2
[ppm]

(b)

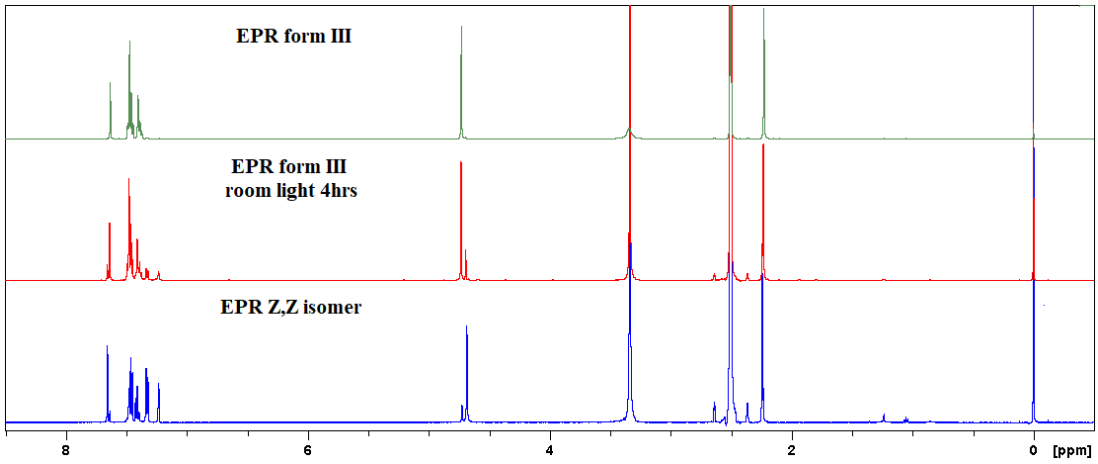
EPR form III
EPR form III
room light 4hrs
EPR Z,Z isomer
8
6
4
2
0
[ppm]

(c)

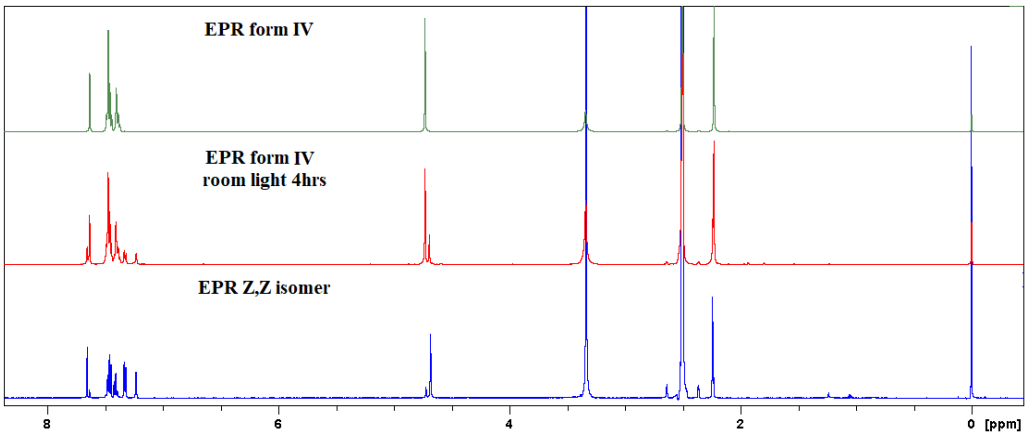

(d)

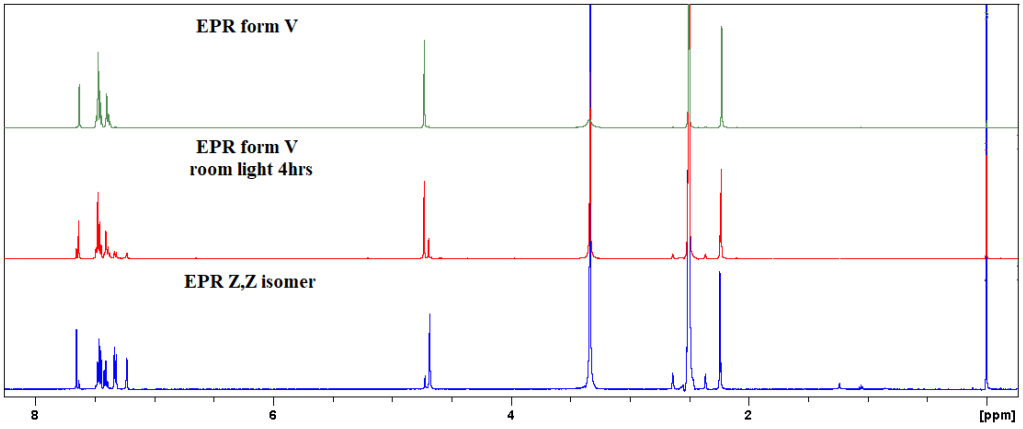

(e)

Figure 4.27 ^{1}H NMR spectrum of EPR polymorphs, (a) form I, (b) form II, (c) form III, (d) form IV and (e) form V before and after exposure to light shows that the E,Z isomer of EPR transforms to the Z,Z isomer within 4 h to about the same extent. Inter-conversion of the E,Z and Z,Z isomer in solution is seen based on the separation of proton signals at 4.69-4.73 ppm (2H, N-CH_2), and the peak at 7.64-7.66 ppm (1H, most downfield aromatic) and appearance of new proton signals at 7.23 and 7.32-7.34 ppm.

4.4 Conclusions

In summary, epalrestat is a highly polymorphic drug compound due to conformational and synthon differences. The O–H···O + C–H···O synthon of $R_2^2(9)$ ring motif observed in polymorphs I and II is as such rare for carboxylic acids, the carboxylic acid dimer being the most common synthon. The different colors for epalrestat polymorphs are ascribed to conformation changes leading to chromophore conjugation and UV-Vis maxima differences. Polymorph I appears to be the most stable modification due to extended hydrogen bonding through $R_2^2(9)$ and $R_4^4(22)$ ring synthons in its X-ray

structure and highest crystal density. There are no phase transitions noted in the DSC of form I compared to the other polymorphs, which exhibit thermal events (exo-endotherm) prior to the melting event. The phase transformations through two possible pathways, one directly to form I and the other via Z,Z isomer, is being explored in detail as well as the overall crystal landscape of epalrestat.

4.5 Experimental Section

Materials and Methods

Epalrestat was gift sample from Symed Laboratories Ltd., Hyderabad, India and used without further purification. All other chemicals were of analytical or chromatographic grade. Water purified from a deionizer-cum-mixed-bed purification system (AquaDM, Bhanu, Hyderabad, India) was used in the experiments.

Preparation of Epalrestat Forms

EPR form I

The commercial material obtained from Symed Laboratories matches to Form-1 which was confirmed by PXRD and DSC. Block shaped red color single crystals suitable for X-ray diffraction were obtained after 3-4 d upon dissolving 30 mg of EPR in 10 mL of hot ethyl acetate : nitromethane solvent mixture (1:1) and left for slow evaporation at ambient conditions.

^{1}H NMR (DMSO-d_6, 500 MHz) δ ppm: 13.46 (1 H, br s), 7.63 (1 H, s), 7.49-7.40 (4 H, m), 7.40-7.35 (2 H, m), 4.73 (2H, s), 2.23 (3 H, s) (Figure 4.28).

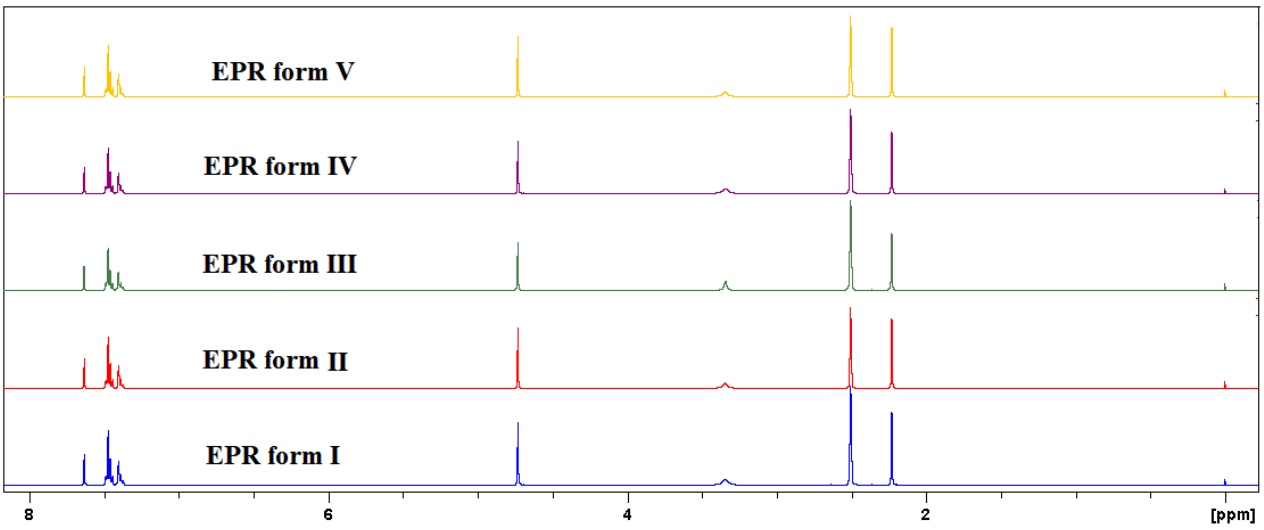

Figure 4.28 ^{1}H NMR spectral overlay of EPR forms recorded in d_6-DMSO.

EPR form II

Diamond shaped orange color single crystals suitable for X-ray diffraction were obtained after 3-4 d upon dissolving 30 mg of EPR in 5 mL of hot 2-propanol solvent and left for slow evaporation at ambient conditions. Form II was obtained in bulk upon dissolving 30 mg of EPR in 10 mL of methanol and heated to get clear solution. This hot solution was rotavaporized immediately to get solid. Formation of form II was confirmed by FT-IR, FT-Raman, ss-NMR, PXRD and DSC.

^{1}H NMR (DMSO-d_6, 500 MHz) δ ppm: 13.46 (1 H, br s), 7.63 (1 H, s), 7.49-7.40 (4 H, m), 7.40-7.35 (2 H, m), 4.73 (2H, s), 2.23 (3 H, s) (Figure 4.28).

EPR form III

Needle morphology yellow color single crystals suitable for X-ray diffraction were obtained after 3-4 d upon dissolving 30 mg of EPR in 10 mL of hot methanol: benzene solvent mixture (1:1) and left for slow evaporation at ambient conitions. Form III was obtained in bulk upon dissolving 50 mg of EPR in 20 mL of nitromethane and heated to get clear solution. This hot solution cooled immediately by keeping in ice to get precipitate. The precipitate was filtered and the formation of form III was confirmed by FT-IR, FT-Raman, ss-NMR, PXRD and DSC.

^{1}H NMR (DMSO-d_6, 500 MHz) δ ppm: 13.45 (1 H, s), 7.63 (1 H, s), 7.49-7.40 (4 H, m), 7.40-7.35 (2 H, m), 4.73 (2H, s), 2.23 (3 H, s) (Figure 4.28).

EPR form IV

EPR form IV was obtained upon heating of amorphous form at 85 °C for 30 min in programmable oven. The formation of form IV was confirmed by FT-IR, FT-Raman, ^{13}C ss-NMR, PXRD, and DSC. Attempts to crystallize the form IV in ethanol, CH_3CN, THF, nitromethane, toluene, acetone, and also mixture of solvents gave polycrystalline powders but no diffraction quality single crystals were obtained.

^{1}H NMR (DMSO-d_6, 500 MHz) δ ppm: 13.45 (1 H, s), 7.64 (1 H, s), 7.50-7.40 (4 H, m), 7.40-7.30 (2 H, m), 4.73 (2H, s), 2.23 (3 H, s) (Figure 4.28).

EPR form V

EPR form IV was obtained upon heating of amorphous form at 160 °C for 30 min in programmable oven. The formation of form IV was confirmed by FT-IR, FT-Raman, ^{13}C ss-NMR, PXRD, and DSC. Attempts to crystallize the form V in ethanol, CH_3CN, THF, nitromethane, toluene, acetone, and also mixture of solvents gave polycrystalline powders but no diffraction quality single crystals were obtained.

^{1}H NMR (DMSO-d_6, 500MHz) δ ppm: 13.46 (1 H, s), 7.63 (1 H, s), 7.49-7.40 (4 H, m), 7.40-7.20 (2 H, m), 4.60 (2H, s), 2.20 (3 H, s) (Figure 4.28).

EPR amorphous form

100 mg of EPR was melted at 225 °C and then immediately dipped in liquid nitrogen to cool down to a glassy state. Formation of amorphous form was confirmed by FT-IR, FT-Raman, ^{13}C ss-NMR, PXRD, and DSC.

EPR Z,Z isomer

Plate morphology yellow color single crystals suitable for X-ray diffraction were obtained after 3-4 d upon dissolving 30 mg of EPR in 10 mL of various solvent mixtures (1:1) such as tetrahydrofuran : heptane, ethanol : benzene, methanol : 1,2-dibromoethane and left for slow evaporation at ambient conditions.

^{1}H NMR (DMSO-d_6, 500 MHz) δ ppm: 13.48 (1 H, s), 7.66 (1 H, s), 7.50-7.35 (2 H, m), 7.40-7.35 (1 H, t), 7.33-7.30 (2 H, d), 7.23 (1 H, s), 4.68 (2H, s), 2.24 (3 H, s) (Figure 4.29).

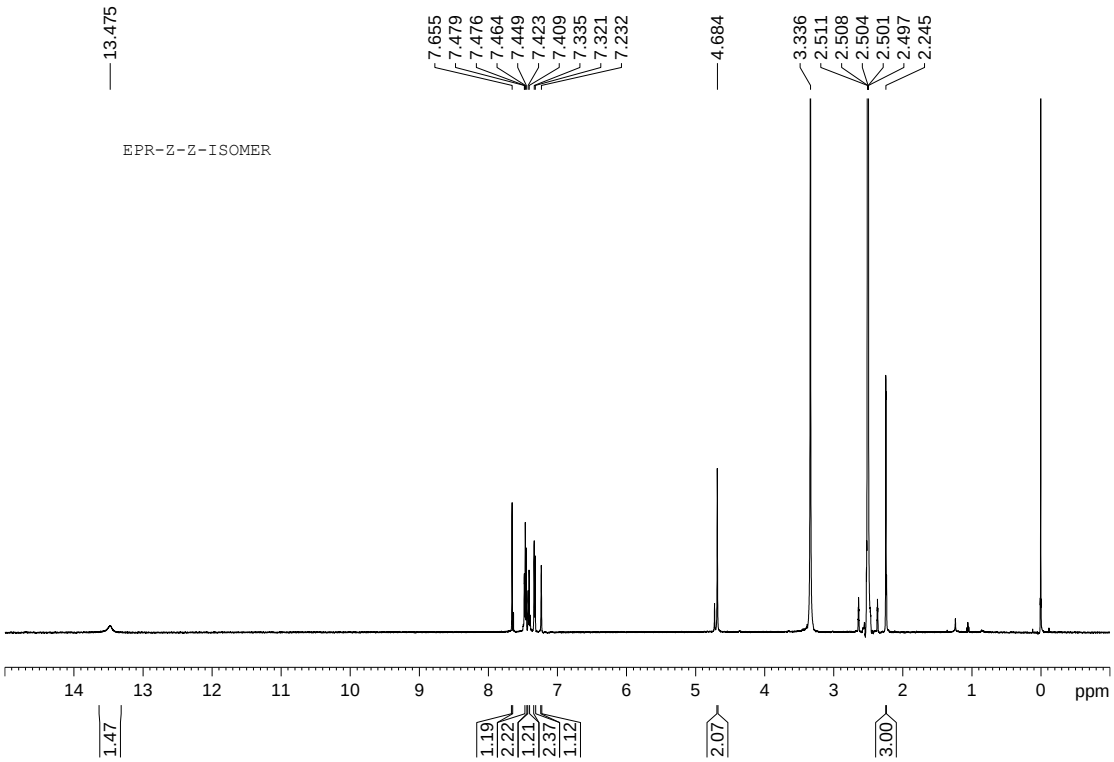

Figure 4.29 ^{1}H NMR spectra of EPR Z,Z isomer recorded in d_6-DMSO.

Grinding and Slurry experiments

Grinding experiments were performed at 100 mg scale. A Retsch mixer-mill equipped with a 5 mL stainless steel grinding jar and SS balls of 4 mm diameter was used for mechanical grinding.

Vibrational Spectroscopy

Thermo-Nicolet 6700 Fourier transform infrared spectrophotometer with NXR-Fourier transform Raman module (Thermo Scientific, Waltham, Massachusetts) was used to record IR and Raman spectra. IR spectra were recorded on samples dispersed in KBr pellets. Raman spectra were recorded on samples contained in standard NMR diameter tubes or on compressed samples contained in a gold-coated sample holder. Data were analyzed using the Omnic software (Thermo Scientific, Waltham, Massachusetts).

Solid-State NMR Spectroscopy

The solid-state ^{13}C NMR spectra were obtained on a Bruker Ultrashield 400 spectrometer (Bruker BioSpin, Karlsruhe, Germany) utilizing a ^{13}C resonant frequency of 400 MHz (magnetic field strength of 9.39 T). Approximately 100 mg of crystalline sample was packed into a zirconium rotor with a Kel-F cap. The crosspolarization, magic angle spinning (CP-MAS) pulse sequence was used for spectral acquisition. Each sample was spun at a frequency of 5.0 ± 0.01 kHz, and the magic angle setting was calibrated by the KBr method. Each data set was subjected to a 5.0 Hz line broadening factor and subsequently Fourier transformed and phase corrected to produce a frequency domain spectrum. The chemical shifts were referenced to TMS using glycine (δglycine = 43.3 ppm) as an external secondary standard. Additionally solution ^{1}H NMR spectra of all the forms were recorded on a Bruker Ultrashield 500 spectrometer (Bruker BioSpin, Karlsruhe, Germany).

Solid-state UV-Vis spectroscopy

Solid-state UV-Visible absorption spectra of EPR forms were recorded on a varian cary 100 spectrophotometer.

Differential Scanning Calorimetry (DSC)

DSC was performed on a Mettler Toledo DSC 822e module. Samples were placed in crimped but vented aluminum sample pans. The typical sample size was 3-4 mg, and the temperature range was 30-300 °C @ 5 °C min^{-1}. Samples were purged by a stream of dry nitrogen flowing at 80 mL min^{-1}.

Hot stage microscopy (HSM)

HSM was performed on a Wagner & Munz PolythermA Hot Stage and Heiztisch microscope. A Moticam 1000 (1.3 MP) camera supported by software Motic Image Plus 2.0ML is used to record images.

X-ray crystallography

X-ray reflections for EPR form I, II, III, and Z,Z isomer were collected at 298 K on Oxford Xcalibur Gemini Eos CCD diffractometer using Mo−Kα radiation (λ = 0.7107 Å). Data reduction was performed using CrysAlisPro (version 1.171.33.55)[30] and OLEX2-1.0[31] was used to solve and refine the structures. All non-hydrogen atoms were refined anisotropically. Hydrogen atoms on hetero atoms were located from difference electron density maps and all C−H hydrogens were fixed geometrically. Hydrogen bond geometries were determined in Platon[32]. X-Seed[33] was used to prepare packing diagrams.

Powder X-ray Diffraction

Powder X-ray diffraction of all the samples were recorded on Bruker D8 Advance diffractometer (Bruker-AXS, Karlsruhe, Germany) using Cu-Kα X-radiation (λ = 1.5406 Å) at 40 kV and 30 mA power. X-ray diffraction patterns were collected over the 2θ range 5-50° at a scan rate of 1° min^{-1}. Powder Cell 2.4[34] was used for Rietveld refinement of experimental PXRD and calculated lines from the X-ray crystal structure.

4.6 References

1. Bernstein, J. *Polymorphism in Molecular Crystals*; Oxford University Press: New York, **2002**.
2. Dey, D.; Chopra, D. *CrystEngComm* **2015**, *17***,** 5288-5298.
3. C. Sun and D. J. Grant, *Pharm. Res.* **2001**, *18***,** 274-280.
4. Davey, R. J. *Chem. Commun.* **2003**, 1463-1467.
5. (a) Koda, A.; Ito, S.; Itai, S.; Yamamoto, K. *J. Pharm. Sci. Technol. Japan.* **2000**, *60*, 43-52. (b) Aiguiar A. J.; Zelmer, J. E. *J. Pharm. Sci.* **1969**, *58*, 983. (c) Florence A. T.; Attwood, D. *Physicochemical Principles of Pharmacy*, Pharmaceutical Press, London, UK, **2006.**
6. Doherty, C.; York, P. *Int. J. Pharm.* **1988,** *47***,** 141-155. (b) Matsuda, Y.; Tatsumi, E. *Int. J. Pharm*. **1990**, *60*, 11-26. (c) De Villiers, M. M.; van der Watt, J. G.; Lo¨tter, A. P. *Int. J. Pharm*. **1992,** *88*, 275-283.
7. Chemburkar, S. R.; Bauer, J.; Deming, K.; Spiwek, H.; Patel, K.; Morris, J.; Henry, R.; Spanton, S.; Dziki, W.; Porter, W.; Quick, J.; Bauer, P.; Donaubauer, J.;

Narayanan, B. A.; Soldani, M.; Riley D.; McFarland, K. *Org. Process Res. Dev.* **2000**, *4*, 413-417.

8. (a) Nangia, A. *J. Ind. Inst. Sci*. **2012,** *87*, 133. (b) Hilfiker, R. Ed. *Polymorphism in the Pharmaceutical Industry*, Wiley-VCH, Weinheim, Germany, **2006**. (c) Goho, A. *Science News*, 2004, **166**, 122-124. (d) Aitipamula S.; Nangia, A. *Supramolecular Chemistry: From Molecules to Nanomaterials*, Gale P. A.; Steed, J. W. Eds., John Wiley & Sons Ltd, West Sussex, U. K, **2012,** 2957–2974.
9. (a) Byrn, S. R.; Pfeiffer R. R.; Stowell, J. G. *Solid-State Chemistry of Drugs*, SSCI, West Lafayette, IN, **1999.** (b) Zhang, G. G. Z.; Law, D.; Schmitt E. A.; Qiu, Y. *Adv. Drug Delivery Rev.* **2004,** *56*, 371-390.
10. (a) Igarashi, R.; Nagase, H.; Furuishi, T.; Tomono, K. *X-ray Structure Analysis Online* **2013**, *29*, 23-24. (b) Ishida, T.; In, Y.; Inoue, M.; Tanaka, C.; Hamanaka, N. *J. Chem. Soc., Perkin Trans. 2*, **1990**, *7*, 1085-1091. (c) Igarashi, R.; Nagase, H.; Furuishi, T.; Tomono, K. *X-ray Structure Analysis Online* **2015**, *31*, 1-2.
11. (a) Umeda, D.; Putra, O. D.; Gunji, M.; Fukuzawa, K.; Yonemochi, E. *Acta Crystallogr.* **2017**, 73, 941−944. (b) Putra, O. D.; Umeda, D.; Fukuzawa, K.; Gunji, M.; Yonemochi, E. *Acta Crystallogr*. **2017,** 73, 1264−1267.
12. Putra, O. D.; Umeda, D.; Nugraha, Y. P.; Furuishi, T.; Nagase, H.; Fukuzawa, K.; Uekusa, H.; Yonemochi, E. *CrystEngComm* **2017**, 19, 2614−2622.
13. Ishida, T.; In, Y.; Inoue, M.; Ueno, Y.; Tanaka, C.; Hamanaka, N. *Tetrahedron Lett.* **1989**, *30*, 959-962
14. Kuduva, S.S.; Craig, D.C.; Nangia, A.; Desiraju, G.R. *J. Am. Chem. Soc.* **1999**, *121*, 1936-1944.
15. Desiraju, G. R.; Das, D. *Chem. Asian J.* **2006,** *1*, 231-244.
16. Sanphui, P.; Bolla, G.; Das, U.; Mukherjee, A.K.; Nangia, A. *CrystEngComm* **2013,** *15*, 34-38.
17. Desiraju, G. R. *Angew. Chem., Int. Ed.* **1995,** *34*, 2311-2327.
18. Nangia, A. *Acc. Chem Res.* **2008**, *41*, 595-604.
19. Suresh, K.; Minkov, V.S.; Namila, K.K.; Derevyannikova, E.; Losev, E.; Nangia, A.; Boldyreva, E.V. *Cryst. Growth Des.* **2015,** *15*, 3498-3510.
20. Yu, L. *J. Phys. Chem. A.* **2002,** *106*, 544-550.
21. (a) Silverstein R. M. *Spectrometric Identification of Organic Compounds*, 6th Ed.; John Wiley & Sons, Inc.: New York, **2002.** (b) Smith, E.; Dent, G. *Modern Raman Spectroscopy, A Practical Approach*, John Wiley: New York, **2005.** (c) Bugay, D.

E.; Brittain, H. G. *Raman Spectroscopy, in Spectroscopy of Pharmaceutical Solids*, New York: Taylor and Francis, **2006,** 271-312.

22. (a) Harris, R. K. *J. Pharm. Pharmacol.* 2007, **59**, 225-239. (b) Vogt, F.G.; Clawson, J.S.; Strohmeier, M.; Edwards, A.J.; Pham, T.N.; Watson, S.A. *Cryst. Growth Des.* 2009, **9**, 921-937. (c) Aliev, A. E.; Harris, K. D. *Supramolecular Assembly via Hydrogen Bonds I,* **2004**. (d) Newman, A.W.; Childs, S.L.; Cowans, B.A. Salt Cocrystal Form Selection, In *Preclinical Development Handbook*, John-Wiley, Hoboken, **2008,** 455-481.
23. (a) Brittain, H. *Am. Pharm. Rev*. **2002,** *5,* 74-80. (b) Stahly, G. P. *Cryst. Growth Des.* **2007,** *7,* 1007-1026.
24. Threlfall, T. L. *Org. Proc. Res. Dev.* **2009,** *13,* 1224-1230.
25. Fucke, K.; Qureshi, N.; Yufit, D.S.; Howard, J.A.; Steed, J.W. *Cryst. Growth Des.* **2010**, *10,* 880-886.
26. Zencirci, N.; Griesser, U.J.; Gelbrich, T.; Apperley, D.C.; Harris, R.K. *Mol. Pharmaceutics*, **2014,** *11,* 338-350.
27. Burger A.; Ramberger, R. *Microchim. Acta II*, **1979,** *72*, 273-316.
28. (a) Phadnis, N. V.; Suryanarayanan, R. *J. Pharm. Sci*. **1997,** *86,* 1256-1263. (b) Otsuka, M.; Teraoka, R.; Matsuda, Y. *Pharm. Res.* 1991, **8**, 1066-1068. (c) Hu, Y.; Erxleben, A.; Hodnett, B. K.; Li, B.; McArdle, P.; Rasmuson, Å.C.; Ryder, A.G. *Cryst. Growth Des.* **2013,** *13,* 3404-3413. (d) Otsuka, M.; Onoe, M.; Matsuda, Y. *Pharm. Res.* **1993**, *10,* 577-582.
29. (a) Henck, J. O. Konformationspolymorphie n-butylsubstituierter Arzneistoffe. Innsbruck: Thesis, p 41 (b) Braun, D.E.; Gelbrich, T.; Kahlenberg, V.; Tessadri, R.; Wieser, J.; Griesser, U.J. *J. Pharm. Sci*., **2009**, *98*, 2010-2026. (c) Griesser, U.J.; Weigand, D.; Rollinger, J.M.; Haddow, M.; Gstrein, E. *J. Therm. Anal. Calorim*., **2004,** *77*, 511-522.
30. *CrysAlis CCD and CrysAlis RED*, Ver. 1.171.33.55; Oxford Diffraction Ltd: Yarnton, Oxfordshire, UK, **2008**.
31. Dolomanov, O. V.; Blake, A. J.; Champness, N. R.; Schröder, *M. J. Appl. Crystallogr*. **2003**, *36,* 1283–1284.
32. Spek, A. L. *PLATON, A Multipurpose Crystallographic Tool*; Utrecht University: Utrecht, Netherlands, **2002**.

33. Barbour, L. J. *X-Seed, Graphical Interface to SHELX-97 and POV-Ray, Program for Better Quality of Crystallographic Figures*; University of Missouri-Columbia, Missouri, U.S.A., **1999**.
34. Powder Cell, *A Program for Structure Visualization, Powder Pattern Calculation and Profile Fitting*, http://www.ccp14.ac.uk/index.html (accessed 31 July, 2014).

CHAPTER FIVE

Epalrestat–Cytosine Cocrystal and Salt Structures: Attempt To Control E,Z → Z,Z Isomerization

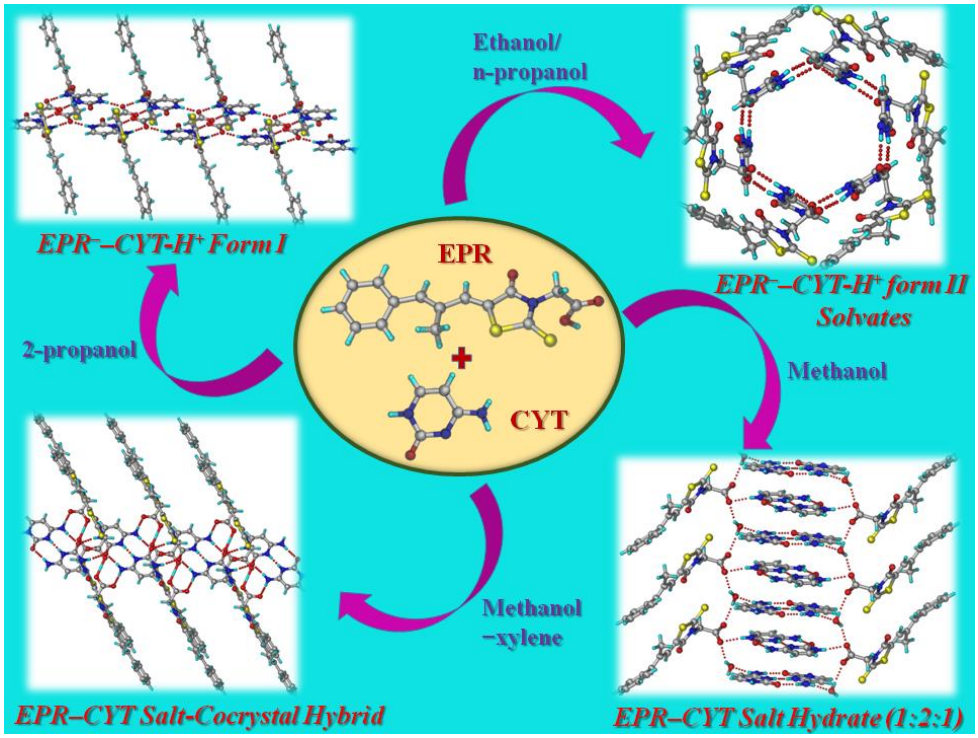

Crystallization of Epalrestat (EPR) and cytosine (CYT) resulted in novel salt polymorphs EPR⁻–CYT-H⁺ form I and solvated form II, a salt-cocrystal hybrid, and salt hydrate (EPR⁻–CYT-H⁺–H_2O, 1:2:1). Attempts to control the E,Z → Z,Z isomerization of EPR through EPR-CYT solid forms was not successful.

5.1 Introduction

The design and crystallization of solid forms such as polymorphs, salts, cocrystals, hydrates, and solvates of active pharmaceutical ingredients (APIs) is practiced to control and modulate the physicochemical and pharmacokinetic properties of APIs,[1-10] such as stability, compressibility, filterability, morphology, dissolution profile, bioavailability, tableting, etc. Salt formation is the most common and effective method, especially for improving the solubility and stability of ionizable drugs.[11] Salts and cocrystals are distinguished based on the proton location, whether it is present on the acid or transferred to the base. The individual components are held together by heteromeric interactions in cocrystals,[12] such as hydrogen bonds, whereas in salts the proton is transferred in the product.[13] It is difficult to predict whether a salt or cocrystal will form in an acid-base complex when their pK_a values are similar. The product can be a neutral cocrystal, an ionic salt, or a continuum of states. The ΔpK_a rule of three[14] states that salts are expected from the reaction of acid and base when ΔpK_a (= pK_a (conjugate acid of base) – pK_a of acid) is greater than 3. If $\Delta pK_a < 0$, then cocrystal is expected, and in the range 0-3, salt-cocrystal continuum or different proton states are observed. Acid-base complexes with $\Delta D_{C\text{-}O} < 0.03$ Å are salts (difference between C–O and C=O distances in COOH group), while $\Delta D_{C\text{-}O} > 0.08$ Å are cocrystals.[14,15] Borderline examples of salt-cocrystal hybrid structures have been reported recently.[14,16]

Salt formation represents the traditional methodology for solid form development with numerous applications in the pharmaceutical industry[3,17]. Perumalla et. al.[18] has reported the improvement in compaction properties of Acetaminophen by synthesising a hydrochloride salt hydrate (ACM.HCl) of this molecule. They have noted that ACM.HCl has higher plasticity compared to the marketed form 1 and hence show excellent tableting properties. Nangia and coworkers[19] documented the improvement in the solubility of antipsychotic drug Olanzapine through mono and dimaleate salts. They have highlighted the significance of counter ion stoichiometry in varying the solubility of drug molecule. The research group of Desiraju[20] reported the saccharinate salts of various Active pharmaceutical ingredients (API's) with improved solubility. They have highlighted the importance of saccharinate counter ion as an able salt former. Puigjaner and coworkers[21] have documented the importance of screening for polymorphs of pharmaceutical salts and their effect on parent molecule solubility. They have reported

three polymorphs of Ziprasidone maleate and demonstrated that the maximum solubility ever documented for Ziprasidone salts was observed in the form C in combination with a high kinetic stability.

5.2 Epalrestat - Literature Reports

Epalrestat (5-[(1*Z*, 2*E*)-2-methyl-3-phenylpropenylidene]-4-oxo-2-thioxo-3-thiazolidineacetic acid; EPR) is a noncompetitive and reversible aldose reductase inhibitor (ARI), used to treat diabetic complications such as diabetic neuropathy, nephropathy, retinopathy, and cataract.[22] By inhibiting aldose reductase enzyme, EPR reduces the accumulation of intracellular sorbitol, which is believed to be the cause of diabetic complications.[23] Among all the recent carboxylic acid ARIs, EPR is the only ARI given marketing approval as a therapeutic drug for diabetic complications.[24] EPR was developed in 1983 and since then has been marketed in Japan, China, India, and Bangladesh. EPR is stable in the dark but isomerizes very easily upon photoirradiation even under a room light in solution to give four isomers, and the structures of these four isomers were reported on the basis of ^{1}H NMR and HPLC spectroscopic techniques.[25] Crystal structures of a guest free form[26a], several solvates (methanol[26b], ethanol[26c], tetrahydrofuron[27a], acetone[27b], dimethyl formamide[28], and dimethyl sulfoxide[28]), and a cocrystal[28] of EPR have been reported. Color polymorphism in Epalrestat (E,Z isomer), its Z,Z isomer, and E,Z to Z,Z isomerization upon exposure light were discussed in the chapter 4.[29]

Cytosine (CYT) is a pyrimidine nucleobase, which can form complementary H-bonds with purine nucleobase guanine in a Watson-Crick base pairing for DNA fragments.[25] Salts, cocrystals, salt hydrates, cocrystal hydrates, and salt cocrystal hydrates of cytosine with various organic and inorganic molecules are reported.[26-28]. With this literature background, to stabilize the EPR from photoisomerisation and thereby to increase therapeutic effect, in this chapter, the solid form screen of EPR with cytosine resulted in EPR–CYT salt polymorphs, EPR^{-}–CYT-H^{+} (polymorphs I and II), salt-cocrystal hybrid and salt hydrate (EPR^{-}–CYT-H^{+}– H_2O, 1:2:1). Chemical structures of EPR and CYT are given Scheme 5.1. All the solid forms were fully characterized by spectroscopic (FT-IR, solution ^{1}H NMR), thermal (differential scanning calorimetry (DSC), hot-stage

microscopy (HSM), and thermogravimetric analysis (TGA)), and X-ray diffraction techniques (single-crystal and powder X-ray diffraction (PXRD)).

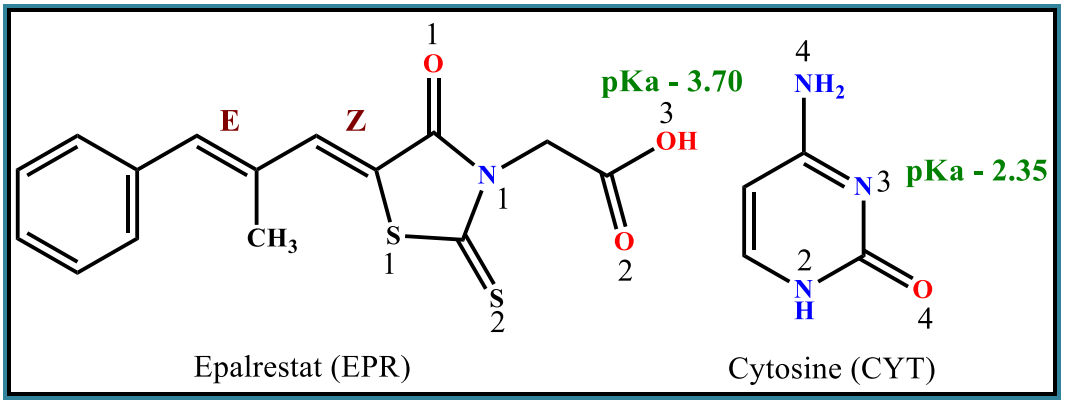

Scheme 5.1 Molecular Structure of Epalrestat (EPR) and Cytosine (CYT) along with Their pK_a Values.[a]

[a] pK_a's were calculated using Marvin[29] 5.10.1, 2012, ChemAxon, http://www.chemaxon.com.

5.3 Results and Discussion

The crystallization outcome of EPR and CYT could be a salt, cocrystal, or salt cocrystal hybrid based on an intermediate ΔpK_a value of 1.35[14] (Scheme 5.1). In the present study we have obtained novel salt polymorphs EPR^-–CYT-H^+ form I and form II, salt-cocrystal hybrid, and salt hydrate (EPR^-–CYT-H^+–H_2O, 1:2:1) forms of EPR with CYT using different techniques such as solution crystallization from different solvents, solvent-assisted grinding, and controlled heating experiments. To our knowledge, this is the first report on salt and salt-cocrystal hybrid products[30] for the same components under different crystallization conditions (Figure 5.1). The 2-amino-pyrimidinium−carboxylate two-point heterosynthon (5) (Scheme 5.2) was observed in the crystal structure of EPR^-–CYT-H^+ form I and form II solvated structures. The stoichiometry of EPR^-–CYT-H^+ form II ethanol and n-propanol salt solvates was estimated as 1:1:0.036 and 1:1:0.043, respectively, by ^{1}H NMR spectroscopy. The CYT-$H^+\cdots H^+$-CYT base pairing (synthon 1) was observed in the crystal structure of a salt-cocrystal hybrid and salt hydrate. The crystallographic information is given in Table 5.1, and hydrogen bonds are listed in Table 5.2.

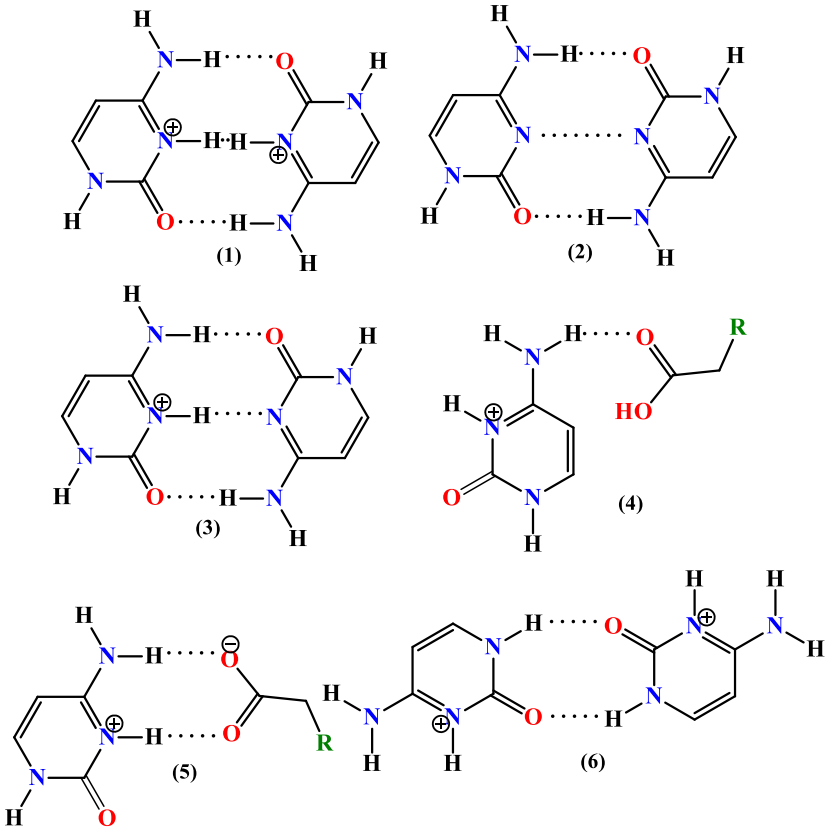

Scheme 5.2 Different Hydrogen Bond Synthons Observed in the Crystal Structures of EPR–CYT Crystal forms. (1) Three-point CYT-H^+···H^+-CYT base pair. (2) Three-point CYT···CYT base pair. (3) Three-point CYT-H^+···CYT base pair. (4) Single point N–H···O bond. (5) Two point 2-amino-pyrimidinium–carboxylate heterosynthon. (6) Two point N–H···O dimer synthon.

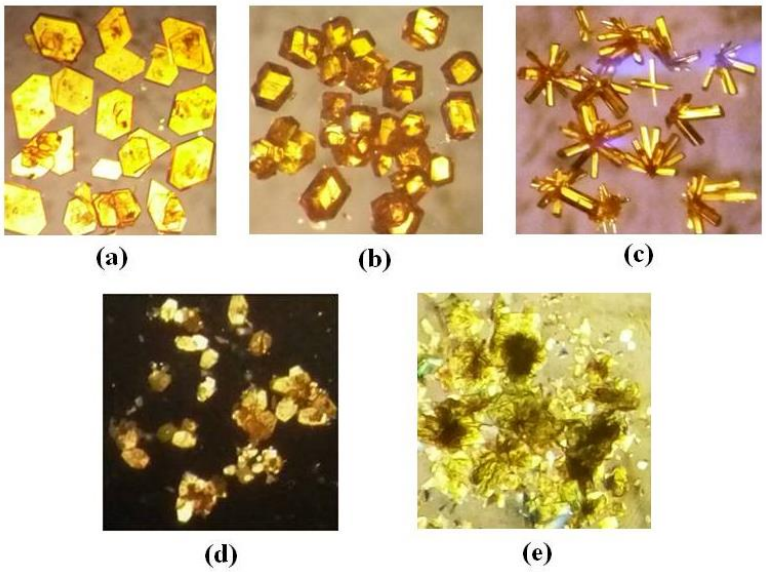

Figure 5.1 Crystal morphology and color images of EPR–CYT solid forms. (a) EPR^{-}–CYT-H^{+} form I, yellow hexagons. (b) EPR^{-}–CYT-H^{+} form II ethanol solvate, yellow blocks. (c) EPR^{-}–CYT-H^{+} form II n-propanol solvate, yellow rods. (d) EPR–CYT salt-cocrystal hybrid, yellow hexagons. (e) EPR-CYT salt hydrate, yellow plates.

Table 5.1 X-ray Crystallographic Data on EPR–CYT Sutructres.

Crystal structure	EPR^{-}–CYT-H^{+} form I	EPR^{-}–CYT-H^{+} form II EtOH solvate[a]	EPR^{-}–CYT-H^{+} form II n-PrOH solvate[a]	EPR–CYT salt-cocrystal hybrid	EPR^{-}–CYT-H^{+}–H_2O (1:2:1)
Chemical formula	C_{15} H_{12} N O_3 S_2 . C_4 H_6 N_3 O	C_{15} H_{12} N O_3 S_2 . C_4 H_6 N_3 O . (C2 H6 O)$_{0.036}$	C_{15} H_{12} N O_3 S_2 . C_4 H_6 N_3 O . (C3 H8 O)$_{0.043}$	2(C_{15} $H_{12.3}$ N O_3 S_2) . 2(C_4 $H_{5.7}$ N_3 O)	C_{15} H_{12} N O_3 S_2 . 2(C_4 $H_{5.50}$ N_3 O) . H_2 O
Crystal system	Triclinic	Trigonal	Trigonal	Triclinic	Triclinic
Formula weight	430.49	430.49	430.49	860.99	559.62
Space group	*P-1*	*R-3*	*R-3*	*P-1*	*P-1*
T [K]	298	298	298	100	298
a [Å]	7.752(5)	33.0523(19)	33.0862(17)	8.4676(11)	6.546(3)
b [Å]	8.438(5)	33.0523(19)	33.0862(17)	8.4700(12)	9.669(4)
c [Å]	16.449(10)	10.5319(8)	10.5570(11)	14.260(2)	20.714(9)
α [°]	82.180(11)	90	90	93.910(6)	86.019(7)
β [°]	83.806(10)	90	90	90.820(6)	84.346(7)
γ [°]	68.151(10)	120	120	107.023(5)	76.409(7)
Z	2	18	18	1	2
V [Å^3]	987.4(10)	9964.2(16)	10008.4(17)	975.0(2)	1266.7(9)
D_{calc} [g cm^{-3}]	1.448	1.291	1.286	1.466	1.467

Reflns. collected	9475	34494	32327	21925	12094
Unique reflns.	3477	4359	3930	3423	4467
Observed reflns.	2235	3242	2918	2841	2384
R_1 [I>2(I)]	0.0554	0.0482	0.0595	0.0915	0.0692
wR_2 (all)	0.1309	0.1446	0.1612	0.2666	0.1889
Goodness-of-fit	1.014	1.085	1.032	1.081	0.976
Diffractometer	Bruker Smart-Apex	Bruker Smart-Apex	Bruker Smart-Apex	Bruker D8 QUEST	Bruker Smart-Apex

[a] The stoichiometry of solvent was estimated by ^{1}H NMR integration.

Table 5.2 Hydrogen Bond Metrics in Crystal Structures.

Hydrogen bond	H···A (Å)	D···A (Å)	D–H···A (º)	Symmetry Code
EPR$^-$–CYT-H$^+$ form I				
N2–H2A···O3	1.92	2.781(4)	177	1-x,-y,1-z
N3–H3A···O2	1.80	2.655(4)	173	1-x,1-y,1-z
N4–H4A···O3	1.96	2.868(4))	154	1-x,1-y,1-z
N4–H4B···O1	2.17	3.020(4	179	-1+x,1+y,z
C4–H4···O4	2.53	2.984(5)	108	1+x,y,-1+z
C14–H14B···O4	2.42	3.087(5)	130	1-x,-y,1-z
C18–H18···O1	2.51	3.246(4)	136	-1+x,1+y,z
C19–H19···S2	2.79	3.597(4)	145	-x+1,-y+1,-z+1
C10–H10···S2	2.99	3.761(5)	133	x+1,+y,+z
C9–H9A···S1	2.74	3.193(6)	112	Intra
C14–H14A···S2	2.69	3.198(5)	114	Intra
EPR$^-$–CYT-H$^+$ form II EtOH Solvate				
N2–H2A···O3	1.94	2.818(2)	160	x,y,-1+z
N3–H3A···O3	1.94	2.689(2)	174	x-y,x,1-z
N4–H4A···O2	2.12	2.906(2)	175	x-y,x,1-z
N4–H4B···O2	2.11	2.927(2)	166	x,y,-1+z
C7–H7···S2	2.87	3.757(3)	159	x-y,x,1-z
C19–H19···O4	2.51	3.005(2)	114	y,-x+y,-z
C18–H18···O1	2.67	3.411(4)	137	x-y-1/3,+x-2/3,-z+1/3+1
C18–H18···O2	2.70	3.383(2)	131	-y+1/3,+x-y-1/3,+z-1/3
C9–H9C···S1	2.59	3.133(2)	116	Intra
C10–H10···O1	2.54	2.891(2)	103	Intra
C14–H14A···O1	2.42	2.793(2)	102	Intra
EPR$^-$–CYT-H$^+$ form II n-Propanol Solvate				
N2–H2A···O3	2.01	2.793(2)	164	x,y,1+z
N3–H3A···O3	1.85	2.685(3)	175	x-y,x,-z
N4–H4A···O2	2.05	2.902(3)	173	x-y,x,-z

N4–H4B···O2	2.13	2.937(3)	156	x,y,1+z
C7–H7···S2	2.88	3.761(3)	160	x-y+1/3,+x-1/3,-z+2/3
C19–H19···O4	2.53	3.019(3)	113	y,-x+y,1-z
C18–H18···O1	2.75	3.412(6)	132	x-y-1/3,+x-2/3,-z+1/3+1
C18–H18···O2	2.68	3.398(4)	137	-y+1/3,+x-y-1/3,+z+2/3
C9–H9B···S1	2.67	3.136(3)	110	Intra
C10–H10···O1	2.55	2.895(3)	103	Intra
C14–H14A···O1	2.44	2.808(3)	102	Intra
EPR–CYT Salt-Cocrystal Hybrid				
N2–H2A···O4	1.96	2.820(4)	164	2-x,2-y,-z
N3–H3A···N3	2.33	2.863(4)	155	1-x,2-y,-z
N4–H4A···O3	2.55	2.918(4)	106	-x,1-y,-z
N4–H4A···O4	2.02	2.882(4)	167	1-x,2-y,-z
N4–H4B···O2	1.94	2.806(4)	169	x,y,z
C4–H4···O2	2.48	3.357(5)	154	1-x,-y,1-z
C19–H19···O3	2.39	3.115(4)	133	1+x,y,z
O3–H3B···O3	1.22	2.444(3)	180	-x,1-y,-z
C10–H8···O1	2.54	2.903(4)	103	Intra
C14–H14A···O1	2.39	2.816(4)	105	Intra
C9–H9A···S1	2.53	3.157(4)	122	Intra
EPR^{-}–CYT-H^{+}–H_2O (1:2:1)				
N2–H2A···O3	1.91	2.778(13)	172	-1+x,1+y,z
N3–H3A···N3	2.03	2.827(13)	176	1-x,1-y,-z
N4–H4A···O4	1.90	2.811(13)	173	1-x,1-y,-z
N4–H4B···O6	2.19	2.997(14)	169	x,-1+y,z
N5–H5A···O2	2.04	2.884(13)	169	-1+x,y,z
N5–H5A···O3	2.62	3.183(5)	124	x-1,+y,+z
N6–H6A···N6	1.90	2.802(13)	166	-x,1-y,-z
N7–H7A···O5	1.94	2.799(13)	175	-x,1-y,-z
N7–H7B···O6	2.34	3.175(15)	165	1-x,1-y,-z
O6–H6B···O3	2.18	2.948(14)	172	-1+x,1+y,z
O6–H6C···O2	2.32	3.027(14)	152	x,1+y,z
C4–H4···O5	2.48	3.201(15)	134	-x,1-y,1-z
C6–H6···O1	2.54	3.241(15)	132	1-x,-y,1-z
C7–H7···O1	2.52	3.354(15)	149	1-x,-y,1-z
C23–H23···O3	2.60	3.216(15)	124	-1+x,y,z
C23–H23···O4	2.42	3.212(15)	143	x,-1+y,z
C18–H18···S2	2.99	3.856(5)	154	x-1,+y,+z
C9–H9A···S1	2.71	3.197(15)	112	Intra
C10–H10···O1	2.50	2.871(13)	104	Intra
C14–H14B···O1	2.43	2.821(13)	104	Intra

5.3.1 Crystal Structure Analysis

Epalrestat-Cytosine Salt EPR^{-}–CYT-H^{+} Form I

Crystallization of EPR and CYT in a 1:1 ratio from i-propanol resulted in yellow color hexagonal-shaped plate morphology crystals of EPR^{-}–CYT-H^{+} form I which was solved in triclinic space group *P*-1. The 2-amino-pyridinium–carboxylate synthon (5) (N4–H4A···O3, 1.96 Å, 154º, and N3–H3A^{+}···O2, 1.80 Å, 173º) was observed (Figure 5.2a). Two adjacent heterodimeric motifs $R_2^2(8)$ connect through the N–H···O hydrogen bond (N4–H4B···O1, 2.17 Å, 179º) to make a tetrameric ring motif $R_4^4(18)$. These tetrameric ring motifs further connect through N–H···O hydrogen bond (N2–H2A···O3^{-}, 1.92 Å, 177º) and form 1D tape (Figure 5.2b). The overall packing in the crystal lattice is shown in Figure 5.2c.

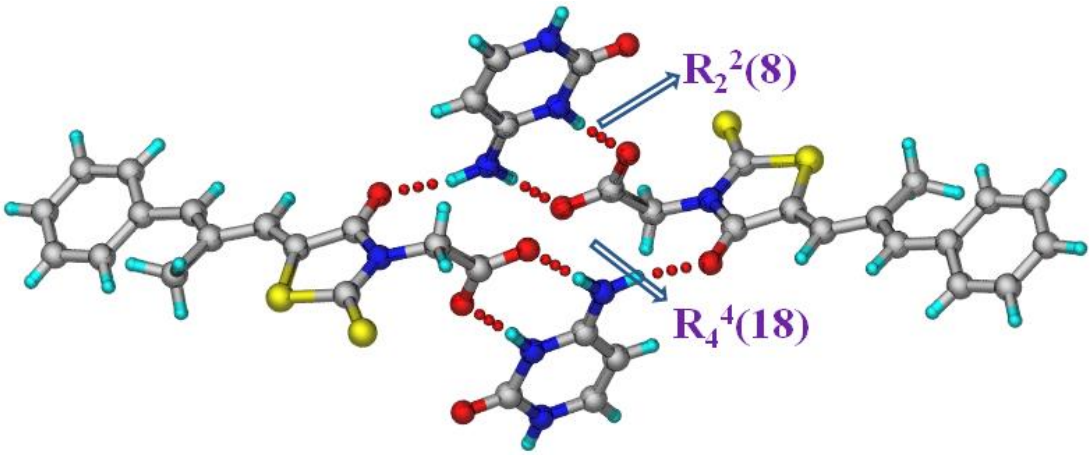

(a)

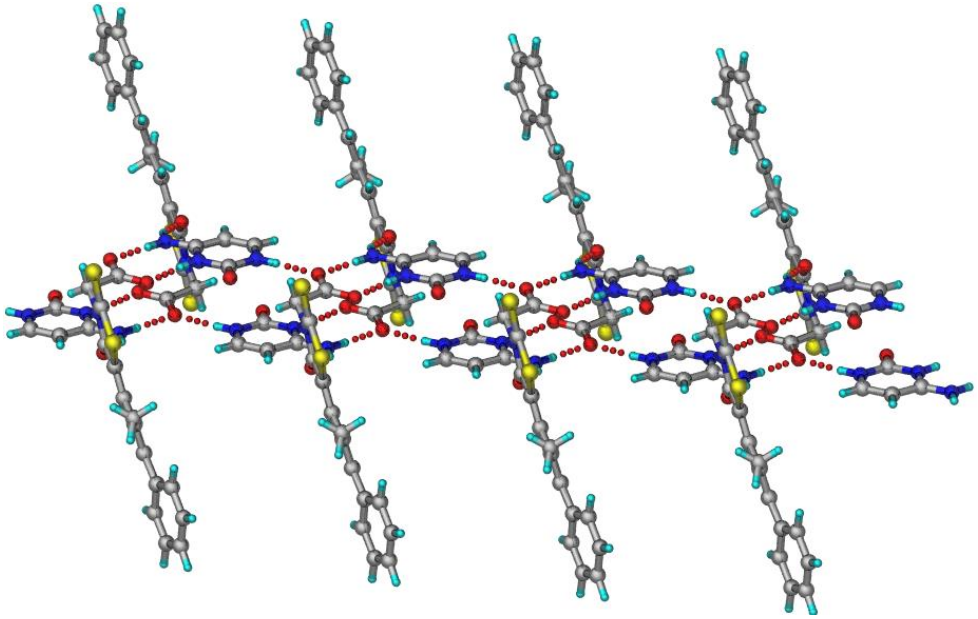

(b)

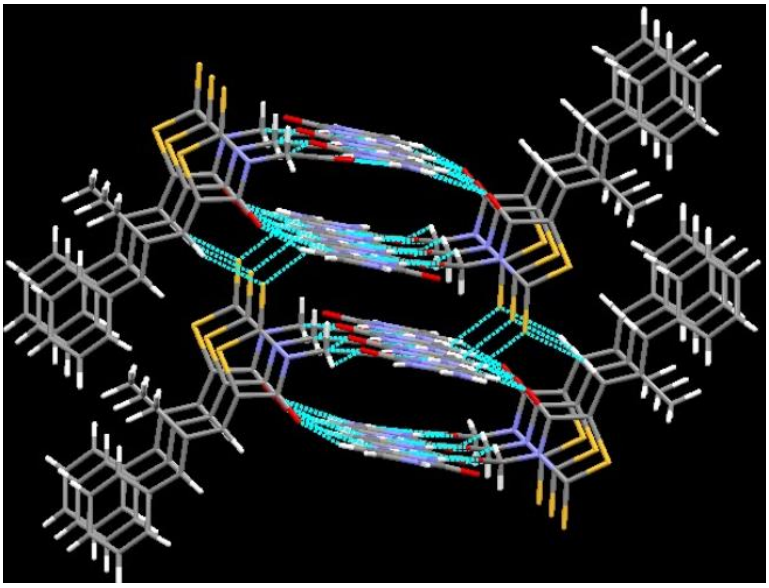

(c)

Figure 5.2 (a) $R_2^2(8)$ dimeric and $R_4^4(18)$ tetrameric assembly of cytosinium cation and EPR anion in the crystal structure of EPR^{-}–CYT-H^{+} form I formed via 2-amino-pyrimidinium−carboxylate heterosynthon and N–H···O hydrogen bonds. (b) Tetrameric ring motifs are connecting through N−H···O hydrogen bonds. (c) The overall 3D packing in the crystal structure.

Epalrestat-Cytosine Salt EPR^{-}–$CYT\text{-}H^{+}$ Form II Ethanol and n-Propanol Solvates.

Crystallization of EPR and CYT in a 1:1 ratio from alcoholic solvents such as ethanol and n-propanol resulted in EPR^{-}–$CYT\text{-}H^{+}$ form II solvates which crystallized in the trigonal space group *R*-3. The asymmetric unit consists of a carboxylate anion of epalrestat (EPR^{-}), and a protonated cytosine ($CYT\text{-}H^{+}$). The hexameric network through 2-amino-pyrimidinium−carboxylate heterosynthon ($N3^{+}$–H3A···$O3^{-}$ 1.94 Å, 174º and N4–H4A···O2, 2.12 Å, 175º) and N−H···O H-bonds (N2–H2A···O3, 1.94 Å, 160º and N4–H4B···O2, 2.11 Å, 166º) is shown in Figure 5.3a. Such a network extends into a channel or solvent-accessible hexagonal voids (Figure 5.3b and 5.3c). Similar to carbamazepine form II,[31] the inclusion of solvent molecules ethanol and n-propanol was observed in the rhombohedral crystal structure of EPR^{-}–$CYT\text{-}H^{+}$ form II. The solvent molecules in the voids are disordered, and the diffuse electron density could not be located as discrete solvent atoms. However, ^{1}H NMR integration and thermogravimetric analysis (TGA) of freshly prepared solvate crystals confirmed the number of solvent molecules. The crystal structures were treated by the squeeze program to remove residual electron density corresponding to disordered solvent molecules.[32] After using the squeeze program, the highest residual peak (Q peak) was reduced from 0.99 to 0.44 for EPR^{-}–$CYT\text{-}H^{+}$ form II EtOH solvate and 0.96 to 0.49 for EPR^{-}–$CYT\text{-}H^{+}$ form II n-PrOH solvate. Since desolvation did not cause any change in the powder XRD pattern and it is different from the powder XRD pattern of the previously discussed EPR^{-}–$CYT\text{-}H^{+}$ structure, the two forms may be classified as EPR^{-}–$CYT\text{-}H^{+}$ polymorphs I and II and the solvent inclusion structures as solvates. The torsion angles ι_4 (N1-C14-C15-O3) are different in the two structures (Table 5.3), and the overlay of the carboxylate anion fragment is shown in Figure 5.4.

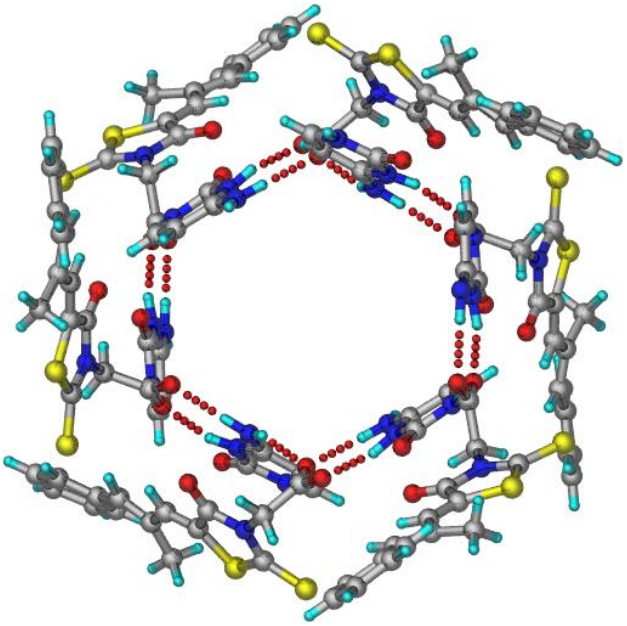

(a)

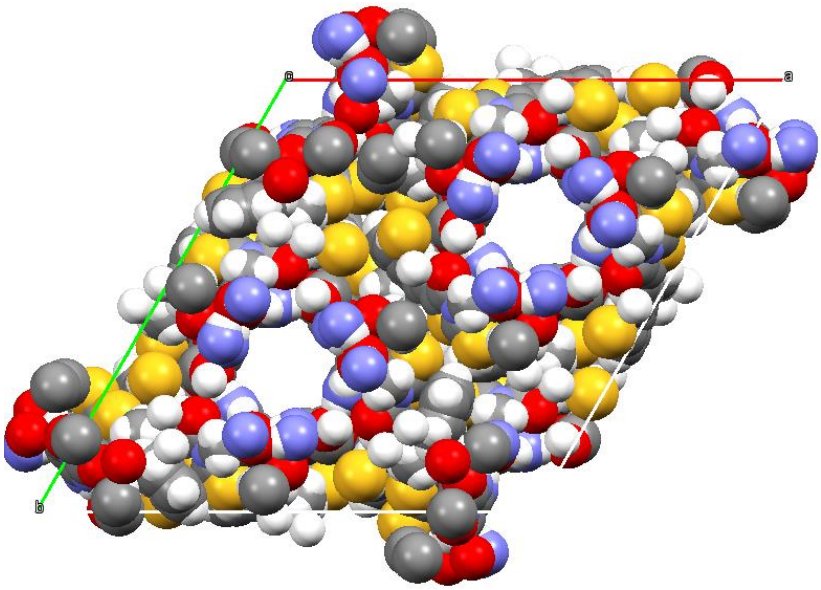

(b)

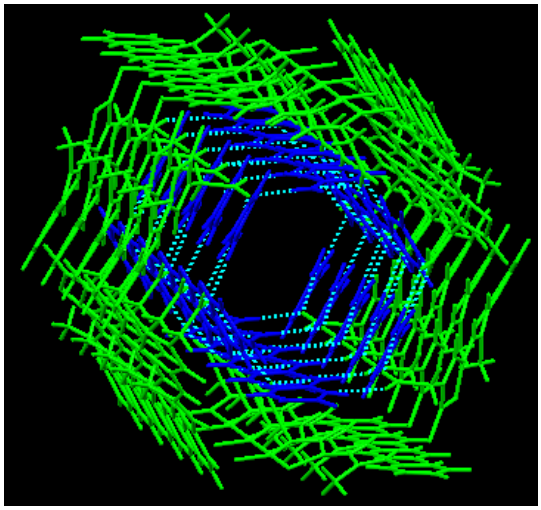

(c)

Figure 5.3 (a) Hexameric network of EPR^- and $CYT\text{-}H^+$ through 2-amino-pyrimidinium−carboxylate heterosynthon and $N{-}H\cdots O^-$ hydrogen bond in the solvated structures. (b) Space filling representation of EPR^-–$CYT\text{-}H^+$ form II viewed down the c-axis. (c) Channel-like structure in the crystal structure of EPR^-–$CYT\text{-}H^+$ form II (green and blue coded).

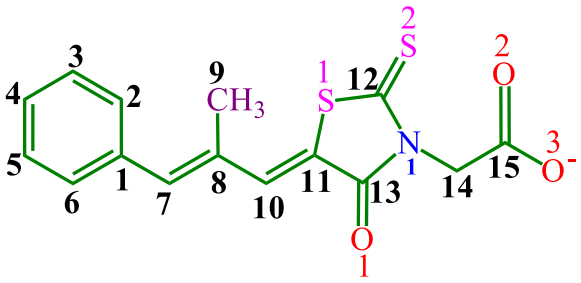

τ_1 (O1-C13-N1-C14), τ_2 (C13-N1-C14-C15), τ_3 (N1-C14-C15-O2), τ_4 (N1-C14-C15-$O3^-$)

Table 5.3 Torsion Angles of EPR^- Conformers in the EPR– CYT Salt Polymorphs.

Crystal Form	τ_1 (°)	τ_2 (°)	τ_3 (°)	τ_4 (°)
EPR^-–$CYT\text{-}H^+$ form I	1.02	71.88	15.89	-164.99
EPR^-–$CYT\text{-}H^+$ form II solvates	4.42	97.86	-15.17	165.42

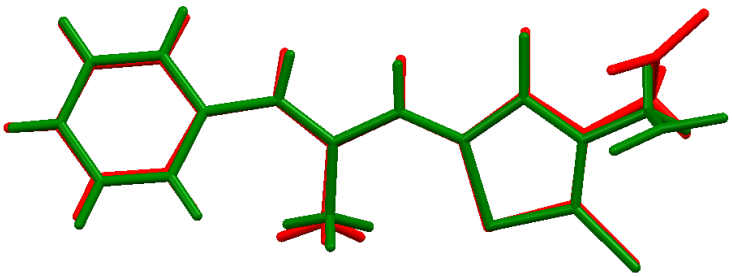

Figure 5.4 Overlay diagram of the carboxylate anion of epalrestat found in the EPR–CYT salt polymorphs. Color code: Red = EPR^- in EPR^-–CYT-H^+ form I, Green = EPR^- in EPR^-–CYT-H^+ form II.

Epalrestat-Cytosine Salt-Cocrystal Hybrid

Crystallization of EPR and CYT from methanol−xylene solvent mixture (1:1) resulted in hexagonal shaped plate crystals of the EPR–CYT salt cocrystal hybrid which were solved in triclinic space group *P*-1. One molecule each of epalrestat (EPR) and cytosine (CYT) is present in the asymmetric unit. Salts and cocrystals can be distinguished by X-ray diffraction using the ΔD_{C-O} (difference between C−O and C=O bond distances) of a carboxylic acid group. Structures with $\Delta D_{C-O} < 0.03$ Å are salts, and $\Delta D_{C-O} > 0.08$ Å are cocrystals[14,15] since the carboxyl anion possesses two similar D_{C-O} values; however, a neutral carboxyl acid group has different D_{C-O} values. In this crystal structure, the C−O and C=O bond distances of the acid group of EPR are 1.288 Å, 1.216 Å ($\Delta D_{C-O} = 0.072$), which is an intermediate distance between the salt and cocrystal. This structure can therefore be assigned as a salt cocrystal hybrid with partial proton transfer (Table 5.4). O−C−C angles (112.4° and 121.3°) of the carboxylic acid show an intermediate state and partial transfer of the proton to the N3 atom of CYT. Site occupancy factors (s.o.f.) for the H3A atom attached to N3 and the H3B atom attached to O3 were fixed as 0.30 and 0.70 because refinements were unstable at other than this ratio.[33] EPR interacts with the CYT through N−H···O H-bond (N4–H4B···O2, 1.94 Å, 169º) (Figure 5.5a). The carboxylic acid proton of EPR is partially transferred to the N3 atom of the cytosine base. The partially protonated cytosine makes a cytosine dimer (CYT-H^+··· H^+-CYT) synthon (3) through two N−H···O H-bonds (N4–H4A···O4, 2.02 Å, 167º) and two N^+−H···N^+ H-bonds (N3–H3A···N3, 2.33 Å, 155º). These dimeric units are held together by N−H···O dimer synthon (N2–H2A···O4, 1.96 Å, 164º) and in a 1D tape (Figure 5.5b). EPR molecules are anchored with this 1D tape through the N−H···O H-

bond (N4–H4B···O2, 1.94 Å, 169º) in a 2D chain (Figure 5.5c). Whether the crystal structure contains synthons (3) which are randomly oriented in the unit cell or a symmetric synthon (1) across the entire structure is difficult to differentiate in the centrosymmetric *P*-1 space group. That is, whether it is a synthon (1) throughout the structure or an average of N–H···N^+ or N^+···H–N synthons (3) is difficult to differentiate in the centrosymmetric *P*-1 space group setting. This type of CYT-H^+···H^+-CYT base pairing is rare but has been observed in some of the crystal structures of charge-transfer complexes of cytosine.[34,35] A search of the Cambridge Structural Database (CSD) on cytosine synthons in the CSD[36] resulted in 10 hits which are listed in Table 5.5.

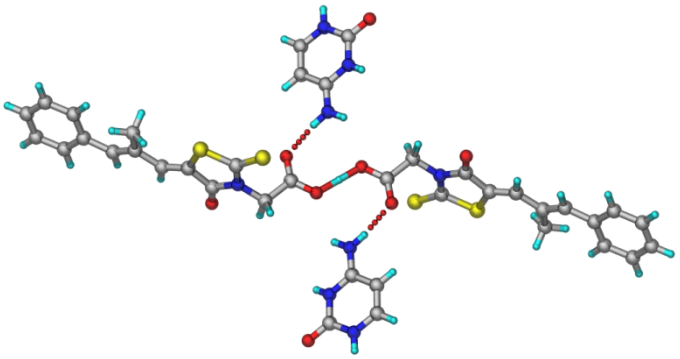

(a)

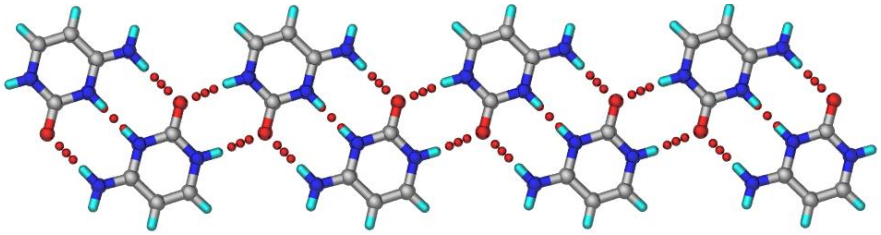

(b)

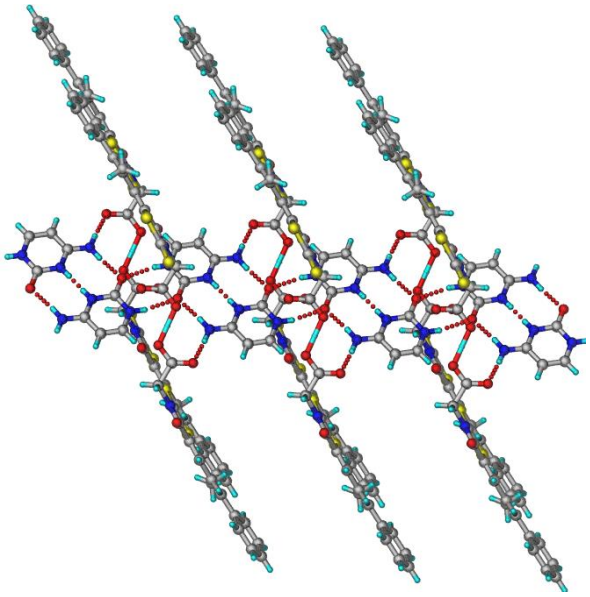

(c)

Figure 5 (a) N–H···O H-bond between EPR and CYT. (b) 1D tape formed through the CYT-H^+···H^+-CYT base pair and N–H···O dimer synthon. (c) 2D chain formed through N–H···O H-bond and CYT-H^+···H^+-CYT base pair.

Table 5.4 $\Delta D_{C\text{-}O}$ Values in EPR–CYT Structures.

Crystal structure	$D_{C=O}$ (Å)	$D_{C\text{-}O}$ (Å)	$\Delta D_{C\text{-}O}$ (Å)
EPR^-–CYT-H^+ form I	1.243	1.262	0.019
EPR^-–CYT-H^+ form II ethanol solvate	1.239	1.259	0.02
EPR^-–CYT-H^+ form II n-propanol solvate	1.244	1.257	0.013
EPR–CYT salt-cocrystal hybrid	1.216	1.288	0.072
EPR-CYT salt hydrate	1.238	1.276	0.038

Table 5.5 CSD search for the synthon (1).

No.	**Refcode**
1	LIWSIU
2	LIWSOA
3	UDIKUP01
4	UDILIE
5	ODICOU
6	GITYEN
7	OYEREQ
8	ZEYKAR
9	TAZXAU
10	TAZXEY

Epalrestat-Cytosine Salt Hydrate EPR^{-}–CYT-H^{+}–H_2O (1:2:1)

Crystallization of EPR and CYT in a 1:2 ratio from methanol solvent resulted in plate shape crystals of salt-cocrystal hydrate which was solved in triclinic space group *P*-1. The asymmetric unit consists of a carboxylate anion of epalrestat (EPR^{-}), two half protonated cytosines (CYT-H^{+}), and a water molecule. The proton from EPR was equally transferred to the two cytosines with site occupancy factor (s.o.f.) of 0.5 for the H3A atom attached to N3 and 0.5 for the H6A atom attached to the N6**.** Two half protonated cytosine molecules are making CYT-H^{+}···H^{+}-CYT base pairing through two N–H···O H-bonds (two N4–H4A···O4, 1.90 Å, 173º, in one CYT-H^{+}···H^{+}-CYT base pair, two N7–H7A···O5, 1.94 Å, 175º, in another CYT-H^{+}···H^{+}-CYT base pair) and two N^{+}–H···N^{+} H-bonds (two $N3^{+}$–H3A···$N3^{+}$, 2.03 Å, 176º, in one CYT-H^{+}···H^{+}-CYT base pair, two $N6^{+}$–H6A···$N6^{+}$, 1.90 Å, 166º, in another CYT-H^{+}···H^{+}-CYT base pair). A water molecule connects two EPR^{-} molecules through O–H···O and O–H···O^{-} H-bonds (O6–H6B···$O3^{-}$, 2.18 Å, 172º and O6–H6C···O2, 2.32 Å, 152º) and form 1D chain. These 1D chains propagate antiparallel connected by CYT-H^{+}···H^{+}-CYT base pair and carboxylate–pyridinium single point synthon (N5–H5A···O2, 2.04 Å, 169º) and N–H···O H-bond (N4–H4B···O6, 2.19 Å, 169º) (Figure 5.6).

Whenever two cytosine molecules are present in an ionic structure, it is observed that CYT-H^{+} hydrogen bonds with cytosine (CYT) through a set of triple hydrogen bonds consisting two N–H···O and one N^{+}–H···N hydrogen bond[27,28] (synthon 3 in Scheme 2). It is difficult to unambiguously differentiate between synthon (3) CYT-H^{+}···CYT and CYT-H^{+}···H^{+}-CYT synthon (1) distributed randomly in the periodic array from the X-ray structure reflections data.

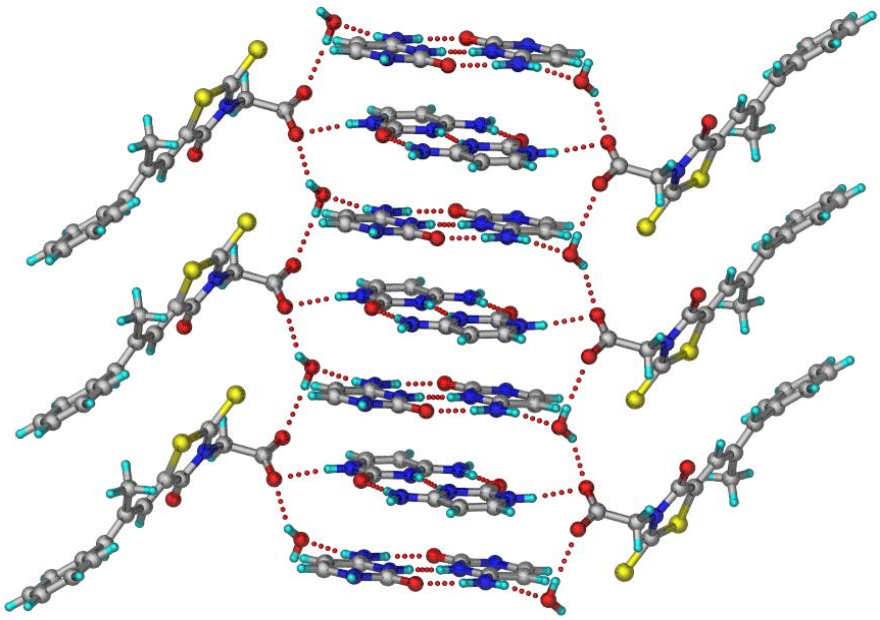

Figure 5.6 CYT-H^+···H^+-CYT base pairs and carboxylate−pyridinium synthon in the crystal structure of EPR^-–CYT-H^+–H_2O (1:2:1).

5.3.2 Powder X-ray Diffraction

The PXRD of the novel solid forms prepared in this work confirm the bulk solid-phase purity and homogeneity of each crystalline phase which showed an excellent overlay of the experimental powder pattern with the calculated lines from the crystal structure (Figure 5.7). Controlled desolvation of EPR^-–CYT-H^+ form II ethanol and n-propanol solvates at 230 and 240 °C for 30 min resulted in EPR^-–CYT-H^+ form II (Figures 5.8 and 5.9) without any solvent present, and the PXRD of this product is different from that of the original EPR^-–CYT-H^+ form I crystallized from i-ProH and similar to the PXRD line pattern of form II solvates. We term these two crystal forms of EPR^-–CYT-H^+ as I and II, since they represent polymorphs of the same salt. Furthermore, dehydration of EPR–CYT salt hydrate (1:2:1) at 160 °C for 30 min resulted in a PXRD of the product that appears to be predominantly EPR^-–CYT-H^+ form II and smaller amounts of residual CYT by visual matching of peaks (Figure 5.10).

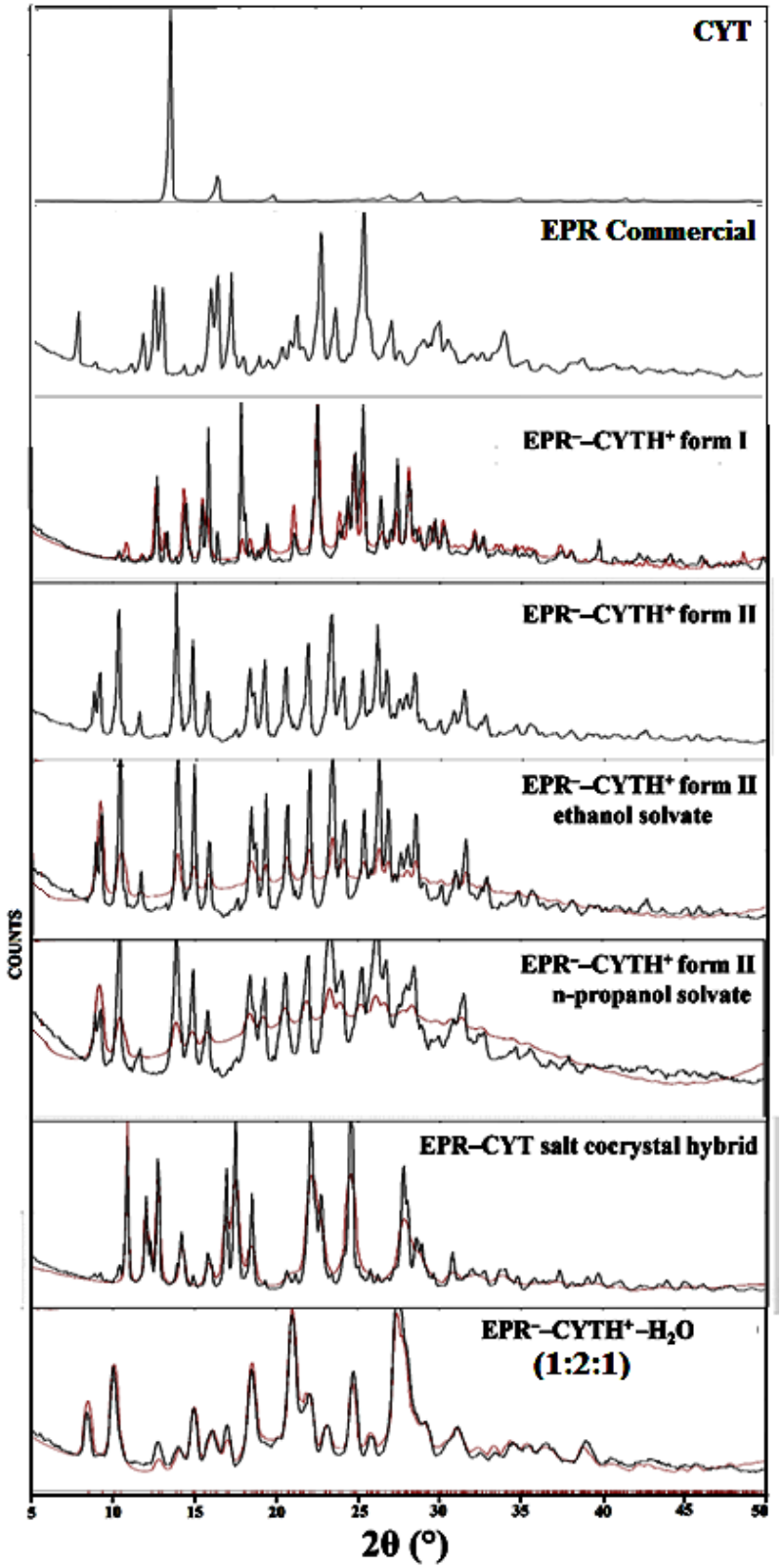

Figure 5.7 Overlay of experimental PXRD (black) of EPR solid forms matches with the calculated lines from the X-ray crystal structure (red).

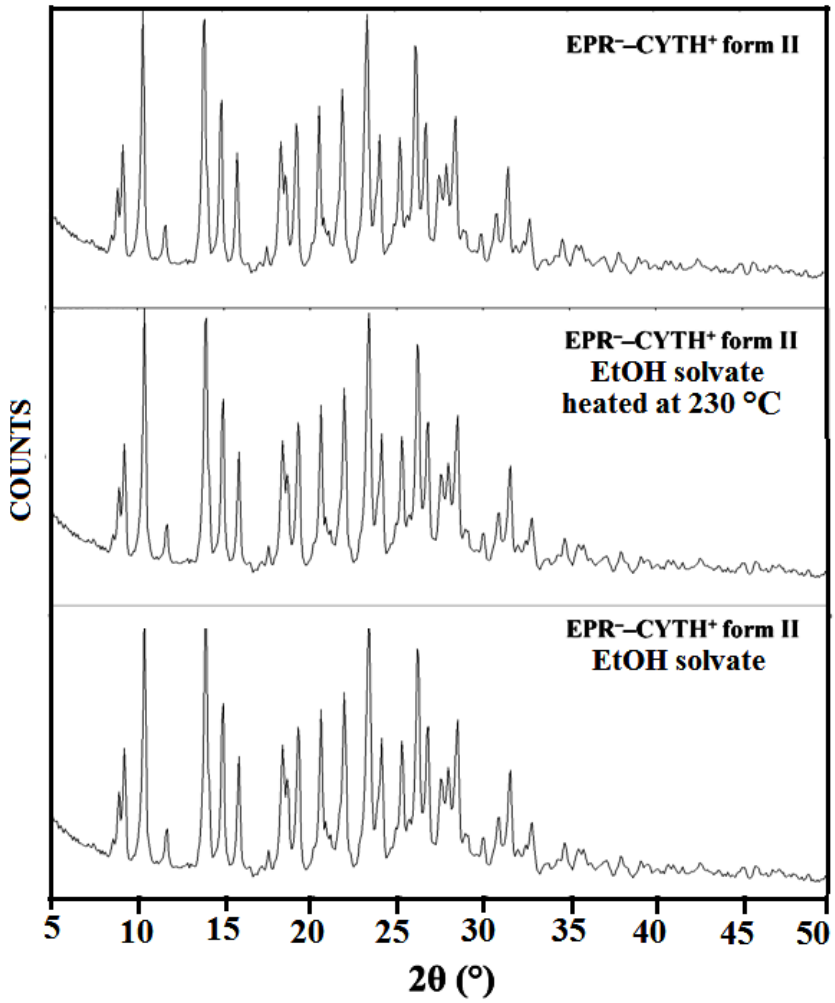

Figure 5.8 PXRD plot of EPR^{-}–CYT-H^{+} form II EtOH solvate to show the formation of EPR^{-}–CYT-H^{+} form II upon heating at 230 °C.

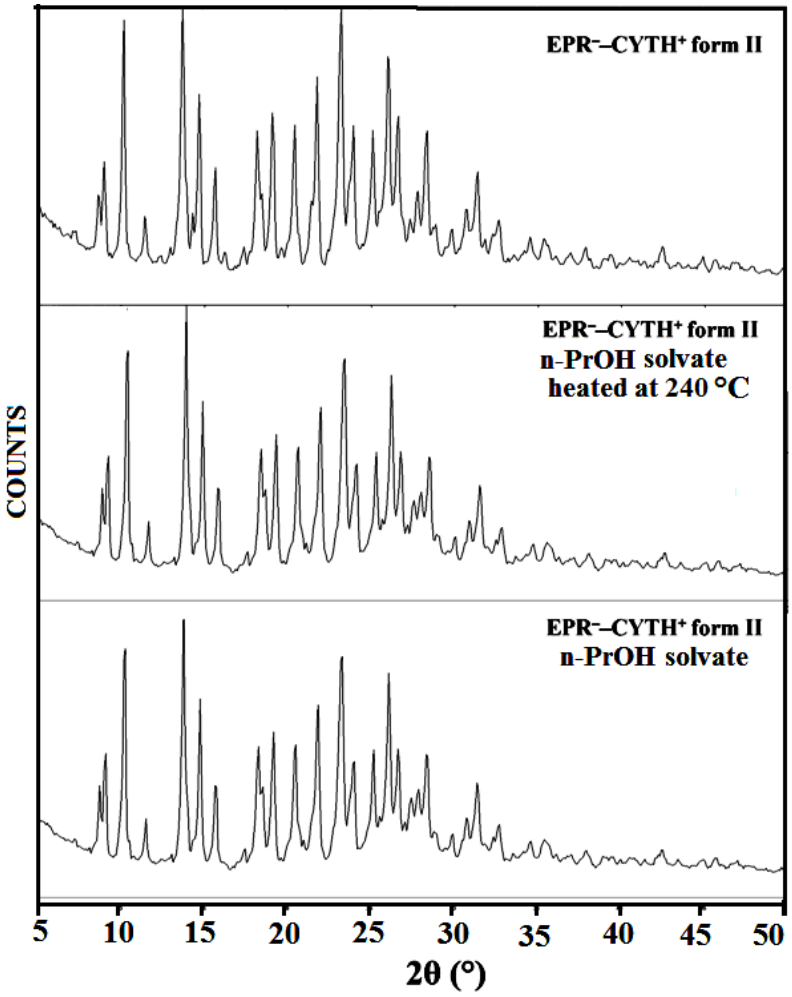

Figure 5.9 PXRD plot of EPR^{-}–CYT-H^{+} form II n-PrOH solvate to show the formation of EPR^{-}–CYT-H^{+} form II upon heating at 240 °C.

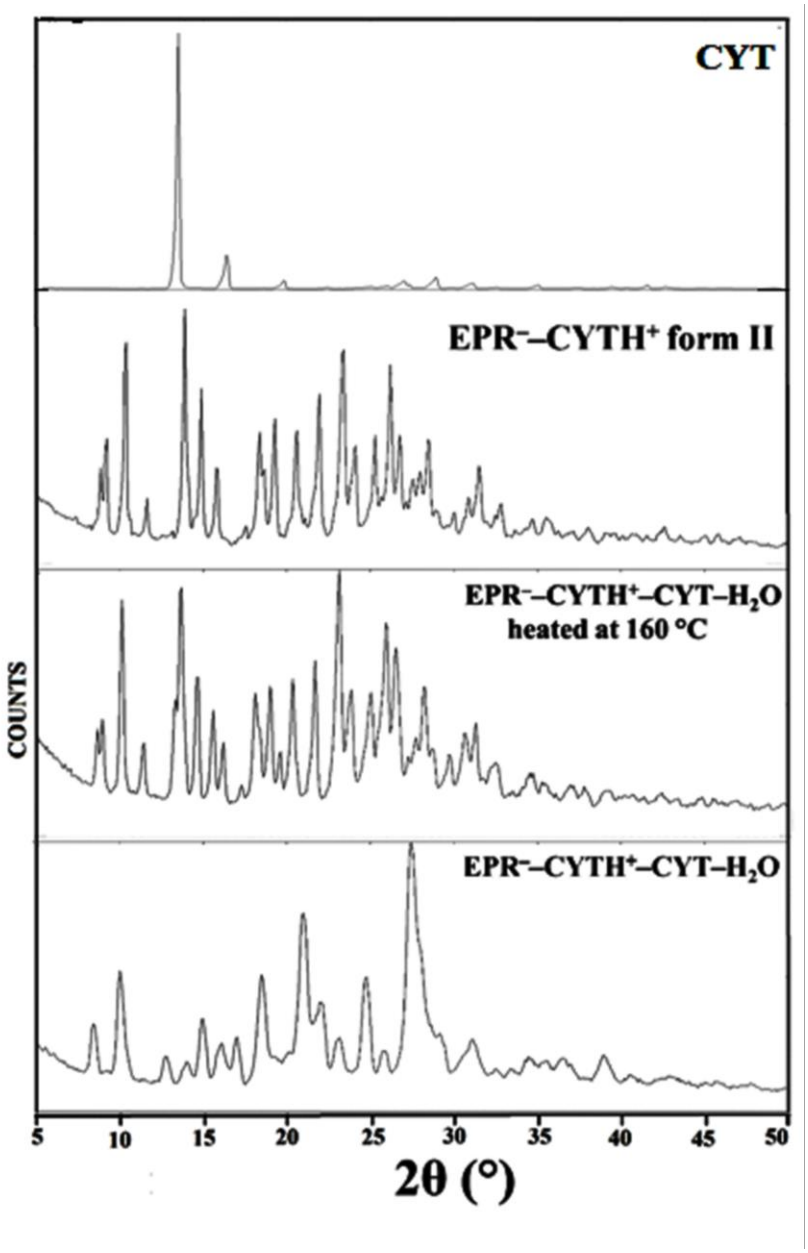

Figure 5.10 PXRD plot of EPR^{-}–CYT-H^{+}–CYT–H_2O to show the formation of EPR^{-}–CYT-H^{+} form II upon dehydration.

5.3.3 Spectroscopic Analysis

A shift in the vibrational frequency of product with respect to the starting materials indicates the formation of new hydrogen bonds.[37] In the IR spectrum of EPR, the carboxylic acid and ketone carbonyl stretching frequencies are at 1677.5 and 1746.5 cm^{-1}, and NH_2 asymmetric and symmetric stretching frequencies of CYT are at 3378.6 and 3170.9 cm^{-1}. Significant shifts in these vibrational frequencies were observed in

EPR–CYT solid forms (Table 5.6, Figure 5.11). The asymmetric and symmetric stretching frequencies of the carboxylate group (COO^-) of EPR^-–CYT-H^+ form I, form II, and form II solvates were observed at 1643.9, 1412.0; 1666.2, 1410.9; 1669.4, 1411.6, and 1663.1, 1411.2 cm^{-1}. The stretching frequency of the carboxylic group in EPR–CYT salt hydrate is at 1522.5 cm^{-1} (weaker C–O stretch of COOH) and for the carboxylate at 1669.8 cm^{-1} (asymmetric) and 1413.0 cm^{-1} (symmetric). Similarly, the EPR–CYT salt cocrystal hybrid exhibits stretching frequency for the carboxylic group at 1518.2 cm^{-1} (weaker C–O stretch of COOH) and for the carboxylate at 1670.1 cm^{-1} (asymmetric) and 1413.0 cm^{-1} (symmetric). In these two spectra, the carbonyl C=O stretch of the COOH group is overlapping with the ketone C=O stretch of the cytosine molecule, and the C–O stretch of COOH is at a different wave number.

Solution ^1H NMR spectra of EPR^-–CYT-H^+ form II ethanol and n-propanol solvates in DMSO-d_6 showed the stoichiometry as 1:1:0.036 for ethanol solvate and 1:1:0.043 for n-propanol solvate (Figure 5.12).

Table 5.6 FT-IR Stretching Frequency of EPR–CYT Crystal Forms (in cm^{-1})

Solid form	$–NH_2$ asym stretch	$–NH_2$ sym stretch	Ketone C=O stretch	Carboxylic C=O stretch	$–COO^-$ asym stretch	$–COO^-$ sym stretch
EPR	---	---	1746.5	1677.5	-	-
EPR^-–CYT-H^+ form II	3388.2	3112.6	1746.5, 1688.9	---	1643.9	1412.0
EPR^-–CYT-H^+ (after desolvation)	3378.8	3106.7	1731.1, 1704.7	---	1666.2	1410.9
EPR^-–CYT-H^+ form II ethanol solvate	3375.5	3112.6	1722.3, 1705.1	---	1669.4	1411.6
EPR^-–CYT-H^+ form II n-propanol solvate	3375.8	3109.6	1722.3, 1701.6	---	1663.1	1411.2
EPR–CYT salt cocrystal hybrid	3376.80	3186.5	1722.3, 1710.4	---	1670.1	1413.0
EPR^-–CYT-H^+– H_2O (1:2:1)	3371.9	3189.5	1720.1, 1710.4	---	1669.8	1413.0
CYT	3378.6	3170.9	1659.2	---	-	-

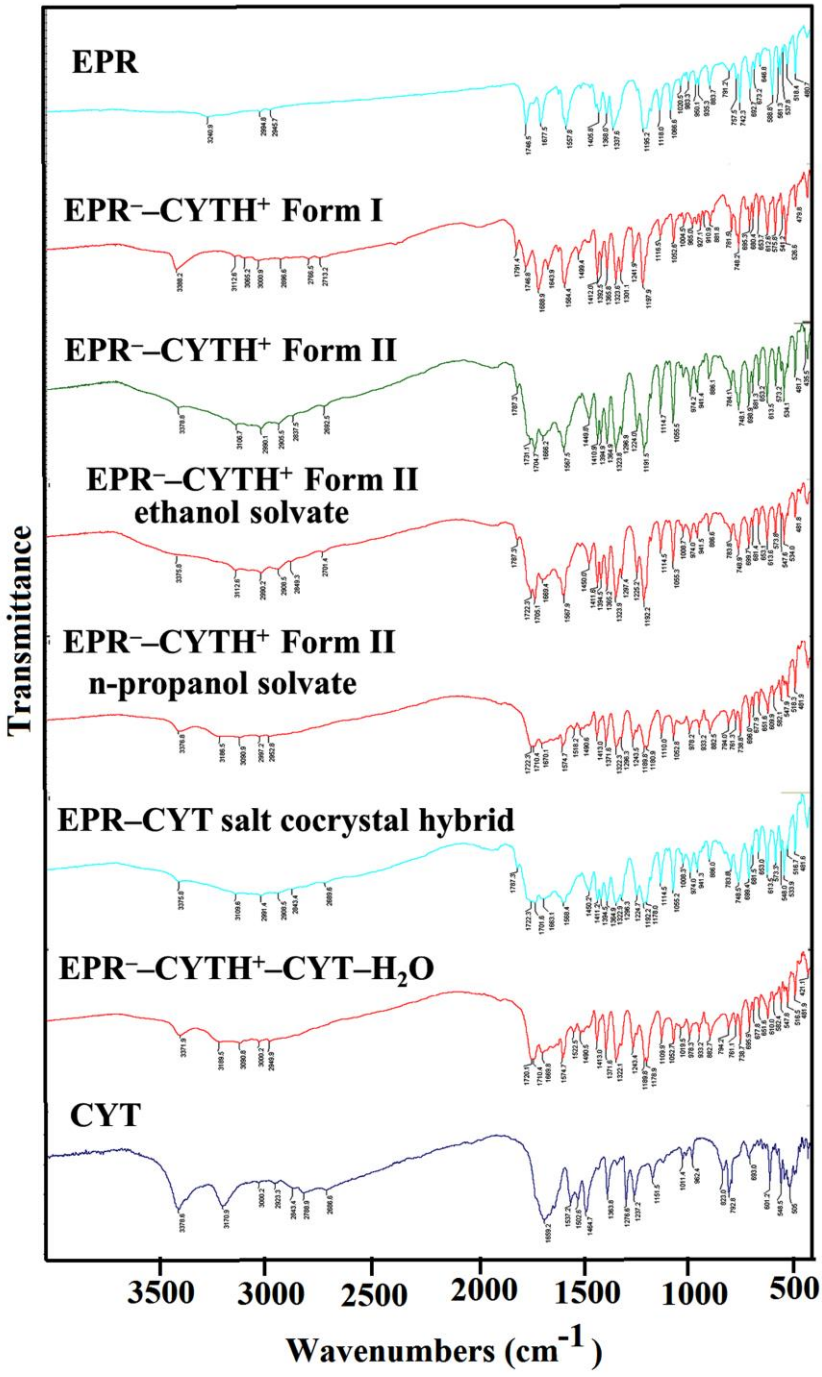

Figure 5.11 FT-IR spectral overlay of EPR–CYT solid forms.

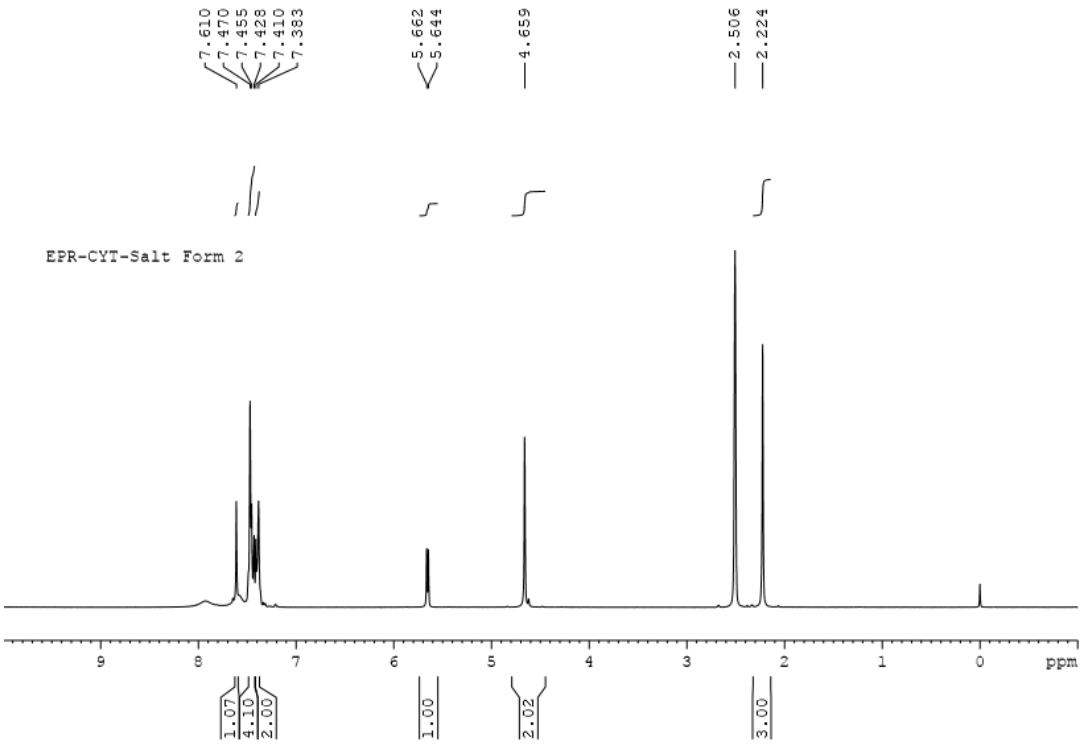
7.610
7.470
7.455
7.428
7.410
7.383
5.662
5.644
4.659
2.506
2.224
EPR-CYT-Salt Form 2
9
8
7
6
5
4
3
2
1
0
ppm
1.07
4.10
2.00
1.00
2.02
3.00

(a)

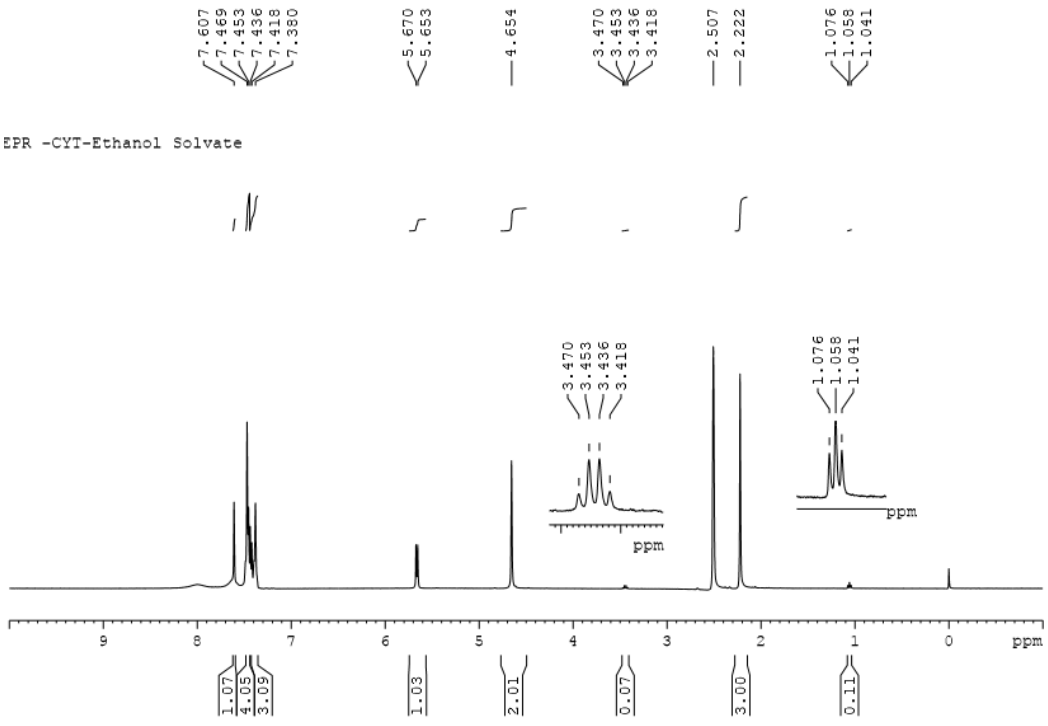
7.607
7.469
7.453
7.436
7.418
7.380
5.670
5.653
4.654
3.470
3.453
3.436
3.418
2.507
2.222
1.076
1.058
1.041
EPR -CYT-Ethanol Solvate
ppm
ppm
9
8
7
6
5
4
3
2
1
0
ppm
1.07
4.05
3.09
1.03
2.01
0.07
3.00
0.11

(b)

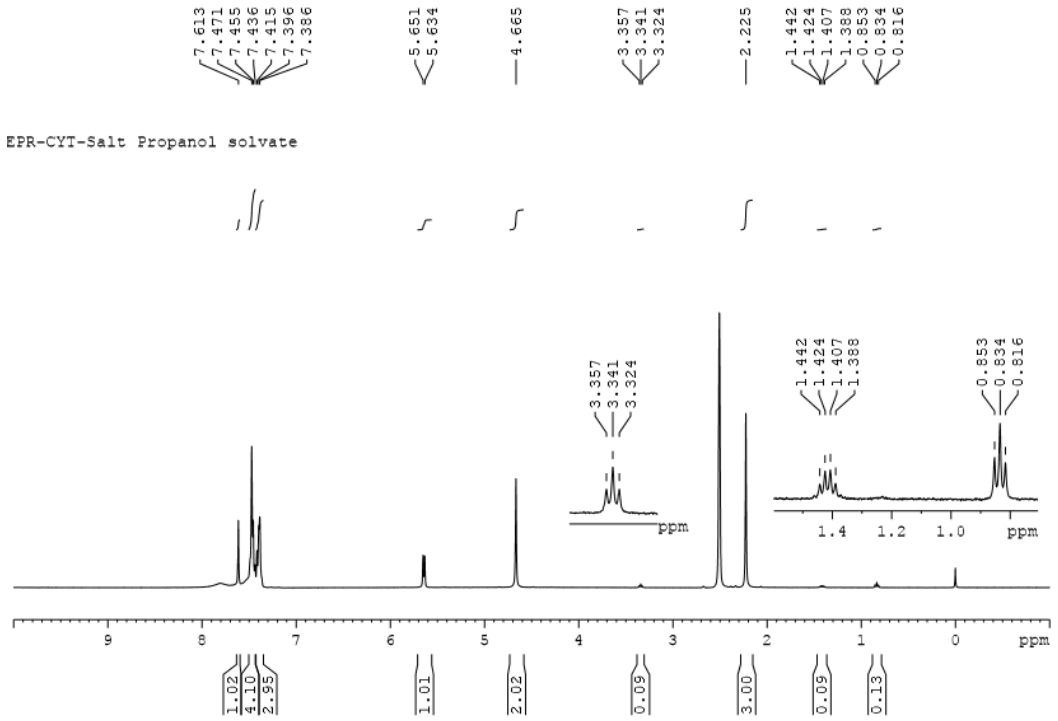

(c)

Figure 5.12 ^{1}H NMR spectra in DMSO-d_6. (a) Desolvated EPR^{-}–$CYT\text{-}H^{+}$. (b) EPR^{-}–$CYT\text{-}H^{+}$ ethanol solvate. (c) EPR^{-}–$CYT\text{-}H^{+}$ n-propanol solvate. The stoichiometry of the solvebnt was determined by NMR integration, 1:1:0.036 for the ethanol solvate and 1:1:0.043 for n-propanol solvate.

5.3.4 Thermal Analysis

Differential scanning calorimetry (DSC)

Differential scanning calorimetry (DSC) of EPR^{-}–$CYT\text{-}H^{+}$ form I and EPR^{-}–$CYT\text{-}H^{+}$ form II exhibited a single melting endotherm without any phase transformation up to T_{onset} of 240.8 and 250.4 °C. EPR–CYT salt hydrate, EPR^{-}–$CYT\text{-}H^{+}$ form II ethanol, and n-propanol solvates showed two endotherm peaks in DSC (Figure 5.13 and Table 5.7). The lower T endotherm is ascribed to water/ solvent loss, and the higher T endotherm is the melting event. The EPR–CYT salt-cocrystal hybrid showed a single melting endotherm at T_{onset} of 250.2 °C. We observed a small endotherm peak in the DSC thermogram of the salt-cocrystal hybrid before a melting event, due to the presence of trace EPR^{-}–$CYT\text{-}H^{+}$ form II (Figure 5.14). Thermal analysis shows that the melting point

of EPR^{-}–CYT-H^{+} form II is ~10 °C higher than that of EPR^{-}–CYT-H^{+} form I, and the rhombohedral polymorph II is designated thermodynamic modification.

Hot stage microscopy and Thermo gravimetric analysis on the solvated and hydrate crystals are consistent with the above discussion (see Figure S7 to S11).

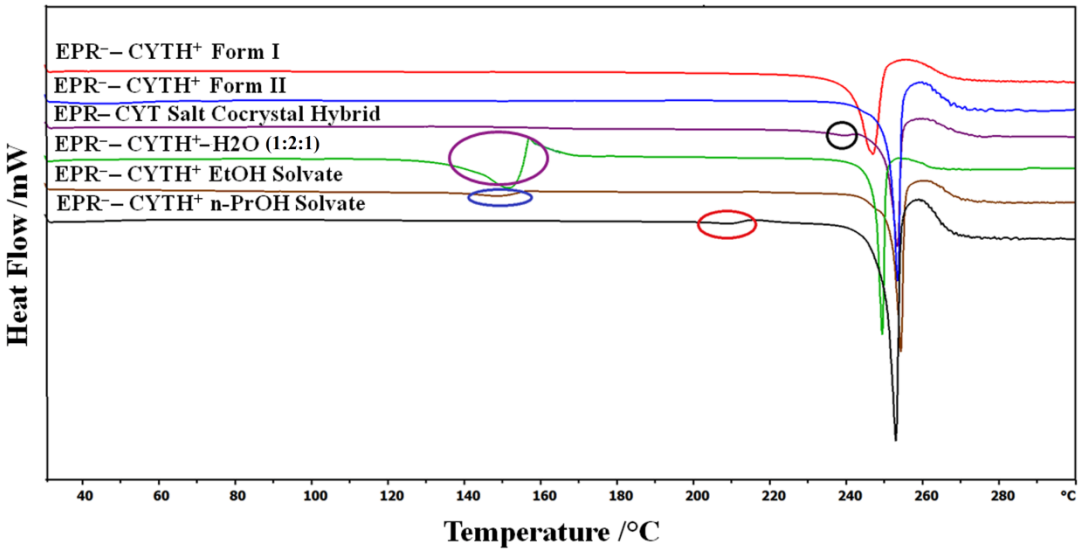

Figure 5.13 DSC thermogram of EPR–CYT solid forms at heating rate of 5 °C min^{-1}. The color circles show loss of water, ethanol, and n-propanol solvent and the black circle indicates the presence of trace EPR^{-}–CYT-H^{+} form II as impurity in the salt-cocrystal hybrid.

Table 5.7 Melting Points of EPR-CYT Solid forms.

Drug/ Coformer	**M.p. of drug/coformer (°C)**	**Solid form**	**M.p. of solid form (°C) T_{onset}/ T_{peak}**
EPR	222.1/224.4	-	-
CYT	320-325	EPR^{-}–CYT-H^{+} form I	240.8/ 246.6
CYT	---	EPR^{-}–CYT-H^{+} form II	250.4/ 252.4
CYT	---	EPR–CYT salt cocrystal hybrid	250.2/ 252.6
CYT	---	EPR^{-}–CYT-H^{+}–H_2O (1:2:1)	247.1/ 248.4
CYT	---	EPR^{-}–CYT-H^{+} form II ethanol solvate	251.3/ 253.3
CYT	---	EPR^{-}–CYT-H^{+} form II n-propanol solvate	249.3/ 251.7

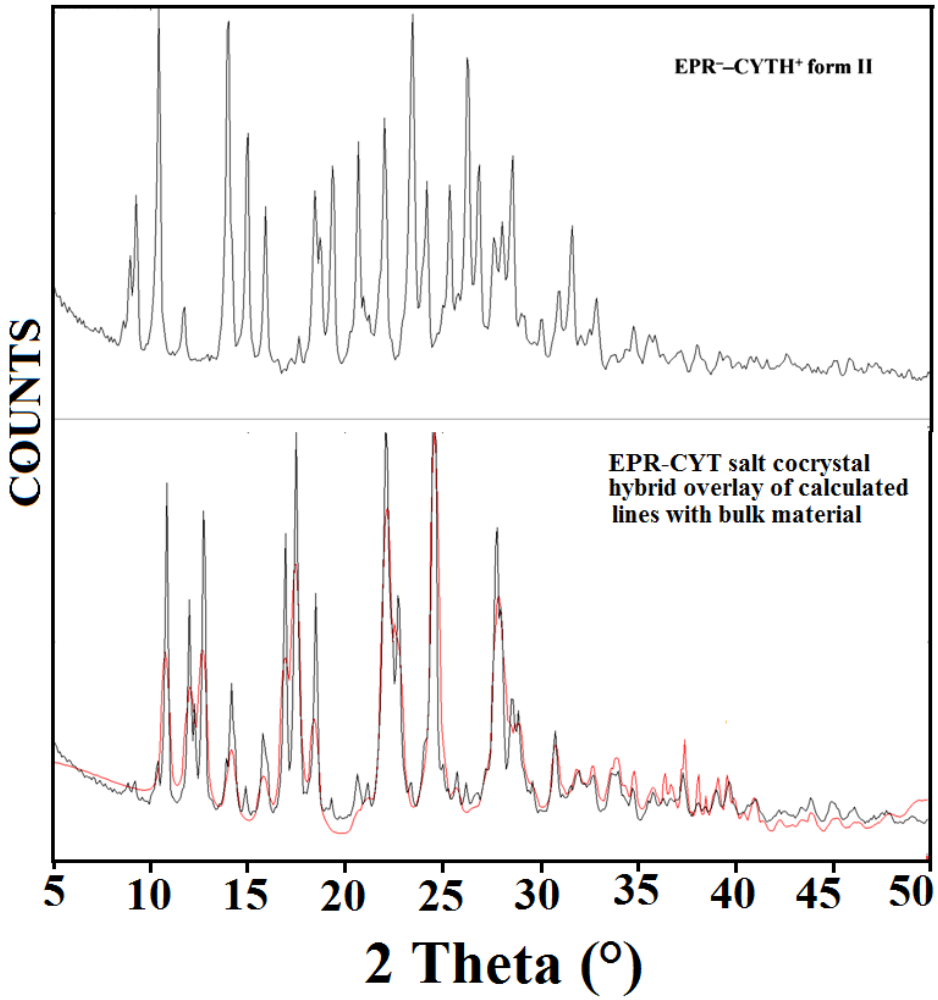

Figure 5.14 PXRD plot showing the presence of EPR^{-}–CYT-H^{+} form II impurity in trace amounts in the EPR-CYT salt cocrystal hybrid bulk sample which was used for the differential scanning calorimetry (DSC) analysis.

Hot Stage Microscopy (HSM)

Hot stage microscopy (HSM) measurements on single crystals of EPR–CYT was carried out to visually observe the thermal events during heating. The solid form was placed on a glass slide and heated from 30 °C to 300 °C on the hot stage microscope. EPR^{-}–CYT-H^{+} form I started melting at 250 °C which was complete at 256 °C (Figure 5.15). No morphological changes were observed. EPR^{-}–CYT-H^{+} ethanol and n-propanol solvate crystals faded and became dark between 165-230 °C and 170-186 °C respectively, and then melting occurred at 254 °C and 256 °C indicating loss of solvent and jumping of crystals on HSM bench at 235 °C and 240 °C. EPR^{-}–CYT-H^{+}–H_2O (1:2:1) crystals turned dark between 165-180 °C (dehydration) prior to melting at 250 °C.

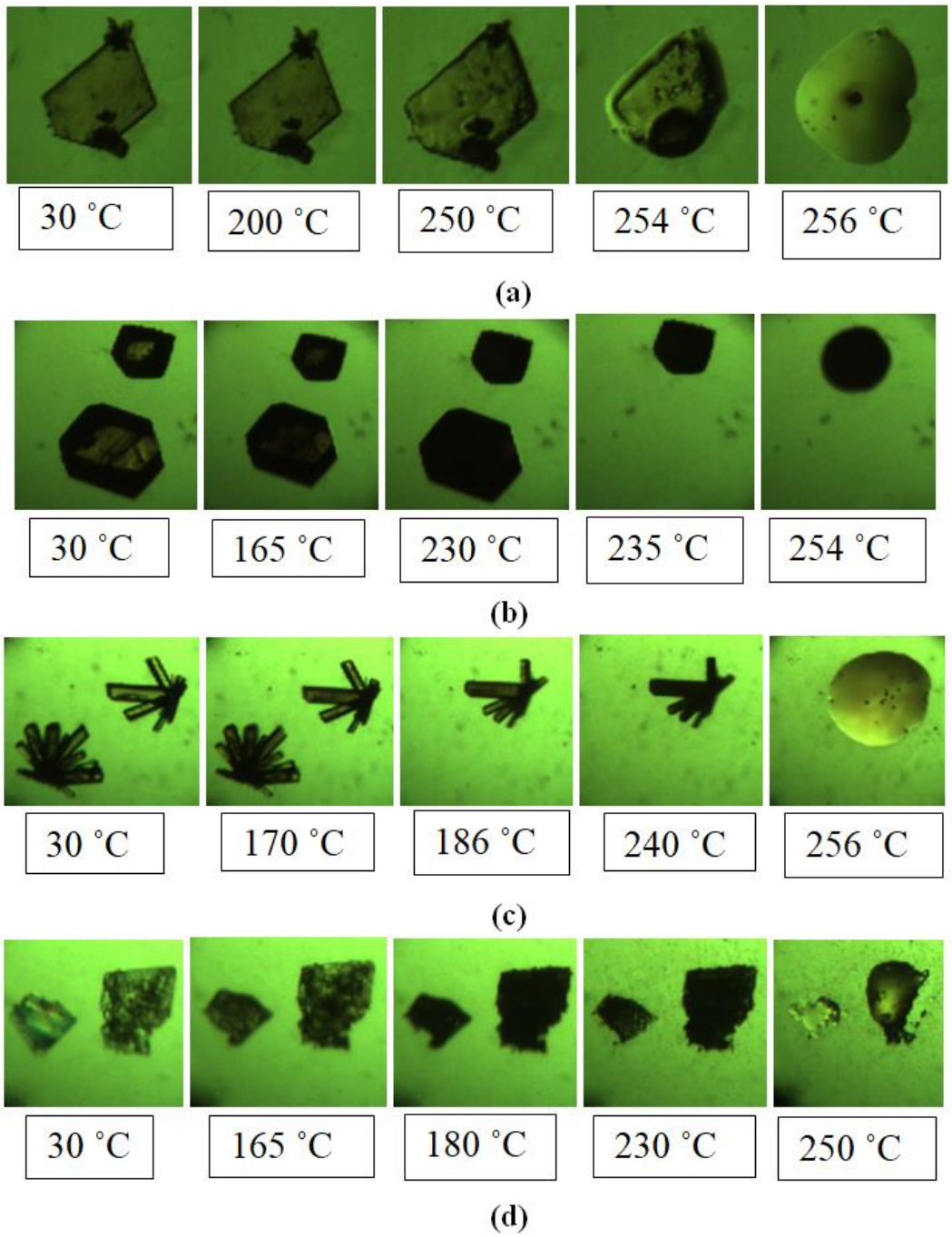

Figure 5.15 HSM snapshots of EPR–CYT solid forms. (a) No changes were observed in crystal morphology of EPR^{-}–CYT-H^{+} form I. (b) EPR^{-}–CYT-H^{+} ethanol solvate faded to dark between 165-230 °C indicating solvent loss. (c) EPR^{-}–CYT-H^{+} n-propanol solvate faded to dark between 170-240 °C indicating solvent loss. (d) EPR^{-}–CYT-H^{+}–H_2O (1:2:1) solvate faded to dark between 165-180 °C indicating water loss.

Thermogravimetric analysis (TGA)

Thermogravimetric analysis (TGA) of EPR–CYT solid forms gave data on weight loss during heating. TGA of pure EPR^{-}–CYT-H^{+} form II did not show any weight change and confirmed the absence of any solvent (Figure 5.16). The weight loss for EPR^{-}–CYT-H^{+} ethanol solvate is 0.05 molecules of ethanol (obsd. 0.52%, Figure 5.17) and that for n-propanol solvate is 0.04 molecules of n-propanol (obsd. 0.54%, Figure 5.18). The weight loss in TGA matched with one water molecule for EPR^{-}–CYT-H^{+}–CYT–H_2O (calc. 3.21%, obs. 3.15%; Figure 5.19).

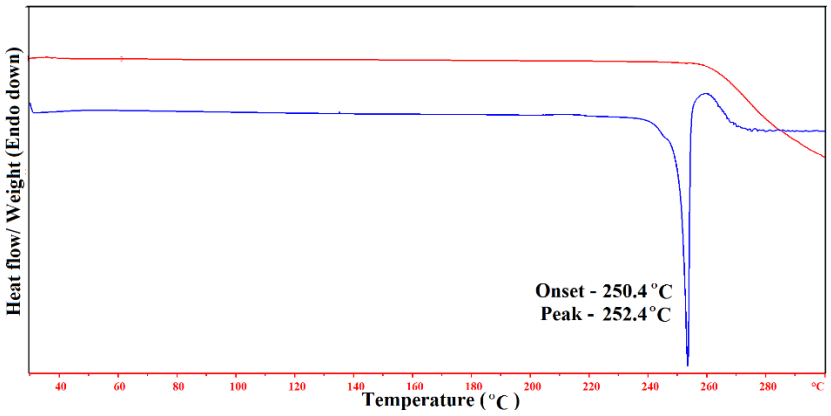

Figure 5.16 DSC (blue) and TGA (red) of EPR^{-}–CYT-H^{+} form II did not exhibit a visible transition before melting at 250 °C.

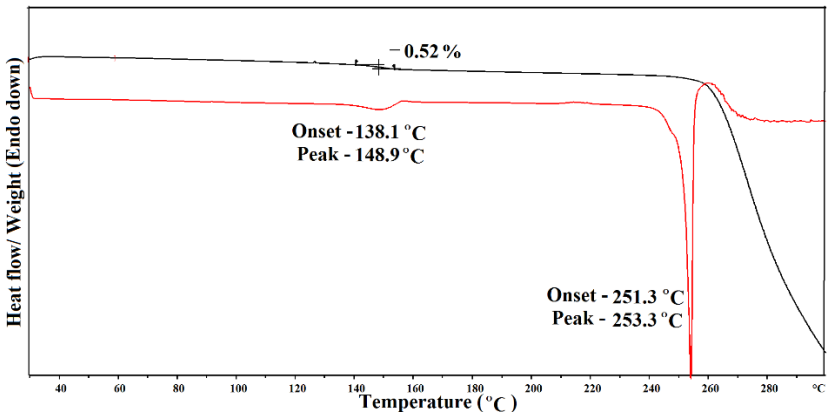

Figure 5.17 DSC (red) and TGA (black) of EPR^{-} –CYT-H^{+} form II ethanol solvate showed solvent loss at 138-148 °C before melting.

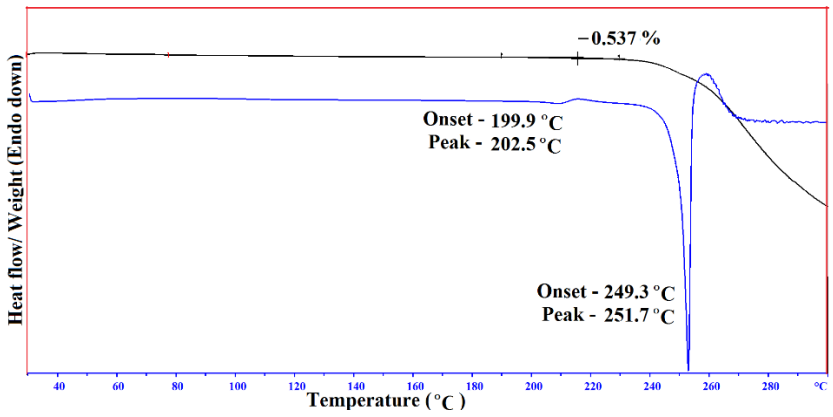

Figure 5.18 DSC (blue) and TGA (black) of EPR^{-}–CYT-H^{+} form II n-propanol solvate showed solvent loss at 200-202 °C before melting.

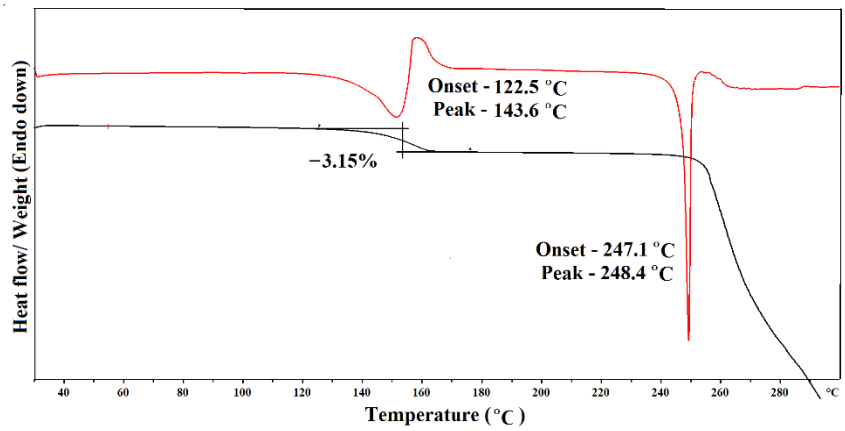

Figure 5.19 DSC (red) and TGA (black) of EPR^{-}–CYT-H^{+}–H_2O (1:2:1) showed water loss at 122-143 °C before melting.

5.3.5 Photostability Study of EPR–CYT Crystal Forms

In general, the stronger hydrogen bonds in cocrystals and salts compared to the native drug structure result in improved physicochemical and stability properties.[6,10] It was our expectation that the stronger synthons in salt-cocrystal structures will constrain the Epalrestat molecule in the crystal lattice and thereby slow down the E,Z to Z,Z isomerization compared to that in the reference drug.[20] The isomerization of E,Z to Z,Z isomer for Epalrestat is known in the literature[20]. Epalrestat polymorphs did not exhibit positive results toward this end.[20] Epalrestat (form I) and each of the novel EPR–CYT forms crystallized in this study were subjected to normal sunlight for 24 h, and then the

^{1}H NMR spectrum was recorded in DMSO-d_6 immediately after sample preparation. However, the transformation of E,Z to Z,Z isomer as visualized from the appearance of new peaks for the latter Z,Z isomer is similar in all cases (Figure 5.20, see the small dots corresponding to the latter isomer).

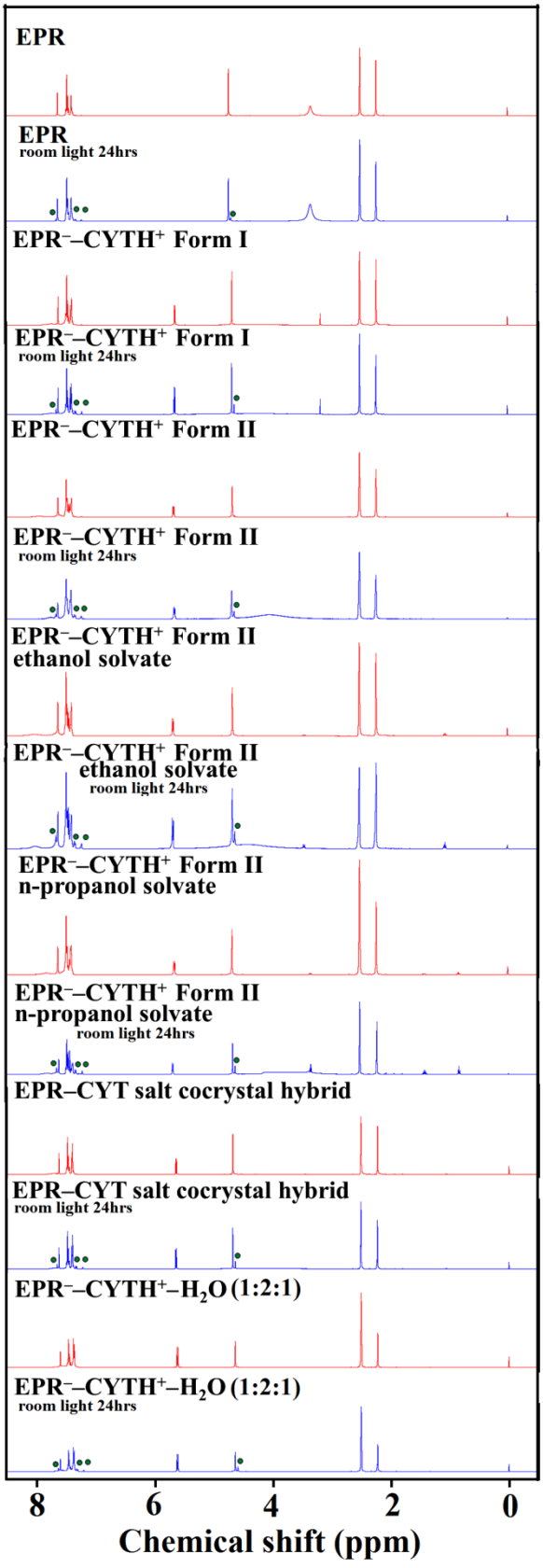
EPR
EPR
room light 24hrs
EPR⁻–CYTH⁺ Form I
EPR⁻–CYTH⁺ Form I
room light 24hrs
EPR⁻–CYTH⁺ Form II
EPR⁻–CYTH⁺ Form II
room light 24hrs
EPR⁻–CYTH⁺ Form II
ethanol solvate
EPR⁻–CYTH⁺ Form II
ethanol solvate
room light 24hrs
EPR⁻–CYTH⁺ Form II
n-propanol solvate
EPR⁻–CYTH⁺ Form II
n-propanol solvate
room light 24hrs
EPR–CYT salt cocrystal hybrid
EPR–CYT salt cocrystal hybrid
room light 24hrs
EPR⁻–CYTH⁺–H2O (1:2:1)
EPR⁻–CYTH⁺–H2O (1:2:1)
room light 24hrs
8
6
4
2
0
Chemical shift (ppm)

Figure 5.20 ^{1}H NMR spectrum of EPR and its cytosine salts before and after exposure to light shows that the E,Z isomer of EPR (drug) transforms to the Z,Z isomer within 24 h to about the same extent. Inter-conversion of the E,Z and Z,Z isomers in solution is seen based on the separation of proton signals at 4.69-4.73 ppm (2H, N-CH_2) and the peak at 7.64-7.66 ppm (1H, most downfield aromatic) and appearance of new proton signals at 7.23 and 7.32-7.34 ppm. The singlet at 3.35 is DMSO proton signal.

5.4 Conclusions

Solid form screening of EPR with CYT resulted in novel salt polymorphs EPR^{-}–CYT-H^{+} form I and form II, salt-cocrystal hybrid and salt hydrate (EPR^{-}–CYT-H^{+}–H_2O, 1:2:1). The ΔpK_a value of EPR and CYT is 1.35. In this report, we have obtained both salts and salt-cocrystal hybrid from different conditions with the same ΔpK_a value. Ethanol and n-propanol solvent molecules are incorporated in the rhombohedral voids of EPR^{-}–CYT-H^{+} form II, and the stoichiometries of EPR^{-}–CYT-H^{+} form II ethanol and EPR^{-}–CYT-H^{+} form II n-propanol solvates were calculated as 1:1:0.036 and 1:1:0.043 by ^{1}H NMR spectroscopy. The rare CYT-$H^{+}\cdots H^{+}$-CYT motif was observed in the crystal structure of the salt-cocrystal hybrid and salt-cocrystal hydrate. Even as novel EPR–CYT crystal structures were analyzed in this study, the objective to control the olefin isomerization is still an ongoing challenge.

5.5 Experimental Section

Materials and Methods

Epalrestat was a gift sample from Symed Laboratories Ltd., Hyderabad, India, and used without further purification. It corresponds to the polymorph I of our previous study.[20] Cytosine (purity >99.8%) was purchased from Sigma-Aldrich, Hyderabad, India. All other chemicals were of analytical or chromatographic grade. Water purified from a deionizer-cum-mixed-bed purification system (AquaDM, Bhanu, Hyderabad, India) was used in the experiments.

Preparation of EPR–CYT Solid Forms

EPR^{-}–CYT-H^{+} form I

EPR^{-}–CYT-H^{+} salt was obtained from the crystallization of EPR–CYT (1:1) ground material from i-propanol solvent. Hexagonal shaped plate crystals suitable for X-ray

diffraction were obtained after 3-4 d. The formation of salt was confirmed by FT-IR, PXRD and single crystal X-ray diffraction.

EPR^{-}–CYT-H^{+} form II ethanol solvate

EPR^{-}–CYT-H^{+} form II ethanol solvate was obtained by co-grinding EPR and CYT (1:1) in a mortar-pestle for 30 min by adding a catalytic amount (two or three drops) of EtOH solvent. The product was confirmed as EPR^{-}–CYT-H^{+} form II ethanol solvate by FT-IR, PXRD and DSC. Yellow color block shaped single crystals suitable for X-ray diffraction were obtained upon crystallizing 30 mg of the ground material from 6 mL of hot EtOH and left for slow evaporation.

^{1}H NMR (DMSO-d_6, 400MHz) δ ppm: 7.60 (1 H, s), 7.47 (4 H, m), 7.42 (3 H, m), 5.65 (1 H, d), 4.65 (2 H, s), 3.45 (0.07 H, q), 2.22 (3 H, s), 1.06 (0.11 H, t). CH_3CH_2OH peaks were observed at 3.45 (q) and 1.06 (t) but in a concentration ratio of 0.036 compared to EPR by proton integration.

EPR^{-}–CYT-H^{+} form II n-propanol solvate

EPR^{-}–CYT-H^{+} form II n-propanol solvate was obtained by co-grinding EPR and CYT (1:1) in a mortar-pestle for 30 min by adding a catalytic amount (two or three drops) of n-propanol. The product was confirmed as EPR^{-}–CYT-H^{+} form II n-propanol solvate by FT-IR, PXRD and DSC. Yellow color rod shaped single crystals suitable for X-ray diffraction were obtained upon crystallizing 30 mg of ground material in 6 mL hot n-PrOH and left for slow evaporation.

^{1}H NMR (DMSO-d_6, 400 MHz) δ ppm: 7.61 (1 H, s), 7.47 (4 H, m), 7.39 (3 H, m), 5.65 (1 H, d), 4.67 (2 H, s), 3.34 (0.09 H, t), 2.23 (3 H, s), 1.42 (0.09 H, q), 0.83 (0.13 H, t). $CH_3CH_2CH_2OH$ peaks were observed at 3.34 (t), 1.42 (q) and 0.83 (t) but in a concentration ratio of 0.043 compared to EPR by proton integration.

EPR^{-}–CYT-H^{+} form II

EPR^{-}–CYT-H^{+} desolvated form II was obtained by heating of EPR^{-}–CYT-H^{+} form II ethanol or n-propanol solvate at 230 °C and 240 °C for 30 min in a programmable oven. Dehydration of EPR–CYT salt hydrate at 160 °C for 30 min in a programmable oven also resulted in EPR^{-}–CYT-H^{+} form II but with slight contaminations. The formation of

EPR^{-}–CYT-H^{+} form II was confirmed by FT-IR, PXRD, DSC, TGA and solution ^{1}H NMR spectroscopy.

^{1}H NMR (DMSO-d_6, 400 MHz) δ ppm: 7.61 (1 H, s), 7.47 (4 H, m), 7.41 (2 H, m), 5.64 (1 H, d, J 8 Hz), 4.66 (2 H, s), 2.22 (3 H, s).

EPR–CYT salt-cocrystal hybrid

EPR–CYT salt-cocrystal hybrid was obtained upon co-grinding EPR and CYT in a 1:1 stoichiometric ratio for 5 min by liquid-assisted grinding (dry EtOH solvent). The formation of a salt-cocrystal hybrid was confirmed by FT-IR, PXRD and DSC. The ground material (about 30 mg) was dissolved in 8 mL of hot methanol−xylene solvent mixture (1:1) and left for slow evaporation at ambient conditions. Plate morphology crystals suitable for X-ray diffraction were obtained after 3-4 d upon solvent evaporation.

EPR^{-}–CYT-H^{+}–H_2O (1:2:1 salt hydrate)

The salt hydrate was obtained upon grinding 150 mg of a 1:2 stoichiometric ratio of EPR and CYT for 30 min by liquid-assisted grinding (water). The formation of salt hydrate was confirmed by FT-IR, FT-Raman, ss-NMR, PXRD and DSC. An amount of 30 mg of the ground material was dissolved in 6 mL of hot CH_3OH and left for slow evaporation at ambient conditions. Plate morphology crystals suitable for X-ray diffraction were obtained after 3-4 d upon solvent evaporation.

Vibrational Spectroscopy

Thermo-Nicolet 6700 Fourier transform infrared spectrophotometer with NXR-Fourier transform Raman module (Thermo Scientific, Waltham, Massachusetts) was used to record IR spectra. IR spectra were recorded on samples dispersed in KBr pellets. Data were analyzed using the Omnic software (Thermo Scientific, Waltham, Massachusetts).

Solution NMR Spectroscopy

Solution ^{1}H NMR spectra of EPR-CYT solid forms were recorded on a Bruker Ultrashield 400 spectrometer (Bruker BioSpin, Karlsruhe, Germany).

Differential Scanning Calorimetry (DSC)

DSC was performed on a Mettler Toledo DSC 822e module. Samples were placed in crimped but vented aluminum sample pans. The typical sample size is 3-4 mg, and the temperature range is 30-250 °C @ 5 °C/min. Samples were purged by a stream of dry nitrogen flowing at 80 mL/min.

Hot Stage Microscopy (HSM)

HSM was performed on a Wagner & Munz, PolythermA Hot Stage and Heiztisch microscope. A Moticam 1000 (1.3 MP) camera supported by software Motic Image Plus 2.0 ML was used to record images.

X-ray Crystallography

X-ray reflections for EPR^{-}–CYT-H^{+} form I, EPR^{-}–CYT-H^{+} form II ethanol solvate, EPR^{-}–CYT-H^{+} n-propanol solvate and EPR–CYT salt hydrate were collected at 298 K on Bruker SMART-APEX CCD diffractometer equipped with a graphite monochromator and Mo-Kα fine-focus sealed tube (λ = 0.71073 Å). Data reduction was performed using Bruker SAINT Software.[38] Intensities were corrected for absorption using SADABS,[39] and the structure was solved and refined using SHELX-97. [40,41] EPR^{-}–CYT-H^{+} form II ethanol and n-propanol solvates were treated with the squeeze program to remove the solvent peaks using the CrysAlisPro (version 1.171.33.55) [42] and OLEX2-1.0 [43] softwares. X-ray reflections for EPR–CYT salt-cocrystal hybrid were collected at 100 K on Bruker D8 QUEST. The structure was solved and refined using APEX 2 software. All non-hydrogen atoms were refined anisotropically. Hydrogen atoms on heteroatoms were located from difference electron density maps and all C−H hydrogens were fixed geometrically. Hydrogen bond geometries were determined in Platon.[44] X-Seed[45] was used to prepare packing diagrams.

Powder X-ray Diffraction

Powder X-ray diffraction of all the samples were recorded on Bruker D8 Advance diffractometer (Bruker-AXS, Karlsruhe, Germany) using Cu-Kα X-radiation (λ= 1.5406 Å) at 40 kV and 30 mA power. X-ray diffraction patterns were collected over the 2θ range 5-50° at a scan rate of 1º min^{-1}. Powder Cell 2.4[46] (Federal Institute of Materials Research and Testing, Berlin, Germany) was used for Rietveld refinement of experimental PXRD and calculated lines from the X-ray crystal structure.

5.6 References

1. Bernstein, J. *Polymorphism in Molecular Crystals*; Clarendon, Oxford, U. K., **2002**.
2. Haleblian, J.; McCrone, W. *J. Pharm. Sci.* **1969**, *58*, 911–929.
3. Serajuddin, A. T. M. Adv. *Drug Delivery Rev.* **2007**, *59*, 603–616.
4. Bhatt, P. M.; Ravindra, N. V.; Banerjee, R.; Desiraju, G. R. *Chem. Commun.* **2005**, 1073–1075.
5. Steed, J.W. *Trends Pharmacol. Sci.* **2013**, *34*, 85-193.
6. Duggirala, N.K.; Perry, M.L.; Almarsson, Ö.; Zaworotko, M.J. *Chem. Commun.* **2016**, *52*, 640-655.
7. Suresh, K.; Goud, N. R.; Nangia, A. *Chemistry–An Asian J*. **2013**, *8*, 3032-3041.
8. Schultheiss, N.; Newman, A. *Cryst. Growth Des.* **2009**, *9*, 2950-2967.
9. Babu, N.J.; Nangia, A. *Cryst. Growth Des.* **2011**, *11*, 2662-2679.
10. Bolla, G.; Nangia, A. *Chem. Comm.* **2106**, *52*, 8342-8360.
11. Maddileti, D.; Swapna, B.; Nangia, A. *Cryst. Growth Des.* **2014**, *14*, 2557-2570.
12. G. R. Desiraju, J. J. Vittal and A. Ramanan, *Crystal Engineering. A Textbook*, World Scientific Publishing, Singapore, 2011.
13. Suresh, K.; Nangia, A. *Cryst. Growth Des.* **2014**, *14*, 2945-2953.
14. Childs, S.L.; Stahly, G. P.; Park, A. *Mol. Pharmaceutics* **2007**, *4*, 323-338.
15. Das, B.; Baruah, J.B. *J. Mol. Struct*. **2011**, *1001*, 134-138.
16. Thipparaboina, R.; Kumar, D.; Mittapalli, S.; Balasubramanian, S.; Nangia, A.; Shastri, N. R. *Cryst. Growth Des.* **2015**, *15*, 5816-5826.
17. (a) Berge, S. M.; Bighley, L. D.; Monkhouse, D. C. *J. Pharm. Sci.* **1977**, *66*, 1-19. (b) Sarma, B.; Thakuria, R.; Nath N. K.; Nangia, A. *CrystEngComm* **2011**, *13*, 3232-3240. (c) Ong, W.; Cheung, E. Y.; Schultz, K. A.; Smith, C.; Bourassa, J.; Hickey, M. B. *CrystEngComm* **2012**, *14*, 2428-2434.
18. Perumalla, S. R.; Shi, L.; Sun, C. C. *CrystEngComm* **2012**, *14*, 2389-2390.
19. Thakuria, R.; Nangia, A. *CrystEngComm* **2011,** *13*, 1759-1764.
20. (a) Banerjee, R.; Bhatt, P. M.; Ravindra, N. V.; Desiraju, G. R. *Cryst. Growth Des.* **2005**, *5*, 2299-2309. (b) Bhatt, P. M.; Ravindra, N. V.; Banerjee, R.; Desiraju, G. R. *Chem. Commun*. **2005,** *8*, 1073-1075.
21. Portell, A.; Barbas, R.; Font-Bardia, M.; Dalmases, P.; Prohens, R.; Puigjaner, C. *CrystEngComm* **2009,** *11*, 791-795.

22. Hotta, N.; Akanuma, Y.; Kawamori, R.; Matsuoka, K.; Oka, Y.; Shichiri, M.; Toyota, T.; Nakashima, M.; Yoshimura, I.; Sakamoto, N.; Shigeta, Y. *Diabetes Care* **2006**, *29*, 1538-1544.
23. Hotta, N.; Sakamoto, N.; Shigeta, Y.; Kikkawa, R.; Goto, Y. *J. Diabetes Complications* **1996**, *10*, 168-172.
24. Zhu, C. *Diabetes Mellitus - Insights and Perspectives*, *InTech* **2013**, 17–46.
25. Ishida, T.; In, Y.; Inoue, M.; Ueno, Y.; Tanaka, C.; Hamanaka, N. *Tetrahedron Lett*. **1989**, *30*, 959-962.
26. (a) Igarashi, R.; Nagase, H.; Furuishi, T.; Tomono, K. *X-ray Structure Analysis Online* **2013**, *29*, 23-24. (b) Igarashi, R.; Nagase, H.; Furuishi, T.; Tomono, K. *X-ray Structure Analysis Online* **2015**, *31*, 1-2. (c) Ishida, T.; In, Y.; Inoue, M.; Tanaka, C.; Hamanaka, N. *J. Chem. Soc., Perkin Trans. 2*, **1990**, *7*, 1085-1091.
27. (a) Umeda, D.; Putra, O. D.; Gunji, M.; Fukuzawa, K.; Yonemochi, E. Acta Crystallogr. 2017, 73, 941−944. (b) Putra, O. D.; Umeda, D.; Fukuzawa, K.; Gunji, M.; Yonemochi, E. Acta Crystallogr. 2017, 73, 1264−1267.
28. Putra, O. D.; Umeda, D.; Nugraha, Y. P.; Furuishi, T.; Nagase, H.; Fukuzawa, K.; Uekusa, H.; Yonemochi, E. CrystEngComm 2017, 19, 2614−2622.
29. Swapna, B.; Suresh, K.; Nangia, A. *Chem. Commun.* 2016, *52*, 4037-4040.
30. Watson, J. D.; Crick, F. H. C. *Nature* **1953**, *171*, 964-967.
31. Perumalla, S.R.; Suresh, E.; Pedireddi, V.R. *Angew. Chem. Int. Ed*. **2005**, *44*, 7752-7757.
32. Sridhar, B.; Nanubolu, J.B; Ravikumar, K. *CrystEngComm* **2012**, *14*, 7065-7074.
33. Cherukuvada, S.; Bolla, G.; Sikligar, K.; Nangia, A. *Cryst. Growth Des.* **2013**, *13*, 1551-1557.
34. Marvin, 5.10.1, 2012, ChemAxon, http://www.chemaxon.com (accessed 25 January 2017).
35. Aitipamula, S.; Banerjee, R.; Bansal, A.K.; Biradha, K.; Cheney, M.L.; Choudhury, A.R.; Desiraju, G.R.; Dikundwar, A.G.; Dubey, R.; Duggirala, N.; Ghogale, P.P. *Cryst. Growth Des.* **2012**, *12*, 2147-2152.
36. Cabeza, A.J.C.; Day, G.M.; Motherwell, W.S.; Jones, W. *Chem. Commun.* **2007**, 16, 1600-1602.

37. Nauha, E.; Saxell, H.; Nissinen, M.; Kolehmainen, E.; Schäfer, A.; Schlecker, R. *CrystEngComm* **2009**, *11*, 2536-2547.
38. Pan, F.; Kalf, I.; Englert, U. *Acta Cryst., Sect. C: Struct. Chem.* **2015**, *71*, 653-657.
39. Yoshida, Y.; Maesato, M.; Ishikawa, M.; Nakano, Y.; Hiramatsu, T.; Yamochi, H.; Saito, G. *Chem. – Eur. J.* **2013,** *19*, 12325-12335.
40. Murata, T.; Saito, G.; Nishimura, K.; Enomoto, Y.; Honda, G.; Shimizu, Y.; Matsui, S.; Sakata, M.; Drozdova, O.O.; Yakushi, K. *Bull. Chem. Soc. of Jpn.* **2008**, *81*, 331-344.
41. Cambridge Structural Database, ver. 5.37. ConQuest 1.18, December 2015 release, November 2016 update, CCDC, www.ccdc.cam.ac.uk.
42. Silverstein, R. M. *Spectrometric Identification of Organic Compounds*, 6th Ed.; John Wiley & Sons, Inc.: New York, **2002**.
43. *SAINT-Plus*, version 6.45; Bruker AXS Inc.: Madison, Wisconsin, U.S.A., **2003**.
44. SADABS, *Program for Empirical Absorption Correction of Area Detector Data*; Sheldrick, G. M. University of Göttingen: Göttingen, Germany, **1997**.
45. *SMART*, version 5.625 and *SHELX-TL*, version 6.12, Bruker AXS Inc.: Madison, Wisconsin, USA, **2000**.
46. Sheldrick, G. M. *SHELXS-97* and *SHELXL-97*, University of Göttingen: Göttingen, Germany, **1997**.
47. *CrysAlis CCD and CrysAlis RED*, Ver. 1.171.33.55, Oxford Diffraction Ltd: Yarnton, Oxfordshire, UK, **2008**.
48. Dolomanov, O. V.; Blake, A. J.; Champness, N. R.; Schröder, *M. J. Appl. Crystallogr*. **2003**, *36*, 1283-1284.
49. Spek, A. L. *PLATON, A Multipurpose Crystallographic Tool*; Utrecht University: Utrecht, Netherlands, **2002**.
50. Barbour, L. J. *X-Seed, Graphical Interface to SHELX-97 and POV-Ray, Program for Better Quality of Crystallographic Figures*; University of Missouri-Columbia, Missouri, U.S.A., **1999**.
51. Powder Cell, *A Program for Structure Visualization, Powder Pattern Calculation and Profile Fitting*, http://www.ccp14.ac.uk/index.html.

CHAPTER SIX

Improved Photostability of Aldose Reductase Inhibitor Epalrestat Through Cocrystallization

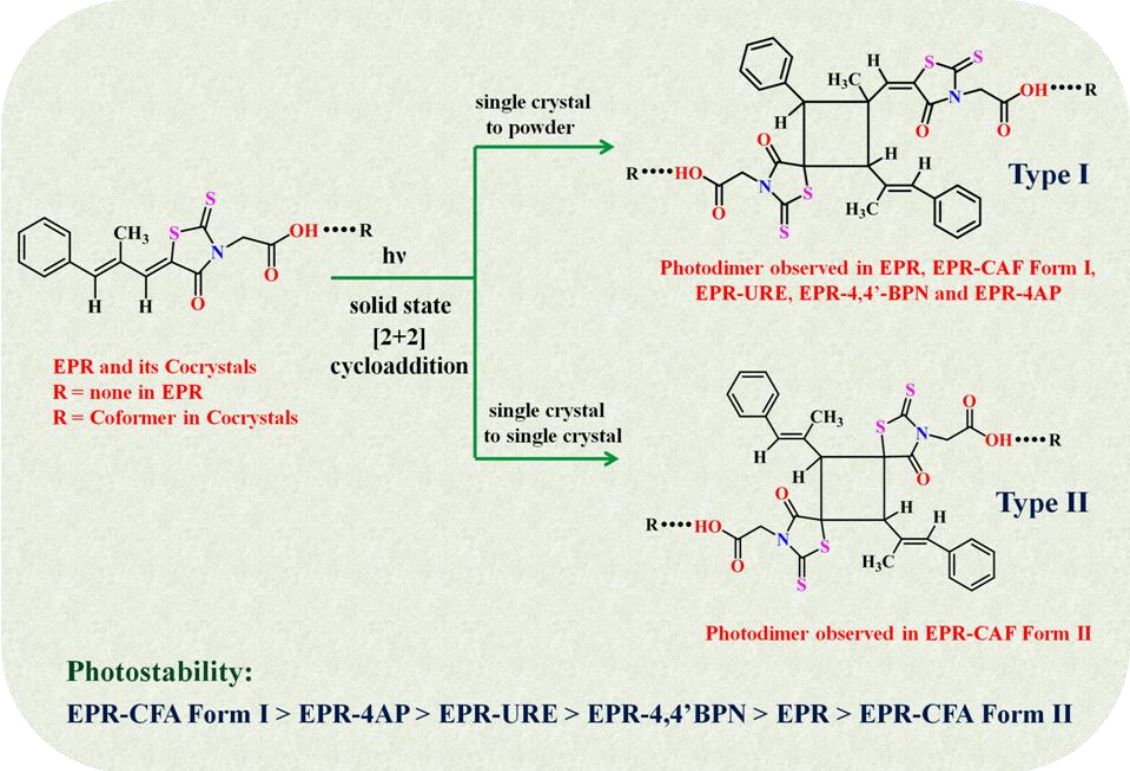

Novel cocrystal forms of Epalrestat (EPR) with conformers such as, caffeine (CAF), acetamide (ACT), urea (URE), 4,4'-bipyridine (4,4'-BPN) and 4-amino pyridine (4AP) were prepared by liquid assisted grinding. The cocrystals exhibit good stability towards photodimerization and percentage of EPR remaining after photodimerization in EPR and its cocrystal forms is 30% (EPR), 86.7% (EPR-CAF Form I), 0% (EPR-CAF Form II), 50% (EPR-URE), 55% (EPR-4AP) and 34% (EPR-4,4'-BPN).

6.1 Introduction

A cocrystal is a multi-component crystalline arrangement of two or more compounds in a stoichiometric ratio coexisting through noncovalent interactions in solid state under ambient conditions. [1,2] Crystal engineering approach has proven to be a successful design strategy for obtaining new cocrystal forms of active pharmaceutical ingredients (APIs) with desired physicochemical properties without affecting the drug's pharmacological behavior.[3-7] Cocrystals have recently been used to successfully modify API stability, [8] solubility,[9] dissolution rate,[10] bioavailability,[11] permeability,[12] and mechanical properties,[13] etc. As a result, cocrystals have recently gained increasing importance as a new class of solid forms in pharmaceutical materials. Chemical and physical instability is one of the major obstacles on the journey from the API to a marketable drug product.[14] The cocrystallization approach offers a unique opportunity to show the power and the ability of crystal engineering to solve real-world problems.[15] For example, Tan et al. showed that the 1:1 cocrystal of nitrofurantoin with 4-hydroxybenzoic acid had better physicochemical and photostability than the API itself.[16] Teraoka et al. improved the solid state photostability of antihypertensive drug, furosemide by forming cocrystals with caffeine, urea and nicotinamide.[17] X. Mei and coworkers[18] have been reported the remarkable improvement in the dissolution and photostability of vitamin K3 (menadione, MD) by making cocrystals with naphthoic acids and sulfamerazine coformers. They showed that, when MD and cocrystals in powder form exposed to UV irradiation for up to 5 days the color change from yellow to amber was found with pure MD due to chemical degradation. Furthermore, the residual content was found to be 15.6% for MD after 5 days of UV treatment. Under the same illumination condition, no apparent degradation or decoloring was observed for the three cocrystals (Figure 6.1). With these literature reports, in this chapter we highlight, cocrystallization approach is a viable approach for improving the photostability of an aldose reductase inhibitor, epalrestat.

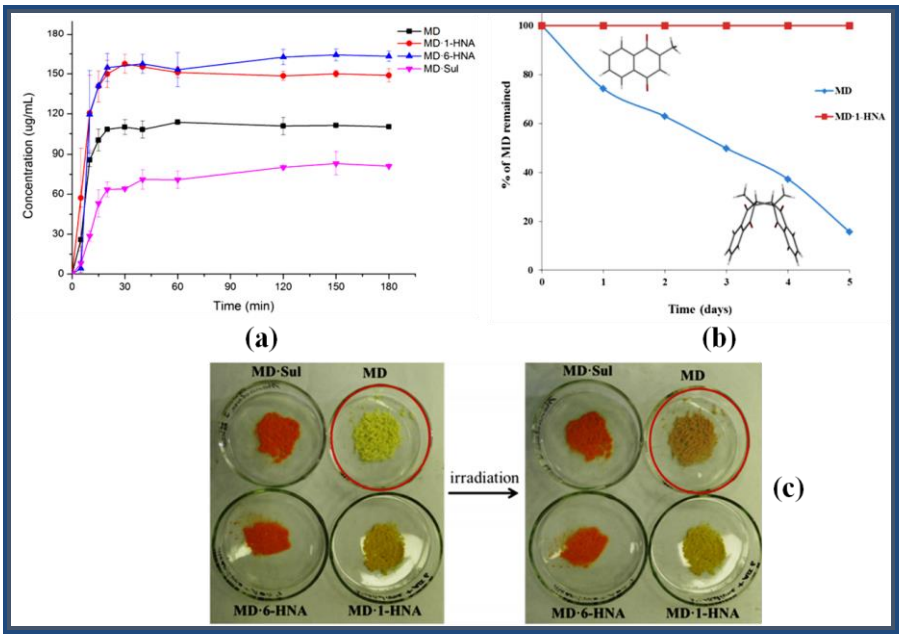

Figure 6.1 (a) Powder dissolution profiles of menadione (MD) and its cocrystals in pH 6.8 phosphate buffer. (b) Comparison of MD assay values for pure MD powder and MD·1-HNA after UV irradiation for 5 days. (c) Change in the physical appearance of MD and its cocrystals after UV irradiation for 5 days.

6.2 Literature Reports on Epalrestat

Epalrestat (EPR; Scheme 6.1) is an aldose reductase inhibitor used to treat diabetic neuropathy, retinopathy, and nephropathy which are the most severe long-term complications observed in patients with diabetes mellitus.[19] Currently, EPR is the only aldose reductase inhibitor that is given marketing approval as a therapeutic drug for diabetic complications.[20] By inhibiting the aldose reductase enzyme, it reduces intercellular sorbitol deposition that is thought to be causing diabetic complications.[19] EPR is stable in the dark but quickly isomerizes in solution upon photoirradiation, even under ambient light irradiation, resulting four isomers, the structures of which were determined using NMR and UV spectroscopic techniques.[21] Several solvates of EPR such as methanol,[22,23] ethanol,[24] dimethyl formamide,[25] dimethyl sulfoxide,[25] tetrahydrofuran[26] and acetone[27] have been reported. Guest free structure of EPR was reported by Igarashi et al.[28] Color polymorphs, crystal structure of Z,Z isomer and salts/salt polymorphs of EPR were reported by our group.[29,30] Uekusa et al. reported the zwitterionic cocrystal of EPR with betaine coformer with

improved solubility.[31] E. Yonemochi and his coworkers have reported EPR-caffeine cocrystal with enhanced solubility.[25]

6.3 Preparation of Epalrestat Cocrystals

In chapter 4 and 5 we discussed E,Z to Z,Z photoisomerization, color polymorphs and salts/salt polymorphs of EPR. However, control of E,Z to Z,Z photoisomerization of EPR is still a challenge. During the photostability studies, we found that EPR undergoes photodimerization in the solid state, but this transformation is not reported in the literature so far. Therefore, in this chapter we have focused our attention in preparing cocrystal forms of EPR and discover their polymorphs to control/stop the photoisomerization and photodimerization of EPR. Various solid form screening methods like solvent assisted grinding, slurry grinding and fast evaporation under controlled vacuum (rotary evaporator) conditions were used to prepare cocrystals.[32,33] On subjecting EPR and different coformers to the above methods in various stoichiometric ratio, we obtained novel cocrystals with caffeine (CAF, 1:1), acetamide (ACT, 1:1), urea (URE, 1:1), 4,4′-bipyridine (4,4′-BPN, 1:0.5) and 4-aminopyridine (4AP, 1:1) (Scheme 6.1). We used solution crystallization method from various solvents and solvent mixtures to isolate polymorphs of these cocrystals. After several crystallization experiments, we obtained two polymorphs of the 1:1 EPR-Caffeine (CAF) cocrystal. These cocrystals and cocrystal polymorphs were characterized by thermal, spectroscopic and diffraction methods.

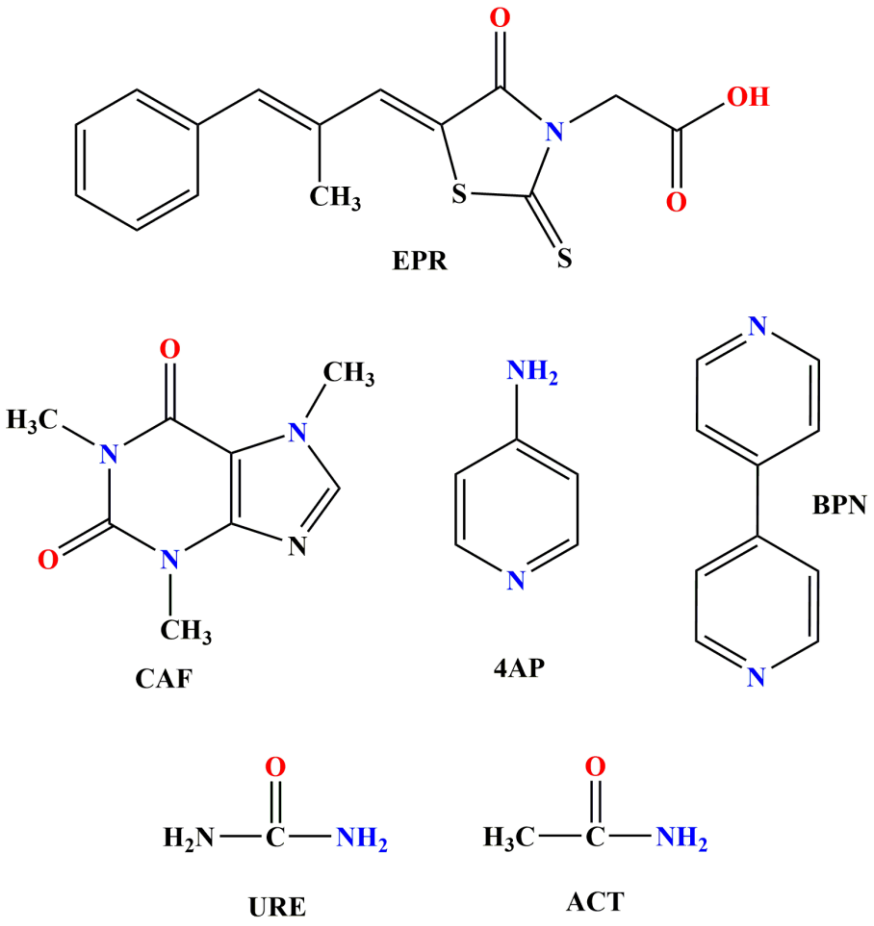

Scheme 6.1 Epalrestat and coformers discussed in this study.

6.4 Results and Discussion

Five new cocrystals of EPR with various coformers i.e; CAF, ACT, URE, 4,4'-BPN and 4AP were synthesized and characterized by spectroscopic (FT-IR, ^{1}H NMR), differential scanning calorimetry (DSC), X-ray diffraction (powder X-ray diffraction (PXRD), single crystal XRD) techniques. A comparison of the experimental PXRD patterns with those calculated from corresponding single crystal data and DSC established the phase purity of the solids. The same batches of samples were used for IR spectroscopy and photostability studies. Supramolecular synthons observed in EPR cocrystals are shown in scheme 6.2. Crystallographic parameters are listed in Table 6.1 and hydrogen bond distances in Table 6.2.

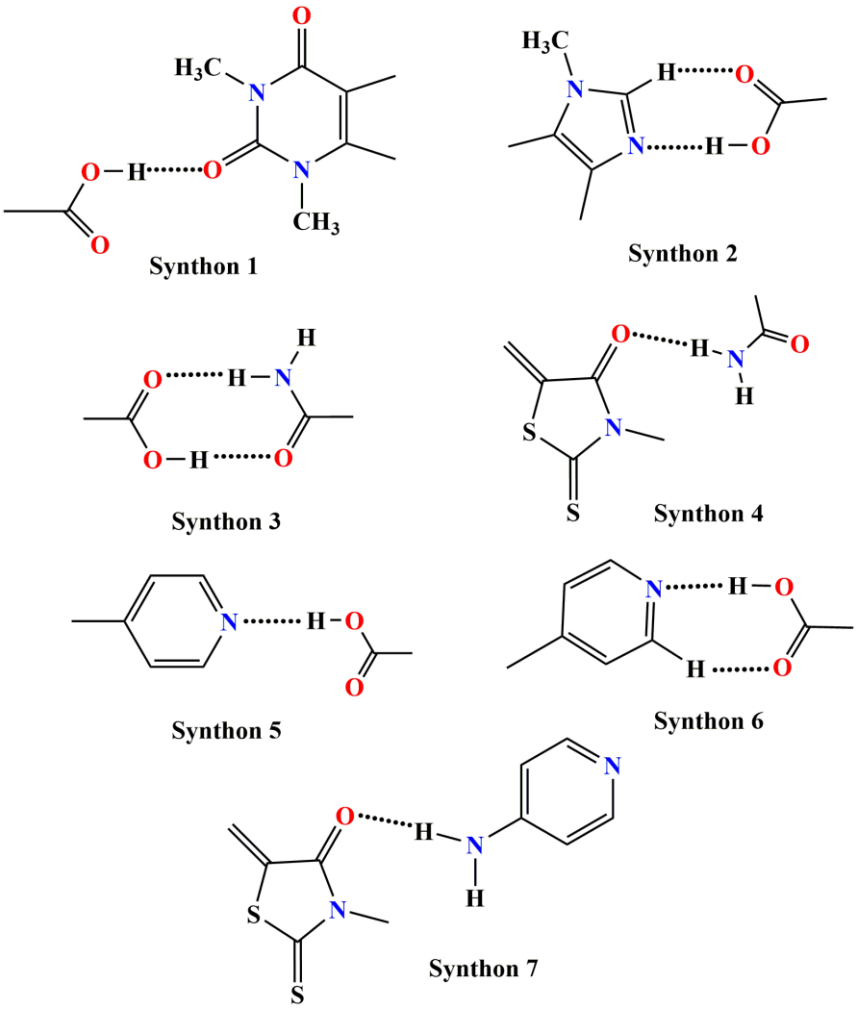

Scheme 6.2 Schematic representations of supramolecular synthons in EPR cocrystals observed in this study.

Table 6.1 Crystallographic parameters of EPR cocrystals

Crystal structure	EPR–CAF Form I This study	EPR–CAF Form I Reported[a]	EPR–CAF Form II	EPR–CAF Form II Dimer	EPR–ACT	EPR–URE	EPR–4,4'-BPN(1:0.5)	EPR–4AP
Chemical formula	$C_{15}H_{13}NO_3S_2.C_8H_{10}N_4O_2$	$C_{15}H_{13}NO_3S_2.C_8H_{10}N_4O_2$	$C_{15}H_{13}NO_3S_2.C_8H_{10}N_4O_2$	$C_{30}H_{26}N_2O_6S_4.2(C_8H_{10}N_4O_2)$	$C_{15}H_{13}NO_3S_2.C_2H_5NO$	$C_{15}H_{13}NO_3S_2.CH_4N_2O$	$C_{15}H_{13}NO_3S_2.C_5H_4N$	$C_{15}H_{13}NO_3S_2.C_5H_6N_2$
Crystal system	Triclinic	Triclinic	Triclinic	Triclinic	Triclinic	Triclinic	Triclinic	Monoclinic
Formula weight	513.58	513.58	513.58	1027.17	378.45	379.45	397.48	413.50
Space group	*P-1*	*P-1*	*P-1*	*P-1*	*P-1*	*P-1*	*P-1*	*P* $2_1/c$
T [K]	298	173	298	298	298	298	298	298
a [Å]	7.9450(5)	7.7900(4)	7.927(10)	7.9896(3)	7.7468(4)	7.4109(15)	8.599(3)	8.0562(6)
b [Å]	8.4238(5)	8.4073(4)	8.889(11)	8.9031(3)	7.8094(5)	7.7869(11)	8.604(3)	34.431(2)
c [Å]	19.8289(11)	19.8594(10)	18.45(2)	18.0670(6)	16.319(1)	16.280(2)	14.188(5)	7.2976(5)
α [°]	83.478(5)	84.159(3)	84.63(2)	84.546(2)	82.430(3)	88.613(12)	88.076(5)	90
β [°]	88.560(5)	88.907(2)	85.01(2)	85.518(2)	78.550(3)	77.622(15)	86.635(5)	106.464(2)
γ [°]	62.497(6)	62.877(3)	65.616(19)	66.446(2)	68.265(3)	67.124(16)	67.486(5)	90
Z	2	2	2	1	2	2	2	4
V [Å^3]	1168.93(13)	1151.06(10)	1178(3)	1171.60(7)	896.99(9)	843.7(3)	968.0(6)	1941.2(2)
D_{calc} [g cm^{-3}]	1.459	-	1.449	1.456	1.401	1.494	1.364	1.415
Reflns. collected	7190	-	7455	18590	17551	5633	9244	14851
Unique reflns.	4118	-	4035	4143	3184	2958	3400	3418
Observed reflns.	3622	-	2703	2554	2504	1678	2595	3207
R_1 [I>2(I)]	0.0760	0.0700	0.0817	0.0669	0.0412	0.0817	0.0715	0.0455
wR_2 (all)	0.2239	-	0.2174	0.1823	0.1163	0.1706	0.2201	0.1151
Goodness-of-fit	1.047	1.193	1.044	1.090	1.134	0.894	1.045	1.105
Diffractometer	Oxford Xcalibur Gemini	-	Bruker Smart Apex	Bruker Smart Apex	Bruker D8 QUEST	Oxford Xcalibur Gemini	Bruker Smart Apex	Bruker Smart Apex

[a] Reported crystal structure in ref. 25.

Table 6.2 Hydrogen Bond Distances and Angles in EPR Cocrystals.

Hydrogen bond D–H···A	**H···A (Å)**	**D···A (Å)**	**D–H···A (º)**	**Symmetry Code**
EPR–CAF Form I				
O3–H3A···O5	1.94	2.675(5)	172	1-x,2-y,-z
C2–H2···O2	2.64	3.421(5)	143	-x+1,-y+1,-z+1
C5–H5···O2	2.62	3.324(5)	134	-x+2,-y,-z+1
C6–H6···S1	2.98	3.899(4)	176	x+1,+y-1,+z
C9–H9A···S1	2.55	3.168(5)	122	---[a]
C10–H10···O1	2.54	2.891(5)	103	---[a]
C14–H14B···O1	2.43	2.824(6)	104	---[a]
C17–H17C···O1	2.62	3.435(2)	144	-x+1,-y,-z+1
C20–H20B···O4	2.37	2.814(6)	108	---[a]
C20–H20B···N2	2.60	3.367(6)	137	x,1+y,z
C22–H22B···N2	2.42	2.817(6)	104	---[a]
EPR–CAF Form II				
O3–H3A···N2	1.87	2.715(6)	175	-x+1,-y+1,-z+1
C5–H5···O4	2.60	3.323(7)	135	-1+x,y,-1+z
C5–H5···O1	2.58	3.317(8)	137	-x,-y,-z
C9–H9A···S1	2.61	3.199(7)	120	---[a]
C10–H10···O1	2.49	2.855(6)	103	---[a]
C14–H14B···O1	2.43	2.817(7)	104	---[a]
C14–H14B···O4	2.49	3.360(7)	149	1-x,-y,1-z
C16–H16···O2	2.40	3.057(8)	127	-x+1,-y+1,-z+1
C17–H17C···O5	2.59	3.522(8)	162	1+x,-1+y,z
C20–H20B···O4	2.26	2.718(7)	109	---[a]
C22–H22B···O5	2.34	2.714(7)	104	---[a]
EPR–CAF Form II Dimer				
O3–H3A···N2	1.80	2.706(5)	171	x,y,1+z
C4–H4···O3	2.51	3.340(7)	149	-x,1-y,1-z
C5–H5···O4	2.48	3.295(7)	147	-1+x,y,z
C9–H9B···S1	2.71	3.231(5)	115	---[a]
C9–H9B···O1	2.50	3.110(6)	121	1-x,-y,1-z
C10–H10···O1	2.41	2.902(5)	110	---[a]
C14–H14A···O1	2.44	2.842(6)	104	---[a]
C14–H14A···O4	2.40	3.271(6)	150	1-x,-y,1-z
C16–H16···O2	2.45	3.098(7)	127	x,y,-1+z
C20–H20A···O4	2.25	2.696(7)	108	---[a]
C22–H22A···O5	2.35	2.765(7)	105	---[a]
EPR–ACT				
N2–H2A···O2	2.01	2.942(4)	166	1-x,1-y,-z
N2–H2B···O1	2.20	2.994(3)	165	-x+1,-y+1,-z+1
O3–H3A···O4	1.62	2.498(3)	170	1-x,1-y,-z
C4–H4···O3	2.68	3.234(3)	119	-x+2,-y+1,-z+1
C9–H9B···S1	2.55	3.165(3)	122	---[a]
C10–H10···O1	2.52	2.873(3)	103	---[a]

C14–H14A···S2	2.71	3.173(3)	110	---[a]
EPR–URE				
N2–H2A···O2	2.21	3.065(10)	171	-1+x,y,z
N2–H2B···O1	2.65	3.341(9)	139	-x+1,-y+1,-z+1
O3–H3A···O4	1.66	2.414(10)	156	x,y,z
N3–H3B···O2	2.10	2.946(10)	167	x,y,z
N3–H3C···O1	2.17	2.967(8)	155	1-x,1-y,1-z
C4–H4···O3	2.60	3.128(1)	117	-x+1,-y+1,-z
C9–H9A···S1	2.29	3.144(8)	147	---[a]
C10–H10 ···O1	2.50	2.848(9)	102	---[a]
C14–H14A···S2	2.71	3.157(7)	109	---[a]
EPR–4,4'-BPN				
O3–H3A···N2	1.66	2.569(5)	175	1-x,-y,1-z
C6–H6···S1	2.94	3.868(5)	175	x,+y+1,+z
C9–H9A···S1	2.83	3.146(6)	100	---[a]
C9–H9C···S2	2.99	3.886(9)	156	-x,-y,-z
C10–H10···O1	2.53	2.886(5)	103	---[a]
C14–H14B···O1	2.46	2.831(6)	104	---[a]
C17–H17···O2	2.64	3.466(7)	149	x+1,+y+1,+z
C19–H19···O2	2.69	3.523(6)	149	-x+1,-y,-z+1
EPR–4AP				
O3–H3A···N2	1.95	2.732(2)	159	x,1/2-y,1/2+z
N3–H3B···O1	2.24	3.048(3)	158	-1+x,y,-1+z
N3–H3C···O3	2.19	3.076(3)	161	-1+x,1/2-y,-1/2+z
C3–H3···O2	2.44	3.166(3)	135	1-x,-y,2-z
C9–H9A···S1	2.56	3.141(3)	119	---[a]
C10–H10···O1	2.54	2.887(3)	102	---[a]
C14–H14B···S2	2.73	3.147(2)	106	---[a]
C16–H16···S2	2.82	3.586(3)	141	x,-y+1/2,+z+1/2
C19–H19···O3	2.57	3.347(3)	141	-1+x,1/2-y,-1/2+z
C20–H20···O2	2.39	3.034(3)	126	x,1/2-y,-1/2+z

[a] = Intramolecular hydrogen bond

6.4.1 Crystal Structure Description

Epalrestat-Caffeine Form I (EPR-CAF Form I)

Cocrystallization of EPR and CAF in 1:1 ratio in tetrahydrofuran: n-heptane solvent mixture afforded orange color needle crystals of form I which solved and refined in triclinic *P*-1 space group. This crystal structure contains one molecule each of EPR and CAF in the asymmetric unit. The CAF molecule in this crystal structure is disordered at the imidazole ring. The carboxylic acid group of EPR connects the carbonyl group on CAF through single point O–H···O hydrogen bond (synthon 1) (O3–H3A···O5, 1.87Å,

175º). The EPR and CAF molecules extend into 2D ladder (Figure 6.1b) through C–H··· π interactions and C–H···O hydrogen bonds (C5–H5···O2, 1.80Å, 162º).

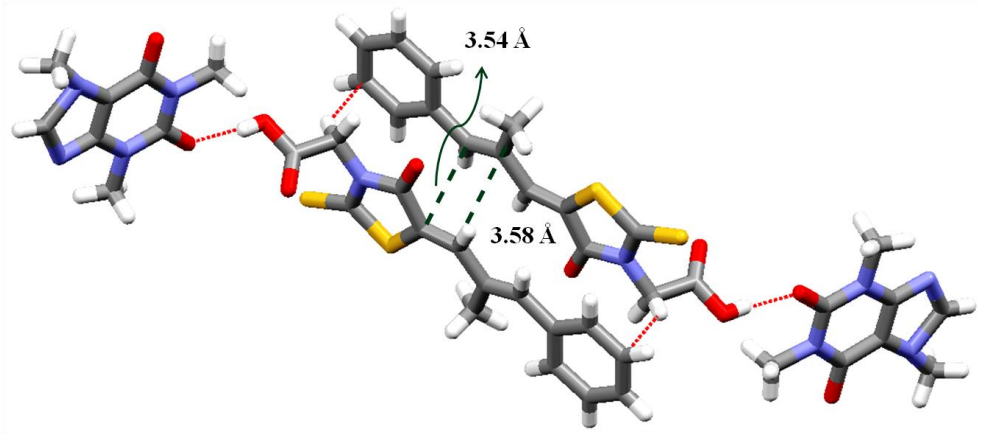

(a)

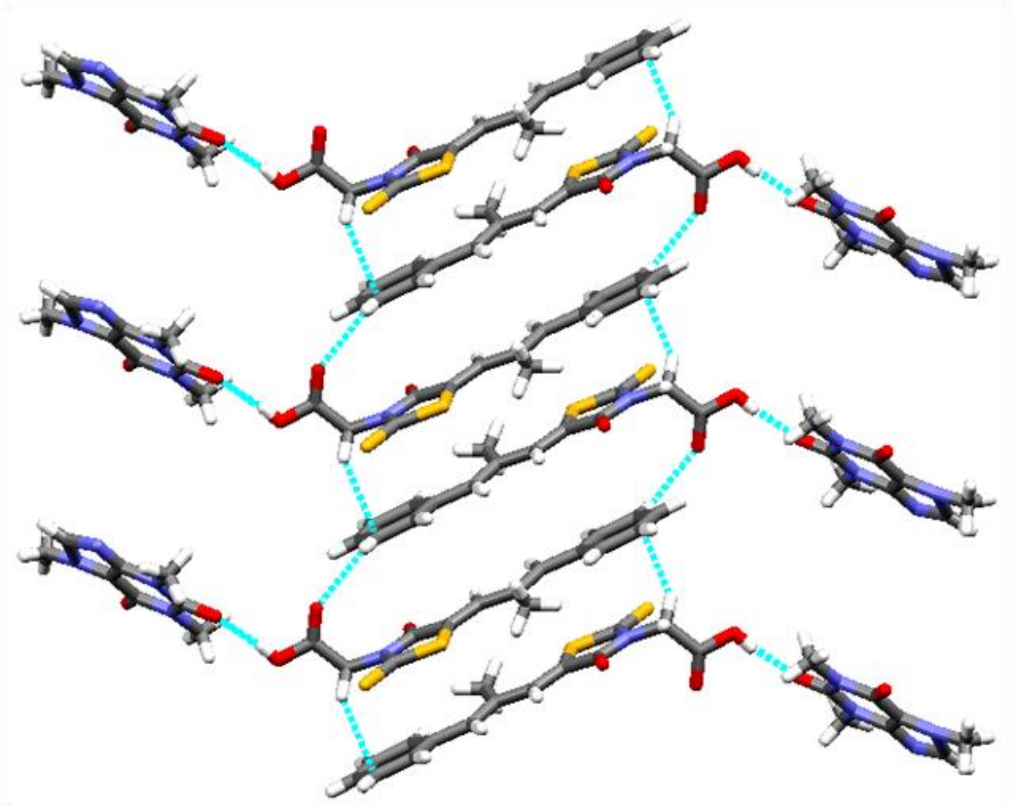

(b)

Figure 6.1 (a) Parallel alignment of adjacent olefinic double bonds in the crystal structure of EPR–CAF Form I. (b) 2D ladder formed via synthon 1, along with C–H··· π interactions and C–H···O hydrogen bonds.

Epalrestat-Caffeine Form II (EPR-CAF Form II)

Cocrystallization of EPR and CAF in 1:1 ratio in methanol solvent afforded yellow color plate crystals of form II which solved and refined in triclinic *P*-1 space group. The crystal structure is sustained by the robust heterodimer[34] (synthon 2) of imidazole and acid groups via O–H···N and C–H···O hydrogen bonds (O3–H3A···N2, 1.87 Å, 175°; C16–H16···O2, 2.40 Å, 127°) in $R_2^2(7)$ ring motif[35] (Figure 6.2b). Two adjacent heterodimeric motifs $R_2^2(7)$ connect through the C−H···π interactions and extend into 2D ladder via π–π interactions between EPR molecules and C–H···O hydrogen bond (C17–H17C···O5, 2.59 Å, 162°) between CAF molecules (Figure 6.2b).

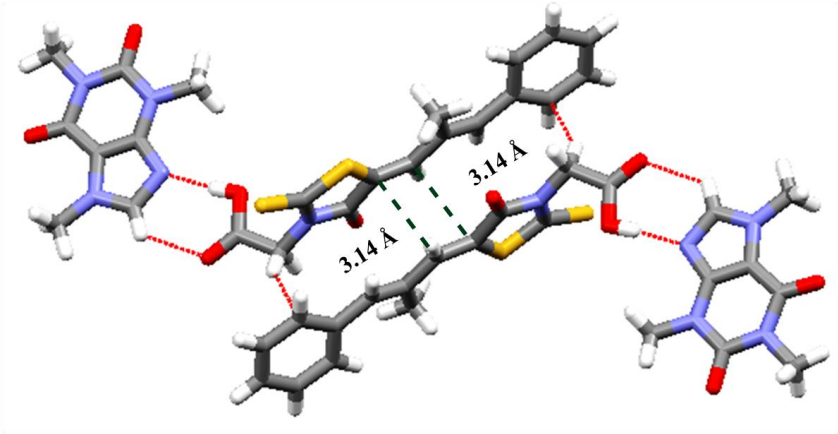

(a)

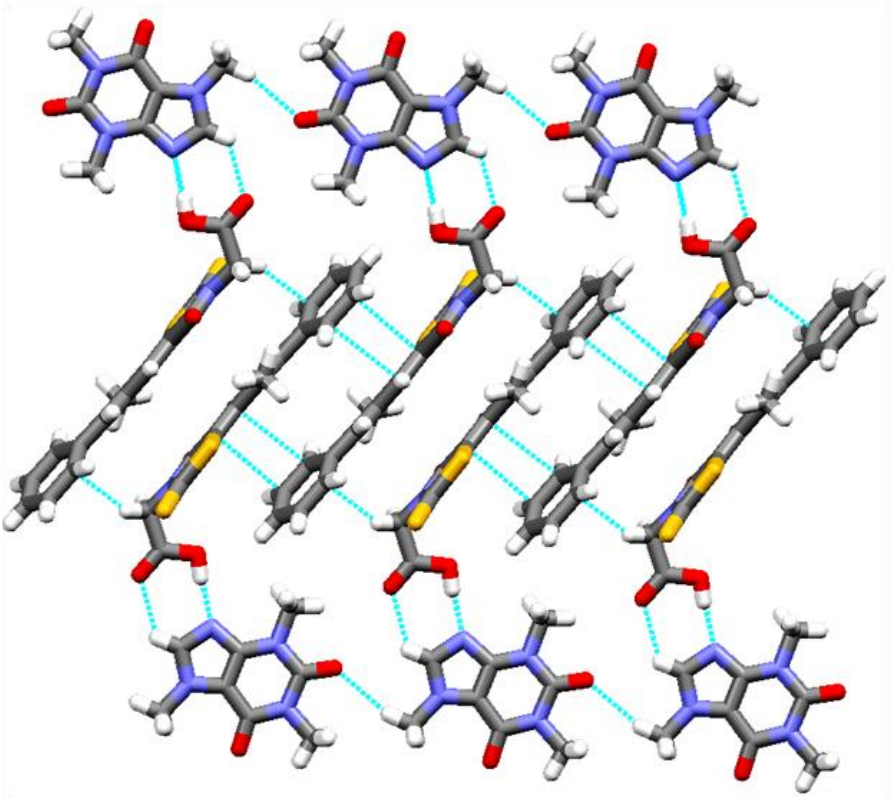

(b)

Figure 6.2 (a) Parallel alignment of adjacent olefinic double bonds in the crystal structure of EPR–CAF Form II. (b) Formation of a 2D network via synthon 2, C–H···O, C−H···π and π–π interactions.

Epalrestat-Caffeine Form II Dimer (EPR-CAF Form II Dimer)

It crystallizes in the triclinic *P*-1 space group with one molecule caffeine and half molecule of EPR dimer in the asymmetric unit. In the crystal structure, EPR dimer interacts with the coformer, CAF through the robust heterodimer[34] (synthon 2) of imidazole and acid groups via O–H···N and C–H···O hydrogen bonds (O3–H3A···N2, 1.80 Å, 171°; C16–H16···O2, 2.45 Å, 127°) in $R_2^2(7)$ ring motif[35] and weak C–H···O interactions (C5–H5···O4, 2.48 Å, 147°) which leads to the formation of 2D sheet like structure (Figure 6.3b).

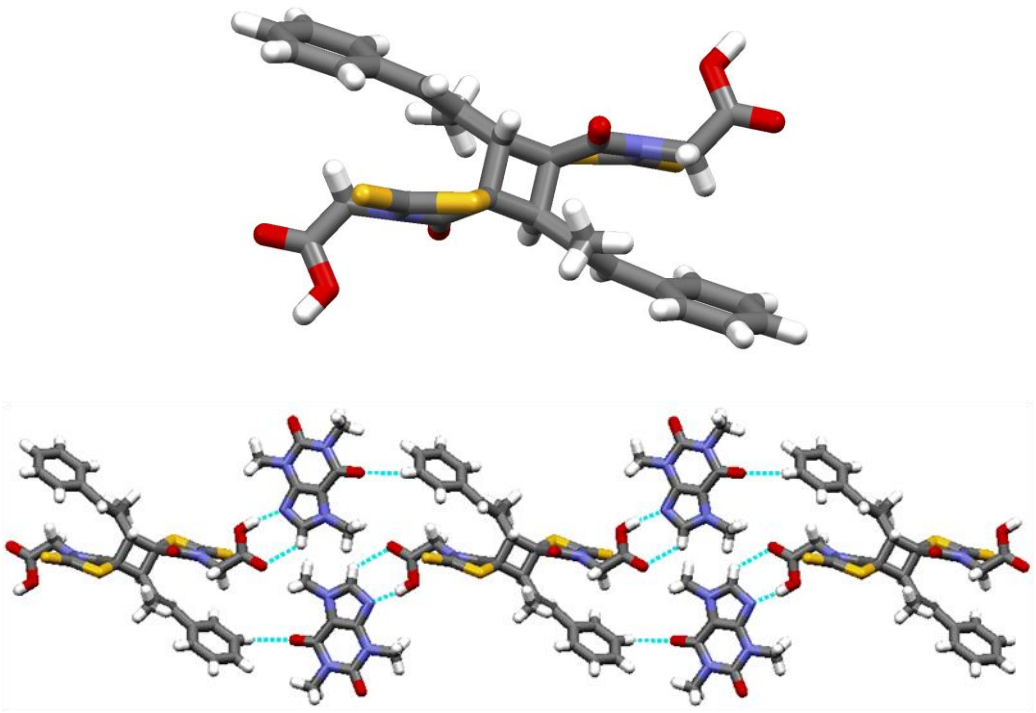

Figure 6.3 (a) EPR dimer observed in the crystal structure of EPR–CAF Form II dimer. (b) 2D sheet like structure formed via synthon 2 and C–H···O hydrogen bonds.

Epalrestat-Acetamide (EPR-ACT)

Cocrystallization of EPR and ACT in 1:1 ratio in nitromethane solvent afforded yellow color plate crystals of EPR-ACT cocrystal which solved and refined in triclinic *P*-1 space group. The asymmetric unit consists of one molecule of EPR and one molecule of ACT. Carboxylic acid group of EPR and amide group of ACT forms acid-amide heterodimer[34] (synthon 3) via O–H···O and N–H···O hydrogen bonds (O3–H3A···O4, 1.62 Å, 170°; N2–H2A···O2, 2.01 Å, 166°) in $R_2^2(8)$ ring motif[35] (Figure 6.4a). Two adjacent heterodimeric motifs $R_2^2(8)$ connect through the N−H···O hydrogen bond (N2–H2B···O1, 2.20 Å, 165º) to make a tetrameric ring motif $R_4^4(18)$. These tetrameric ring motifs further connect through C−H···O hydrogen bond (C4–H4···O3, 2.68 Å, 119º) and form 1D tape (Figure 6.4b).

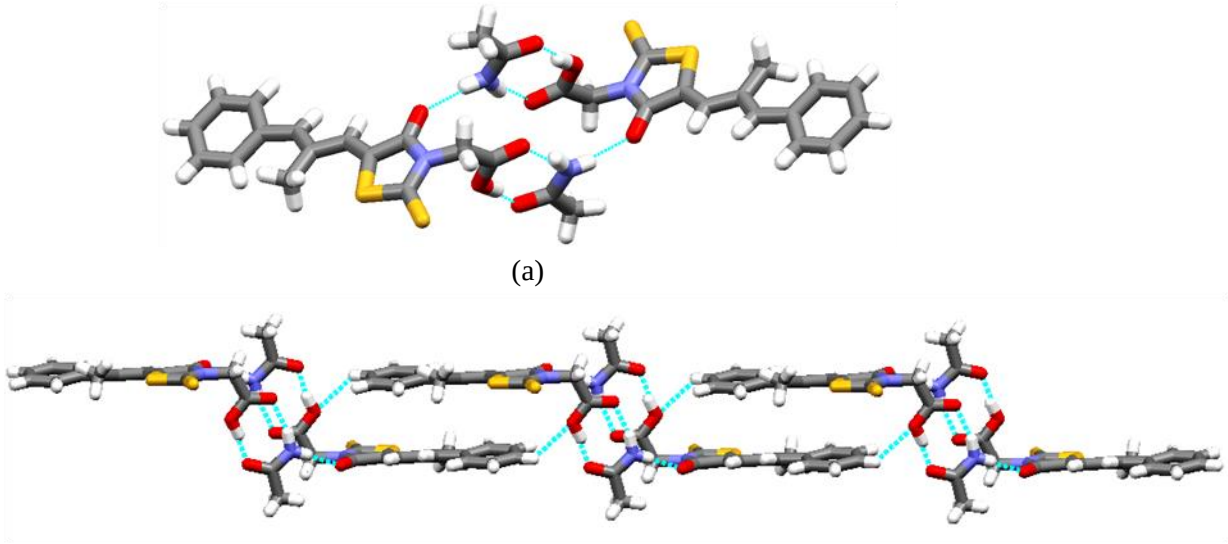

(a)

(b)

Figure 6.4 (a) $R_2^2(8)$ dimeric and $R_4^4(18)$ tetrameric assembly in the crystal structure of EPR–ACT cocrystal formed via acid-amide heterosynthon and N–H···O hydrogen bonds. (b) Tetrameric ring motifs connected through C−H···O hydrogen bonds.

Epalrestat-Urea (EPR-URE)

Cocrystallization of EPR and URE in 1:1 ratio in ethyl acetate-nitromethane solvent mixture afforded yellow color plate crystals of EPR-URE cocrystal which solved and refined in triclinic *P*-1 space group. The asymmetric unit consists of one molecule each of EPR and URE. Carboxylic acid group of EPR and amide group of URE forms acid-amide heterodimer[34] (synthon 3) via O–H···O and N–H···O hydrogen bonds (O3–H3A···O4, 1.66 Å, 156°; N3–H3B···O2, 2.10 Å, 167°) in $R_2^2(8)$ ring motif (Figure 6.5a). Two adjacent heterodimeric motifs $R_2^2(8)$ connect through the N−H···O hydrogen bond (N3–H3C···O1, 2.17 Å, 155º) to make a tetrameric ring motif $R_4^4(18)$.[35] These tetrameric ring motifs extend into zigzag tapes through N−H···O hydrogen bonds (N2–H2A···O2, 2.21 Å, 171º). The zigzag tapes extend as corrugated sheet-like structure through C–H···π interactions and C–H···O hydrogen bonds (C9–H9B···π ; C4–H4···O3, 1.66 Å, 156°) (Figure 6.5b).

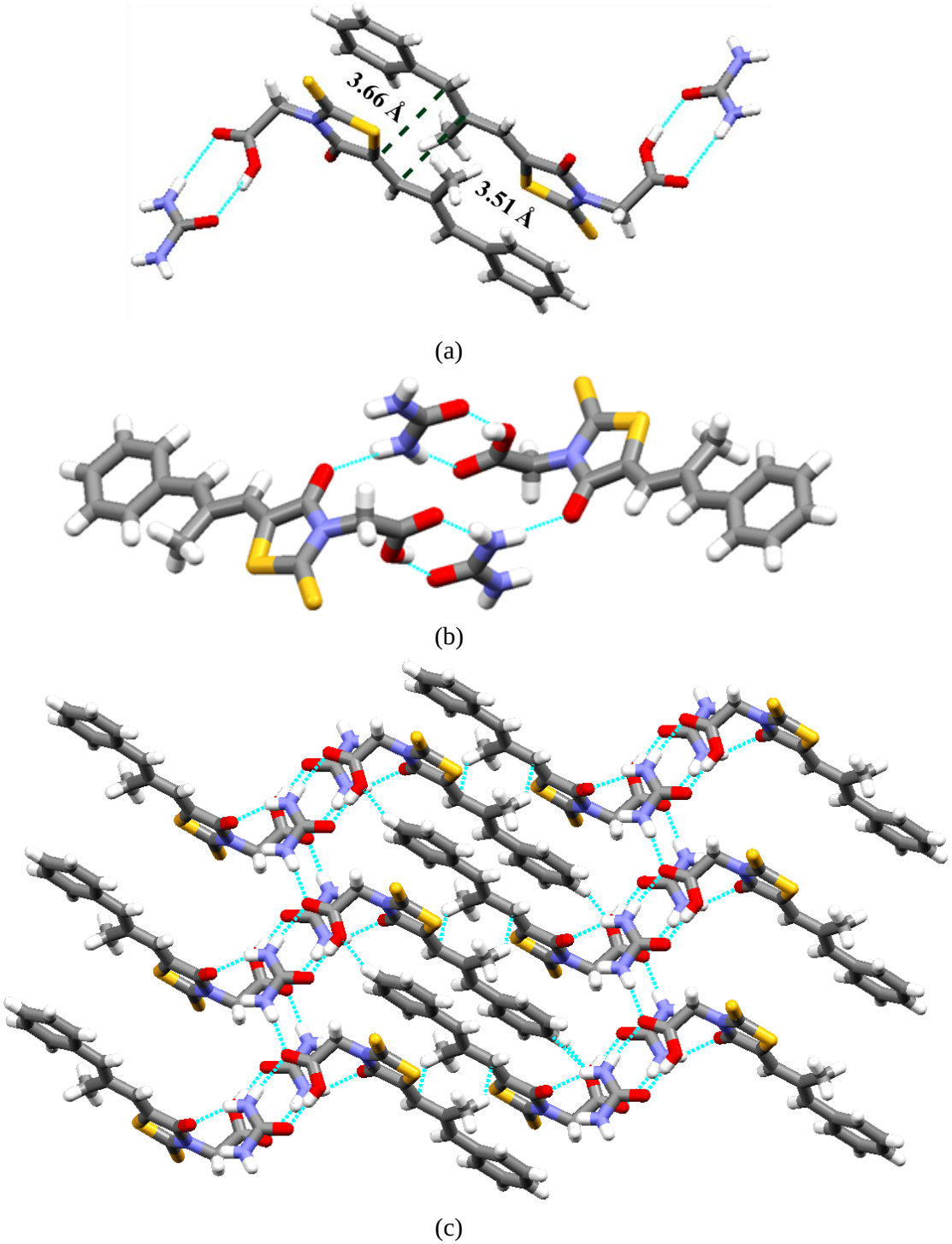

(a)

(b)

(c)

Figure 6.5 (a) Parallel alignment of adjacent olefinic double bonds in the crystal structure of EPR–URE cocrystal. (b) $R_2^2(8)$ dimeric and $R_4^4(18)$ tetrameric motifs in the crystal structure of EPR–URE cocrystal formed via acid-amide heterosynthon and N–H···O hydrogen bonds. (c) Corrugated sheet-like structure formed by C–H···π interactions and C–H···O hydrogen bonds.

Epalrestat-4,4′-Bipyridine (EPR-4,4'-BPN)

The cocrystal of EPR and BPN crystallizes in triclinic space group *P*-1 with one molecule of EPR and half molecule of BPN in the asymmetric unit. In the crystal structure BPN binds with two EPR molecules via robust acid–pyridine synthon[36] (synthon 5) (O3–H3A···N2, 1.66 Å, 175º) to form a trimer. The adjacent trimers are linked via bifurcated C–H···O interactions. Two adjacent EPR molecules are connected by the C–H···S interactions (C9–H9C···S2, 2.99 Å, 156º) that lead to the formation of ladder like structure (Figure 6.6b).

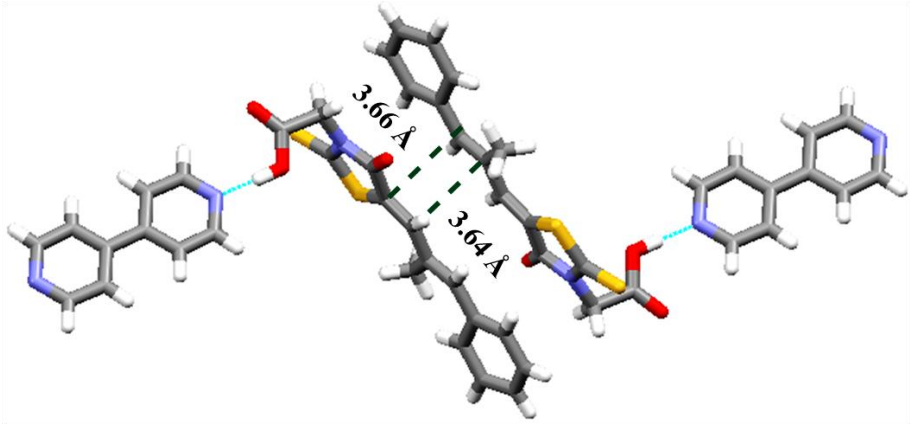

(a)

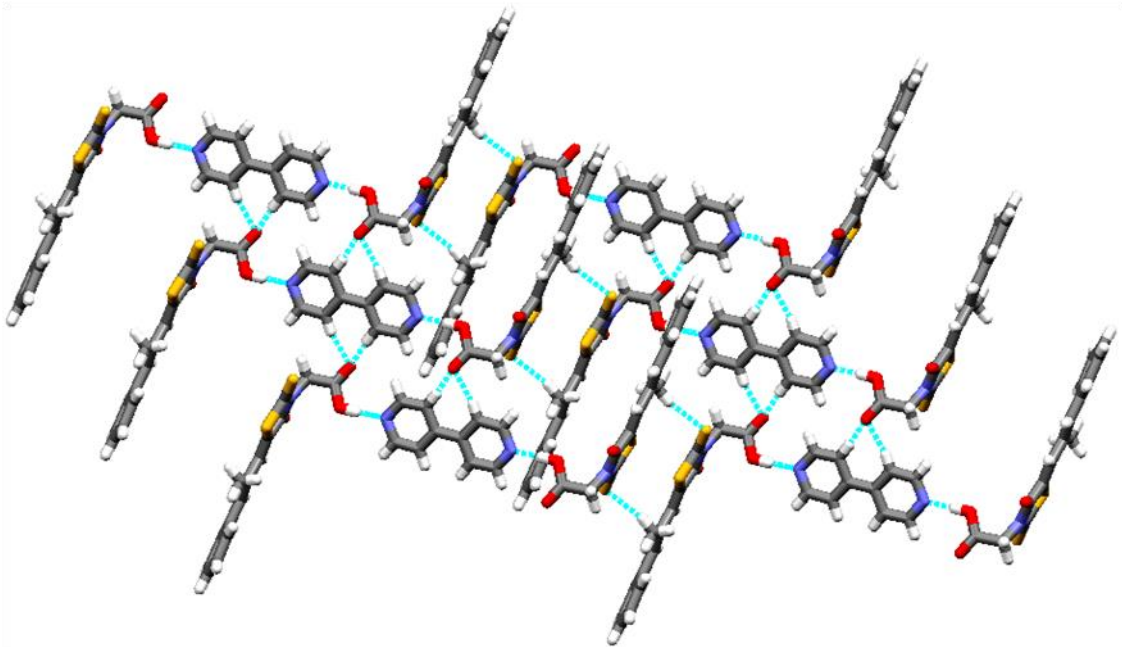

(b)

Figure 6.6 (a) Parallel alignment of adjacent olefinic double bonds in the crystal structure of EPR–4,4'-BPN. (b) Ladder like structure formed via acid-pyridine synthon and bifurcated C–H···O interactions and C–H···S interactions.

Epalrestat-4-Aminopyridine (EPR-4AP)

The cocrystal EPR-4AP crystallizes in the monoclinic $P2_1/c$ space group with one molecule of each EPR and 4AP in the asymmetric unit. The coformer, 4AP molecule possesses two strong hydrogen bonding functional groups: a pyridyl nitrogen and a amine group at the para position on its phenyl ring. In the crystal structure, the pyridyl nitrogen of 4AP interacts with the carboxylic acid group of EPR molecule via O–H···N and C–H···O hydrogen bonds (synthon 6) (O3–H3A···N2, 1.95 Å, 159º; C20–H20···O2, 2.39 Å, 126º) and one of the two amine hydrogens of 4AP forms N–H···O hydrogen bond (synthon 7) (N3–H3B···O1, 2.24 Å, 158º) with the carbonyl O-atom of EPR that eventually leads to a 1D zigzag tape shown in figure 6.7a. Adjacent tapes join by weak C–H···O interactions to form a ladder (figure 6.7b). The second hydrogen of the NH_2 group of 4AP forms N–H···O hydrogen bond (N3–H3C···O3, 2.19 Å, 161º) with the carboxylic O-atom of EPR from another adjacent tape.

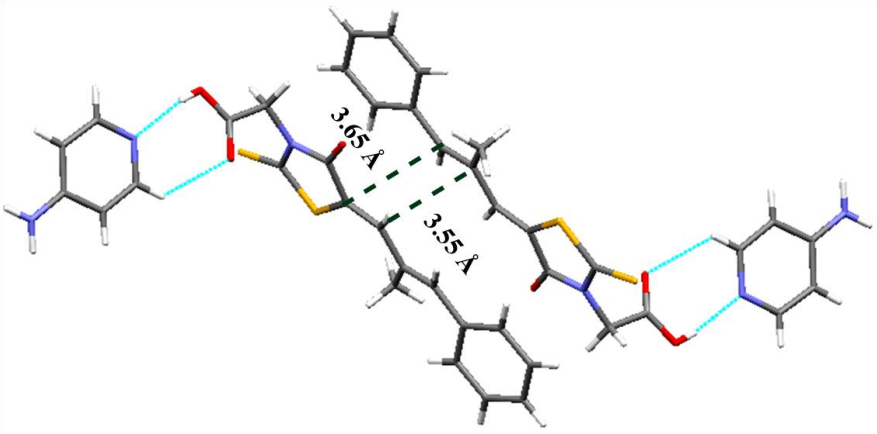

(a)

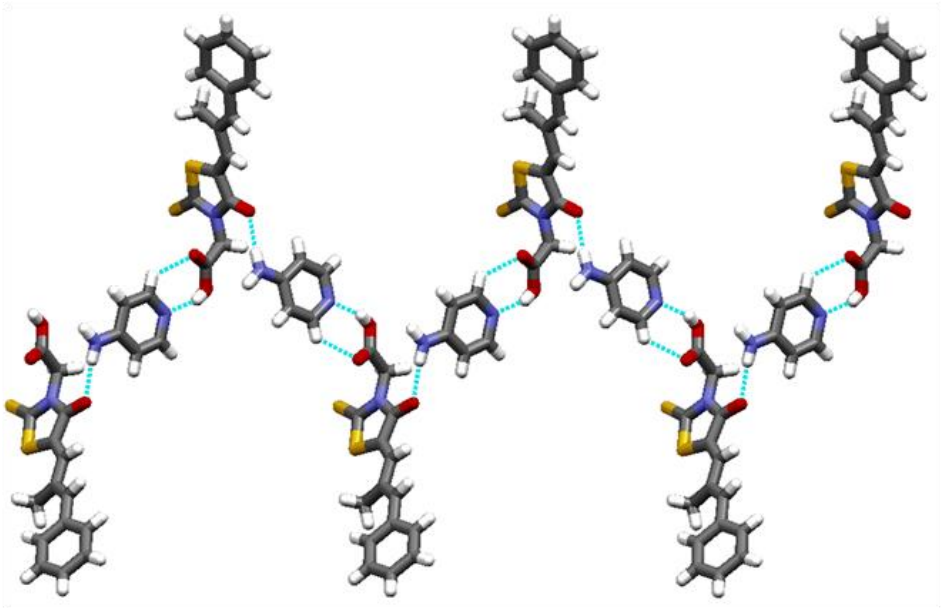

(b)

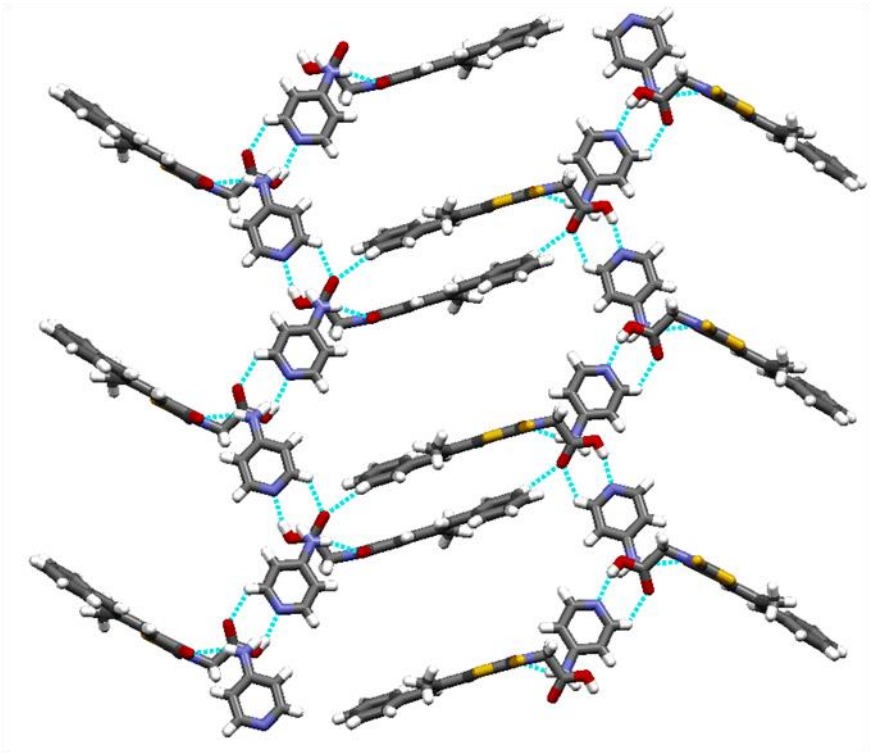

(c)

Figure 6.7 (a) Parallel alignment of adjacent olefinic double bonds in the crystal structure of EPR–4AP. (b) 1D zigzag tape formed via synthon 6 and synthon 7. (c) Adjacent tapes are connected by weak C–H···O interactions to form a ladder network.

Epalrestat (EPR Form I)

EPR Form I crystallizes in triclinic space group $P\bar{1}$ with two molecules (Z'=2) in the asymmetric unit. Two symmetry-independent molecules are connected via O–H···O and C–H···O hydrogen bonds a $R_2^2(9)$ dimeric motif. Such motifs are held together by O–H···O hydrogen bonds in a tetrameric $R_4^4(22)$ motif. In this structure, EPR molecules are arranged in a head to tail orientation with shortest C=C distances of 3.52 Å, 3.58 Å and 3.68 Å, 3.79 Å in the two symmetry independent sets (Figure 6.8).

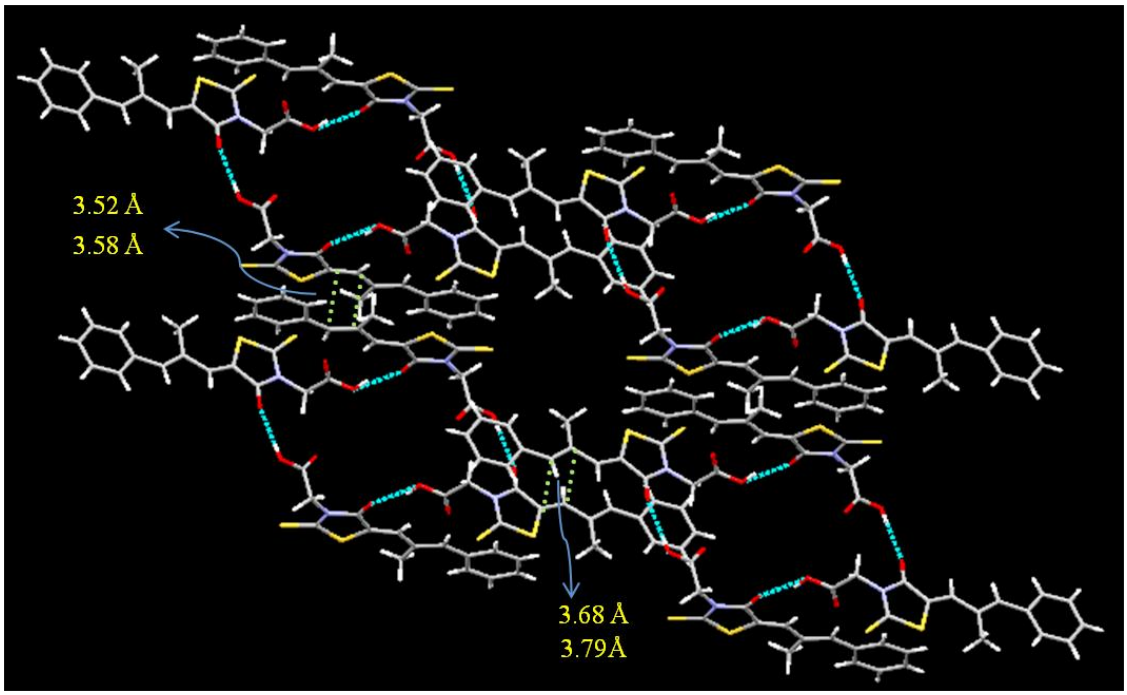

Figure 6.8 Reactive C=C bonds are parallel to each other and are within Schmidt's topochemical reactive distance of 4.2 Å.

6.4.2 Powder X-ray diffraction Analysis

Powder diffraction is a reliable method for determining the novelty of different solid forms by their unique diffraction patterns. It allows for easy distinction of the modified solid materials from their starting components.[37] When single crystals are not available for analysis, this technique becomes much more important. The identification of polymorphic impurities in a mixture of polymorphs, bulk purity of polymorphs, cocrystals or salts, amorphous content in a crystalline material, and structure solution of a crystalline material from powder diffraction data have all recently been added to its list

of applications.[37-39] PXRD was used to determine the bulk phase purity of EPR cocrystals in this study. The five cocrystals powder diffraction lines showed an excellent overlay of the experimental PXRD pattern with the calculated lines from the X-ray crystal structure, confirming the bulk phase purity (Figure 6.9).

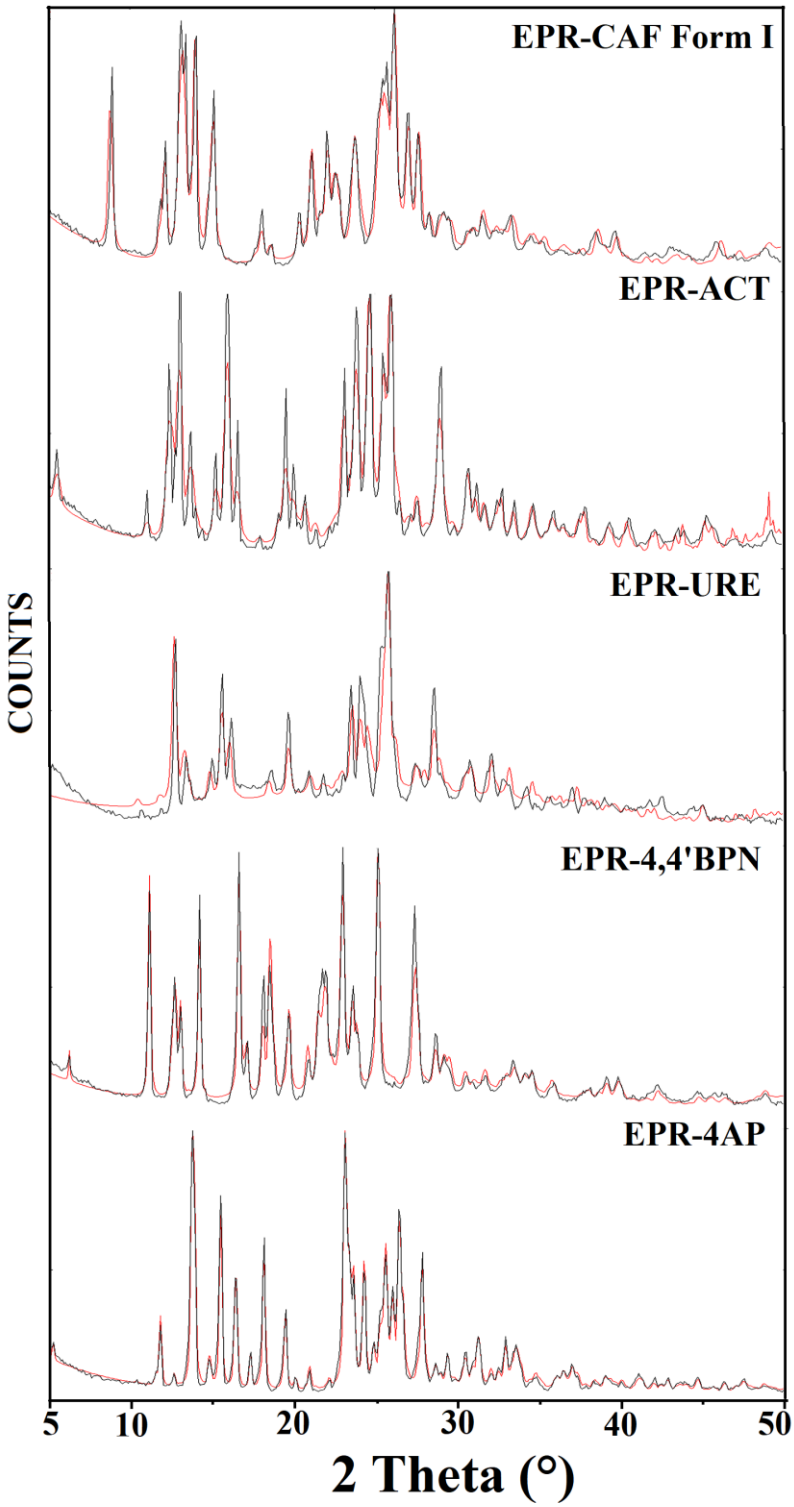

Figure 6.9 Overlay of experimental PXRD (black) patterns of EPR solid forms showed good match with their calculated line patterns from the X-ray crystal structures (red) indicating bulk purity and homogeneity of each phase.

6.4.3 Infrared Spectroscopy

Infrared spectroscopy (IR) is a reliable technique for determining co-crystal formation. Usually cocrystals show the stretching frequency (ν_s) bands of both the starting components associated with characteristic shifts.[40] In the IR spectrum of EPR, cyclic ketone and carboxylic acid C=O stretching frequencies appeared at 1748.9 and 1686.4 cm^{-1}. Significant changes in these vibrational modes were observed on forming cocrystal (Figure 6.10). In EPR-CAF Form I, the C=O stretching modes of EPR shifted to 1749.0, 1697.8 cm^{-1}. The carbonyl stretching frequencies of CAF shifted from 1700.8, 1658.1 cm^{-1} to 1719.3, 1641.5 cm^{-1}. The C=N stretch of CAF shifted from 1549.9 cm^{-1} to 1562.3 cm^{-1}. Similar differences were also observed in the stretching frequencies of other cocrystals. While the C=O stretching frequencies appeared at 1703.1, 1619.7 and 1576.7 cm^{-1} in EPR-ACT, they showed up at 1760.7, 1710.4 and 1688.0 cm^{-1} in EPR-URE and 1722.3, 1704.5 cm^{-1} in EPR-4,4'-BPN and 1691.2, 1572.0 in EPR-4AP. The corresponding NH_2 asymmetric and symmetric stretching frequencies were observed at 3420.2 and 3198.4 cm^{-1} in EPR-ACT, 3488.1 and 3441.6 cm^{-1} in EPR-URE and 3415.3, 3332.8 cm^{-1} in EPR-4AP. The C=N stretch was observed at 1604.7 cm^{-1} in EPR-4,4'-BPN and 1654.2 cm^{-1} in EPR-4AP. The detailed peak assignment for the free EPR and each cocrystal is given in Table 6.3.

Table 6.3 List of major FT-IR stretching frequencies in the EPR cocrystals and their individual components (in cm^{-1}**)**.

Solid form	–NH_2 asym stretch	–NH_2 sym stretch	Ketone C=O stretch	Carboxylic C=O stretch	C=N stretch
EPR	---	---	1748.9	1686.4	---
EPR–CAF Form I	---	---	1749.0, 1719.3, 1641.5	1697.8	1562.3
CAF	---	---	1700.8, 1658.1	---	1549.9
EPR–ACT	3420.2	3198.4	1703.1, 1619.7	1576.7	---
ACT	3376.0	3177.6	1670.5	---	---
EPR–URE	3488.1	3441.6	1760.7, 1710.4	1688.0	---
URE	3442.8	3347.4	1682.3	---	---
EPR–4,4'-BPN	---	---	1722.3	1704.5	1604.7
4,4'-BPN	---	---	---	---	1589.7
EPR–4AP	3415.3	3332.8	1691.2	1572.0	1654.2
4AP	3436.4	3301.6	---	---	1649.0

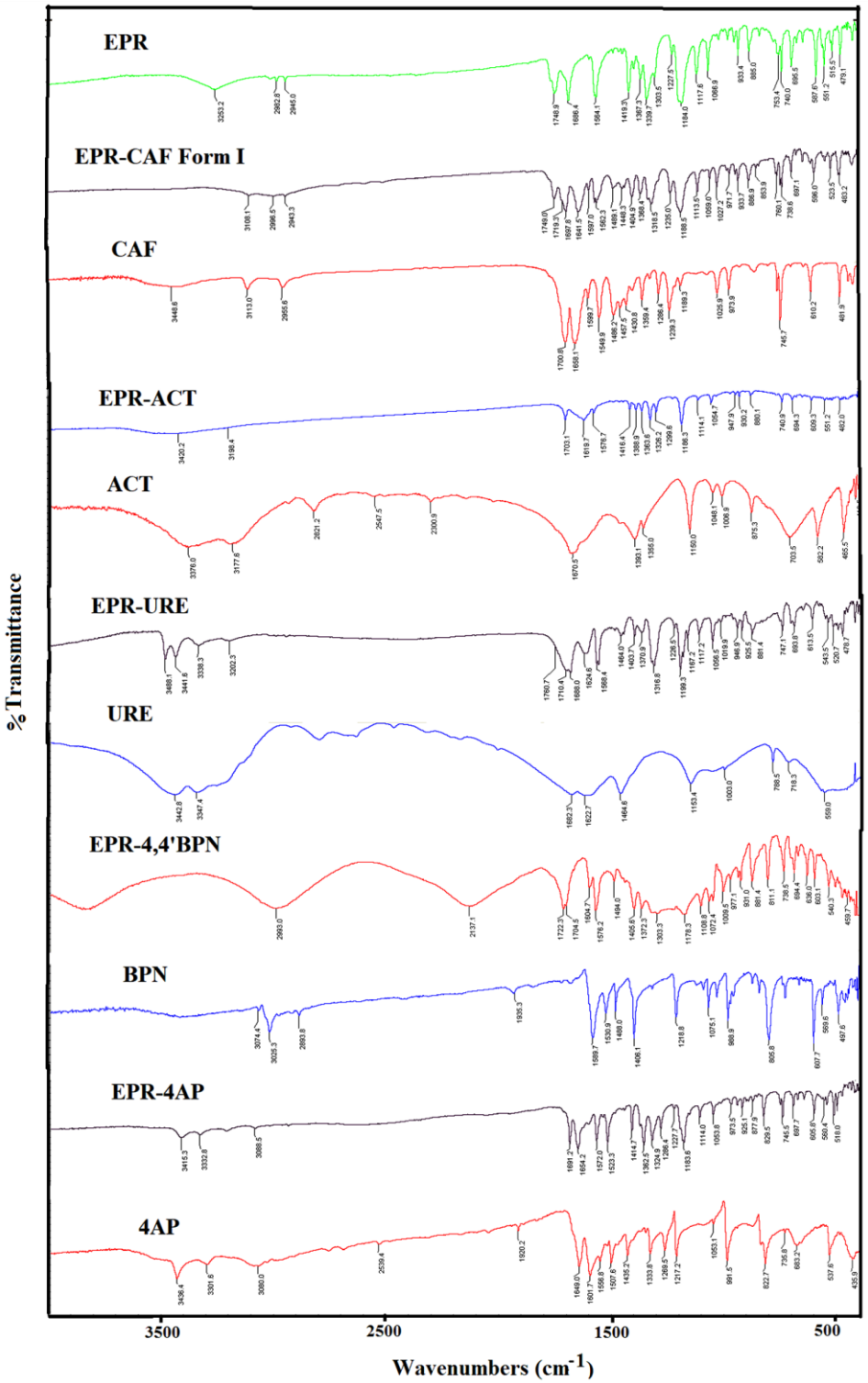

Figure 6.10 Overlay of IR spectra of EPR cocrystals in comparison to their individual components.

6.4.4 Thermal Analysis

Differential scanning calorimetry (DSC) was used to study the thermal behavior of EPR cocrystals.[41-43] The DSC thermograms for all the EPR cocrystals showed a single endothermic transition corresponding to the melting event. The melting point of all the cocrystals was different from either of the individual components confirming the formation of a new phase. The melting transition temperature of all the cocrystals lies in between that of EPR and the coformer, except EPR–CAF which is lower (Figure 6.11 and Table 6.4). The melting point of the cocrystal correlated, in general, with the melting point of the coformer, except CAF cocrystal.

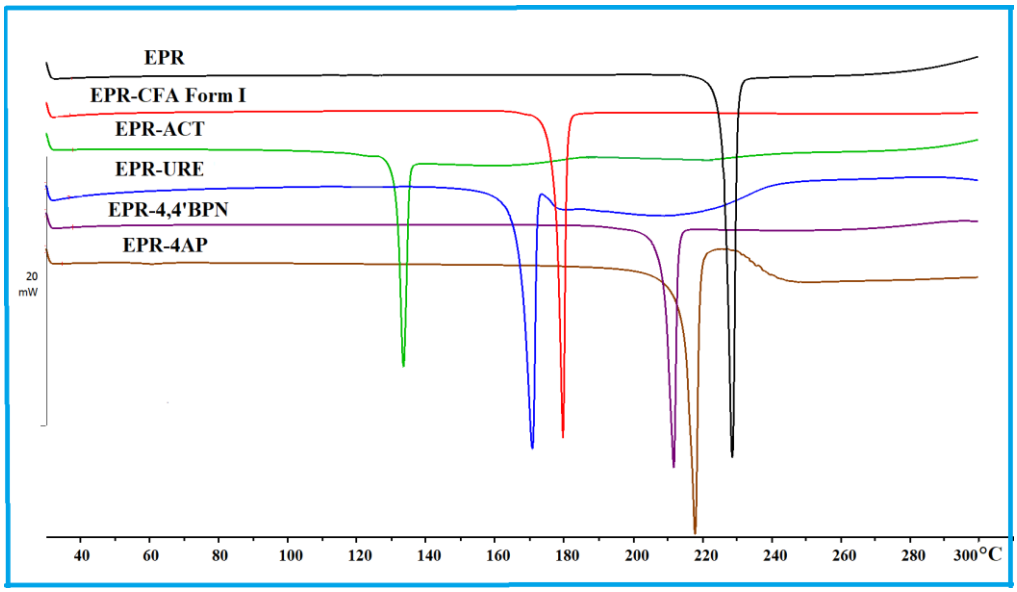

Figure 6.11 DSC heating curves of EPR and its cocrystals at heating rate of 5 °C min^{-1}. The sharp endotherm is the melting point of the cocrystal.

Table 6.4 Melting points of EPR cocrystals and their coformers.

S.No	EPR Cocrystal	Melting Point (°C)	Coformer	Melting Point (°C)
1	EPR–CAF Form I	177–181	caffeine	235–238
2	EPR–ACT	131–135	acetamide	79–81
3	EPR–URE	167–172	urea	133–135
4	EPR–BPN	208–212	4,4'-bipyridine	114
5	EPR–4AP	214–219	4-aminopyridine	155–158

Melting point of EPR 224 °C

6.4.5 Photostability Studies

When irradiated with UV light, EPR undergoes photoisomerization in solution state and [2 + 2] cycloaddition (photodimerization) in the solid state. Therefore, cocrystals of EPR were prepared and their stability studies were carried out in this chapter.

Photodimerization studies:

In the crystal structure of EPR, the molecules of EPR do stack one on top of one another in a parallel fashion leading to a head-tail arrangement. In this assembly, the intermolecular packing distance between the C=C carbon atoms is 3.56 Å, 3.58 Å and 3.68 Å, 3.79 Å within the Schmidt's topochemical limit for photodimerization[44-46] (Figure 6.8). Because of this reason, it was found that EPR undergoes [2 + 2] cycloaddition in the solid state by applying UV light. In this regard, cocrystals of EPR were prepared with various conformers and irradiated with UV light in a broadband mercury photoreactor in order to explore their photoreactivity. The extent of the photoreaction was studied in regular interval via ^{1}H NMR spectroscopy. When EPR-ACT cocrystal was irradiated with UV light, the sample became gummy after 2 h. Therefore, irradiation was discontinued after 2 h in this case. The ^{1}H NMR spectrum of EPR in d_6-DMSO obtained from irradiation of EPR in solid-state (powder form) using UV lamp for 7 d showed cyclobutane protons peaks at 3.60 and 3.98 ppm in addition to signals from unreacted EPR. The methyl group protons were also shifted upfield from 2.23 ppm to 1.94 ppm and 1.80 ppm, respectively. This observation is consistent with the formation of type I head-tail photodimer in quantitatively yield. Prolonged irradiation of EPR beyond 7 d duration did not improve the percentage of photodimerized product. Peaks corresponding to EPR and EPR dimer in the ^{1}H NMR spectrum of EPR and all cocrystals except EPR-CAF Form II were similar after UV irradiation, and confirmed the formation of type I head-tail dimer whereas EPR-CAF Form II gives type II head-tail dimer after UV irradiation (Scheme 6.3). The percentage of photoreaction was calculated from the integration of the NMR signals (CH_3 group protons) and found to be 70% (EPR), 13.3% (EPR-CFA Form I), 100% (EPR-CFA Form II), 50% (EPR-URE), 66% (EPR-4,4'BPN) and 45% (EPR-4AP) (Figure 6.13-6.18). From the stability studies we established the stability order as EPR-CFA Form I > EPR-4AP > EPR-URE > EPR-4,4'BPN > EPR > EPR-CFA Form II. From the above studies we conclude that EPR-CAF Form I is the most stable solid form in photodimerization reaction.

When single crystals of EPR-CFA Form I, EPR-URE, EPR-4,4'BPN, EPE-4AP and EPR were exposed to UV-light, the samples experienced extensive cracking and disintegrated to a powder state during the cycloaddition reaction. Due to the loss of the single crystalline nature during the photoreaction, the crystal structures of the photodimers of EPR and its cocrystals except EPR-CFA Form II could not be determined by X-ray crystallography. Our attempts to grow single crystals were also not successful.

Single crystals of EPR-CFA Form II, in contrast to EPR-CFA Form I, EPR-URE, EPR-4,4'BPN, EPE-4AP and EPR were determined to maintain crystal integrity during the course of the photodimerization, which suggested that the reaction proceeds via a single crystal to single crystal (SCSC) transformation.[47-49] Single-crystal X-ray diffraction study confirmed the reaction to occur in an SCSC manner. EPR-CFA Form II was completely converted to type II head-tail photodimer after just 10 min. Thus, the time required for [2+2] photodimerization in EPR-CFA Form II was shorter than in EPR-CAF Form I, EPR-URE, EPR-4,4'BPN, EPE-4AP and EPR.

Photoisomerization studies:

All the cocrystal forms exposed to UV light in solution state and their photoisomerization studies were carried out through ^{1}H NMR spectroscopy. Whereas the reaction is slowed down, but photoisomerization does occur and none of the cocrystal topology results is stoppage of the photoisomerization of EPR (Figure 6.19).

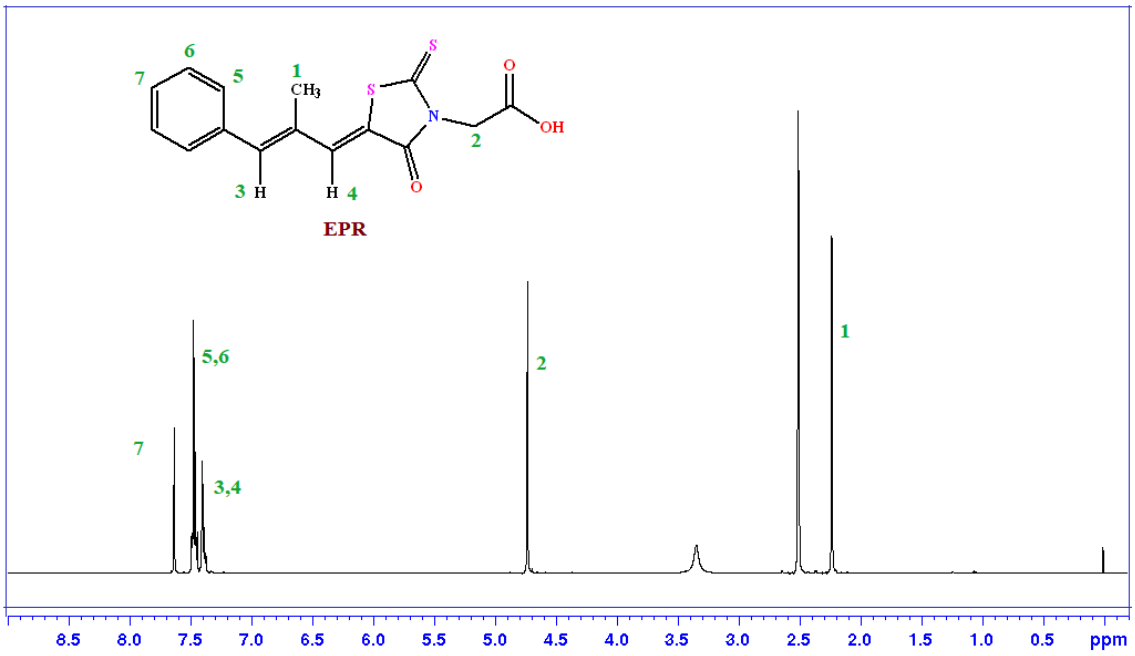

Figure 6.12 ^{1}H NMR spectrum of the EPR compound.

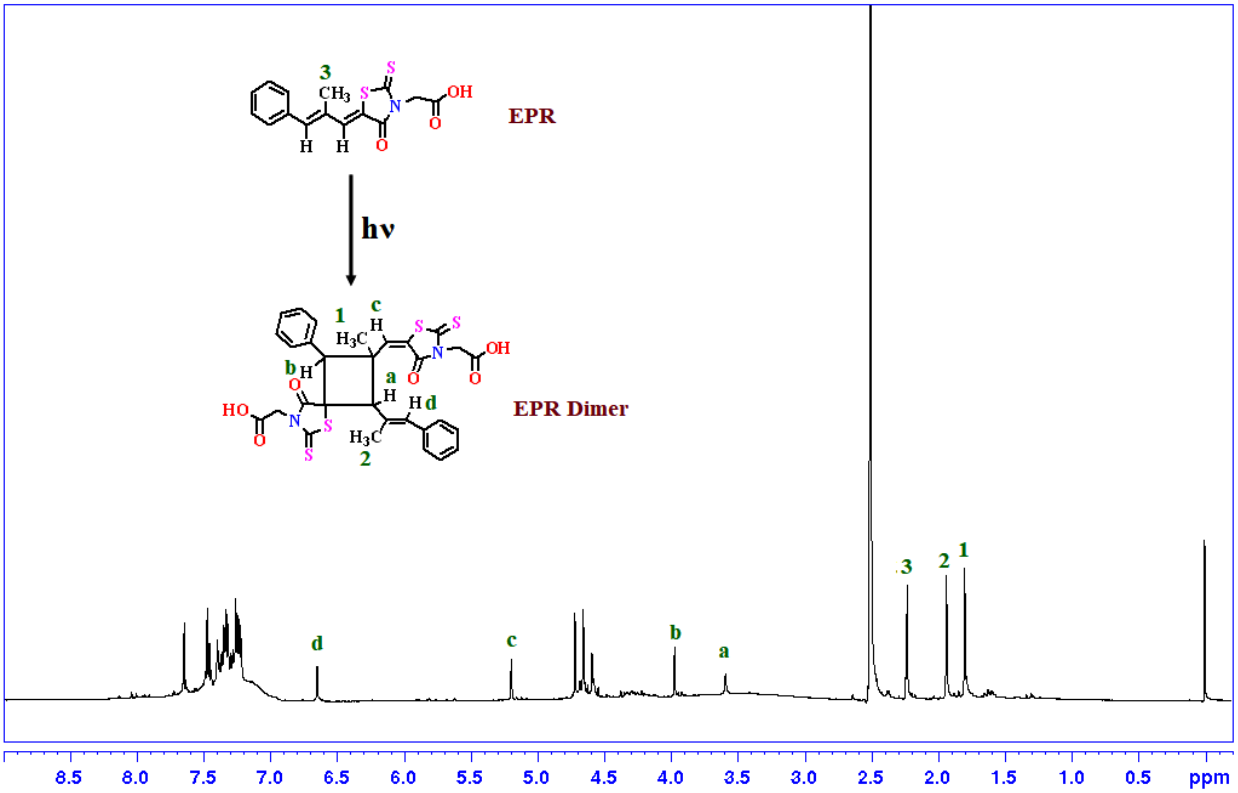

Figure 6.13 ^{1}H NMR spectrum of the EPR compound after irradiation for 7 days which shows the mixture of unreacted EPR and the photodimerized product (70% photoreaction).

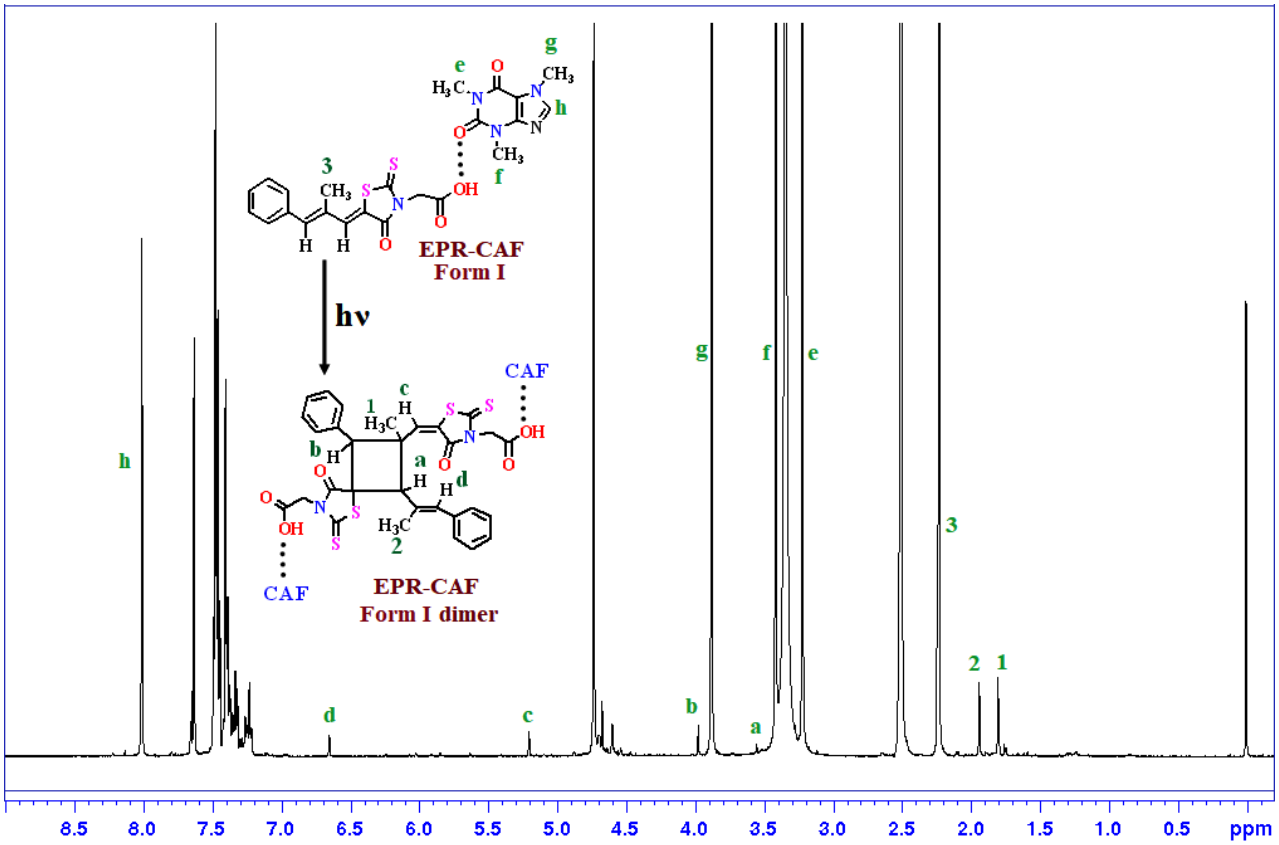

Figure 6.14 ^{1}H NMR spectrum of the EPR-CAF cocrystal Form I after irradiation for 7 days which shows the mixture of unreacted EPR-CAF cocrystal Form I and the photodimerized product (13.3% photoreaction).

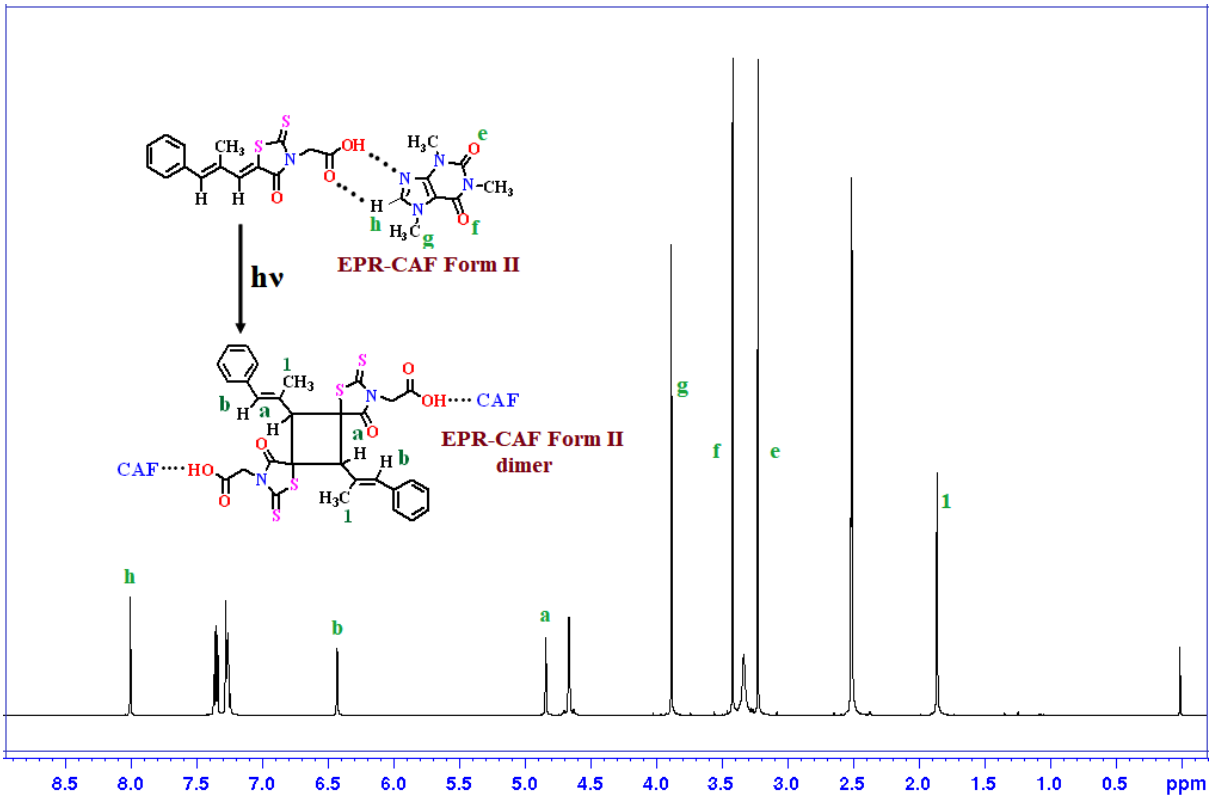

Figure 6.15 ^{1}H NMR spectrum of the EPR-CAF cocrystal Form II dimer (100% photoreaction).

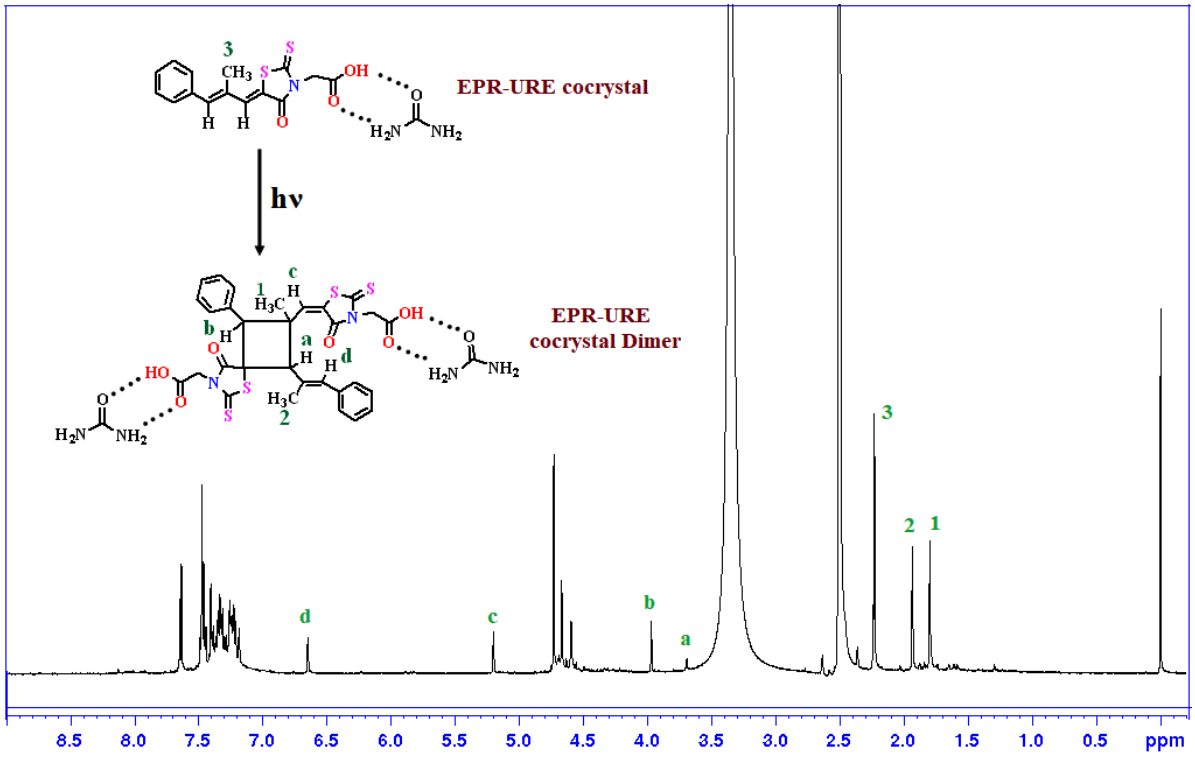

Figure 6.16 ^{1}H NMR spectrum of the EPR-URE cocrystal after irradiation for 7 days which shows the mixture of unreacted EPR-URE cocrystal and the photodimerized product (50% photoreaction).

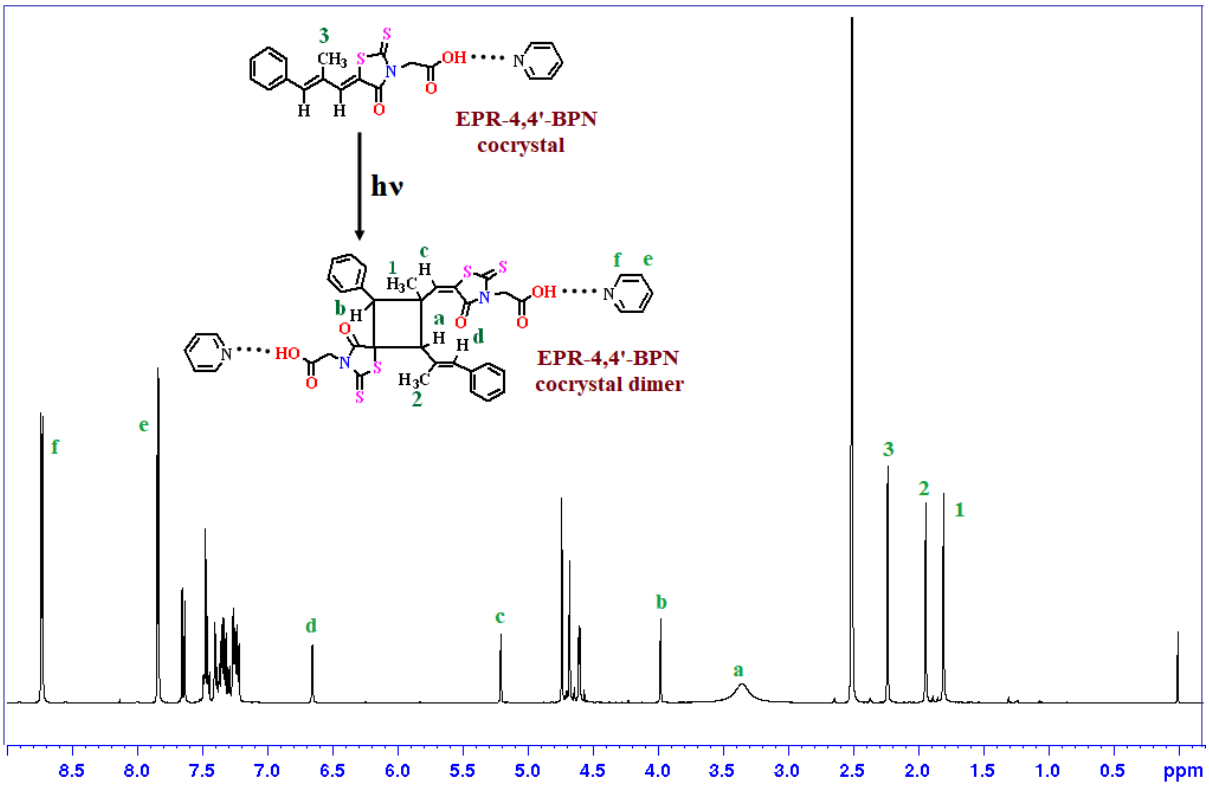

Figure 6.17 ^{1}H NMR spectrum of the EPR-4,4'-BPN cocrystal after irradiation for 7 days which shows the mixture of unreacted EPR-4,4'-BPN cocrystal and the photodimerized product (66% photoreaction).

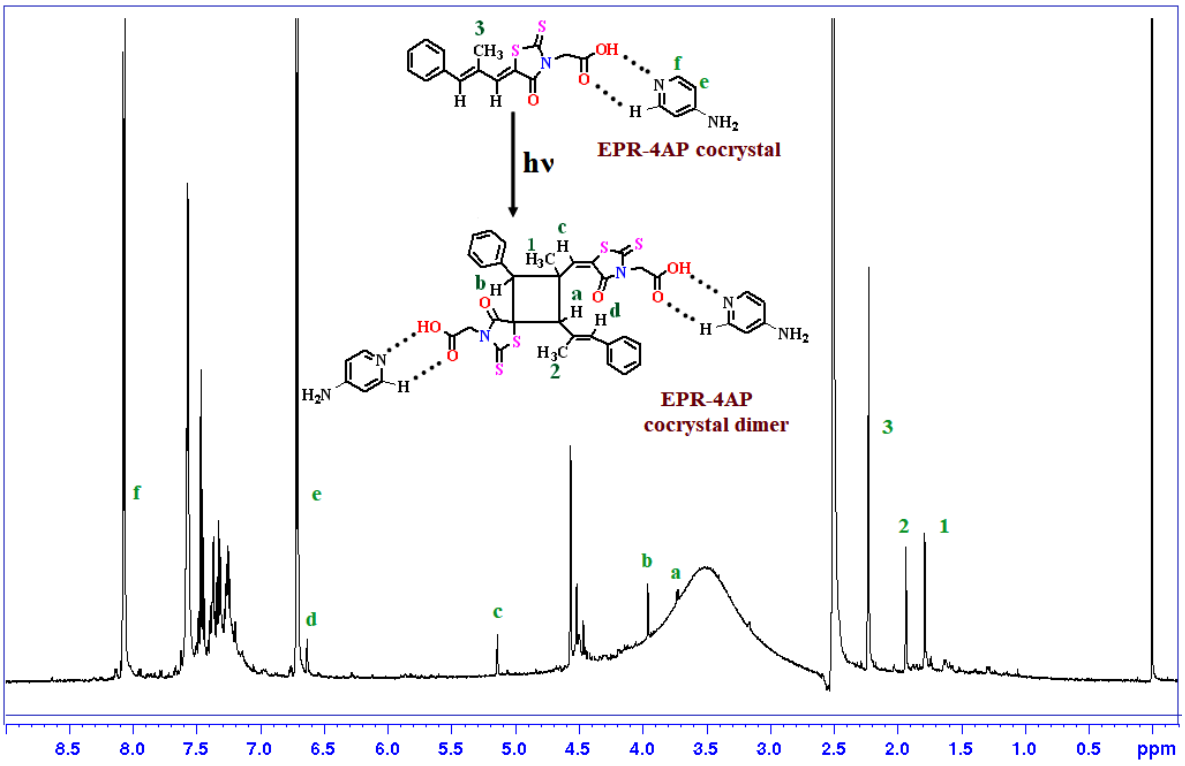

Figure 6.18 ^{1}H NMR spectrum of the EPR-4AP cocrystal after irradiation for 7 days which shows the mixture of unreacted EPR-4AP cocrystal and the photodimerized product (45% photoreaction).

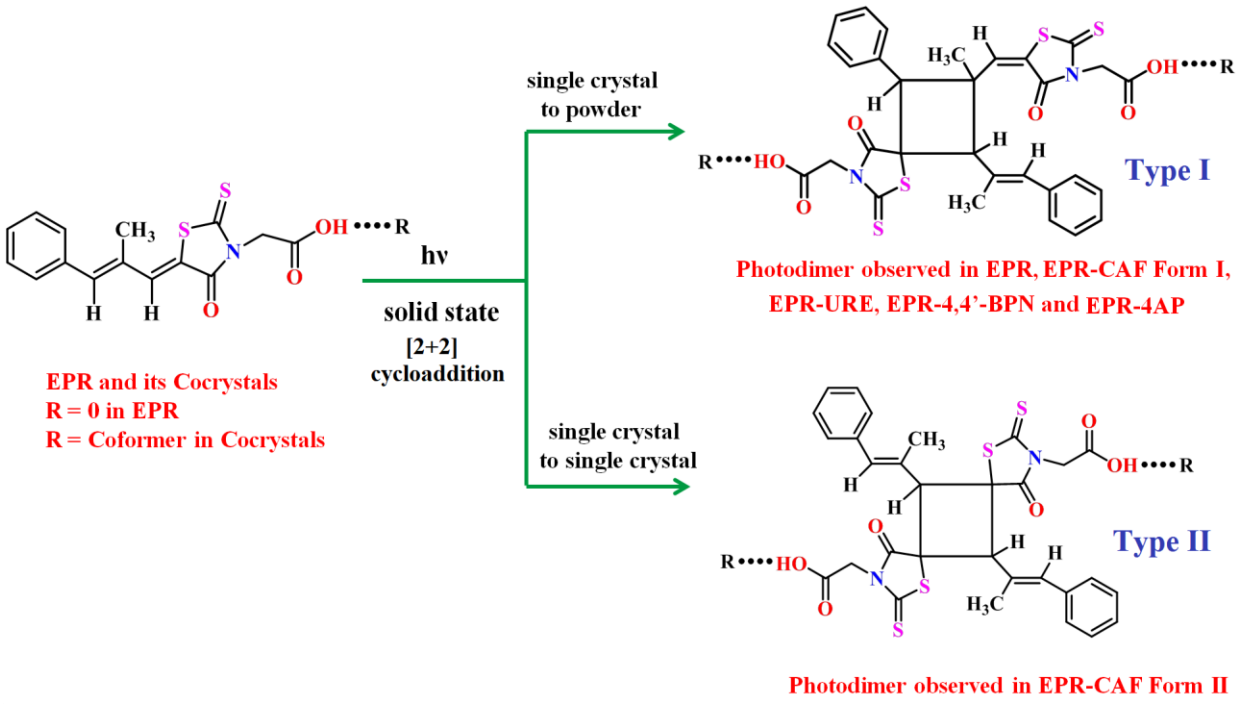

Scheme 6.3 Solid-state [2+2] photodimerization of EPR and its cocrystals.

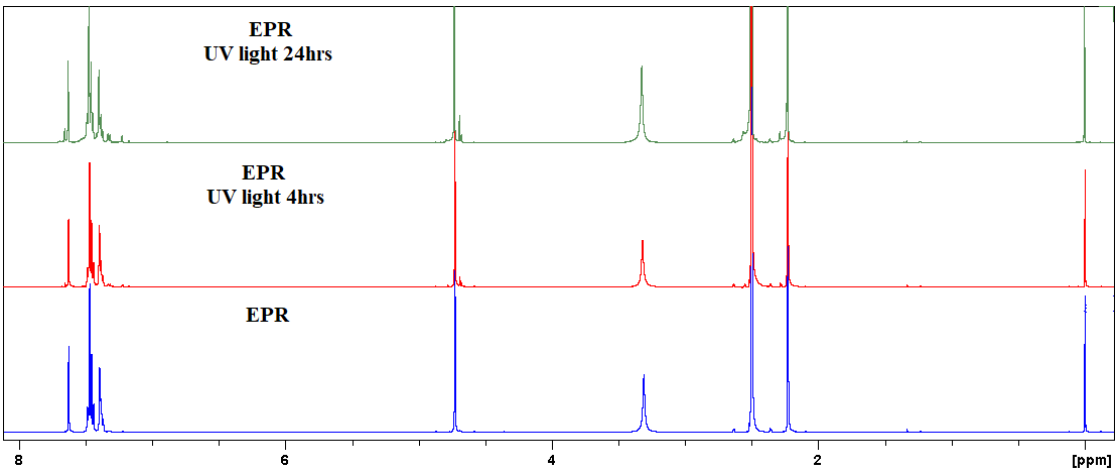
EPR
UV light 24hrs
EPR
UV light 4hrs
EPR
8
6
4
2
[ppm]

(a)

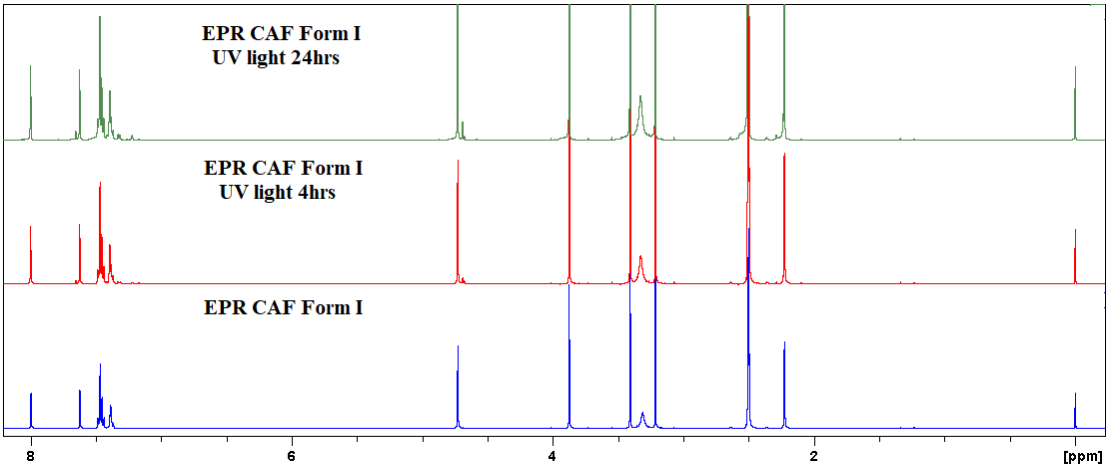
EPR CAF Form I
UV light 24hrs
EPR CAF Form I
UV light 4hrs
EPR CAF Form I
8
6
4
2
[ppm]

(b)

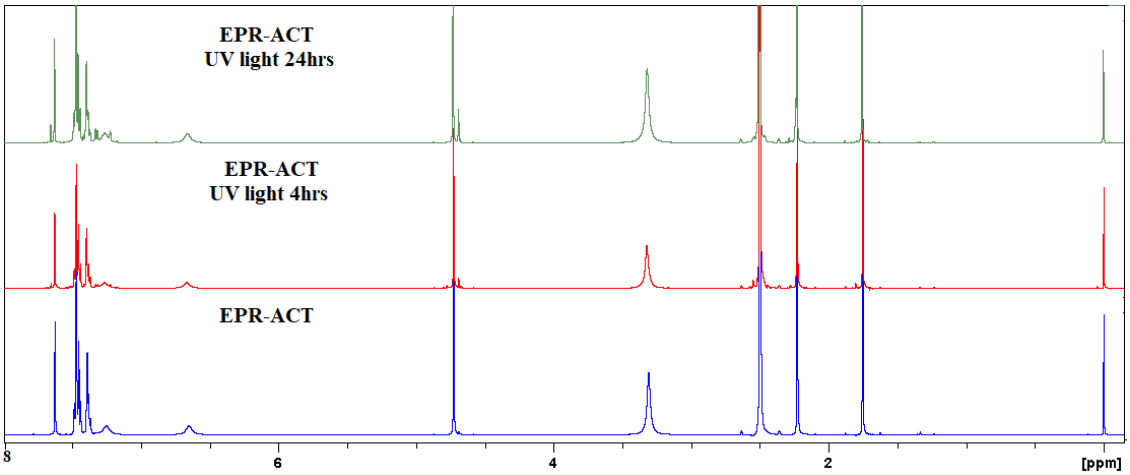
EPR-ACT
UV light 24hrs
EPR-ACT
UV light 4hrs
EPR-ACT
8
6
4
2
[ppm]

(c)

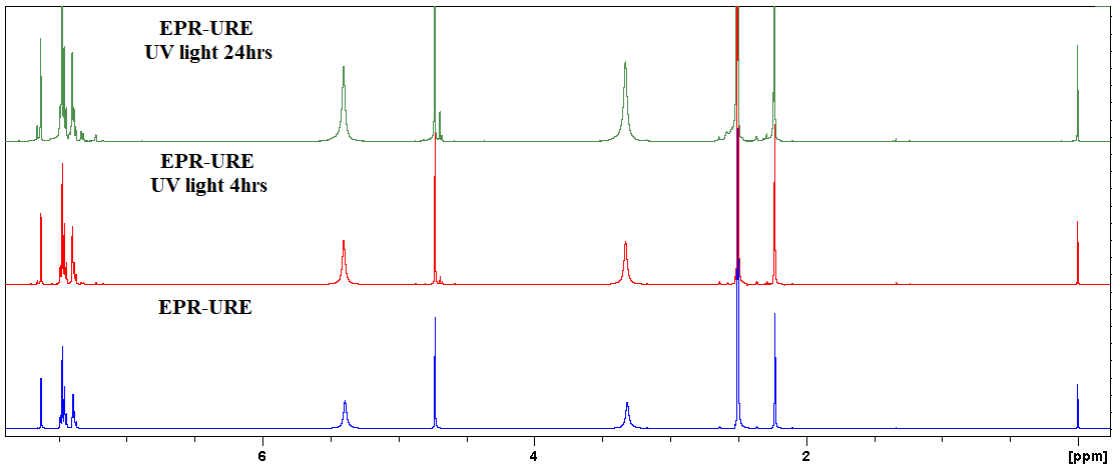
EPR-URE
UV light 24hrs
EPR-URE
UV light 4hrs
EPR-URE
6
4
2
[ppm]

(d)

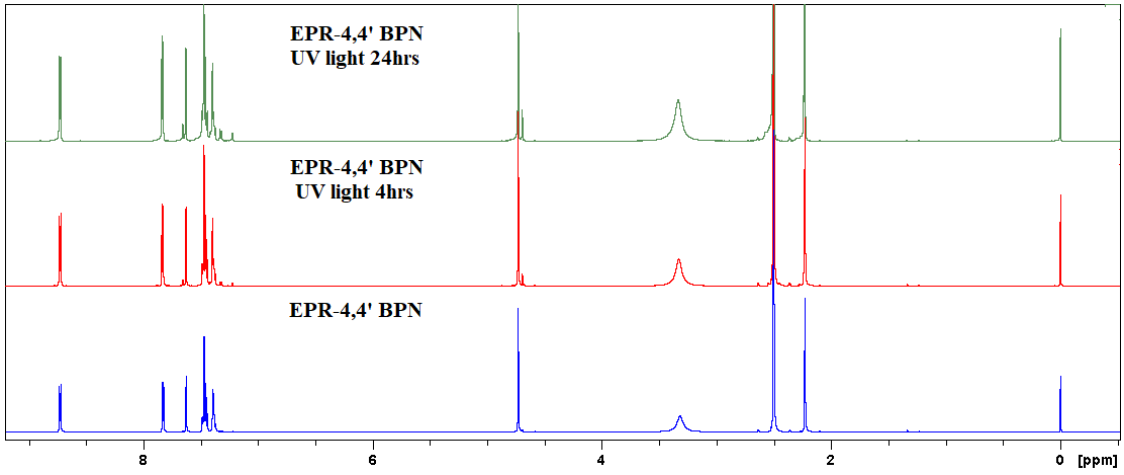
EPR-4,4' BPN
UV light 24hrs
EPR-4,4' BPN
UV light 4hrs
EPR-4,4' BPN
8
6
4
2
0
[ppm]

(e)

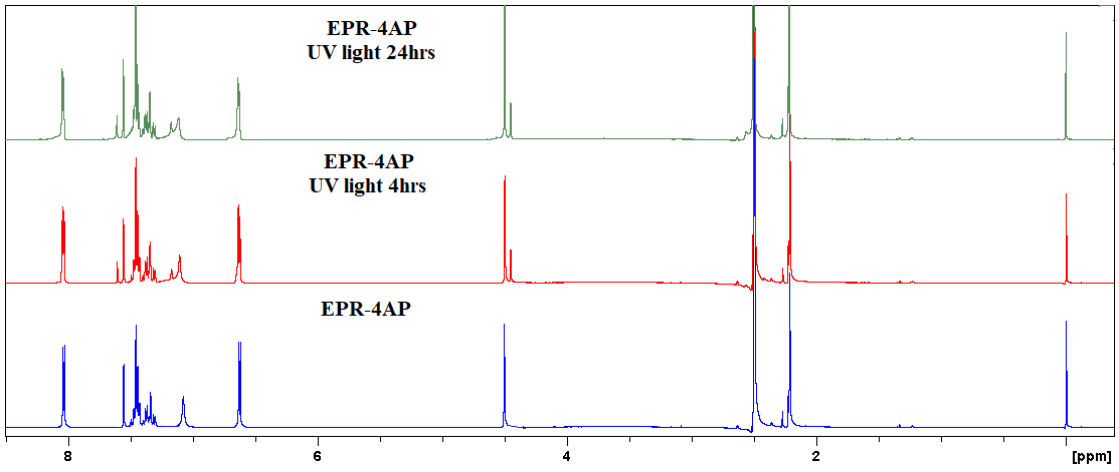
EPR-4AP
UV light 24hrs
EPR-4AP
UV light 4hrs
EPR-4AP
8
6
4
2
[ppm]

(f)

Figure 6.19 ^{1}H NMR spectrum of EPR cocrystals, (a) pure EPR, (b) EPR-CAF Form I, (c) EPR-ACT, (d) EPR-URE (e) EPR-4,4'BPN and (f) EPR-4AP before and after exposure to UV light shows that the E,Z isomer of EPR transforms to the Z,Z isomer within 4 h to about the same extent. Inter-conversion of the E,Z and Z,Z isomer in solution is seen based on the separation of proton signals at 4.69-4.73 ppm (2H, N-CH_2), and the peak at 7.64-7.66 ppm (1H, most downfield aromatic) and appearance of new proton signals at 7.23 and 7.32-7.34 ppm.

6.4.6 Correlating reactivity with molecular crystal packing

From the photodimerization studies, we established the photoreactivity order of EPR and its cocrystals as EPR-CFA Form I < EPR-4AP < EPR-URE < EPR-4,4'BPN < EPR < EPR-CFA Form II. In the crystal structure of EPR-CFA Form II, the distance between centroids of two reactive double bonds is 3.413 Å and the reactive double bonds are aligned in a parallel orientation (θ=0.00, Table 6.5). Therefore, it was found that this is the more reactive cocrystal form among all. But photoreactivity of other cocrystals doesn't follow either the distance criteria or parallel alignment criteria (Table 6.5). This could be explained from the following discussion.

Schmidt[44-46] postulated the following topochemical principle based on the photoreactivity of α-, β- and γ- forms of cinnamic acid and its derivatives:

1. The distance between centroids of two reactive double bonds must be within a distance of 4.2 Å.

2. The photoreactive double bonds of the nearest neighbour molecules must be aligned in a parallel orientation.

In addition to the distance (d) between the reactive double bonds, several other useful geometrical parameters were proposed to assess the nature of double bond alignment.[50] They are θ, θ_1 and θ_2, and also the displacement of double bonds, d1 and d2, with respect to one another (Scheme 6.4). The angle θ denotes the rotational angle of one double bond with respect to the other, while θ_1 represents the obtuse angle of the parallelogram formed by the double bond carbons, whereas θ_2 represents the angle between the plane of the reactive bonds and the plane of the olefin. The ideal values for θ, θ_1, and θ_2 for the best overlap of p-orbitals are 0°, 90° and 90° respectively. θ_1 reflects the displacement along the double bond axis, while θ_2 is a measure of its displacement in the molecular plane.

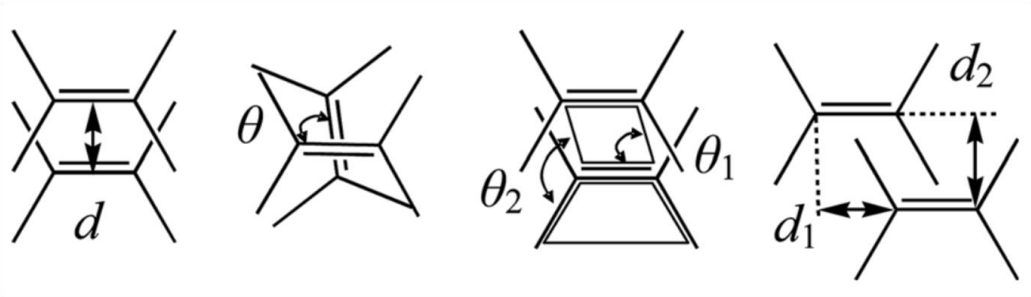

Scheme 6.4 Geometrical parameters used in the relative representation of reactant double bonds.

These rules are a powerful tool for determining a compound's photoreactivity or photostability. However, several molecules have been reported to react when the C=C bonds are not parallel and the distances are greater than 4.2 Å. Similarly, there are examples where the reactive double bonds being within 4.2 Å were photoinert.[51-53] Since Schmidt's topochemical postulate was first proposed, it has become clear that molecules in a crystal go through a variety of motions at room temperature, some of which may aid photoreactivity in the solid state.[54-55] However, some of these motions only occur when molecules are activated to the excited state, and they do not occur at room temperature in the absence of light. It is also important to note that the amount of free space surrounding the reactant molecules, which allows for some molecular motion in the crystal lattices, has a big impact on the crystals' reactivity. As a result, the reaction cavity and lattice energy play an important role in controlling the solid-state reactivity.[56-58]

Table 6.5 Relative Orientations of Reactive Double Bonds in EPR and its Cocrystal Structures.

Crystal structure	*d*(Å)	*θ* (deg)	*θ*$_1$ (deg)	*θ*$_2$(deg)	d$_1$(Å)	d$_2$(Å)	Yield (%)
EPR							
Pair I	3.731	13.83	81.29	76.44	0.8380	3.582	70
Pair II	3.550	15.64	94.26	78.09	0.1513	3.522	
EPR–CFA Form I	3.554	15.12	79.01	80.36	0.7410	3.460	13.3
EPR–CFA Form II	3.413	0.00	95.77	88.04	0.3431	3.396	100
EPR–URE	3.582	13.16	87.97	73.49	0.3287	3.647	50
EPR–4,4'BPN	3.646	14.43	85.72	89.33	0.1616	3.659	66
EPR–4AP	3.592	13.37	92.57	84.91	0.4804	3.615	45

6.5 Conclusions

In this chapter novel cocrystal forms of EPR with various conformers such as caffeine (1:1), acetamide (1:1), urea (1:1), 4,4'-bipyridine (1:0.5), and 4-aminopyridine (1:1) in a fixed stoichiometry are reported. All the cocrystal forms were characterized by thermal, spectroscopic and X-ray diffraction techniques. EPR-CAF cocrystal exhibited polymorphic behavior i.e. dimorphic. The main objective of this work was to obtain stable solid forms of EPR to stop/control the undesired photoinstability. Among the novel cocrystals of EPR synthesized, EPR-CAF Form I showed good photostability towards photodimerization. Unfortunately, all the cocrystal forms are undergoing photoisomerization and none of the cocrystals is able to completely stop the photoisomerization of EPR. The polymorphism of cocrystals in the context of photoreactivity is not well documented. To our knowledge, the only reported examples are polymorphs of cyclobutene tetracarboxylic acid and 1,2-bis(4-pyridyl)ethylene cocrystal, (cbta)-2(4,4'-bpe). The photoreaction takes place in SCSC manner in the Form II of (cbta)-2(4,4' -bpe) cocrystal and the reaction completes in shorter time compared to Form I.[59] One polymorph of 2(resorcinol)-2(4,4'-bpe) cocrystal is photoactive while the other one is photostable.[60]

6.6 Experimental Section

Epalrestat was a gift sample from Symed Laboratories Ltd., Hyderabad, India, and used without further purification. It corresponds to the polymorph I of our previous study.[29] All coformers (purity > 99.8%) were purchased from Sigma-Aldrich (Hyderabad, India). Solvents (purity > 99%) were purchased from Hychem Laboratories (Hyderabad, India).

Preparation of EPR solid forms

EPR–CAF Form I (1:1): This form was obtained upon grinding about 100 mg of a 1:1 stoichiometric ratio of EPR and CAF for 30 min by CH_3CN liquid-assisted grinding. The formation of cocrystal was confirmed by FT-IR, PXRD and DSC. 40 mg of the ground material was dissolved in 8 mL of hot tetra hydro furan: n-heptane solvent mixture (1:1, v/v) and left for slow evaporation at room temperature. Orange color needle crystals suitable for X-ray diffraction were obtained after 3-4 d upon solvent evaporation.

EPR–CAF Form II (1:1): Yellow color plate crystals of EPR–CAF Form II suitable for X-ray diffraction were obtained upon dissolving about 30 mg of a 1:1 stoichiometric ratio of EPR and CAF physical mixture in 6 mL of methanol solvent and left for slow evaporation at room temperature. Attempts to produce EPR–CAF Form II in bulk through various methods such as solvent assisted gringing, dry gringing, slurry grinding and rotary evaporation (fast evaporation) were unsuccessful.

EPR–ACT: The cocrystal was obtained by grinding EPR and ACT in 1:1 stoichiometry with a few drops of CH_3CN added in a liquid-assisted method for 30 min. The formation of cocrystal was confirmed by FT-IR, PXRD and DSC. Yellow color plate crystals suitable for X-ray diffraction were obtained when 30 mg of the ground product was dissolved in nitromethane solvent and left for slow evaporation at room temperature for 4-5 days.

EPR–URE: This cocrystal was obtained by grinding EPR and UER in 1:1 stoichiometry with a few drops of CH_3CN added in a liquid-assisted method for 30 min. The formation of cocrystal was confirmed by FT-IR, PXRD and DSC. Yellow color plate crystals suitable for X-ray diffraction were obtained when 40 mg of the ground product was dissolved in ethyl acetate-nitromethane solvent mixture (2:1 v/v, 8 mL) and left for slow evaporation at room temperature for 4-5 days.

EPR–4,4'-BPN (1:0.5): This cocrystal was obtained upon grinding about 100 mg of a 1:0.5 stoichiometric ratio of EPR and 4,4'-BPN for 30 min by CH_3CN liquid-assisted grinding. The formation of cocrystal was confirmed by FT-IR, PXRD and DSC. 40 mg of the ground material was dissolved in 8 mL hot tetrahydrofuran -methanol solvent mixture (1:1, v/v) and left for slow evaporation at room temperature. Yellow color block crystals suitable for X-ray diffraction were obtained after 3-4 d upon solvent evaporation.

EPR–4AP: This cocrystal was obtained by grinding EPR and 4AP in 1:1 stoichiometry with a few drops of CH_3CN added in a liquid-assisted method for 30 min. The formation of cocrystal was confirmed by FT-IR, PXRD and DSC. Yellow color block crystals suitable for X-ray diffraction were obtained when 30 mg of the ground product was dissolved in 6 mL of ethanol solvent and left for slow evaporation at room temperature for 4-5 days.

Photostability experiments of EPR and its cocrystals:

Photodimerization: Photodimerization studies on EPR and its cocrystals were carried out as follows. Samples of approximately 10-15 mg of powdered EPR and its cocrystals were spread evenly between two pyrex glass plates. The slides were kept together with scotch tape on their four edges. The glass plates were then exposed to ultraviolet radiation from a 450 W high pressure mercury lamp for 7 days. For uniform irradiation the samples were turned around every 12 h and respread between the plates every 24 h. The extent of the photoreaction was studied at regular intervals using ^{1}H NMR spectroscopy.

Photoisomerization: about 3mg of EPR was dissolved in DMSO-d_6 solvent in the NMR tube and exposed to ambient light. ^{1}H NMR was recorded after 24hrs of exposure. The above procedure was repeated for each cocrystal by keeping the amount of EPR constant.

Solution NMR spectra were recorded on Bruker Avance 400 MHz spectrometer (Bruker-Biospin, Karlsruhe, Germany).

EPR: ^{1}H NMR (DMSO-d_6, δ, ppm): 7.63 (1 H, s), 7.49-7.40 (4 H, m), 7.40-7.35 (2 H, m), 4.73 (2H, s), 2.23 (3 H, s) (Figure 6.12).

EPR Dimer: ^{1}H NMR (DMSO-d_6, δ, ppm): 1.80 (s, 2.1H), 1.94 (s, 2.1H), 2.23 (s, 1.8H), 3.6 (s, 0.7H), 3.98 (s, 0.7H), 4.59 (s, 1.4H), 4.66 (s, 1.4H), 4.72 (s, 1.2H), 5.2 (s, 0.7H), 6.65 (s, 0.7H), 7.22-7.28 (m, 3.4H), 7.32-7.35 (m, 2.8H), 7.39-7.40 (m, 1.2H), 7.44-7.48 (m, 2.4H), 7.65 (s, 1.4H). The peak at δ 3.6 ppm is slightly overlapped by the solvent peak. 70% photoreaction (Figure 6.13).

EPR-CAF Form I Dimer: ^{1}H NMR (DMSO-d_6, δ, ppm): 1.80 (s, 0.4H), 1.94 (s, 0.4H), 2.23 (s, 5.2H), 3.22 (s, 6H), 3.42 (s, 6H), 3.6 (s, 0.14H), 3.88 (s, 6H), 3.98 (s, 0.13H), 4.59 (s, 0.27H), 4.66 (s, 0.26H), 4.73 (s, 3.47H), 5.2 (s, 0.13H), 6.65 (s, 0.12H), 7.22-7.28 (m, 0.8H), 7.32-7.35 (m, 1.06H), 7.39-7.40 (m, 3.47H), 7.44-7.48 (m, 6.94H), 7.65 (s, 1.74H), 8.0 (s, 2H). The peak at δ 3.6 ppm is overlapped by the solvent peak. 13.3% photoreaction (Figure 6.14).

EPR-CAF Form II Dimer: ^{1}H NMR (DMSO-d_6, δ, ppm): 1.86 (s, 6H), 3.22 (s, 6H), 3.42 (s, 6H), 3.88 (s, 6H), 4.66 (s, 4H), 4.84 (s, 2H), 6.43 (s, 2H), 7.24-7.28 (m, 6H), 7.34-7.37 (m, 4H), 8.00 (s, 2H). X% photoreaction (Figure 6.15).

EPR-URE Dimer: ^{1}H NMR (DMSO-d_6, δ, ppm): 1.80 (s, 1.5H), 1.94 (s, 1.5H), 2.23 (s, 3.0H), 3.7 (s, 0.5H), 3.98 (s, 0.5H), 4.59 (s, 1H), 4.66 (s, 1H), 4.72 (s, 2H), 5.2 (s, 0.5H), 6.65 (s, 0.5H), 7.22-7.26 (m, 3H), 7.31-7.35 (m, 2H), 7.39-7.40 (m, 2H), 7.46-7.48 (m, 4H), 7.65 (s, 1H). The peak at δ 3.6 ppm is slightly overlapped by the solvent peak. 50% photoreaction (Figure 6.16).

EPR-4,4'BPN Dimer: ^{1}H NMR (DMSO-d_6, δ, ppm): 1.80 (s, 2H), 1.94 (s, 2H), 2.23 (s, 2H), 3.98 (s, 0.65H), 4.59 (s, 1.3H), 4.66 (s, 1.3H), 4.72 (s, 1.4H), 5.2 (s, 0.65H), 6.65 (s, 0.65H), 7.22-7.28 (m, 3.47H), 7.32-7.35 (m, 2.7H), 7.39-7.40 (m, 1.4H), 7.44-7.48 (m, 2.67H), 7.65 (s, 1.33H), 7.83-7.84 (d, 4H), 8.72-8.73 (d, 4H). One peak is buried under the solvent peak at δ 3.6 ppm. 66% photoreaction (Figure 6.17).

EPR-4AP Dimer: ^{1}H NMR (DMSO-d_6, δ, ppm): 1.80 (s, 1.37H), 1.94 (s, 1.37H), 2.23 (s, 3.3H), 3.6 (s, 0.45H), 3.98 (s, 0.45H), 4.47 (s, 0.9H), 4.50 (s, 0.9H), 4.57 (s, 2.2H), 5.2 (s, 0.45H), 6.64 (s, 0.45H), 6.7 (d, 6H), 7.22-7.28 (m, 2.9H), 7.32-7.35 (m, 1.8H), 7.37-7.40 (m, 2.2H), 7.44-7.48 (m, 4.4H), 7.63 (s, 1.1H), 8.0 (d, 6H). One peak is buried under the solvent peak at δ 3.6 ppm and one more peak is overlapped by the solvent peak at δ 3.98 ppm. The peak at δ 7.63 ppm is merging with the NH_2 peak. 45% photoreaction (Figure 6.18).

Vibrational spectroscopy

Thermo-Nicolet 6700 FT-IR-NIR spectrometer with NXR FT-Raman module (Thermo Scientific, Waltham, MA) was used to record IR spectra. IR spectra were recorded on samples dispersed in KBr pellets. Data were analyzed using the Omnic software (Thermo Scientific, Waltham, MA).

Thermal analysis

Differential scanning calorimetry was performed on Mettler-Toledo DSC 822e module, (Mettler-Toledo, Columbus, OH). Samples were placed in crimped but vented aluminum pans for DSC experiments. The typical sample size is 3-5 mg for DSC. The temperature

range for the heating curves was 30-300°C, and the sample was heated at a rate of 5 °C/min. Samples were purged in a stream of dry nitrogen flowing at 80 mL/min.

X-ray crystallography

X-ray reflections for EPR–CAF Form II and EPR–4,4'-BPN were collected on Bruker SMART-APEX CCD diffractometer equipped with a graphite monochromator and Mo-Kα fine-focus sealed tube (λ = 0.71073 Å). Data reduction was performed using Bruker SAINT Software.[61] Intensities were corrected for absorption using SADABS,[62] and the structures were solved and refined using SHELX-97.[63-64] X-ray reflections for EPR–ACT were collected on Bruker D8 QUEST CCD diffractometer. X-ray reflections for EPR–4AP and EPR–CAF Form II Dimer were collected on Bruker APEX-II CCD diffractometer. The structures were solved and refined using APEX-III software.[65] All non-hydrogen atoms were refined anisotropically. Hydrogen atoms on heteroatoms were located from difference electron density maps and all C−H hydrogens were fixed geometrically. Hydrogen bond geometries were determined in Platon.[66] X-ray reflections on EPR-CAF Form I and EPR-URE were collected on Oxford CCD X-ray diffractometer (Yarnton, Oxford, UK) equipped with Mo-Kα radiation (λ = 0.71073 Å) source. Data reduction was performed using CrysAlisPro 171.33.55 software.[67] Crystal structures were solved and refined using Olex2-1.0[68] with anisotropic displacement parameters for non-H atoms. Hydrogen atoms were experimentally located through the Fourier difference electron density maps in all crystal structures. All O–H and C–H atoms were geometrically fixed using HFIX command in SHELX-TL program of Bruker-AXS. Mercury[69] was used to prepare packing diagrams. X-ray reflections for all the crystal structures were collected at 298 K.

Powder X-ray diffraction

Powder X-ray diffraction was recorded on Bruker D8 Advance diffractometer (Bruker-AXS, Karlsruhe, Germany) using Cu-Kα X-radiation (λ = 1.5406 Å) at 40 kV and 30 mA power. X-ray diffraction patterns were collected over the 2θ range 5–50° at a scan rate of 5°/min. Powder Cell 2.4[70] (Federal Institute of Materials Research and Testing, Berlin, Germany) was used for Rietveld refinement of experimental PXRD and calculated lines from the x-ray crystal structure.

6.7 References

1. Weyna, D. R.; Shattock, T.; Vishweshwar, P.; Zaworotko, M. J. *Cryst. Growth Des*. **2009,** *9*, 1106–1123.
2. Aitipamula, S.; Banerjee, R.; Bansal, A. K.; Biradha, K.; Cheney, M. L.; Choudhury, A. R.; Desiraju, G. R.; Dikundwar, A. G.; Dubey, R.; Duggirala, N.; Ghogale, P. P.; Ghosh, S.; Goswami, P. K.; Goud, N. R.; Jetti, R. R. K. R.; Karpinski, P.; Kaushik, P.; Kumar, D.; Kumar, V.; Moulton, B.; Mukherjee, A.; Mukherjee, G.; Myerson, A. S.; Puri, V.; Ramanan, A.; Rajamannar, T.; Reddy, C. M.; Rodriguez-Hornedo, N.; Rogers, R. D.; Row, T. N. G.; Sanphui, P.; Shan, N.; Shete, G.; Singh, A.; Sun, C. C.; Swift, J. A.; Thaimattam, R.; Thakur, T. S.; Kumar Thaper, R.; Thomas, S. P.; Tothadi, S.; Vangala, V. R.; Variankaval, N.; Vishweshwar, P.; Weyna, D. R.; Zaworotko, M. J. *Cryst. Growth Des*. **2012,** *12*, 2147−2152.
3. Desiraju, G. R. *Crystal Engineering: The Design of Organic Solids*; Elsevier: New York, 1989.
4. Desiraju, G. R. *Angew. Chem., Int. Ed*. **2007**, *46*, 8342–8356.
5. Almarsson, Ö; Zaworotko, M. J. *Chem. Commun*. **2004**, 1889–1896.
6. Chattoraj, S.; Shi, L.; Chen, M.; Alhalaweh, A.; Velaga, S.; Sun, C. C. *Cryst. Growth Des*. **2014**, *14*, 3864−3874.
7. Landenberger, K. B.; Bolton, O.; Matzger, A. J. *Angew. Chem., Int. Ed*. **2013**, *52*, 6468−6471.
8. Swapna, B.; Mannava, M.C.; Nangia, A. *J. Pharm. Sci*. **2018**, *107*, 1667-1679.
9. Good, D. J.; Rodriguez-Hornedo, N. *Cryst. Growth Des*. **2009**, *9*, 2252–2264.
10. Thakuria, R.; Nangia, A. *CrystEngComm* **2011**, *13*, 1759–1764.
11. Suresh, K.; Mannava, M.C.; Nangia, A. *Chem. Commun*. **2016,** *52*, 4223-4226.
12. Mannava, M.C.; Gunnam, A.; Lodagekar, A.; Shastri, N.R.; Nangia, A.K.; Solomon, K.A. *CrystEngComm* **2021**, *23*, 227-237.
13. Chattoraj, S; Shi, L; Sun, C. C. *CrystEgComm* **2010,** *12*, 2466–2472.
14. Guidance for Industry: Q1A Stability Testing of New Drug Substances and Products, U.S. Food and Drug Administration, August **2003** (Revision 2).
15. Seddon, K. R.; Zaworotko, M. *Crystal Engineering: The Design and Application of Functional Solids; NATO-ASI Series*, Kluwer, Norwell, MA, **1999**, vol. 539.
16. Vangala, V. R.; Chow, P. S.; Tan, R. B. H. *CrystEngComm* **2011**, *13*, 759−762.

17. Teraoka, R.; Fukami, T.; Furuishi, T.; Nagase, H.; Ueda, H.; Tode, C.; Yutani, R.; Kitagawa, S.; Sakane, T. *Chemical and Pharmaceutical Bulletin* **2019**, *67*, 940-944.
18. Zhu, B.; Wang, J.R.; Zhang, Q.; Mei, X. *Cryst. Growth Des*. **2016**, *16*, 483-492.
19. Maruthi, R.; Chandan, R.S.; Tengli, A.K. *Research Journal of Pharmacy and Technology*. **2021**, *14*, 11-13.
20. Tatsunami, R.; Murao, Y.; Sato, K. *Yakugaku Zasshi: Journal of the Pharmaceutical Society of Japan*. **2020**, *140*, 1381-1388.
21. Ishida, T.; In, Y.; Inoue, M.; Ueno, Y.; Tanaka, C.; Hamanaka, N. *Tetrahedron Lett*. **1989**, *30*, 959-962.
22. Igarashi, R.; Nagase, H.; Furuishi, T.; Tomono, K.; Endo, T.; Ueda, H. Anal. Sci. *X-Ray Struct. Anal. Online* **2015**, *31*, 1−2.
23. Nagase, H.; Kobayashi, M.; Ueda, H.; Furuishi, T.; Gunji, M.; Endo, T.; Yonemochi, E. *X-Ray Struct. Anal. Online* **2016**, *32*, 7−9.
24. Ishida, T.; In, Y.; Inoue, M.; Tanaka, C.; Hamanaka, N. *J. Chem. Soc., Perkin Trans. 2* **1990**, *2*, 1085−1091.
25. Igarashi, R.; Nagase, H.; Furuishi, T.; Endo, T.; Tomono, K.; Ueda, H. *X-Ray Struct. Anal. Online* **2013**, *29*, 23−24.
26. Umeda, D.; Putra, O. D.; Gunji, M.; Fukuzawa, K.; Yonemochi, E. Acta Crystallogr. **2017**, *73*, 941−944.
27. Putra, O. D.; Umeda, D.; Fukuzawa, K.; Gunji, M.; Yonemochi, E. *Acta Crystallogr*. **2017**, *73*, 1264−1267.
28. Igarashi, R.; Nagase, H.; Furuishi, T.; Tomono, K. *X-ray Structure Analysis Online* **2013**, *29*, 23-24.
29. Swapna, B.; Suresh, K.; Nangia, A. *Chem. Commun*. **2016**, *52*, 4037−4040.
30. Swapna, B.; Nangia, A. *Cryst. Growth Des*. **2017**, *17*, 3350−3360.
31. Putra, O.D.; Umeda, D.; Nugraha, Y.P.; Nango, K.; Yonemochi, E.; Uekusa, H. *Cryst. Growth Des.* **2018,** *18*, 373-379.
32. N. Shan, F. Toda and W. Jones, *Chem Commun*, **2002**, *20*, 2372-2373.
33. P. P. Bag, M. Patni and C. M. Reddy, *CrystEngComm*, **2011**, *13*, 5650-5652.
34. Walsh, R. D. B.; Bradner, M. W.; Fleishman, S.; Morales, L. A.; Moulton, B.; Rodríguez-Hornedo, N.; Zaworotko, M. J. *Chem. Commun.* **2003**, 186.

35. Bernstein, J.; Davis, R. E.; Shimoni, L.; Chang, N. L. *Angew. Chem., Int. Ed. Engl.* **1995**, *34*, 1555–1573.
36. Walsh, R. D. B.; Bradner, M. W.; Fleischman, S.; Morales, L. A.; Moulton, B.; Rodriguez-Hornedo, N.; Zaworotko, M. J. *Chem. Commun.* **2003**, *2*, 186–187.
37. Harris, K. D. M.; Tremayne, M.; Kariuki, B. M. *Angew. Chem. Int. Ed*. **2001**, *40*, 1626-1651.
38. Harris, K. D.; Tremayne, M.; Lightfoot, P.; Bruce, P. G. *J. Am. Chem. Soc.* **1994**, *116*, 3543-3547.
39. Cheung, E. Y.; Kitchin, S. J.; Harris, K. D. M.; Imai, Y.; Tajima, N.; Kuroda, R. *J. Am. Chem. Soc.* **2003**, *125*, 14658-14659.
40. Sanphui, P.; Sarma, B.; Nangia, A. *Cryst. Growth Des*. **2010**, *10*, 4550–4564.
41. Jones, W.; Motherwell, W. D. S.; Trask, A. V. *MRS Bull.* **2006**, *31*, 875.
42. Stanton, M. K.; Bak, A. *Cryst. Growth Des*. **2008**, *8*, 3856.
43. Stanton, M. K.; Tufekcic, S.; Morgan, C.; Bak, A. *Cryst. Growth Des*. **2009**, *9*, 1344.
44. Cohen, M. D.; Schmidt, G. M. J. *J. Chem. Soc*. **1964**, 1996.
45. Cohen, M. D.; Schmidt, G. M. J.; Sonntag, F. I. *J. Chem. Soc*. **1964**, 2000.
46. Schmidt, G. M. J. *Pure Appl. Chem*. **1971**, *27*, 647.
47. Halasz, I. *Cryst. Growth Des*. 2010, 10, 2817.
48. Friscic, T.; MacGillivray, L. R. *Z. Kristallogr*. **2005**, *220*, 351.
49. Barbour, L. J. *Aust. J. Chem.* **2006**, *59*, 595.
50. Gnanaguru, K.; Ramasubbu, N.; Venkatesan, N.; Ramamurthy, V. *J. Org. Chem.*, **1985**, *50*, 2337.
51. Biradha K, Santra R. *Chemical Society Reviews*. **2013**, *42*, 950-67.
52. Yang, S.-Y.; Naumov, P.; Fukuzumi, S. *J. Am. Chem. Soc*. **2009**, *131*, 7247.
53. Ramamurthy, V.; Venkatesan, K. *Chem. ReV.* **1987**, *87*, 433-481.
54. Dunitz, J. D.; Scomkaher, V.; Trueblood, K. N. *J. Phys. Chem.* **1988**, *92*, 856.
55. Harada, J.; Ogawa, K. In Topics in Stereochemistry; Denmark, S. E., Siegel, J. S., Eds.; John Wiley & Sons, Inc: **2006**, *25*, 31.
56. Cohen, M. D. *Angew. Chem., Int. Ed*. Engl., **1975**, *14*, 386.
57. Gavezzotti, A. *J. Am. Chem. Soc.*, **1983**, *105*, 5220.

58. Kearsley, S. K. *The Prediction of Chemical Reactivity within Organic Crystals Using Geometric Criteria, in Organic Solid State Chemistry,* ed. Desiraju, G. R. Elsevier, New York, **1987**, 69–115.
59. Bhattacharya, S.; Stojakovic, J.; Saha, B. K.; MacGillivray, L. R. *Organic Letters*. **2013**, *15*, 744-747.
60. Friscic, T.; MacGillivray, L. R. *Chem. Commun*. **2009**, 773.
61. *SAINT-Plus*, version 6.45; Bruker AXS Inc.: Madison, Wisconsin, U.S.A., **2003**
62. SADABS, *Program for Empirical Absorption Correction of Area Detector Data*; Sheldrick, G. M. University of Göttingen: Göttingen, Germany, **1997**.
63. *SMART*, version 5.625 and *SHELX-TL*, version 6.12;, Bruker AXS Inc.: Madison, Wisconsin, USA, **2000**.
64. Sheldrick, G. M. *SHELXS-97* and *SHELXL-97*; University of Göttingen: Göttingen, Germany, **1997**.
65. Bruker. APEX3, SAINT and SADABS. Bruker AXS Inc. **2016**, Madison, Wisconsin, USA.
66. Spek, A. L. *PLATON, A Multipurpose Crystallographic Tool*; Utrecht University: Utrecht, Netherlands, **2002**.
67. *CrysAlis CCD and CrysAlis RED*, Ver. 1.171.33.55; Oxford Diffraction Ltd: Yarnton, Oxfordshire, UK, **2008**.
68. Dolomanov, O. V.; Blake, A. J.; Champness, N. R.; Schröder, *M. J. Appl. Crystallogr*. **2003**, *36*, 1283–1284.
69. Mercury 3.8, Cambridge Crystallographic Data Centre.
70. Powder Cell, *A Program for Structure Visualization, Powder Pattern Calculation and Profile Fitting*, http://www.ccp14.ac.uk/index.html (accessed 31 July, 2014).

CHAPTER SEVEN

CONCLUSIONS AND FUTURE PROSPECTS

This thesis focuses on the identification, characterization and application of various single and multiple component solid forms of Active pharmaceutical Ingredients (APIs). Extensive studies on various solid forms such as polymorphs, cocrystals, salts and polymorphic cocrystals and salts of several APIs were carried out with the main objective of understanding and solving the problems associated with them.

Isoniazid (INH) is a key drug ingredient in the fixed dose combination (FDC) for the treatment of tuberculosis (TB). INH is highly soluble in aqueous medium and stable in pure form, but it degrades due to cross reactions when it is part of the FDC. In Chapter 2, we performed a cocrystal screen with pharmaceutically acceptable molecules from the generally regarded as safe (GRAS) list to improve the physiochemical properties of INH. Cocrystals with acidic conformers like vanillic acid (VLA), ferulic acid (FRA), caffeic acid (CFA), and the hydroxyl coformer resorcinol (RES) have been reported. INH–VLA and INH–FRA are dimorphic while INH–CFA is trimorphic. Form-1 of INH-FRA and INH-VLA are two-dimensional isostructural structures. All cocrystal structures are sustained by the expected acid–pyridine synthon, except the isostructural cocrystals which have the hydroxyl–pyridine synthon. Except for the INH–RES cocrystal, all cocrystal forms were found to be stable for a six-month test period when they were tested in accelerated ICH conditions of 40 ºC and 75% RH for stability. Form-2 of INH-FRA and INH-VLA have good slurry stability, and Form-1 of INH-CFA is the most stable crystalline form of INH, according to slurry conditions and grinding experiments.

The primary goal in Chapter 3 was to improve the stability of FDC formulation of anti-tuberculosis drugs. The classic FDC of four TB drugs, namely Rifampicin (RIF), Isoniazid (INH), Pyrazinamide (PZA) and Ethambutol Dihydrochloride (EDH) has the twin issues of physical stability and rifampicin cross-reaction in the 4FDC. The major reason for these quality issues is the interaction between RIF and INH to yield

isonicotinyl hydrazone (HYD) in drug tablets. Pharmaceutical cocrystals of INH with caffeic acid (PZA + EDH + RIF + INH-CFA cocrystal) and vanillic acid (PZA + EDH + RIF + INH-VLA cocrystal) are able to stabilize the FDC formulation compared to the reference batch (PZA + EDH + RIF + INH). Stability studies under accelerated humidity and temperature stress conditions of 40 °C and 75% relative humidity showed that the physical stability of the cocrystal formulation was superior by PXRD and SEM analysis, and chemical purity was analyzed by HPLC. Changes in the composition and structure were monitored on samples drawn at 7, 15, 22, and 30 days of storage. FDC-INH-CFA cocrystal batch exhibited greater stability compared to FDC-INH-VLA cocrystal and FDC reference drug batches. The superior stability of INH-CFA cocrystal is attributed to the presence of stronger hydrogen bonds and cyclic O–H···O synthon in the crystal structure.

In Chapter 4, we described five crystalline polymorphs and an amorphous phase of an aldose reductase inhibitor, Epalrestat together with configurational isomerism and color behavior. Form I (deep red), form II (deep orange), form III (bright yellow), form IV (yellow), form V (orange) are in the E,Z configuration of the drug, and a Z,Z isomer (bright yellow). Two pathways are identified for polymorph conversion: direct transformation of E,Z isomer and another pathway via the Z,Z isomer to the E,Z polymorphs. From a pharmaceutical perspective, the stability of polymorphs was established by grinding, solvent slurry and thermal conditions as: Form I (thermodynamic) > Form II > Form V > Form III > Form IV (least stable).

In Chapter 5, Cocrystallization of the antidiabetic drug Eparlestat (EPR) with cytosine (CYT) gave EPR^{-}–CYT-H^{+} form I, a salt-cocrystal hybrid structure, salt hydrate (EPR^{-}–CYT-H^{+}–H_2O, 1:2:1), and nonstoichiometric solvates of EPR^{-}–CYT-H^{+} with EtOH/n-PrOH included in the rhombohedral symmetry voids, referred to as form II. Desolvation of EPR^{-}–CYT-H^{+} form II solvates resulted in an unsolvated form II of EPR^{-}–CYT-H^{+} which was characterized by DSC, TGA, and NMR. The carboxylate···cytosinium synthon was observed in the salt structure along with the uncommon CYT-H^{+}···H^{+}-CYT base pairing in the structures of salt-cocrystal hybrid and salt hydrate. The crystalline forms were characterized by spectroscopic (IR, NMR),

thermal (DSC, HSM, TGA), powder X-ray diffraction (PXRD) and single crystal X-ray diffraction (SC-XRD) techniques. The intent of using the salt/ salt-cocrystal forms as a means to stop the E,Z → Z,Z isomerization of EPR was not successful in photoirradiation experiments.

In Chapter 6, cocrystallization of Epalrestat (EPR) with various coformers was performed with the intention that the resulting cocrystals would have the appropriate hydrogen bonding interactions to control/stop the photoisomerization and photodimerization of EPR. Liquid assisted grinding (LAG) resulted in cocrystals of EPR with caffeine (CAF), acetamide (ACT), urea (URE), 4,4′-bipyridine (BPN) and 4-amino pyridine (AP). Except EPR-BPN (1:0.5), all the cocrystals were found to be 1:1 (API: coformer) stoichiometry. The EPR-CAF cocrystal was shown to exhibit polymorphism, i.e: dimorphic. Since C=C bonds lie parallel and separated by less than 4.2 Å in EPR and its cocrystal forms, they are undergo (2+2) cycloaddition in the solidstate when exposed to UV light. Formation of type I head-tail dimer was observed in the case of EPR and all cocrystals except EPR-CAF Form II which gives type II head-tail dimer after UV irradiation. All the solid forms were exposed to UV light for the period of 7 days and in the certain time intervals samples were withdrawn and their ^{1}H NMR spectroscopy studies were done. EPR-CAF form II undergoing 100% photodimerization within in time period of 10 min. Percentage of EPR remaining after photodimerization in EPR and its cocrystal forms is 30% (EPR), 86.7% (EPR-CFA Form I), 0% (EPR-CFA Form II), 50% (EPR-URE), 34% (EPR-4,4' BPN) and 55% (EPR-4AP). From the stability studies we conclude that EPR-CAF Form I is the most stable solid form in photodimerization reaction. All the cocrystal forms exposed to UV light in solution state and their photoisomerization studies were carried out through ^{1}H NMR spectroscopy. Unfortunately, all the cocrystal forms undergo photoisomerization and none of the cocrystals is able to stop/control the photoisomerization of EPR.

Future prospects

Superior stability of the FDC-INH-CFA cocrystal batch compared to the FDC reference drug batch in chapter 3 can be used as an alternative formulation in future provided its bioavailability is expected to be better than the FDC reference drug batch. We were

unsuccessful in improving the photoisomerization issue of Epalrestat through polymorphs (Chapter 4), salts (Chapter 5), and cocrystals (Chapter 6), though cocrystals were able to decrease the photodimerization. Therefore, it would be interesting to improve the photoisomerization of Epalrestat through methods other than salts/cocrystals/polymorphs for better therapeutic efficacy.

ABOUT THE AUTHOR

Battini Swapna, daughter of Mr. Vishnumurthy and Mrs. Bhagyamma, was born in Mothkur, Yadadri Bhuvanagiri District, Telangana, India. She received primary education at Harividyalayam school and secondary education at A.P Residential School for Girls, Choutuppal. She completed Intermediate (B.P.C., 2004-06) in Biology, Physics and Chemistry at Sri Chaitanya Junior College for Girls, Hyderabad. She pursued Bachelor of Science (B.Sc., Biochemistry, Genetics and Chemistry, 2006-09) at St Pious X degree&pg college for women, Hyderabad and Master of Science (M. Sc., Organic Chemistry, 2009-11) from University College of Science, Osmania University, Hyderabad. She qualified CSIR-UGC-JRF National Eligibility test and ranked 88th for 'Junior Research Fellowship' (JRF) held in June 2011 and was awarded research fellowship by University Grant Commission (UGC). She then joined (in 2012) Prof. Ashwini Nangia's Research Group, School of Chemistry, University of Hyderabad, as a PhD Student and was upgraded as a 'Senior Research Fellow' (SRF) in 2014. Her research interest deals with the polymorphism in single and multiple component crystal forms of active pharmaceutical ingredients. During her PhD registration she has taken break from research work due to family reasons from April 2018 to December 2020, and re-registered in January 2021 to submit her PhD thesis in July 2021.

List of Publications

1. **High Solubility Crystalline Pharmaceutical Forms of Blonanserin.**

   Maddileti, D.; **Swapna, B**.; Nangia, A. *Cryst. Growth Des.* **2014,** *14*, 2557-2570.

2. **Cocrystals of the Tuberculosis Drug Isoniazid: Polymorphism, Isostructurality, and Stability.**

   Swapna, B.; Maddileti, D.; Nangia. A. *Cryst. Growth Des.* **2014,** *14*, 5991-6005.

3. **Tetramorphs of the Antibiotic Drug Trimethoprim: Characterization and Stability.**

   Maddileti, D.; **Swapna**, **B**.; Nangia. A. *Cryst. Growth Des.* **2015,** *15*, 1745-1756.

4. **Color Polymorphs of Aldose Reductase Inhibitor Epalrestat: Configurational, Conformational and Synthon differences.**

   Swapna, **B**.; Suresh, K.; Nangia. A. *Chem. Commun.* **2016,** *52*, 4037-4040.

5. **Epalrestat–Cytosine Cocrystal and Salt Structures: Attempt To Control *E,Z* → *Z,Z* Isomerization**.

   Swapna, B.; Nangia. A. *Cryst. Growth Des.* **2017,** *17*, 3350-3360.

6. **Blonanserin N-Oxide Lowers Glucose Levels in Insulinogenic Cells and Animal Models.**

   Maddileti, D.; Mannava, C.; **Swapna, B**.; Tejpal, R.; Konga, D. B.; Rao Khandavilli, U. B.; Kokkonda, V.; Medipelli, S. R; Mummareddy, S.; Ernest, K.; Kona, K .; Vangalapudi, L.; Nangia, A. *J Pharm Drug Devel*. **2017**, *4***,** 1-8.

7. **Improved Stability of Tuberculosis Drug Fixed-Dose Combination Using Isoniazid-Caffeic Acid and Vanillic Acid Cocrystal.**

   Swapna, **B**.; Mannava, M. K. C.; Nangia, A. *J. Pharm. Sci.* **2018**, *107***,** 1667-1679.

8. **Improved Photostability of Aldose Reductase Inhibitor Epalrestat Through Cocrystallization**

   Swapna, **B**.; Nangia, A. (to be communicated)

Patents Filed:

9. Improved Stability of Fixed Dose Combination of Anti-TB Drugs Via Cocrystals.

   D. Maddileti, S. Mittapalli, **B. Swapna,** S. Cherukuvada and A. Nangia.

   Indian Patent, 2014, Provisional Patent Application No. 5833/CHE/2014.

10. N-Alkyl N-Heterocyclic Piperazine N-Oxide Compounds for the Treatment Of Type-II Diabetes

    D. Maddileti, M. K. C. Mannava, **B. Swapna,** R. Tejpal, D.B. Konga, K. Ernest, K. Kona, L. Vangalapudi, U. B. R. Khandavilli, V. Kokkonda, S.R. Medipelli, A. Nangia.

    Provisional Patent Application No. No. 2971/CHE/2015.

Conferences, Symposia and Workshops Attended

1. Attended the work shop on "**Computational Chemistry"** conducted by School of chemistry, University of Hyderabad, December 02-14, 2013.

2. Participated in A. P. Science Congress-2013 **"Innovation in Science and Technology for Emerging Knowledge Society"** conducted by A. P. Akademi of Sciences, held at University of Hyderabad, November 14-16, 2013.

3. Presented a poster entitled **"Cocrystals of the Tuberculosis Drug Isoniazid: Polymorphism, Isostructurality, And Stability"** in the **Chemfest 2014** held at University of Hyderabad, Hyderabad, India, during February 2014.

4. Presented a poster entitled **"Cocrystals of the Tuberculosis Drug Isoniazid: Polymorphism, Isostructurality, And Stability"** in the **RSC Road Show** held at University of Hyderabad, Hyderabad, India, during November 7, 2014.

5. Participated in **"The First INDO-TAIWAN Symposium on Recent Trends in Chemical Sciences"** held at University of Hyderabad, November 17-18, 2014.

6. Presented a poster entitled **"Polymorphism of aldose reductase inhibitor Epalrestat."** In **"13th Asian Crystallographic Association"** held in Science City, Kolkata, India, during December 5-8, 2015.

7. Delivered an oral presentation and presented a poster entitled **"Color polymorphs of aldose reductase inhibitor epalrestat: configurational, conformational and synthon differences."** in the "**Chemfest 2016**" **(13th Annual In-house Symposium)** held at University of Hyderabad, Hyderabad, India, during March 18-19, 2016.

8. Delivered an oral presentation entitled **"Applications of Cocrystals in Pharmaceutical Industry to Improve the Stability of Anti-Tuberculosis Fixed Dose Combination Drugs"** in "**Dr. K. V. Rao Scientific Society Annual Science Awards–2016-17"** held on May 27, 2017, Hyderabad, India.

9. Presented a poster entitled **"Salt-cocrystal continuum of epalrestat-cytosine binary solid"** in **"24th Congress and General Assembly of the International Union of Crystallography"** held at HICC, Hyderabad, India, during August 21-28, 2017.

Polymorphism in Single and Multiple Component Crystal Forms of Active Pharmaceutical Ingredients

by Swapna Battini

Polymorphism in Single and Multiple Component Crystal Forms of Active Pharmaceutical Ingredients

ORIGINALITY REPORT

50%	30%	34%	5%
SIMILARITY INDEX	INTERNET SOURCES	PUBLICATIONS	STUDENT PAPERS

PRIMARY SOURCES

1	pubs.acs.org Internet Source	17%
2	Battini Swapna, Ashwini Nangia, "Epalrestat–Cytosine Cocrystal and Salt Structures: Attempt To Control , → , Isomerization ", Crystal Growth & Design, 2017 Publication	12%
3	Swapna Battini, M. K. Chaitanya Mannava, Ashwini Nangia. "Improved Stability of Tuberculosis Drug Fixed-Dose Combination Using Isoniazid-Caffeic Acid and Vanillic Acid Cocrystal", Journal of Pharmaceutical Sciences, 2018 Publication	8%
4	pubs.rsc.org Internet Source	6%
5	baadalsg.inflibnet.ac.in Internet Source	1%

Publication has name of author
14.02.21, Ashwini Nangia

Prof. Ashwini K. Nangia
School of Chemistry
University of Hyderabad
Central University P.O.
Hyderabad 500 046

Ashwini Nangia
14.02.21

Prof. Ashwini K. Nangia
School of Chemistry
University of Hyderabad
Central University P.O.
Hyderabad 500 046

Ashwini Nangia
14.02.21

Prof. Ashwini K. Nangia
School of Chemistry
University of Hyderabad
Central University P.O.
Hyderabad 500 046

Publication has name of author
14.02.21, Ashwini Nangia

Prof. Ashwini K. Nangia
School of Chemistry
University of Hyderabad
Central University P.O.
Hyderabad 500 046

6	Submitted to University of Hyderabad, Hyderabad Student Paper	1 %
7	www.science.gov Internet Source	1 %
8	mafiadoc.com Internet Source	<1 %
9	www.scribd.com Internet Source	<1 %
10	Submitted to University of Bedfordshire Student Paper	<1 %
11	Kuthuru Suresh, Vasily S. Minkov, Kranthi Kumar Namila, Elizaveta Derevyannikova et al. "Novel Synthons in Sulfamethizole Cocrystals: Structure–Property Relations and Solubility", Crystal Growth & Design, 2015 Publication	<1 %
12	Submitted to Jawaharlal Nehru Technological University Student Paper	<1 %
13	citeseerx.ist.psu.edu Internet Source	<1 %
14	journals.iucr.org Internet Source	<1 %

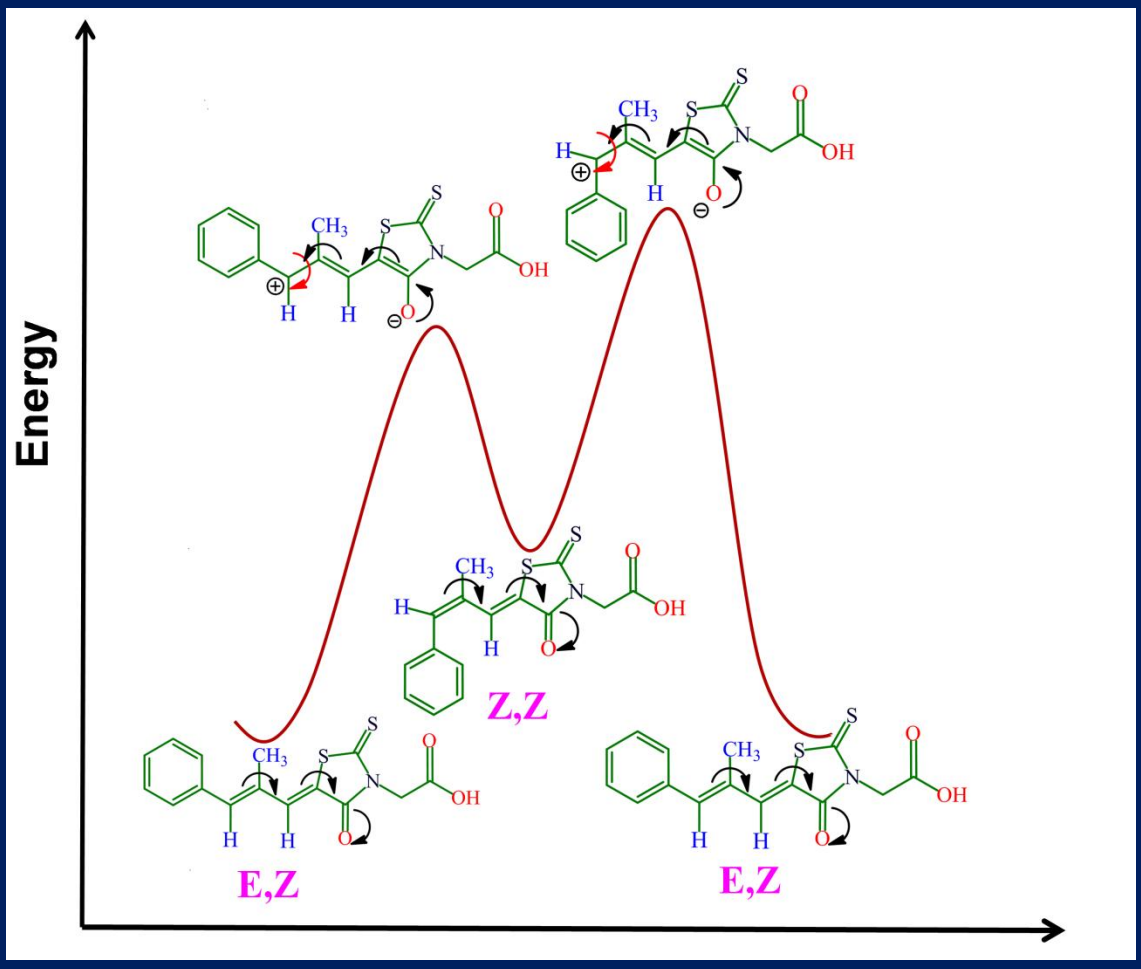
Energy
Z,Z
E,Z
E,Z

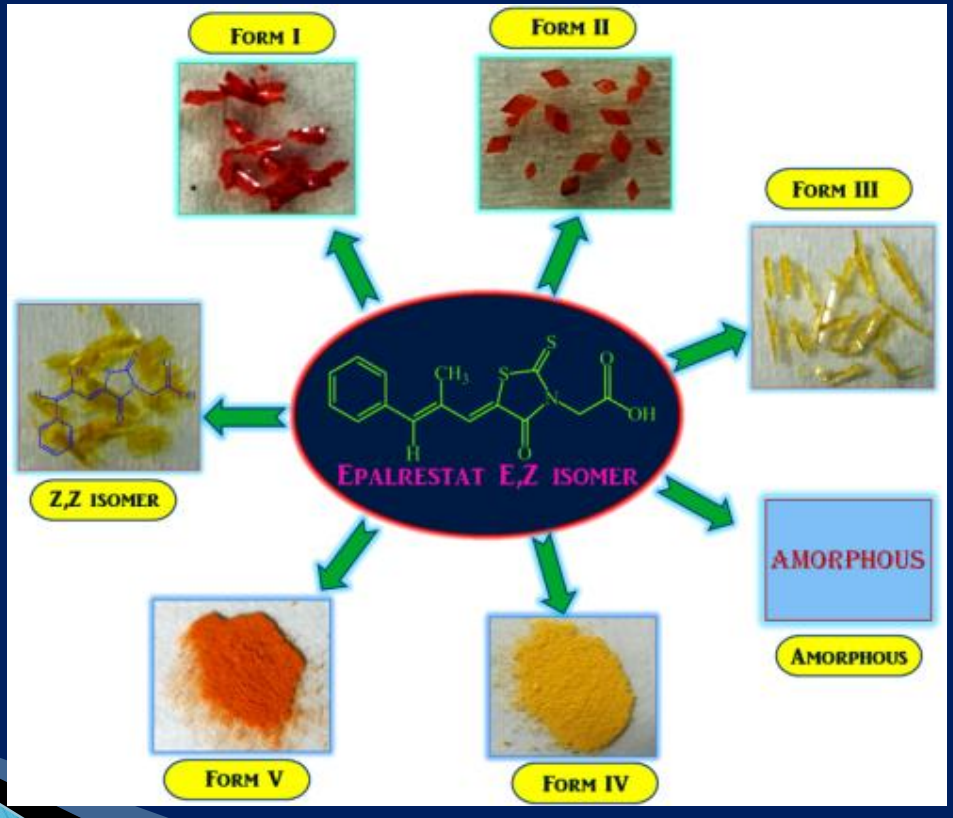
FORM I
FORM II
FORM III
Z,Z ISOMER
EPALRESTAT E,Z ISOMER
AMORPHOUS
AMORPHOUS
FORM V
FORM IV